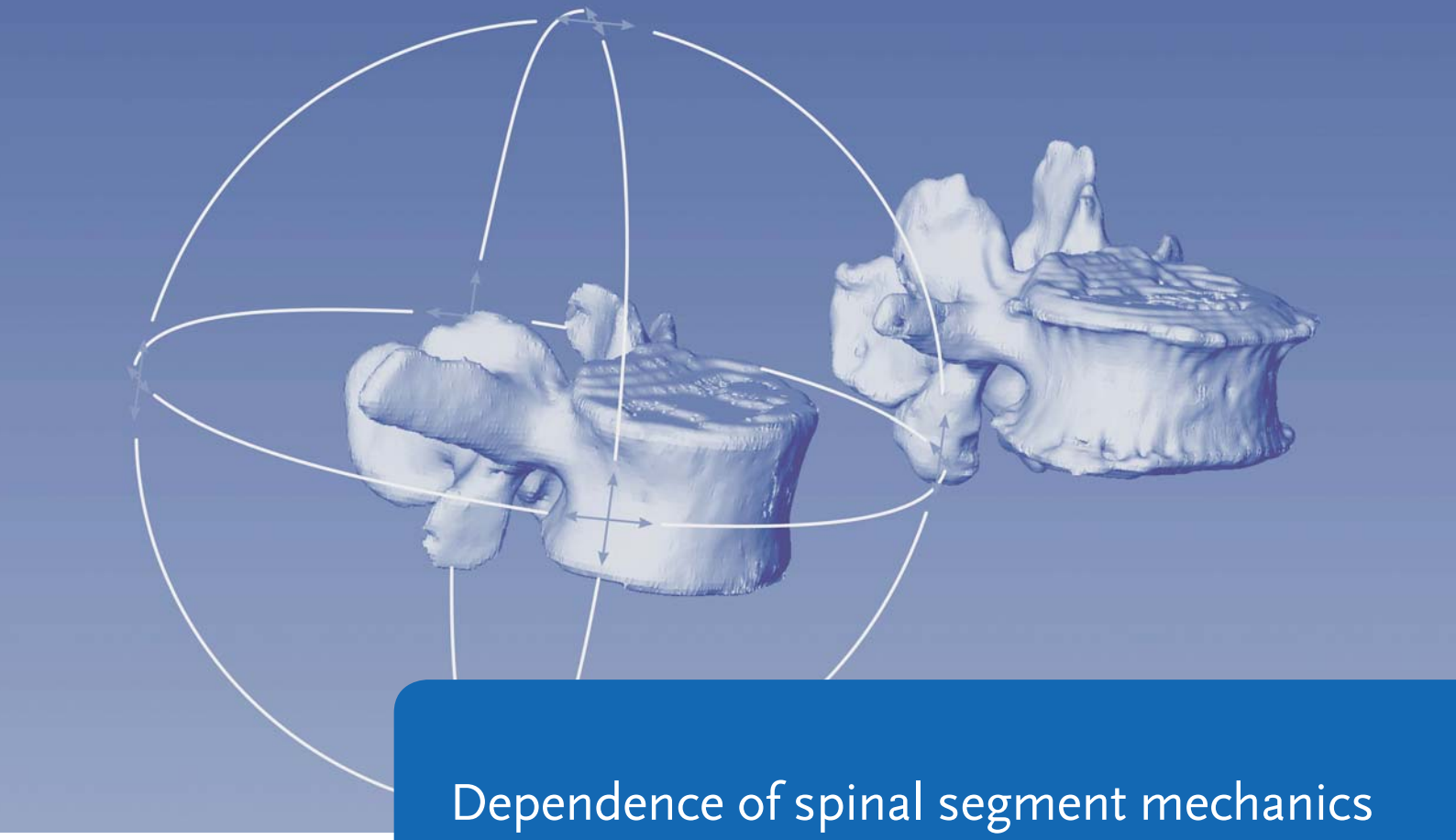

Dependence of spinal segment mechanics on age and posture

G. Huber, Ch. Mischke, D. M. Skrzypiec, H. Seidel

baua:
Bundesanstalt für Arbeitsschutz
und Arbeitsmedizin

Research
Project F 2069

G. Huber
Ch. Mischke
D. M. Skrzypiec
H. Seidel
(eds.)

Dependence of spinal segment mechanics on age and posture

Dortmund/Berlin/Dresden 2010

This publication is the final report of the project ‘Strength and mechanical characteristics of motion segments of the lumbar spine during repetitive loads by compression and shear forces. In-vitro experiments and FE-simulations for different age groups and degrees of flexion’ – Project F 2069 – on behalf of the Federal Institute for Occupational Safety and Health.
The authors of this publication are responsible for the content of their individual contributions, indicated at the beginning of each part. The friendly and pertinent supervision of Dr. Barbara Hinz and the kind support of Birol Aydin, Arne Hothan, Harald Ittrich, Annelie Rehmer, Kay Sellenschloh, Matthias Vollmer, Nadine Wilke and Florian Witt is deeply appreciated.

Editors: Dr.-Ing. Gerd Huber
Dipl.-Ing. Christoph Mischke
Ph.D. Daniel M. Skrzypiec
Dr. med. Helmut Seidel

Authors: (alphabetised)
Dr. rer. nat. Barbara Hinz
Dr.-Ing. Gerd Huber
Dr. med. Anke Klein
B.Sc. Anna Matthaei
Dipl.-Ing. Christoph Mischke
Prof. Dr. Michael M. Morlock
Dipl.-Ing. Helge Paetzold
Dipl.-Ing. Berry Pöpplau
Prof. Dr. Klaus Püschel
Dr. med. Helmut Seidel
Ph.D. Daniel M. Skrzypiec
Dr. med. Felix Stahmer
Prof. Dr. Horst Peter Wölfel

Cover figure: Gerd Huber, TUHH, Hamburg University of Technology
Cover design: Rainer Klemm, Federal Institute for Occupational Safety and Health

Publisher: Federal Institute for Occupational Safety and Health
Friedrich-Henkel-Weg 1-25, 44149 Dortmund, Germany
Telephone: +49 231 9071-0
Telefax: +49 231 9071-2454
E-Mail: poststelle@baua.bund.de
Internet: www.baua.de

Berlin:
Nöldnerstr. 40-42, 10317 Berlin, Germany
Telephone: +49 30 51548-0
Telefax: +49 30 51548-4170

Dresden:
Proschhübelstr. 8, 01099 Dresden, Germany
Telephone: +49 351 5639-50
Telefax: +49 351 5639-5210

All rights reserved, including photomechanical reproduction and the reprinting of extracts.
For environmental reasons this publication was printed on non-chlorine bleached paper.

ISBN 978-3-88261-112-0

List of Contents

Dependence of spinal segment mechanics on age and posture

Abstract

Introduction: Whole-body vibration, commonly experienced in the workplace, may increase the prevalence of low back pain. Finite element (FE) models are supposed to point out the coherence between vibrations and damages, but they need to be improved and validated. The aim was to assess shear strength, dynamic shear and compressive stiffness, and compressive fatigue strength of human functional spinal units (FSUs) with relation to age, posture and individual characteristics. The findings were incorporated in an individualized FE model of FSUs. **Characterisation:** Specimens from age group 20-44 yrs (Young) and 48-64 yrs (Old) were characterised by anthropometric data of donors and by CT based parameters, such as endplate area (AREA) and bone mineral density (BMD). Potting of FSUs was done in 0° (Neutral) and 10° (Flexed) posture. **Shear strength:** L2-L3 FSUs were sheared anteriorly, while a physiological compressive load was applied. The testing groups were: Young-Neutral, Young-Flexed, Young-Creep (additional creep for 1 h) and Old-Neutral. Specimens in flexion tended to have higher failure strength. Specimens tested in neutral posture exhibited increased shear strength with increasing BMD. **Dynamic stiffness:** L4-L5 FSUs were exposed to loading varying in frequency (up to 12 Hz), offset loads and amplitudes. The directions were anterior-posterior shear and axial compression. The groups were Young-Neutral, Young-Flexed and Old-Neutral. The energy ratio and the linearised stiffness in the quasi-static compression tests was the highest for Young-Flexion. Shear pre-load decreased the axial stiffness. The shear quasi-static stiffness however increased with increasing axial compression preload. Axial and shear stiffness increased with increasing test frequency and axial stiffness decreased with increasing amplitude. **Modelling:** A partially individualised FE model of L4-L5 FSUs was created. It incorporates 23 individual geometric parameters derived from CT data. The annulus of the intervertebral disc was modelled as a ground substance with pre-stressed fibres and the nucleus as a viscoelastic liquid-filled cavity. The individualisation improved the modelling, but the behaviour shown in the experiments cannot be completely described yet. The results indicate that individual material parameters and individual descriptions of the facet joints should be taken into account as well. **Fatigue:** The three groups of L4-L5 FSUs were additionally loaded in compression for 300,000 sinusoidal cycles (5 Hz) to initiate fatigue failure. The fatigue strength of young donor's specimens was unexpectedly high. None of them failed in neutral posture. Four specimens from older donors with low BMD failed if exposed to high physiological loads; there was an exponential relationship between cycles to failure and the product of AREA and BMD. Only two of Young-Flexed failed. One had low BMD and was in line with the relationship derived for the specimens from older donors, whereas the second with normal BMD did not. Age and individual characteristics should be considered in the analysis of fatigue strength and thus of whole-body vibration injuries. **Conclusions:** Fundamental data that improve knowledge of spinal behaviour under various loading conditions were delivered. Individualisation of FE models is an important step to generate improved assessment and ultimately improve workplace safety.

Key words: lumbar spine, in vitro, shear, compression, FE-model, dynamic, fatigue

Mechanik der Wirbelsäulenbewegungssegmente in Abhängigkeit von Alter und Haltung

Kurzfassung

Einleitung: Die Prävalenz von Lendenwirbelsäulenbeschwerden kann durch Ganzkörper-Vibrationen, z.B. am Arbeitsplatz, erhöht werden. Finite-Elemente (FE) Modelle könnten bei der Analyse des Schädigungsmechanismus helfen, müssen jedoch verbessert und validiert werden. Ziel war es, die Schubfestigkeit, dynamische Schub- und Kompressionssteifigkeit und Ermüdungsfestigkeit von menschlichen Wirbelsäulenbewegungssegmenten (WBS), abhängig von Alter, Haltung und individuellen Eigenschaften, zu bestimmen. Diese Erkenntnisse flossen in individualisierte FE-Modelle der WBS ein. **Charakterisierung:** Präparate von Spendern im Alter von 20-44 Jahren (Jung) und 48-64 Jahren (Alt) wurden anhand anthropometrischer Daten und CT-Parametern wie Endplattenfläche (AREA) und Knochendichte (BMD) charakterisiert. Die Präparate wurden unter 0° (Neutral) oder 10° (Flexion) getestet. **Schubfestigkeit:** L2-L3 WBS wurden unter physiologischer Kompressionslast mit anteriorem Schub beaufschlagt. Untersucht wurde Jung-Neutral, Jung-Flexion, Jung-Creep (Kriechvorgang für 1 h) und Alt-Neutral. Unter Flexion tendierten die WBS zu höheren Versagenswerten; in neutraler Haltung zeigte sich mit größerer BMD eine höhere Schubfestigkeit. **Dynamische Steifigkeit:** L4-L5 WBS wurden frequenzabhängig (bis 12 Hz) getestet. Für Jung-Neutral, Jung-Flexion und Alt-Neutral wurden Offset und Amplituden für anterior-posterioren Schub und Kompression variiert. Der Anteil der absorbierten Energie und die linearisierte Steifigkeit waren bei quasistatischer Kompression für Jung-Flexion am höchsten. Schubvorlast reduzierte die Axialsteifigkeit. Kompressionsvorlast erhöht jedoch die quasistatische Schubsteifigkeit. Die Axial- und Schubsteifigkeit stieg mit steigender Frequenz; die Axialsteifigkeit verringerte sich mit steigender Amplitude. **Modellierung:** Ein FE-Modell eines L4-L5 WBS, dessen Geometrie anhand 23 Parameter angepasst werden kann, wurde erstellt. Der Annulus wurde als mit vorgespannten Fasern durchzogene Grundsubstanz modelliert, der Nukleus als viskoelastische Flüssigkeit. Die Individualisierung verbesserte die Simulation, jedoch konnte das experimentell bestimmte Verhalten nicht vollends wiedergegeben werden. Individuelle Materialparameter und individuelle Modellierung der Facettengelenke sollten zusätzlich berücksichtigt werden. **Ermüdung:** L4-L5 WBS wurden zusätzlich durch 300.000 Zyklen komprimiert (5 Hz). Die Ermüdungsfestigkeit bei jungen Spendern war unerwartet hoch, von Jung-Neutral versagte keines. Vier WBS aus Alt-Neutral mit niedriger BMD versagten. Ein exponentieller Zusammenhang zwischen Ermüdungsdauer und dem Produkt aus AREA und BMD wurde festgestellt. Aus Jung-Flexion versagten nur zwei Präparate. Eines davon wies eine geringe BMD auf; passend zu dem für Alt-Neutral ermittelten Zusammenhang. Alter und individuelle Parameter sollten bei der Analyse der Ermüdungsfestigkeit und damit bei durch Ganzkörper-Vibrationen induzierten Schädigungen berücksichtigt werden. **Schlussfolgerungen:** Grundlegende Daten über das Verhalten der Wirbelsäule unter verschiedenen Lasten wurden bestimmt. Individualisierbare FE-Modelle sind ein wichtiger Schritt hin zu besseren Beurteilungen. Dies kann schlussendlich zu höherer Arbeitsplatzsicherheit führen.

Schlüsselwörter: Lendenwirbelsäule, in vitro, Schub, Kompression, FE-Modell, dynamisch, Ermüdung

Part I Preface

Helmut Seidel

Detailed knowledge about the biomechanical behaviour and strength of lumbar functional spinal units is crucial for understanding the health risk associated with repetitive loads, such as those caused by whole-body vibration (WBV). The risk assessment according to current international guidelines (ISO 2631-1 1997; ISO 2631-5 2004) and regulations (Directive 2002/44/EC 2002) can be misleading, because their scientific basis is deficient (cf. Griffin, 1998, 2004; Seidel, 2005; Waters et al., 2007; VIBRISKS, 2006). According to the general framework: “On the relationship between whole-body vibration exposure and spinal health” (Seidel, 2005), a reliable risk assessment requires knowledge of (I) the transfer from measurable external loads or exposure to internal forces, (II) the strain caused by internal forces and (III) the tolerance of the structure to sustain the latter. Gaps in knowledge concern all three areas. Epidemiological studies indicate an increased health risk associated with WBV, but have failed to provide the data needed for a quantitative evaluation of WBV. Such an evaluation would entail e.g. determining a critical dose, evaluating high peak values, analysing the significance of posture and individual factors, and examining the frequency weighting and effects of WBV in the x- and y-axes (Seidel, 2005). Systematic research performed and/or initiated by the Federal Institute for Occupational Safety and Health in Germany and supported by the European Commission has addressed the above-mentioned information gaps. Finite element models of the whole body based on human anatomy (Hofmann et al., 2003; Pankoke et al., 2000, 2001; Wölfel, 2006) and validated by experimental data (Hinz et al., 2001; Seidel et al., 1986; Seidel et al., 1997) appear to be a promising way to predict the internal forces acting on the lumbar spine during WBV based on exposure conditions obtained in European countries (VIBRISKS, 2006) and other factors like posture and anthropometric characteristics (Hinz et al., 2008; Seidel et al., 2008b). An in vitro study (Huber et al., 2005) provided a comprehensive data set on the behaviour of functional spinal units under a variety of dynamic compression and shear loadings in a frequency range typical for WBV, i.e. up to 12 Hz. These data were used to elaborate and validate an FE model reflecting the force-induced strain on the functional lumbar spinal unit, i.e. a submodel that can be used to predict the local strain caused by internal forces. Those internal forces are calculated by a FE model of the whole body (Mischke et al., 2007). Fatigue failure of lumbar spinal units was examined in the same in vitro study (Huber et al., 2005), thus enabling the preliminary derivation of a method to predict fatigue failure due to repetitive compression (Seidel et al., 2008a). The fatigue strength of the specimens was surprisingly high; the authors attributed this finding to the young donor age.

Several arguments were considered in mapping out the aims for this study. Given the enormous significance of age-related changes in the lumbar spine with respect to the effects of repetitive loads and the continuously increasing age of the working population in Europe, it was felt that it was important to include older specimens in the study alongside those from younger donors. The fact that shear forces are not addressed in current guidelines and that the disputed factor of 1.4 for WBV in x- and y-axes is applied in the assessment of health risk, but not of comfort (Griffin, 1998;

ISO 2631-1 1997), prompted a more careful examination of the effects of shear forces. Considering the impact of drivers' sitting postures as well as the available resources, shear forces were restricted to the sagittal plane. Based on the results of the former study (Huber et al., 2005), the number of cycles to test compressive fatigue failure was increased and the cyclic load was limited to one high magnitude in order to better simulate real occupational exposure conditions. Tried and tested methods were employed to determine individual characteristics (anthropometric data, bone mineral density and endplate area) in spite of the significant expense. This decision was based on several factors. First of all, it was necessary to learn more about and quantify the real distribution of different biological effects resulting from the same exposure, as this will help to locate individual exposure-effect relationships within the health guidance caution zone (ISO 2631-1 1997). In addition, this information could lead to the possible revision of the currently questionable width of this zone as well as of comparable ranges between threshold and limit values. Second, it was aspired to accommodate the increasing demand for a more individualised assessment of health risk, which is essential for the foreseeable trend towards more personalised prevention and assessment of the causal exposure-effect relationships in individual cases of possible occupational diseases. Furthermore, in order to accelerate the implementation of obtained in vitro results, it was of particular importance that the finite element model was improved and elaborated by individualising the geometric parameters.

Consequently, the study aimed to examine ultimate strength under shear, high-cycle fatigue failure under compression, and stiffness under shear and/or compression. Two groups of human lumbar functional spinal units were obtained from young and old donors so as to investigate the influence of age. Two postures (neutral and flexion) were tested with frequencies of up to 12 Hz in order to reflect normal sitting posture as well as loads typical for occupational whole-body vibration. A further aim was to improve the individualised finite element model and validate it with the experimental data obtained in this study.

The structure of the report reflects its interdisciplinary nature. A brief description may help the reader to navigate through the vast amount of results. As a starting point and reference for all subsequent parts, the first part describes the specimens and the methods used to examine and classify them; this chapter is supplemented by several appendices that document further methodological details. The next chapter presents new essential data about mechanical behaviour under shear loads, followed by an exciting chapter on the dynamic experiments, i.e. various combinations of quasi-static ramp loadings and many different cyclic loadings of up to 12 Hz. Both parts compare the effects of different ages and flexion angles. The part on modelling refers to the results outlined in the preceding chapters and demonstrates the progress made in comparison with the old submodel. The last part describes and compares fatigue experiments with two kinds of specimens (old and young) and two postures (neutral and flexion; young specimens only).

This report illustrates the essential progress made after the first studies published in 2003 and 2005 by Hofmann et al. and Huber et al., respectively. Scientific progress depends on critical discussions of research. The authors therefore welcome and value all comments and suggestions.

Part II Characterisation of Specimens

Gerd Huber, Daniel M. Skrzypiec, Anna Matthaei,
Berry Pöpplau, Klaus Püschel, Michael M. Morlock

1 Introduction

Lumbar spinal specimens were harvested from human male donors. The objective was to obtain specimens from two different age ranges within the working age. The intended age ranges were between 20 and 40 years and around 50 to 60 years. Harvesting was done by the Department of Legal Medicine (University Medical Centre Hamburg-Eppendorf, Germany).

After explantation, the specimens were kept frozen until testing. CT scans were acquired in order to determine spinal characteristics and to eliminate specimens with pathologic deformities. The original data source was delivered by computer tomography (CT) provided by the Diagnostic and Interventional Radiology Department and Clinic (University Medical Centre Hamburg-Eppendorf, Germany). Due to organisational reasons, two different spiral CT scanners had to be used (LWS 1101 to LWS 1108: spiral CT S5VA40A, Siemens, Munich, Germany / LWS 1109 to LWS 1136: Mx8000 IDT 16, Philips Healthcare, DA Best, The Netherlands). For further processing, the CT scans were exported into DICOM format. Endplate area (AREA) and bone mineral density (BMD) were of major interest.

2 Anthropometrical Data

Prior to explantation, several anthropometrical data were measured. The chosen anthropometrical data were the same as those used in the preceding project (F1899, Huber et al., 2005), i.e. age, body height, body weight, acromial height, elbow height, ankle diameter, knee joint diameter, elbow joint diameter and wrist joint diameter (Table II-1, Figure II-1).

Table II-1 Listing of the desired anthropometrical data of the donors

Denotation	Abbreviation	Measurement device
body weight	m_B	scales
body height	h_B	tape measure
acromial height	h_{AC}	tape measure
elbow height	h_{EB}	tape measure
ankle diameter	d_{AN}	anthropometer
knee joint diameter	d_{KN}	anthropometer
elbow joint diameter	d_{EB}	anthropometer
wrist joint diameter	d_{WR}	anthropometer

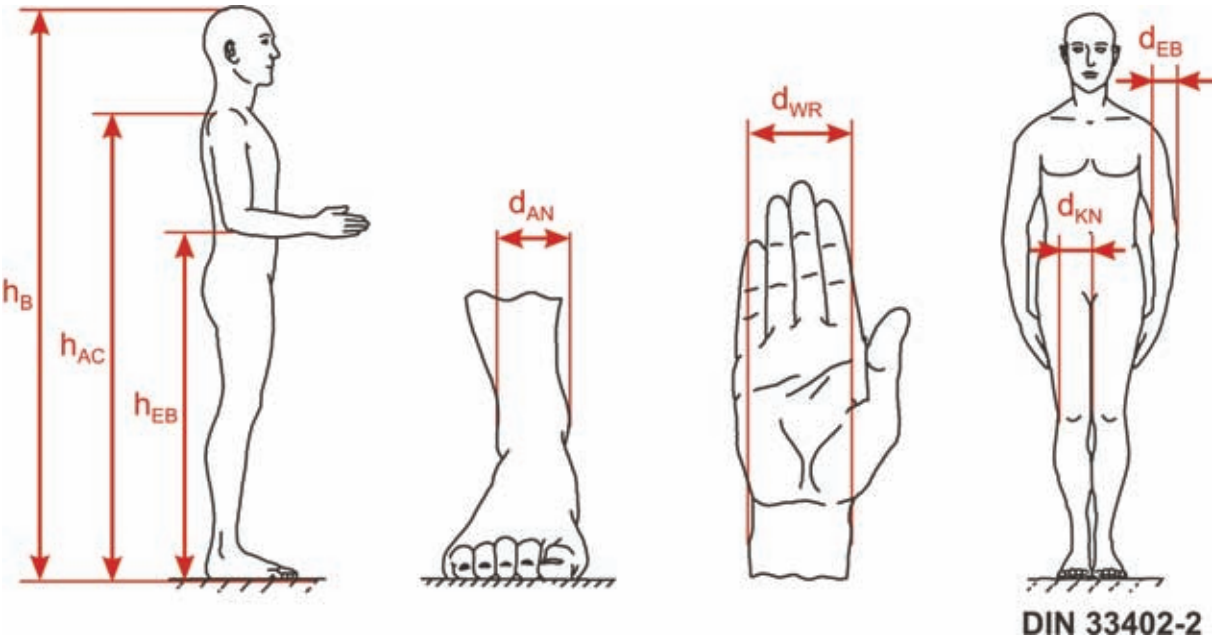

Figure II-1 Diagram of the geometric anthropometrical data (adapted from DIN 33402-2)

After explantation, the specimens were wrapped in saline-soaked gauze, double sealed in plastic bags and kept frozen (<-20°C) until the day of testing. This state-of-the-art storage method has been shown to neither significantly alter the creep behaviour (Dhillon et al., 2001) nor the stiffness (Gleizes et al., 1998) of human spinal specimens.

For the experiments, at least two sets of 18 functional spinal units were needed. However, more specimens were harvested for several reasons. First, it is occasionally necessary to exclude specimens due to damages that are visible only

after computer tomography images have been made. Second, additional specimens were needed to perform pilot measurements with the modified test rig. Furthermore, supplemental tests with L2-L3 were performed during this project (32 shear instead of 18 creep experiments). Figure II-2 gives an overview of the major anthropometrical data of the specimens used.

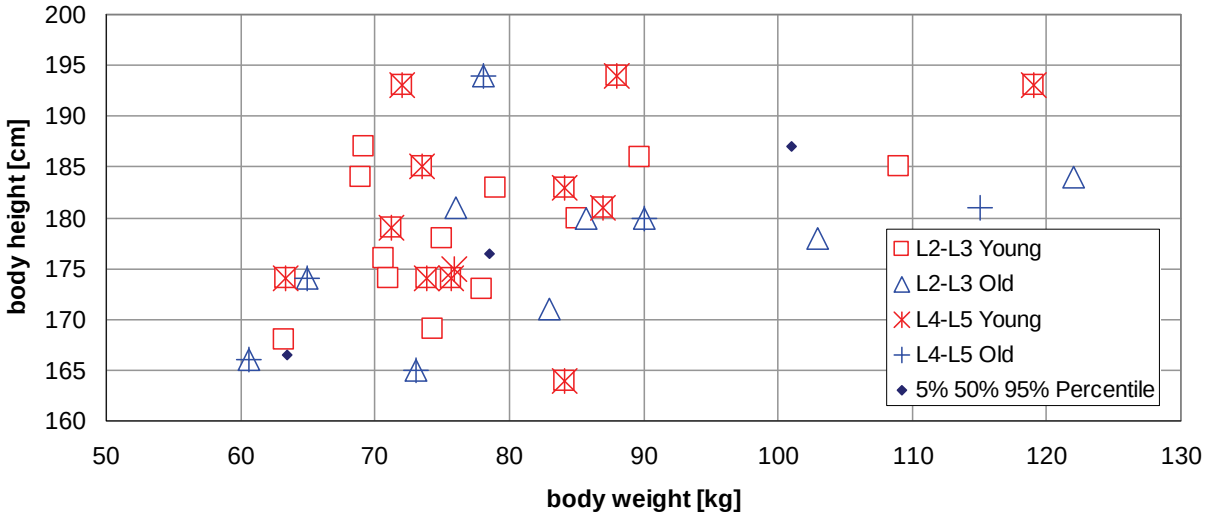

Figure II-2 Donor body weight and height for the 51 functional spinal units in comparison to the 5 %, 50 % and 95 % percentile of 26 to 40 year old men (Draft DIN 33204-2 or FB 1023, respectively)

In Table II-2 all of the harvested specimens and their available anthropometrical data are listed. The majority had been harvested recently (LWS 1101 to LWS 1136). The last eight specimens listed were from the F1899 project (0003, 0004, 0011, 0012, 0028, 0033, 0036, 0052). Those spines were only used in the L2-L3 shear experiments to enlarge the available database. Even though these spines had been stored for a rather long time, no differences were observed between the results derived from those specimens and the recently harvested ones.

Table II-2 Anthropometric data of all specimens harvested and used in this study

LWS	Days till exp.	Age [yrs]	m_B [kg]	h_B [cm]	h_{AC} [cm]	h_{EB} [cm]	d_{AN} [cm]	d_{KN} [cm]	d_{EB} [cm]	d_{WR} [cm]
1101	4	56	65.0	174	154	122	6.8	9.5	7.2	5.2
1102	2	37	99.4	178	151	124	7.5	9.9	7.9	6.1
1103	5	57	82.0	174	152	121	8.0	9.9	7.0	6.5
1104	5	48	78.1	194	170	142	7.5	11.0	8.5	6.5
1105	7	58	62.0	165	144	116	7.0	10.0	8.2	6.7
1106	1	23	84.1	164	144	118	7.1	10.5	7.5	6.2
1107	3	36	75.7	174	147	117	7.0	10.4	8.5	6.0
1108	3	50	115.0	181	155	132	6.7	11.9	9.0	6.4
1109	3	64	83.0	171	145	116	6.9	10.0	7.8	5.8
1110	1	52	90.0	180	156	125	7.2	10.3	7.8	6.2
1111	2	58	71.6	173	149	120	6.9	9.9	6.8	6.0

1112	1	20	63.3	174	147	115	6.5	9.5	7.3	5.5
1113	2	21	75.9	175	150	122	7.0	10.1	7.3	5.5
1114	2	50	91.3	189	164	135	7.1	10.5	7.5	6.0
1115	2	58	128.8	183	152	128	7.3	11.4	8.6	5.5
1116	4	28	79.0	183	143	118	7.0	10.3	8.5	5.5
1117	10	48	101.0	181	149	124	7.3	11.5	9.6	6.2
1118	3	38	66.0	184	153	131	6.6	9.0	8.0	5.7
1119	2	39	73.5	185	143	122	6.5	11.0	8.3	5.4
1120	3	41	84.1	183	148	125	6.8	10.1	9.5	5.8
1121	0	50	85.7	180	145	120	6.9	11.5	9.2	5.3
1122	2	48	122.0	184	147	123	7.2	11.3	10.9	6.0
1123	3	35	119.0	193	156	131	8.5	12.8	9.8	6.9
1124	2	34	71.2	179	140	118	7.5	11.3	8.7	5.9
1125	0	27	87.0	181	143	120	6.9	11.8	9.0	6.0
1126	1	21	72.0	193	150	126	7.8	10.4	7.6	5.6
1127	4	36	92.0	187	156	133	7.2	12.2	9.3	6.5
1128	1	60	103.0	178	137	114	8.0	13.4	11.0	7.8
1129	6	43	70.0	183	141	119	6.3	7.0	8.5	6.3
1130	3	50	76.0	181	137	113	7.1	11.8	9.2	6.5
1131	4	56	73.0	165	127	107	7.0	11.7	9.3	6.7
1132	4	22	63.2	168	134	112	5.9	10.3	8.7	6.1
1133	2	38	88.0	194	151	126	7.2	12.5	9.5	6.5
1134	2	44	70.6	176	139	115	7.3	11.2	9.3	7.0
1135	5	22	73.8	174	135	114	6.7	12.0	9.2	6.2
1136	2	59	60.6	166	127	108	6.0	9.5	9.3	6.1
0003 [1)]	2	37	85.0	180	156	123	6.5	11.0	9.5	5.5
0004 [1)]	3	34	89.7	186	162	128	7.7	10.6	8.2	6.2
0011 [1)]	6	31	69.2	187	149	115	5.7	8.4	7.9	5.8
0012 [1)]	1	42	75.0	178	155	122	5.9	8.8	7.4	6.0
0028 [1)]	6	32	69.0	184	161	120	6.8	9.4	7.6	5.3
0033 [1)]	2	21	109.0	185	159	127	6.9	11.7	9.4	5.8
0036 [1)]	1	30	78.0	173	147	117	6.8	11.2	9.2	6.3
0052 [1)]	≤3	27	71.0	174	155	125	6.4	12.3	9.2	5.9

[1)] Specimens harvested during the project F1899 (Huber et al., 2005)

3 Specimen Preparations

On the day of testing, spinal muscles were removed. The spine was dissected into two FSUs (L2-L3 and L4-L5). Each FSU consisted of two vertebrae and an intervertebral disc. Care was taken to keep the ligaments and disc intact. The FSUs were potted in metal holders using a two-component polymer (Ureol, Vantico, Switzerland). Generally, L2-L3 specimens were used for the shear experiments and L4-L5 specimens were used for the fatigue tests.

For the groups with specimens denoted as ‘Neutral’, the mid-plane of the segment’s disc was mounted parallel to the flange of the test machine. This was achieved by potting and transporting the specimens in a holder that guaranteed parallel alignment of the potting cups (details can be found elsewhere: F1899, Huber et al., 2005). For the flexed groups, both holders were angled 5° in extension during potting (Figure II-3), resulting in 10° flexion when mounted in the hydraulic test machine. The flexion angle was chosen based on Andersson et al. (1979), who found that when posture is changed from a standing position to unsupported sitting at the L4-L5 level, the angle changes by approximately 10° in flexion.

Figure II-3 Holder for potting and transporting the FSUs tested in flexed position

4 Endplate Area

For spinal research, the endplate area is a basic skeletal measure value. It enables individualisation of experimental loads. Based on the assumption that larger structures are able to withstand greater loads, forces are normalised with the help of the corresponding endplate area, resulting in stress values.

To calculate the endplate areas, computer tomography (CT) data records of the spinal specimens were imported to 3D visualisation software (Amira 3.0, Mercury Computer Systems, Inc., Merignac, France). Three-dimensional models of the bony structure were created from the CT data, whereby the soft tissue was separated from the bone by threshold segmentation.

Cutting planes were chosen manually to cut the vertebral body at the height of the endplates. This was done on the inferior and superior sides of the vertebra. The cutting plane was oriented with respect to the vertebral body so as to obtain a close contour with no other parts of the vertebra (like the dorsal process or pedicles) connected to it (Figure II-4).

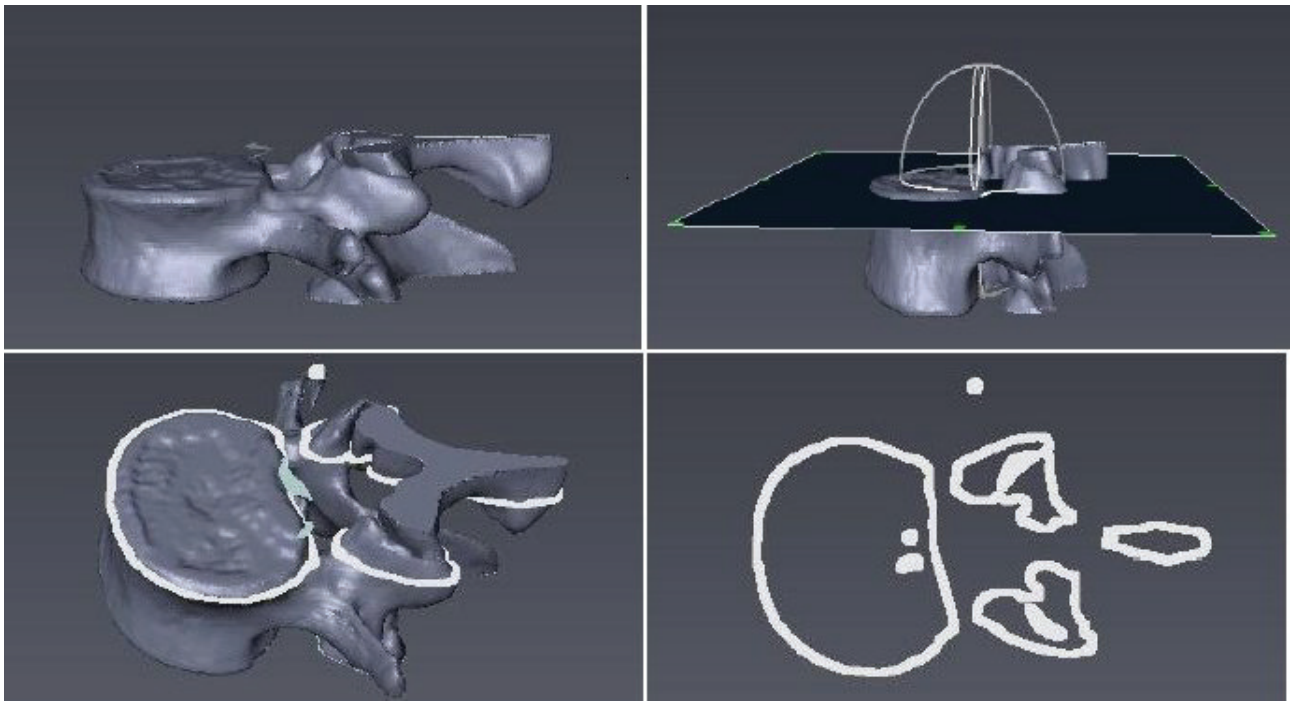

Figure II-4 Steps to determine the contour of the endplate (Matthaei, 2008)

Further data processing was done using a numerical program (Matlab, MathWorks Inc., Natick, MA, USA). In general, these planes, and consequently the derived linesets of the intersection between the spinal structure and cutting plane, are not planar with respect to the orientation of the CT planes. However, the methods that are used to calculate the endplate areas account for two spatial directions only. Therefore, the coordinates of the linesets were transformed so that the area of interest was embedded within the plane of the two direction vectors.

In a recent study (Seidel et al., 2008) a linear approximation was used to transform the three spatial coordinates in order to obtain a two-dimensional description of the endplate area. The original scaling was retained and the point of origin was defined within the cutting plane. Since this method leads to variations at large angles between cutting planes and CT planes, it was generalised using the following method (Matthaei et al., 2008).

According to this method, the 3D CT coordinates of each point within the plane of the endplates are simply multiplied with a rotation matrix consisting of any normalised coordinate system that is adjusted to the plane, i.e. with the vectors of two coordinates parallel to the plane of the endplates. To express the rotation of the CT system with respect to the 2D system, the rotation matrix:

$$R = \left[\vec{x}_s \quad \vec{y}_s \quad \vec{z}_s\right] \tag{II-1}$$

is determined based on the endplate planes in the original coordinate system described by:

$$z = a \cdot x + b \cdot y + c \quad . \tag{II-2}$$

With this linear equation, the Hesse normal form can be obtained. The normal vector

$$\vec{n_0} = \begin{pmatrix} a \\ b \\ -1 \end{pmatrix} \cdot \frac{1}{\sqrt{a^2 + b^2 + 1}} \tag{II-3}$$

is used as $\vec{z}_S$ of the rotation matrix. Any vector whose cross product with $\vec{z}_S$ equals zero is perpendicular to the normal vector and represents $\vec{x}_S$ for the rotation. Another cross product of $\vec{z}_S$ and $\vec{x}_S$ results in the third spatial vector, $\vec{y}_S$. The rotation matrix is thus complete. In order to obtain the needed coefficients from the data points of the linesets, the matrix notation for multiple measuring data is used:

$$\begin{pmatrix} z_1 \\ z_2 \\ \dots \\ z_n \end{pmatrix} = a \cdot \begin{pmatrix} x_1 \\ x_2 \\ \dots \\ x_n \end{pmatrix} + b \cdot \begin{pmatrix} y_1 \\ y_2 \\ \dots \\ y_n \end{pmatrix} + c \quad . \tag{II-4}$$

This is equal to:

$$\vec{z} = \left[\vec{x} \quad \vec{y} \quad \vec{1}\right] \cdot \begin{bmatrix} a \\ b \\ c \end{bmatrix} \quad . \tag{II-5}$$

In this notation $\vec{1}$ describes an n-dimensional vector containing only elements with a value of 1 having the same length as $\vec{x}$ or $\vec{y}$, respectively. Using the abbreviation:

$$\overrightarrow{COEF} = \begin{bmatrix} a \\ b \\ c \end{bmatrix} \tag{II-6}$$

leads to:

$$\vec{z} = \begin{bmatrix} \vec{x} & \vec{y} & \vec{1} \end{bmatrix} \cdot \overrightarrow{COEF} \tag{II-7}$$

or:

$$\vec{z}^{\,T} = \overrightarrow{COEF}^{\,T} \cdot \begin{bmatrix} \vec{x} & \vec{y} & \vec{1} \end{bmatrix}^T \quad , \tag{II-8}$$

respectively. With the help of the pseudo inverse function, a least square fit is finished:

$$\overrightarrow{COEF}^{\,T} = \vec{z}^{\,T} \cdot \mathrm{pinv}\left(\begin{bmatrix} \vec{x} & \vec{y} & \vec{1} \end{bmatrix}^T \right) \quad . \tag{II-9}$$

This gives us:

$$\overrightarrow{COEF} = \mathrm{pinv}\left(\begin{bmatrix} \vec{x} & \vec{y} & \vec{1} \end{bmatrix}^T \right)^T \cdot \vec{z} \quad . \tag{II-10}$$

This generalised method has been verified. Details can be found elsewhere (Matthaei et al., 2008). The cutting plane also went through the posterior elements. This part of the linesets was removed manually.

The area enclosed by the remaining contours of the endplates was determined by the hullfit function afterwards. This was done using a public domain function (hullfit.m, Matlab function by Peter Wasmeier, p.wasmeier@bv.tum.de). The function places a polygon consisting of piecewise linear sections around the selected region and minimises the enclosed area with the help of an additional factor. This factor defines the ratio between the longest and shortest track section. Without this special minimisation factor, it would not have been possible to account for the concave side of the kidney-shaped cross-sectional area of the endplates. A convergence analysis was performed due to the fact that smaller minimisation factors lead to higher accuracy but to increased computing time as well. For three linesets (LWS 1101_4i, LWS 1101_4s and LWS 1101_5i), the endplate area was calculated with different factors (0; 1; 0.75; 0.5; 0.3; 0.2; 0.1; 0.08; 0.05). Figure II-5 shows that the results converge at a value of 0.2 or smaller and the varieties are below 0.1%. For further calculations of the endplate areas, a factor of 0.1 was used, which coped both with demands for accuracy and reasonable computing time.

Following the described method, the areas were partly determined by two independent persons (the superior and inferior endplates of L2 for the specimens LWS 1109 to LWS 1123, those of L3 for all specimens and those of L4 and L5 for the

specimens LWS 1101 to LWS 1123). This was done in order to analyse the variability between different investigators.

The method used to determine the endplate area appears to have been reliable. The calculated endplate areas of the first investigator mostly agreed with those of the second investigator. The slope of the regression for the endplate areas of L4 and L5 was 0.99. As a measure for the repeatability of the method, the statistical parameters of the regression can additionally be taken into account. The comparison of the endplate areas received from the two investigators yielded $R^2_{adjusted} = 0.78$ for the corrected coefficient of determination and the significance $p < 0.001$ (Figure II-6).

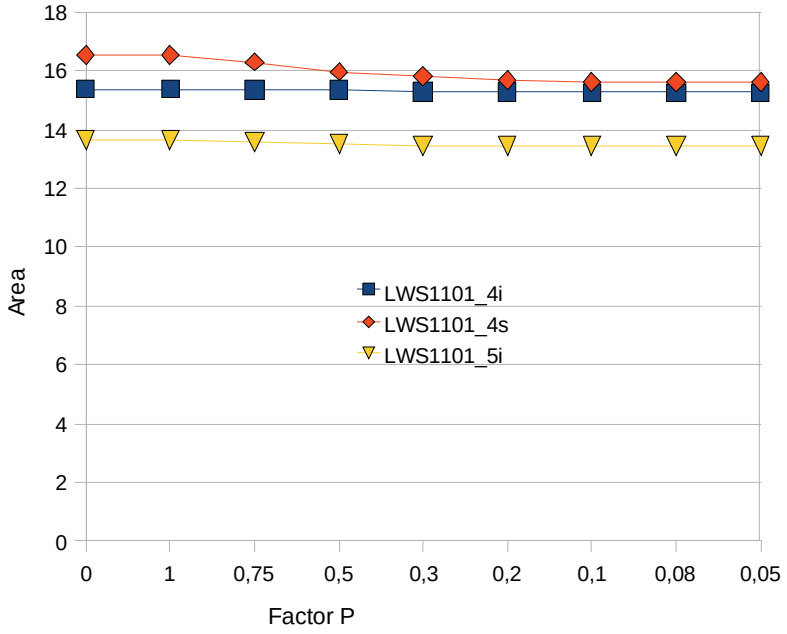

Figure II-5 Convergence analysis of the minimisation factor for the 'hullfit' function

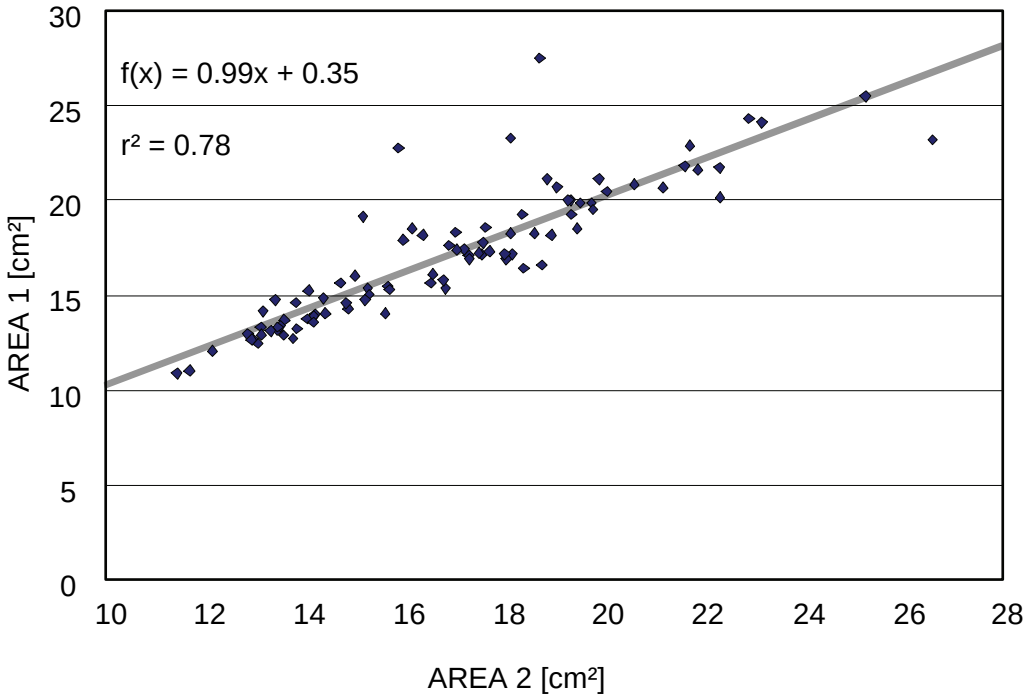

Figure II-6 Linear regression between endplate areas of L4 and L5 as measured by two different investigators

Specimens with distinct deviations between the old and the new values were reviewed. In all cases the deviations could be put down to two reasons. Either the cutting plane was placed such that pedicles and dorsal processes formed a connected area with the endplate (Figure II-7), or contours were not closed and had inclusions within the contour (Figure II-8).

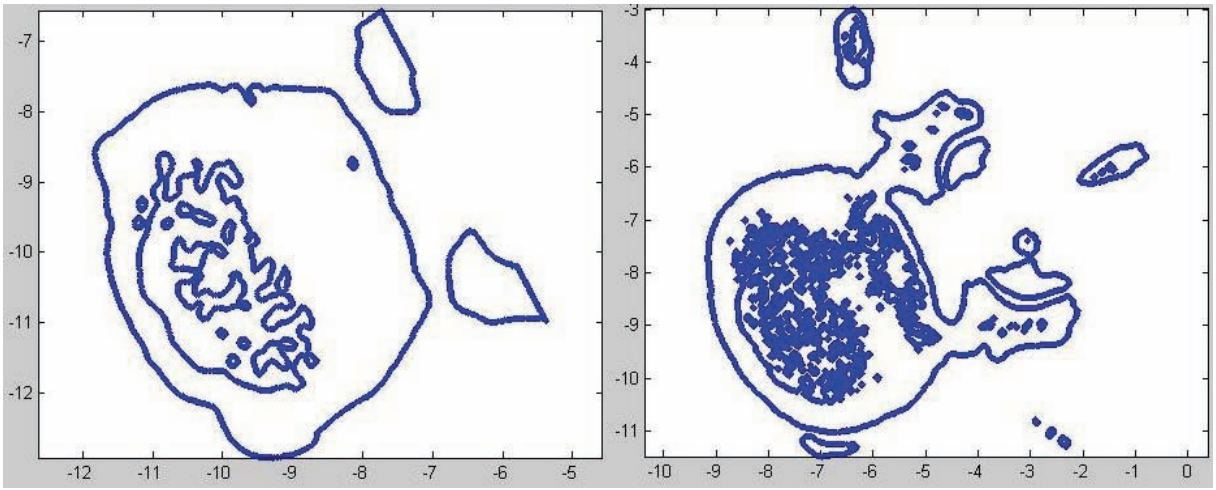

Figure II-7 Comparison of the same endplate (LWS 1117_L5_s) marked by different investigators. The contour at the right did not fulfil the instructions. The cutting plane crossed the pedicle.

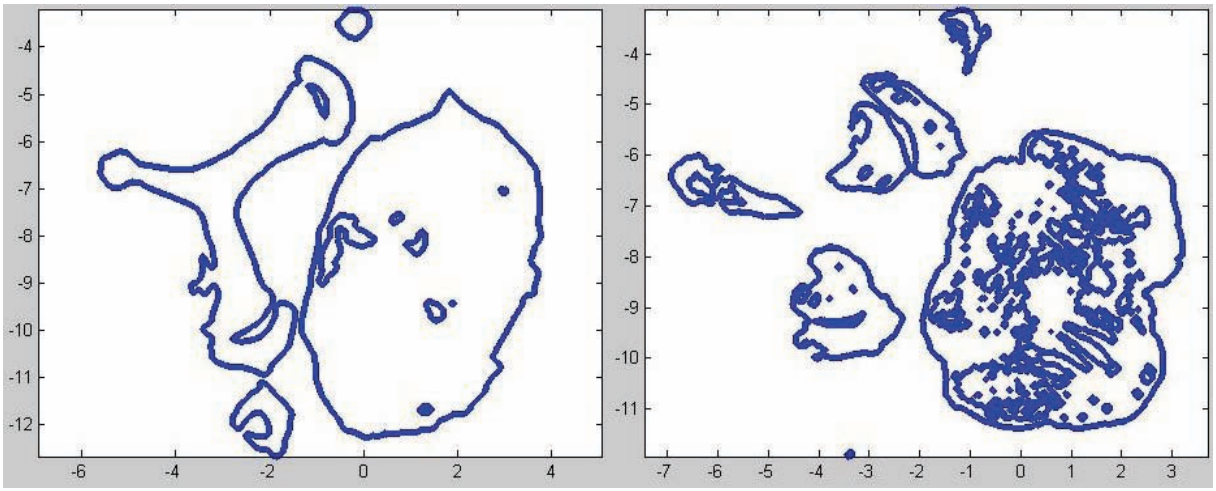

Figure II-8 Comparison of the same endplate (LWS 1110_L5_s) marked by different investigators. The contour at the right did not fulfil the instructions. The cutting plane did not cross the largest area of the endplate.

In Table II-3 the areas of the superior and inferior endplates of the vertebrae L2 to L5 are given. The given values already account for differences between the two investigators' measurements. Values with large discrepancies were repeatedly analysed and controlled.

Table II-3 Area of L2, L3, L4 and L5 endplates (* endplate areas determined by only one investigator)

LWS	L2		L3		L4		L5	
	Superior [cm²]	Inferior [cm²]	Superior [cm²]	Inferior [cm²]	Superior [cm²]	Inferior [cm²]	Superior [cm²]	Inferior [cm²]
1101	15.23*	15.08*	15.22	14.87	15.62	15.35	14.88	13.46
1102	11.57*	16.74*	15.92	17.00	16.53	17.10	16.57	15.01
1103	19.12*	25.97*	23.87	24.63	25.26	19.86	19.47	18.95
1104	16.49*	17.45*	16.67	17.41	17.63	18.53	15.88	15.98
1105	13.40*	12.25*	13.90	13.16	14.08	13.69	14.05	17.03
1106	11.95*	12.30*	12.82	12.67	13.07	13.32	12.86	12.95
1107	13.73*	15.00*	14.85	15.05	14.72	14.84	13.41	13.17
1108	10.26*	15.99*	16.16	15.80	18.05	16.92	18.17	16.90
1109	12.70	13.12	13.76	14.12	14.21	12.90	12.94	11.69
1110	19.75	22.20	20.83	22.27	21.90	21.72	26.60	18.72
1111	14.78	15.46	15.79	16.56	17.71	17.42	18.01	15.67
1112	23.39	14.52	14.56	14.41	15.30	13.39	13.85	11.43
1113	12.79	13.52	13.17	13.64	13.14	13.31	13.31	12.15
1114	19.24	19.94	22.54	24.96	24.63	20.02	19.29	13.83
1115	18.48	25.06	22.09	20.44	22.33	20.48	16.38	21.73
1116	13.55	10.29	14.29	14.93	14.42	14.76	15.18	14.83
1117	17.04	17.92	18.25	18.65	19.06	18.26	18.14	16.83
1118	19.47	18.67	19.83	19.10	18.87	17.77	17.56	16.78
1119	12.05	12.81	13.41	13.23	13.77	13.89	14.17	18.37
1120	16.01	16.94	17.24	18.45	19.35	17.23	18.76	15.71
1121	17.95	18.71	19.91	19.65	21.19	19.87	21.63	
1122	22.23	18.65	19.01	19.38	19.79	20.86	19.91	17.05
1123	21.03	19.61	19.94	19.82	18.62	24.16	22.91	18.40
1124	15.61*	15.58*	15.95	16.42	16.21*	15.60*	14.93*	15.96*
1125	14.98*	15.33*	16.01	17.50	18.07*	17.86*	18.23*	16.69*
1126	17.09*	18.35*	19.01	19.20	19.50*	18.79*	19.07*	16.62*
1127	16.16*	17.04*	17.48	18.85	19.03*	20.36*	20.30*	18.38*
1128	13.60*	14.60*	14.96	18.04	19.37*	17.02*	15.86*	
1129	16.47*	16.71*	17.36	17.02	18.17*	16.96*	17.56*	14.72*
1130	17.16*	17.23*	17.60	17.96	17.33*	17.44*	18.00*	17.79*
1131	18.62*	16.14*	15.33	16.48	16.82*	17.78*	17.09*	14.40*
1132	10.96*	10.77*	11.19	11.36	11.70*	11.84*	12.03*	11.93*
1133	19.61*	21.22*	21.54	18.81	18.82*	18.26*	17.79*	17.10*
1134	16.65*	17.91*	18.25	18.11	18.61*	17.95*	18.29*	
1135	12.98*	13.98*	14.15	14.64	14.77*	13.47*	14.69*	15.67*
1136	16.21*	15.52*	16.36	15.37	16.51*	14.85*	16.78*	14.34*

5 Bone Mineral Density

The bone mineral density (BMD) of vertebrae probably influences their mechanical strength and thus the strength of the complete spinal structure. Hence, for all specimens harvested in this study, the BMD of the central part of each vertebra was determined based on the Hounsfield Units (HU) of the CT scans. BMD was expressed as the concentration of dipotassium phosphate in distilled water (mg K_2HPO_4 per ml).

To determine the bone mineral density of the bony structure inside the vertebrae, a 3D reconstruction program (Amira 3.0, Avizio 5.0, Mercury Computer Systems, Merignac, France) was used. DICOM files were imported directly. Because spongious bone is not a homogeneous structure and CT data are rather noisy, BMD values were mostly analysed within a defined volume (Figure II-9, Figure II-10).

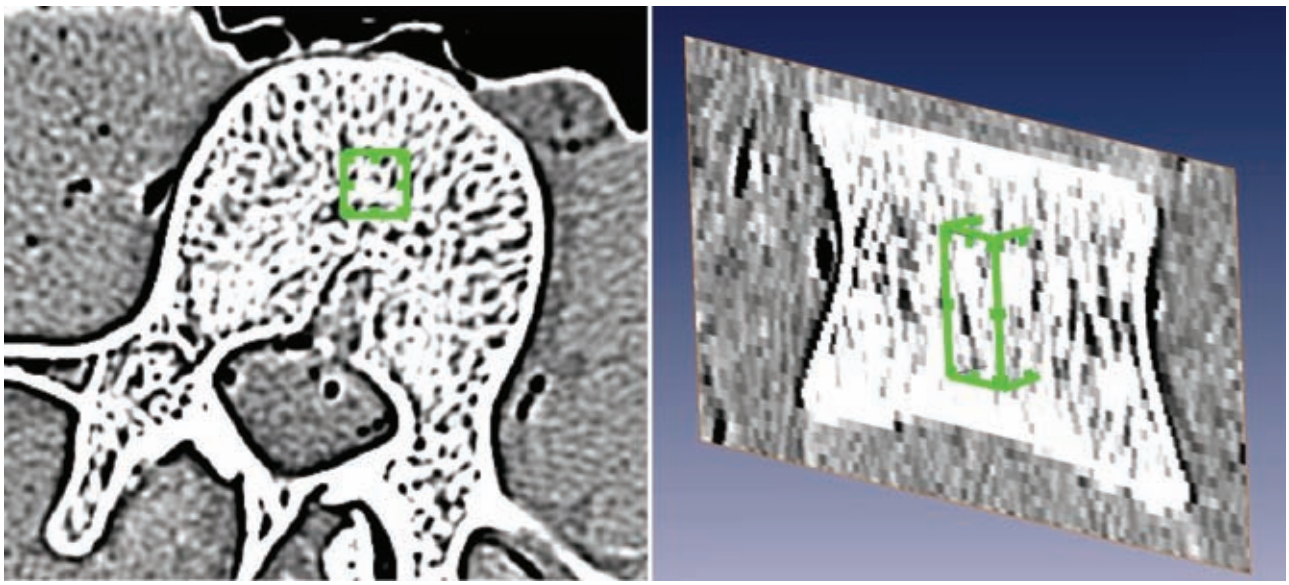

Figure II-9 Location of the bounding box within two views of a vertebra

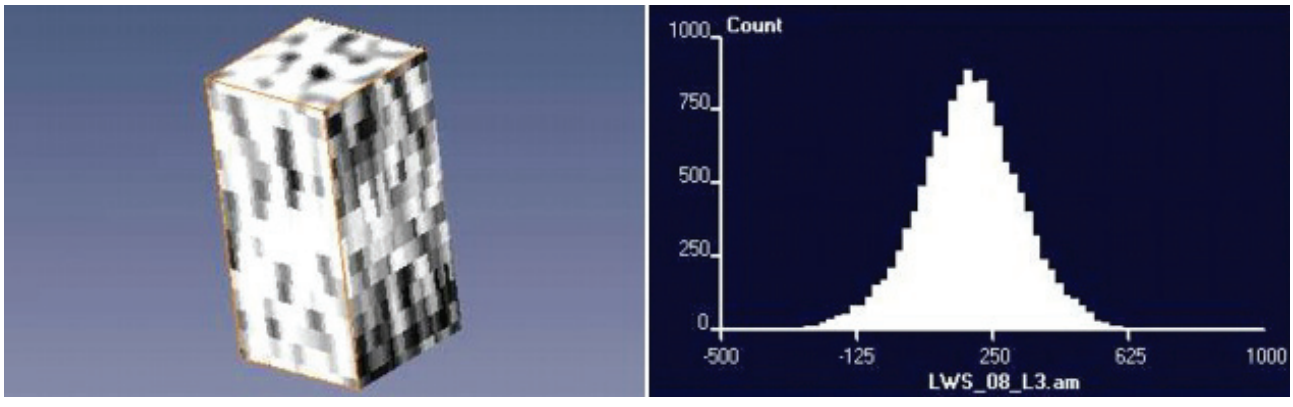

Figure II-10 Extracted bounding box and corresponding histogram of the voxels' HU values

The measurement volume in this study was a bounding box of 30x30x15 voxels, manually placed in the centre of the analysed vertebral body. In cases where the

geometry of the vertebral body did not allow use of the standard size (e.g. if the vertebral bodies were too flat or had bony deformations), a smaller size was substituted to avoid inclusion of cortical bone and endplates (e.g. LWS 1103, L2: 30x30x10 voxels). Since the measured values might be influenced by the investigator's choice of bounding box positioning and orientation, the measurements were performed by two individuals to evaluate the variability between different investigators. The derived values are given at the end of this section (Table II-4, Table II-5, Table II-6, Table II-7).

However, even though the HU scale appears to be rather objective, two problems are associated with it. First of all, this scale can hardly be transformed to material or mechanical properties like mineral content, ash weight or mechanical strength. Second, this scale appears to be different for different types of CT scanners. Therefore, the HU values were converted into the equivalent of BMD using a custom-made dipotassium phosphate (K_2HPO_4) phantom. Dipotassium phosphate is a secondary ortho-phosphate that is mainly used for the composition of buffer solutions. Since human bone also contains phosphate (calcium phosphate), the absorption of X-rays due to K_2HPO_4 is similar to that of the mineral fractions of the bone. However, in contrast to the description of the bone mineral density in HU, the description in equivalents of dipotassium phosphate is independent of the type and the setting of the CT scanner used and therefore allows better comparability – as long as the conversion formula is known.

K_2HPO_4 phantoms were used to estimate a linear conversion formula between the HU and K_2HPO_4 equivalents. A phantom made of three vials with different concentrations of K_2HPO_4 was made. One vial was filled with distilled water and the others contained 100 mg K_2HPO_4 per ml and 500 mg K_2HPO_4 per ml, respectively. The phantom was scanned in both scanners (Siemens: 140 kV, 200 mAs, Kernel B70s and Philips: 140 kV, 200 mAs, Kernel D). The HU were measured in three perpendicular cutting planes and the mean value of the three measurements was calculated to account for deviations within the scanners (Figure II-11).

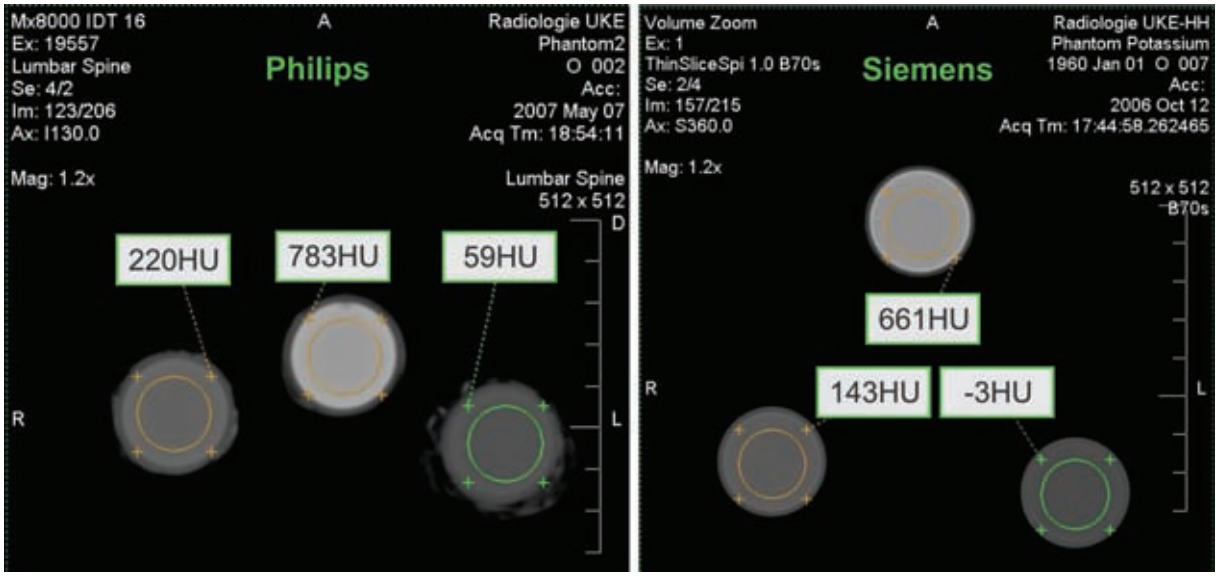

Figure II-11 CT slice from the same phantom recorded in different CT scanners

The phantom showed a high linearity between the concentration of K_2HPO_4 and measured HU; however, there were differences between the two scanners (Figure II-12 and also with respect to data in the literature (Brinckmann et al., 1998). Hence, different conversion parameters were needed to allow a comparison between the measured data.

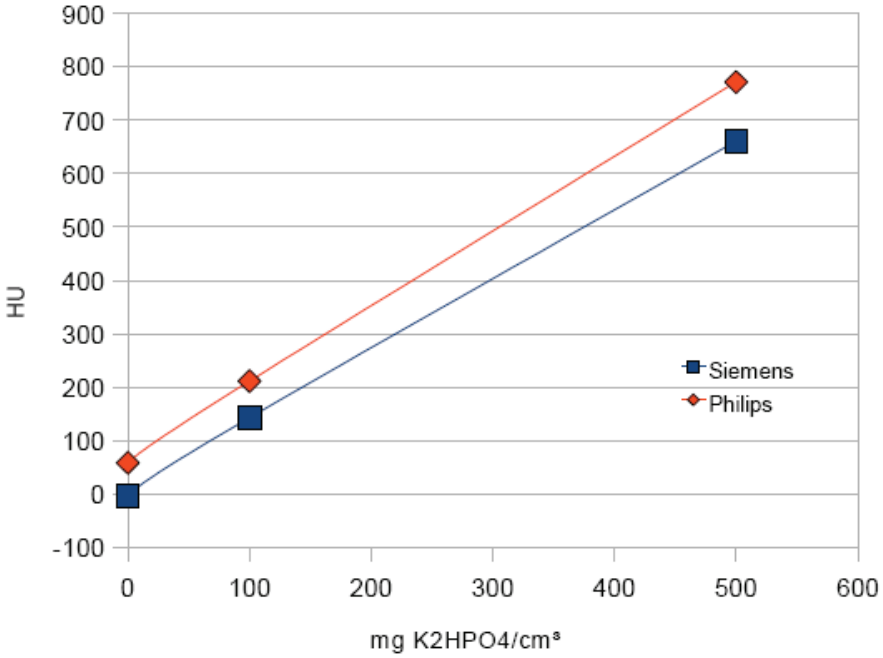

Figure II-12 Relation between concentration of K_2HPO_4 and HU for both CT scanners

Regarding the measured HU as a function of the concentration of K_2HPO_4, the resulting curve does not cross the origin for the Philips scanner. The reason for this effect is the influence of the water in the phantom, which normally does not contribute to the attenuation ($HU_{Water} = 0$) but changes the volumetric fraction of the K_2HPO_4 (20% in 500 mg K_2HPO_4 per ml, 4% in 100 mg K_2HPO_4 per ml). Since only the linearity between pure K_2HPO_4 and measured HU should be taken into account, the influence of the water has to be eliminated from the equation

$$HU = \nu_K \cdot HU_K + \nu_W \cdot HU_W \quad , \tag{II-11}$$

where ν_K is the volume fraction of K_2HPO_4, ν_W the volume fraction of water, HU_K the attenuation of K_2HPO_4 and HU_W the attenuation of water. ν_K and ν_W are known values. By means of the measured Hounsfield Units (for Philips: 771 HU for 500 mg K_2HPO_4/ml, 212 HU for 100 mg K_2HPO_4/ml and 59 HU for water) HU_K can be calculated with the equation

$$HU_K = \frac{1}{\nu_K} \cdot HU - \frac{\nu_W}{\nu_K} \cdot HU_W \tag{II-12}$$

(for Philips this was 3536 HU, as calculated for 500 mg K_2HPO_4/ml concentration). Now corrected values for the three calibration points can be calculated using the equation

$$HU_{corrected} = \nu_K \cdot HU_K \quad . \tag{II-13}$$

The resulting corrected line crosses the origin (Figure II-13) and allows the correct conversion into Hounsfield Units for every concentration of K_2HPO_4.

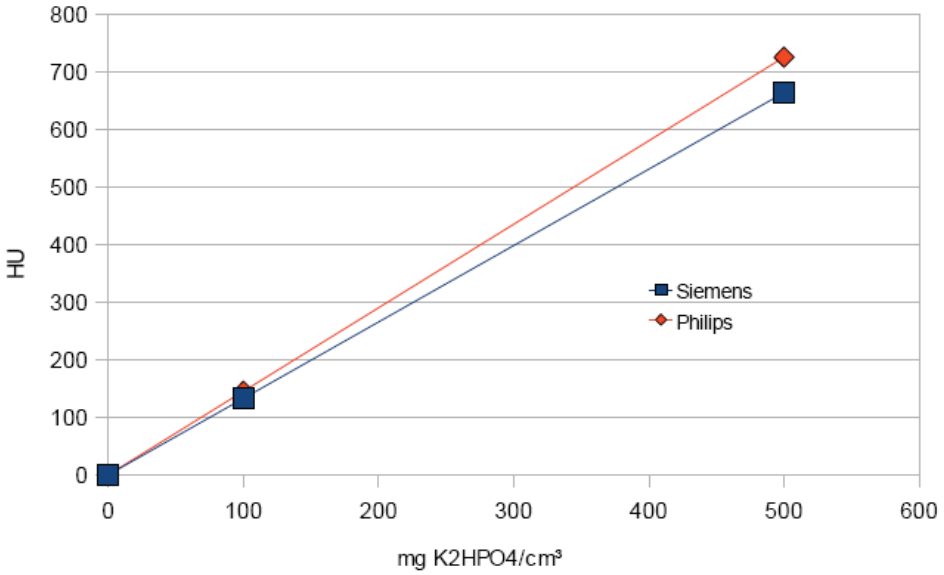

Figure II-13 Relation between HU and concentration of K_2HPO_4 for the Philips and Siemens scanners (corrected)

In this study, the inverse relation is needed. Measured HU has to be expressed as the equivalent of K_2HPO_4. For the first scanner (Siemens), this is:

$$[BMD_{K_2HPO_4}] = 0.7542 \cdot \frac{\frac{mg}{ml}}{HU \cdot [HU]} \tag{II-14}$$

and for the second scanner (Philips), it is:

$$[BMD_{K_2HPO_4}] = 0.69 \cdot \frac{\frac{mg}{ml}}{HU \cdot [HU]} \quad . \tag{II-15}$$

For 77 specimens of different spinal levels, the BMD values (in HU) were determined by two independent investigators. Vertebral bodies with deviations in BMD values of more than 10% were analysed repeatedly by both observers. Overall, the regression between the two data sets is sufficient (Figure II-14). The slope is 0.939 (±0.058) and the corrected coefficient of determination is R^2_{corr} =0.78 ($p < 0.001$).

It appeared that large deviations occurred mostly in cases where the size of the vertebral bodies was small or where bony damages were visible. In these cases the exact positioning within the spongy bone was difficult, and cortical bone and endplates might therefore have been included as well. The allowed reduction of the size of the measurement volume for flat or abnormal vertebrae was only done for the axial coordinate (from 15 voxels to 10 voxels). Some abnormal cases can be seen in Figure II-15. However, the quality of the results depends predominantly on the properties of the specimens and not on the choice of investigator.

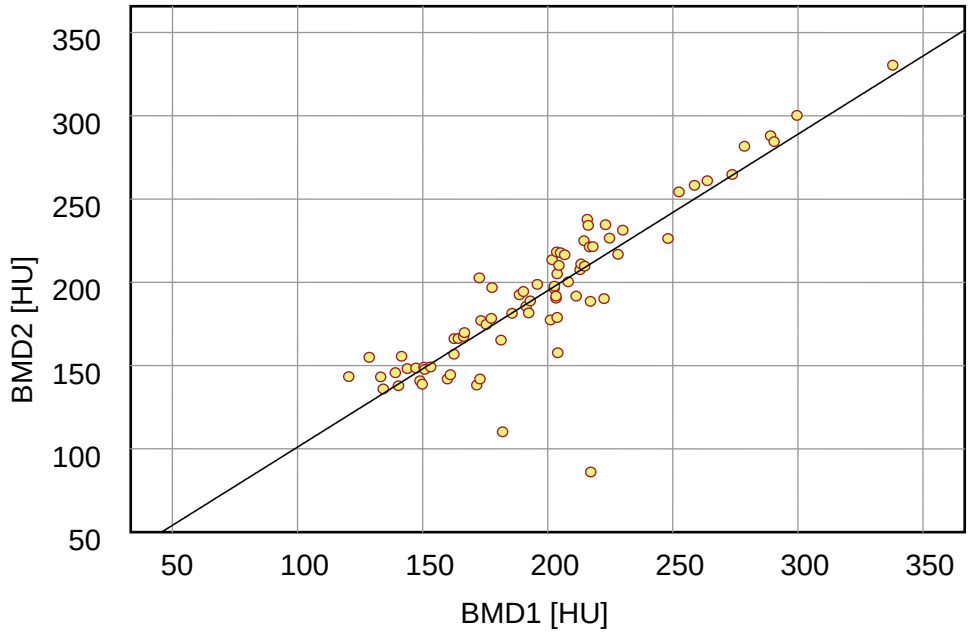

Figure II-14 Regression between the BMD values determined by two independent investigators

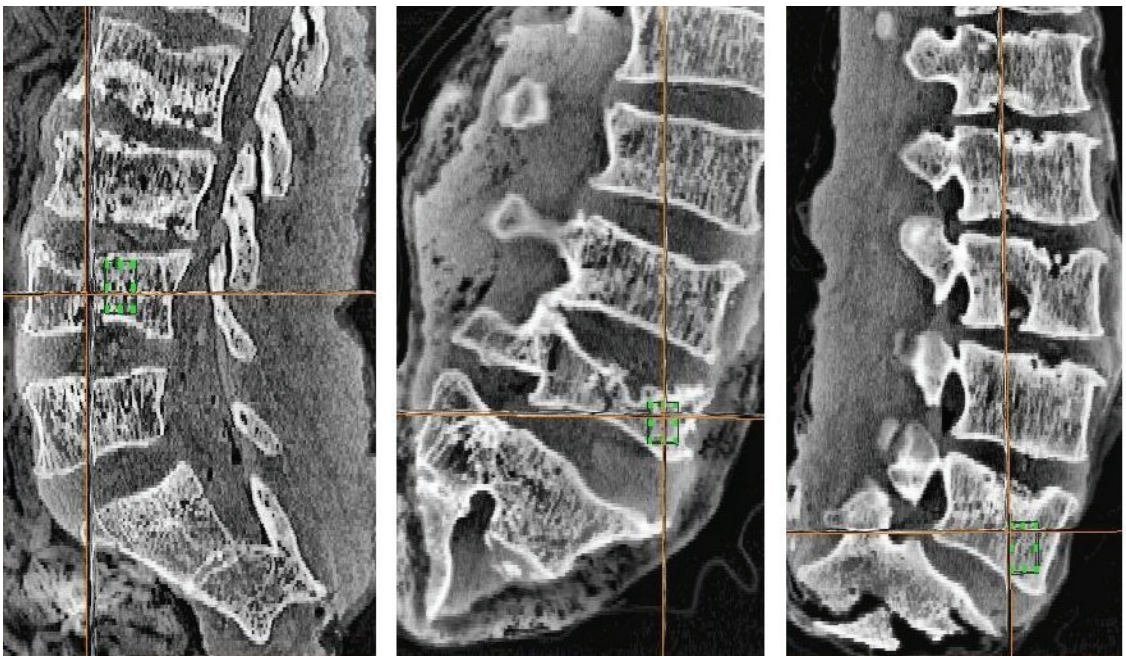

Figure II-15 Positioning of the bounding box in extreme cases, where a smaller volume size was applied (L4, LWS 1103; L4, LWS 1114; L5, LWS 1118)

No differences between the mean BMD of different spinal levels were observed (Figure II-16). Table II-4 shows the measured data as well as the position of the bounding box defined by the minimal index in the x-, y- and z-directions.

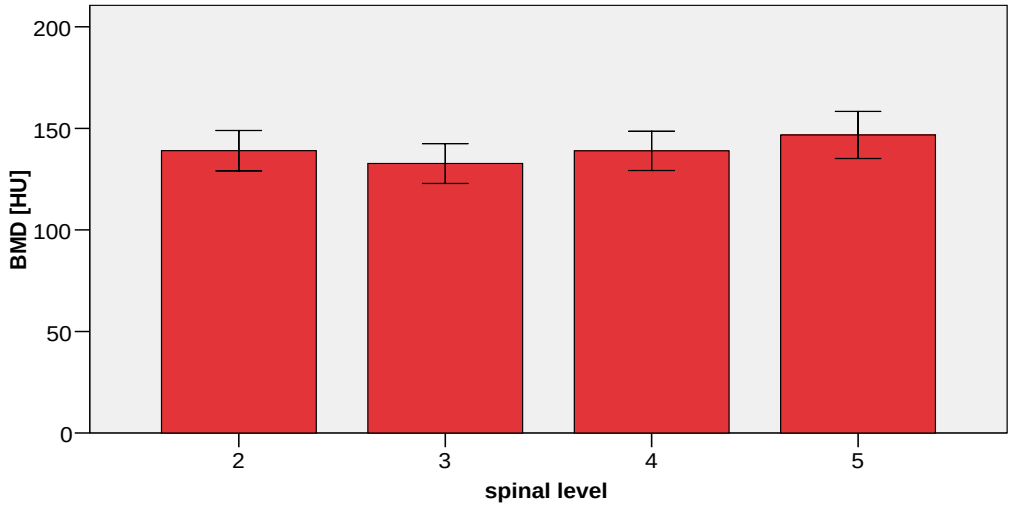

Figure II-16 Mean BMD of the four different spinal levels (error bars showing 95% confidence interval)

Table II-4 Analysed measurement volume and BMD of vertebra L2

LWS	Bounding box [voxels]			Min index [voxels]			Voxel size [mm]			Mean [HU]	STD [HU]	RMS [HU]	BMD [mgK_2HPO_4 per ml]
	x	y	z	x	y	z	x	y	z				
1101	30	30	15	108	80	72	0.3	0.3	1.0	139.1	118.2	182.6	104.9
1102	30	30	15	154	166	18	0.3	0.3	1.0	150.5	142.8	207.5	113.5
1103	30	30	10	202	199	167	0.3	0.3	1.0	202.4	214.9	295.2	152.6
1104	30	30	15	240	214	48	0.3	0.3	1.0	153.2	102.9	184.6	115.6
1105	30	30	15	169	122	168	0.3	0.3	1.0	201.1	133.8	241.6	151.7
1106	30	30	15	201	191	164	0.3	0.3	1.0	214.8	116.6	244.4	162.0
1107	30	30	15	240	226	25	0.3	0.3	1.0	171.6	162.0	236.0	129.4
1108	30	30	15	288	140	141	0.3	0.3	1.0	203.8	242.8	317.0	153.7
1109	30	30	15	93	220	144	0.3	0.3	1.0	275.4	687.7	283.9	190.0
1110	30	30	15	278	213	51	0.3	0.3	1.0	189.7	84.8	207.8	130.9
1111	30	30	15	94	226	175	0.3	0.3	1.0	183.4	65.4	194.8	126.6
1112	30	30	15	147	227	48	0.3	0.3	1.0	201.1	81.5	217.0	138.8
1113	30	30	15	103	96	46	0.3	0.3	1.0	244.8	66.0	253.5	168.9
1114	30	30	15	238	69	51	0.3	0.3	1.0	136.3	78.4	157.3	94.1
1115	30	30	15	267	136	155	0.3	0.3	1.0	141.8	73.3	159.6	97.8
1116	30	30	15	238	203	55	0.3	0.3	1.0	223.1	62.2	231.6	154.0
1117	30	30	15	115	212	160	0.3	0.3	1.0	212.2	96.7	233.2	146.4
1118	30	30	15	271	119	143	0.3	0.3	1.0	194.6	72.7	207.8	134.3
1119	30	30	15	131	71	162	0.3	0.3	1.0	257.6	71.4	267.4	177.8
1120	30	30	15	276	219	96	0.3	0.3	1.0	200.8	63.2	210.5	138.6
1121	30	30	15	242	129	89	0.3	0.3	1.0	191.5	72.4	204.7	132.1
1122	30	30	15	208	245	136	0.3	0.3	1.0	189.9	56.4	198.1	131.0
1123	30	30	15	240	176	88	0.3	0.3	1.0	222.6	58.8	230.3	153.6
1124	30	30	15	278	206	79	0.3	0.3	1.0	184.8	62.6	195.1	127.5
1125	30	30	15	274	211	48	0.3	0.3	1.0	210.9	75.8	224.1	145.5
1126	30	30	15	277	209	208	0.3	0.3	1.0	226.9	67.0	236.6	156.6
1127	30	30	15	179	79	94	0.3	0.3	1.0	252.1	55.6	258.1	173.9
1128	30	30	15	103	198	52	0.3	0.3	1.0	167.9	69.2	181.6	115.9
1129	30	30	15	89	237	180	0.3	0.3	1.0	225.3	54.7	231.9	155.5
1130	30	30	15	276	110	61	0.3	0.3	1.0	134.7	62.9	148.6	92.9
1131	30	30	15	136	104	112	0.3	0.3	1.0	164.5	62.5	176.0	113.5
1132	30	30	13	106	186	93	0.3	0.3	1.0	325.4	77.8	334.5	224.5
1133	30	30	15	120	235	243	0.3	0.3	1.0	199.6	55.9	207.3	137.7
1134	30	30	15	207	219	79	0.3	0.3	1.0	148.2	63.1	161.1	102.3
1135	30	30	15	230	233	216	0.3	0.3	1.0	242.8	57.5	249.5	167.5
1136	30	30	15	137	106	63	0.3	0.3	1.0	133.2	67.2	149.2	91.9

Table II-5 Analysed measurement volume and BMD of vertebra L3

LWS	Bounding box [voxels]			Min index [voxels]			Voxel size [mm]			Mean [HU]	STD [HU]	RMS [HU]	BMD [mgK_2HPO_4 per ml]
	x	y	z	x	y	z	x	y	z				
1101	30	30	15	115	68	111	0.3	0.3	1.0	134.3	113.3	175.7	101.3
1102	30	30	15	222	178	101	0.3	0.3	1.0	159.9	162.7	228.2	120.6
1103	30	30	15	122	134	137	0.3	0.3	1.0	173.0	208.9	271.2	130.4
1104	30	30	15	264	215	88	0.3	0.3	1.0	143.9	108.4	180.1	108.5
1105	30	30	15	114	136	137	0.3	0.3	1.0	166.4	125.2	208.2	125.5
1106	30	30	15	243	190	134	0.3	0.3	1.0	212.9	105.4	237.6	160.6
1107	30	30	15	265	233	63	0.3	0.3	1.0	150.8	182.1	236.5	113.8
1108	30	30	15	293	149	106	0.3	0.3	1.0	191.4	187.5	267.9	144.3
1109	30	30	15	86	225	107	0.3	0.3	1.0	273.7	68.8	282.2	188.9
1110	30	30	15	276	173	91	0.3	0.3	1.0	177.7	81.3	195.4	122.6
1111	30	30	15	56	230	135	0.3	0.3	1.0	162.6	59.2	173.1	112.2
1112	30	30	15	124	212	83	0.3	0.3	1.0	192.4	63.1	202.5	132.7
1113	30	30	15	85	94	82	0.3	0.3	1.0	263.8	70.3	273.0	182.0
1114	30	30	15	212	59	90	0.3	0.3	1.0	120.5	81.3	145.3	83.1
1115	30	30	15	286	106	120	0.3	0.3	1.0	133.2	76.6	153.7	91.9
1116	30	30	15	245	216	93	0.3	0.3	1.0	228.1	54.5	234.6	157.4
1117	30	30	15	101	209	121	0.3	0.3	1.0	208.2	101.1	231.5	143.7
1118	30	30	15	290	114	103	0.3	0.3	1.0	203.8	64.6	213.8	140.6
1119	30	30	15	134	59	122	0.3	0.3	1.0	252.5	69.9	262.0	174.2
1120	30	30	15	278	199	134	0.3	0.3	1.0	217.1	81.3	231.8	149.8
1121	30	30	15	236	89	125	0.3	0.3	1.0	177.5	66.8	189.6	122.5
1122	30	30	15	194	259	175	0.3	0.3	1.0	185.7	57.2	194.4	128.2
1123	30	30	15	268	169	121	0.3	0.3	1.0	201.8	68.2	213.0	139.2
1124	30	30	15	280	208	116	0.3	0.3	1.0	172.3	62.7	183.3	118.9
1125	30	30	15	292	216	87	0.3	0.3	1.0	197.1	71.3	209.6	136.0
1126	30	30	15	358	262	165	0.3	0.3	1.0	218.9	68.4	229.4	151.1
1127	30	30	15	217	86	136	0.3	0.3	1.0	229.9	72.0	240.9	158.6
1128	30	30	15	144	234	88	0.3	0.3	1.0	137.8	76.5	157.6	95.1
1129	30	30	15	104	293	142	0.3	0.3	1.0	219.3	51.8	225.3	151.3
1130	30	30	15	261	105	103	0.3	0.3	1.0	147.0	74.5	164.8	101.5
1131	30	30	15	221	95	148	0.3	0.3	1.0	128.5	68.5	145.6	88.7
1132	30	30	15	108	229	124	0.3	0.3	1.0	278.2	57.0	283.9	191.9
1133	30	30	15	112	329	206	0.3	0.3	1.0	215.4	56.6	222.7	148.6
1134	30	30	15	330	269	117	0.3	0.3	1.0	163.1	69.6	177.3	112.5
1135	30	30	15	257	234	179	0.3	0.3	1.0	234.3	54.3	240.5	161.7
1136	30	30	15	137	111	100	0.3	0.3	1.0	124.6	68.6	142.2	86.0

Table II-6 Analysed measurement volume and BMD of vertebra L4

LWS	Bounding box [voxels]			Min index [voxels]			Voxel size [mm]			Mean [HU]	STD [HU]	RMS [HU]	BMD [mgK_2HPO_4 per ml]
	x	y	z	x	y	z	x	y	z				
1101	30	30	15	109	57	149	0.3	0.3	1.0	141.6	121.4	186.5	106.8
1102	30	30	15	230	176	102	0.3	0.3	1.0	166.7	168.3	236.9	125.8
1103	30	30	15	113	117	105	0.3	0.3	1.0	217.2	213.6	304.6	163.8
1104	30	30	15	293	177	129	0.3	0.3	1.0	148.9	116.0	188.8	112.3
1105	30	30	15	80	205	101	0.3	0.3	1.0	164.3	117.7	202.1	123.9
1106	30	30	15	231	195	102	0.3	0.3	1.0	218.0	115.0	246.5	164.4
1107	30	30	15	249	227	100	0.3	0.3	1.0	181.4	197.8	268.4	136.8
1108	30	30	15	306	149	65	0.3	0.3	1.0	203.6	214.6	295.8	153.5
1109	30	30	15	77	219	67	0.3	0.3	1.0	290.5	72.9	299.5	200.5
1110	30	30	15	258	194	130	0.3	0.3	1.0	223.1	110.3	248.8	153.9
1111	30	30	15	66	199	96	0.3	0.3	1.0	175.5	77.4	191.8	121.1
1112	30	30	15	105	221	124	0.3	0.3	1.0	188.7	58.4	197.5	130.2
1113	30	30	15	88	99	117	0.3	0.3	1.0	278.7	74.9	288.6	192.3
1114	30	30	12	285	126	133	0.3	0.3	1.0	204.0	112.7	233.1	140.8
1115	30	30	15	310	108	83	0.3	0.3	1.0	140.3	77.6	160.4	96.8
1116	30	30	15	244	195	133	0.3	0.3	1.0	214.5	62.3	223.4	148.0
1117	30	30	15	110	186	79	0.3	0.3	1.0	202.7	99.1	225.6	139.8
1118	30	30	15	257	81	67	0.3	0.3	1.0	195.8	74.2	209.4	135.1
1119	30	30	15	131	84	84	0.3	0.3	1.0	258.7	72.8	268.7	178.5
1120	30	30	15	287	194	171	0.3	0.3	1.0	211.4	86.0	228.2	145.9
1121	30	30	15	248	99	126	0.3	0.3	1.0	173.4	64.2	184.9	119.6
1122	30	30	15	190	256	217	0.3	0.3	1.0	204.5	57.0	212.3	141.1
1123	30	30	15	292	175	161	0.3	0.3	1.0	213.3	69.6	224.4	147.2
1124	30	30	15	276	200	154	0.3	0.3	1.0	185.4	72.7	199.2	128.0
1125	30	30	15	290	211	126	0.3	0.3	1.0	202.6	73.1	215.4	139.8
1126	30	30	15	377	268	123	0.3	0.3	1.0	230.8	79.2	244.0	159.2
1127	30	30	15	143	122	179	0.3	0.3	1.0	234.4	73.3	245.6	161.7
1128	30	30	15	163	314	125	0.3	0.3	1.0	148.7	79.3	168.5	102.6
1129	30	30	15	99	286	103	0.3	0.3	1.0	225.9	54.6	232.3	155.9
1130	30	30	15	240	90	142	0.3	0.3	1.0	144.2	68.4	159.6	99.5
1131	30	30	15	252	118	188	0.3	0.3	1.0	125.9	66.5	142.4	86.9
1132	30	30	15	117	228	158	0.3	0.3	1.0	271.2	58.9	277.5	187.1
1133	30	30	15	112	313	161	0.3	0.3	1.0	210.2	74.5	223.0	145.0
1134	30	30	15	354	255	160	0.3	0.3	1.0	150.1	66.1	164.0	103.6
1135	30	30	15	266	235	141	0.3	0.3	1.0	238.9	54.5	245.1	164.9
1136	30	30	15	131	85	138	0.3	0.3	1.0	127.7	66.8	144.1	88.1

Table II-7 Analysed measurement volume and BMD of vertebra L5

LWS	Bounding box [voxels]			Min index [voxels]			Voxel size [mm]			Mean [HU]	STD [HU]	RMS [HU]	BMD [mgK_2HPO_4 per ml]
	x	y	z	x	y	z	x	y	z				
1101	30	30	15	132	72	189	0.3	0.3	1.0	162.5	133.0	210.0	122.6
1102	30	30	15	254	157	145	0.3	0.3	1.0	147.3	155.9	214.5	111.1
1103	30	30	15	115	155	65	0.3	0.3	1.0	222.5	209.8	305.8	167.8
1104	30	30	15	281	168	168	0.3	0.3	1.0	128.7	98.1	161.8	97.0
1105	30	30	15	94	219	65	0.3	0.3	1.0	190.3	122.6	226.4	143.5
1106	30	30	15	230	178	70	0.3	0.3	1.0	224.7	110.8	250.5	169.5
1107	30	30	15	222	231	136	0.3	0.3	1.0	161.1	173.4	236.7	121.5
1108	30	30	15	296	156	23	0.3	0.3	1.0	230.1	200.9	305.4	173.5
1109	30	30	15	113	184	32	0.3	0.3	1.0	289.0	82.8	300.7	199.4
1110	30	30	15	251	188	172	0.3	0.3	1.0	203.3	93.9	223.9	140.3
1111	30	30	15	100	188	60	0.3	0.3	1.0	203.3	71.9	214.7	140.3
1112	30	30	15	105	187	163	0.3	0.3	1.0	206.8	70.9	218.6	142.7
1113	30	30	15	126	142	150	0.3	0.3	1.0	299.6	86.4	311.8	206.7
1114	30	30	15	155	108	158	0.3	0.3	1.0	172.6	78.9	189.8	119.1
1115	30	30	15	323	95	45	0.3	0.3	1.0	149.9	96.3	178.1	103.4
1116	30	30	15	225	196	171	0.3	0.3	1.0	215.8	60.5	224.1	148.9
1117	30	30	15	124	199	35	0.3	0.3	1.0	205.1	109.4	232.5	141.5
1118	30	30	15	248	76	26	0.3	0.3	1.0	248.0	155.5	292.8	171.1
1119	30	30	15	147	120	48	0.3	0.3	1.0	337.9	129.3	361.8	233.2
1120	30	30	15	283	206	208	0.3	0.3	1.0	202.6	69.6	214.2	139.8
1121	30	30	15	241	116	207	0.3	0.3	1.0	193.0	68.9	204.9	133.2
1122	30	30	15	183	191	249	0.3	0.3	1.0	216.2	69.8	227.2	149.2
1123	30	30	15	297	179	200	0.3	0.3	1.0	216.7	73.7	228.9	149.5
1124	30	30	15	247	194	192	0.3	0.3	1.0	216.5	76.5	229.7	149.4
1125	30	30	15	270	210	166	0.3	0.3	1.0	197.6	80.0	213.2	136.3
1126	30	30	15	401	263	79	0.3	0.3	1.0	241.8	69.4	251.5	166.8
1127	30	30	15	191	72	220	0.3	0.3	1.0	258.7	69.7	268.0	178.5
1128	30	30	15	189	297	165	0.3	0.3	1.0	122.6	71.5	141.9	84.6
1129	30	30	15	116	251	64	0.3	0.3	1.0	262.6	72.4	272.4	181.2
1130	30	30	13	188	154	179	0.3	0.3	1.0	181.6	116.8	215.9	125.3
1131	30	30	15	234	161	225	0.3	0.3	1.0	130.0	64.2	145.0	89.7
1132	30	30	15	140	207	194	0.3	0.3	1.0	281.0	56.1	286.5	193.9
1133	30	30	15	115	302	119	0.3	0.3	1.0	218.1	64.1	227.3	150.5
1134	30	30	15	362	248	202	0.3	0.3	1.0	195.0	76.3	209.4	134.6
1135	30	30	15	259	214	104	0.3	0.3	1.0	257.4	54.6	263.1	177.6
1136	30	30	15	128	79	176	0.3	0.3	1.0	129.7	69.5	147.1	89.5

6 Frobin Classification

Frobin et al. (1997) proposed a new technique for measuring disc height from lateral radiographs of the lumbar spine. This technique was based on measuring relative disc height independent of distortion, axial rotation and lateral tilt of the spine. They evaluated the database using 892 lateral views of the lumbar spine of male and female subjects between 16-57 years of age. Data from pathologically deformed vertebrae or discs were excluded but data from spines showing normal age-related changes were included. The normal values gathered in this study can serve as a database for age comparison to evaluate the severity of spinal pathologic changes.

The Frobin classification was evaluated by three observers using a Matlab (MathWorks Inc., Natick, MA, USA) program. Details about the Matlab program, the procedures and definitions are given in Huber et al. (2005).

The results were averaged for three observers. Relative disc height of the tested L2-L3 and L4-L5 specimens versus age is shown in Figure II-17 and Figure II-18.
The average relative disc height was larger by 7% and 11% in comparison to norm values for L2-L3 and L4-L5 specimens, respectively (Table II-8). The lowest disc height was 10% below the norm value and the highest was 42% above the norm value; those values were recorded for L2-L3 specimens.

Detailed results of the Frobin classification are listed in Table II-9 for shear specimens and in Table II-10 for fatigue specimens.

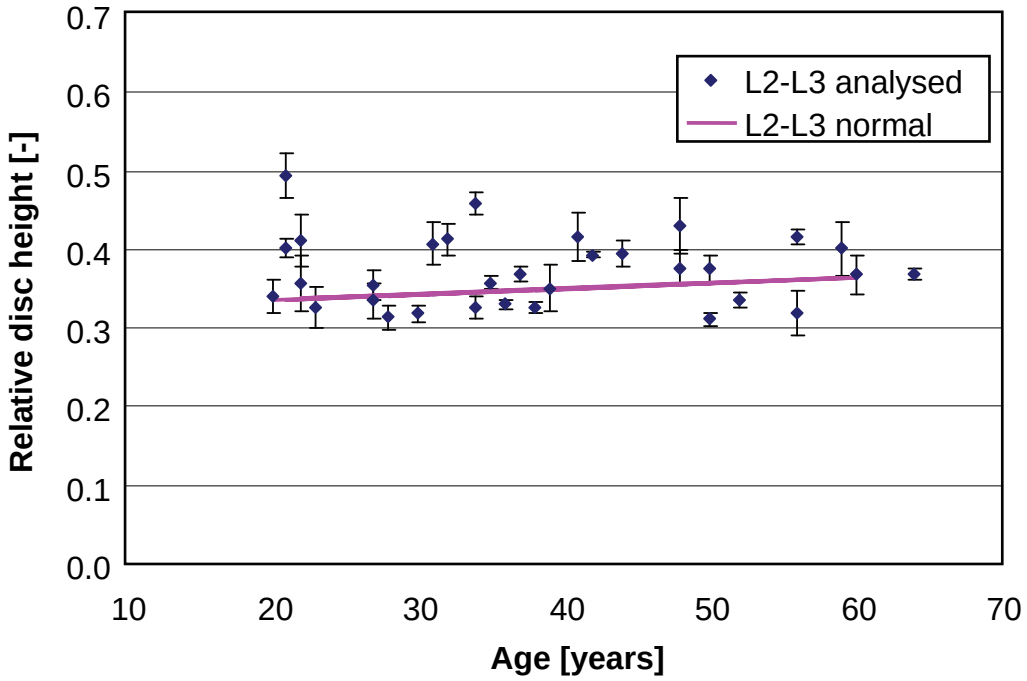

Figure II-17 Age dependence of average values (bars indicate STD) of measured relative disc height of tested L2-L3 specimens in comparison to regression line for normal values from Frobin et al. (1997)

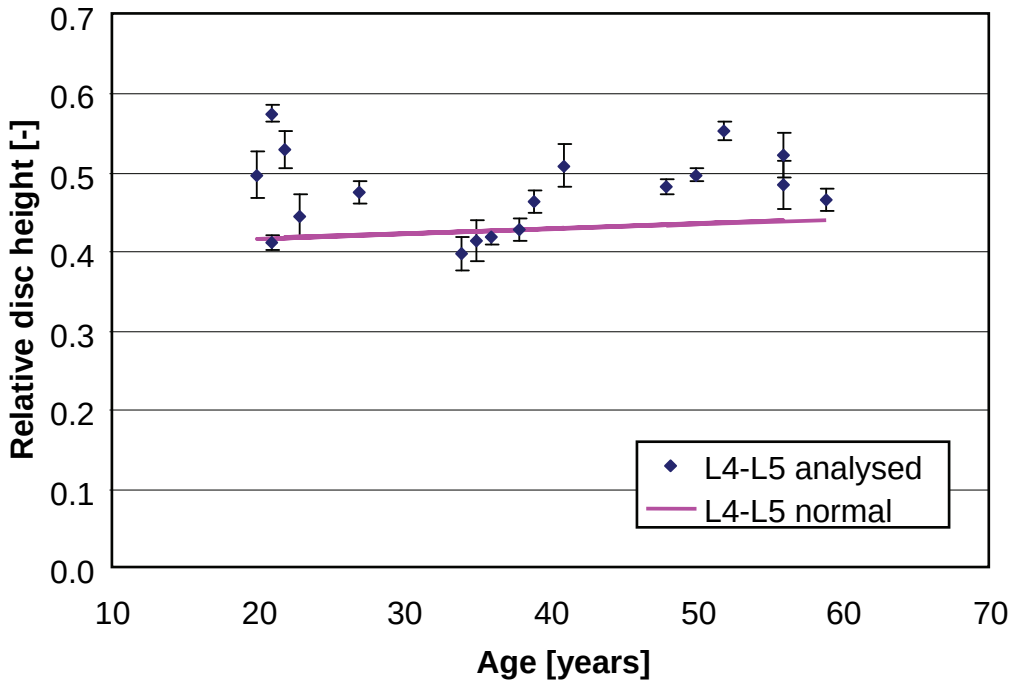

Figure II-18 Age dependence of average values (bars indicate STD) of measured relative disc height of tested L4-L5 specimens in comparison to regression line for normal values from Frobin et al. (1997)

Table II-8 Comparison of disc height of tested specimens to calculated norm values from Frobin et al. (1997)

Type	Minimum value in comparison to norm	Maximum value in comparison to norm	Mean value in comparison to norm
L2-L3	-10%	+42%	+7%
L4-L5	-7%	+34%	+11%

Table II-9 Frobin results of L2-L3 motion segments tested in shear mode (VA: vertebral angle, DH: relative disc height corrected)

LWS	Observer 1		Observer 2		Observer 3		Mean	
	VA [°]	DH [-]	VA [°]	DH [-]	VA [°]	DH [-]	VA [°]	DH [-]
0003	5.0	0.37	4.6	0.38	5.8	0.36	5.1	0.37
0004	4.1	0.44	3.4	0.47	4.3	0.46	4.0	0.46
0011	4.3	0.42	3.3	0.42	3.4	0.38	3.7	0.41
0012	8.3	0.40	9.3	0.39	7.9	0.39	8.5	0.39
0028	4.5	0.41	4.1	0.44	4.9	0.40	4.5	0.41
0033	8.8	0.40	8.6	0.41	9.0	0.39	8.8	0.40
0036	10.7	0.31	11.0	0.33	10.1	0.31	10.6	0.32
0052	9.0	0.32	8.9	0.36	8.8	0.32	8.9	0.33
1101	4.0	0.43	3.5	0.41	3.7	0.42	3.8	0.42
1104	3.6	0.42	9.2	0.47	4.6	0.40	5.8	0.43
1106	5.8	0.33	6.2	0.35	5.8	0.30	5.9	0.33
1107	7.1	0.33	5.6	0.34	5.7	0.32	6.2	0.33
1109	7.8	0.37	7.6	0.37	7.3	0.36	7.6	0.37
1110	1.0	0.34	0.7	0.35	1.3	0.33	1.0	0.34
1112	11.1	0.34	10.9	0.36	10.2	0.32	10.8	0.34
1116	5.7	0.33	5.0	0.31	5.5	0.30	5.4	0.31
1119	7.2	0.36	7.8	0.38	7.2	0.32	7.4	0.35
1120	2.1	0.44	1.9	0.43	3.2	0.38	2.4	0.42
1121	6.6	0.32	6.7	0.32	6.9	0.30	6.7	0.31
1122	10.1	0.39	10.3	0.39	10.1	0.35	10.2	0.38
1123	3.2	0.36	4.4	0.35	5.1	0.36	4.2	0.36
1124	10.8	0.34	11.4	0.33	11.1	0.31	11.1	0.33
1125	6.9	0.37	8.3	0.36	6.7	0.33	7.3	0.35
1126	6.5	0.50	6.4	0.52	6.9	0.46	6.6	0.49
1128	8.3	0.39	8.0	0.38	8.2	0.34	8.2	0.37
1130	5.6	0.39	6.8	0.39	6.2	0.35	6.2	0.38
1131	12.5	0.35	12.6	0.31	14.3	0.29	13.1	0.32
1132	5.0	0.39	4.1	0.37	5.3	0.32	4.8	0.36
1133	6.9	0.33	7.7	0.33	8.0	0.32	7.5	0.33
1134	8.8	0.39	9.0	0.41	9.6	0.38	9.1	0.40
1135	6.9	0.43	6.5	0.44	6.4	0.37	6.6	0.41
1136	2.7	0.41	2.2	0.43	3.3	0.36	2.7	0.40

Table II-10 Frobin results of L4-L5 motion segments tested in fatigue mode (VA: vertebral angle, DH: relative disc height corrected)

LWS	Observer 1		Observer 2		Observer 3		Mean	
	VA [°]	DH [-]	VA [°]	DH [-]	VA [°]	DH [-]	VA [°]	DH [-]
1101	15.2	0.56	15.3	0.52	16.0	0.50	15.5	0.52
1104	10.5	0.49	10.4	0.48	10.5	0.48	10.5	0.48
1106	9.0	0.47	8.8	0.45	8.3	0.42	8.7	0.45
1107	11.9	0.42	11.5	0.43	12.0	0.41	11.8	0.42
1108	4.4	0.49	6.5	0.49	7.8	0.51	6.3	0.50
1110	12.1	0.57	9.6	0.55	11.5	0.54	11.1	0.55
1112	13.3	0.53	14.7	0.49	14.6	0.47	14.2	0.50
1113	21.0	0.41	21.4	0.42	21.9	0.40	21.4	0.41
1119	12.3	0.48	10.0	0.47	9.2	0.45	10.5	0.46
1120	13.5	0.53	14.2	0.52	12.7	0.48	13.5	0.51
1123	12.6	0.44	12.2	0.41	12.1	0.39	12.3	0.41
1124	16.5	0.42	16.6	0.40	17.8	0.37	17.0	0.40
1125	13.7	0.48	14.8	0.49	13.1	0.46	13.9	0.48
1126	12.3	0.58	11.7	0.59	12.1	0.56	12.0	0.58
1131	21.7	0.48	22.7	0.52	20.9	0.46	21.8	0.49
1133	13.7	0.43	13.2	0.45	14.0	0.42	13.6	0.43
1135	13.1	0.54	10.6	0.54	12.9	0.50	12.2	0.53
1136	7.8	0.47	8.5	0.48	7.7	0.45	8.0	0.47

7 Thompson Classification

Thompson et al. (1990) developed a disc degeneration grading system. The system consists of five grades of degeneration according to the descriptions shown in Table II-11. Each grade of degeneration includes four categories: nucleus, annulus, endplate and vertebral body.

Tested motion segments were cut through the mid-sagittal plane using a band saw (Exakt, Norderstedt, Germany). The cut surface was washed briefly in running tepid water to remove debris. After sectioning they were photographed in order to allow evaluation of disc degeneration.

Two observers were asked to evaluate disc degeneration from photographs in terms of a degeneration score based on each described category. Disc sections across different degeneration grades are shown in Figure II-19 and Figure II-20.
This post-test analysis of disc sections was performed for groups of specimens tested in shear and in fatigue. For details of specimens assigned to particular groups, refer to Parts III, IV and VI.

With regard to the specimens tested in shear, 23 out of 32 nuclei were rated the same by the two observers (Table II-12). In eight cases Observer 1 gave a higher grade of degeneration; in one case Observer 2 assessed a higher grade of degeneration. Their evaluations differed by only one grade of degeneration.

For the annulus, 11 out of 32 cases were rated the same by the two observers (Table II-12). In 18 cases Observer 1 gave a higher score and in three cases Observer 2 gave a higher score. Again, the degeneration evaluations differed by only one grade.

For the endplate, the two observers agreed in 18 out of 32 cases (Table II-12). Observer 1 rated four cases higher, and Observer 2 gave higher ratings differing by one degeneration grade in ten cases.

For the vertebral body, the observers agreed in 24 out of 32 cases (Table II-12). In six cases Observer 1 rated the degree of degeneration higher, including one case where the disagreement differed by three degeneration grades and two cases differing by two grades. In two cases Observer 2 rated the degeneration higher, including one case where the disagreement differed by two degeneration grades.

With regard to the specimens used for the fatigue testing, the nuclei of 8 out of 18 cases were rated the same by the two observers (Table II-13). In three cases Observer 1 gave a higher grade of degeneration including one case where the disagreement differed by two degeneration grades. In seven cases Observer 2 gave a higher degeneration rating differing by one grade.

For the annulus, 7 out of 18 cases were rated the same by the two observers (Table II-13). In three cases Observer 1 gave a higher score and in seven cases Observer 2 gave a higher score. The scores differed by only one degeneration grade.

For the endplate, the two observers agreed in 11 out of 18 cases (Table II-13). Observer 1 rated one case higher by two degeneration grades, and Observer 2 gave higher ratings differing by one degeneration grade in six cases.
For the vertebral body, the two observers agreed in 11 out of 18 cases (Table II-13). In seven cases Observer 2 gave a higher degeneration rating, including one case where the disagreement differed by two degeneration grades.

Boxplots for each category of disc degeneration are shown in Figure II-21 for shear specimens and in Figure II-22 for fatigue specimens. In addition, the boxplots of total average disc degeneration for different testing groups are presented in Figure II-23 and Figure II-24.

Motion segments that failed during fatigue testing were rated for an overall mean grade between 3.6 and 4.5, apart from one specimen that was graded 1.8 (LWS 1119). Disc sections are shown in Figure II-25, Figure II-26 and Figure II-27.

Table II-11 Description of the morphologic grade (Thompson et al., 1990)

Grade	Nucleus	Annulus	Endplate	Vertebral body
I	Bulging gel	Discrete fibrous lamellas	Hyaline, uniformly thick	Margins rounded
II	White fibrous tissue peripherally	Mucinous material between lamellas	Thickness irregular	Margins pointed
III	Consolidated fibrous tissue	Extensive mucinous infiltration; loss of annular-nucleus demarcation	Focal defects in cartilage	Early chondrophytes or osteophytes at margins
IV	Horizontal clefts parallel to endplate	Focal disruptions	Fibrocartilage extending from subchondral bone; irregularity and focal sclerosis in subchondral bone	Osteophytes less than 2 mm
V	Clefts extended through nucleus and annulus		Diffuse sclerosis	Osteophytes greater than 2 mm

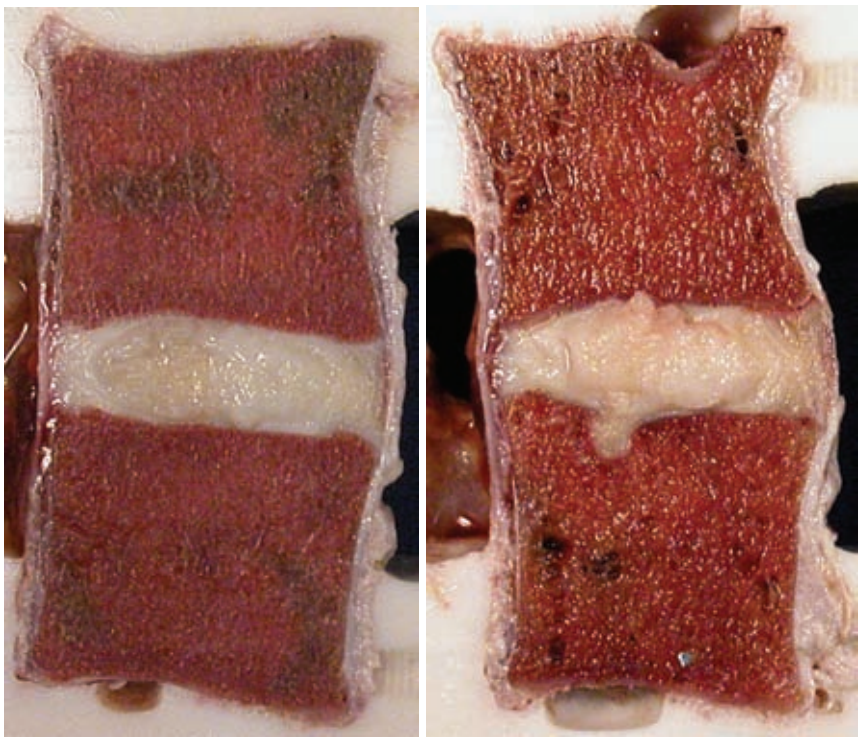

Figure II-19 Motion segment sections of lower degeneration grades: LWS 1116 L2-L3 was graded 1.1 and LWS 0012 L2-L3 was graded 2.5, respectively.

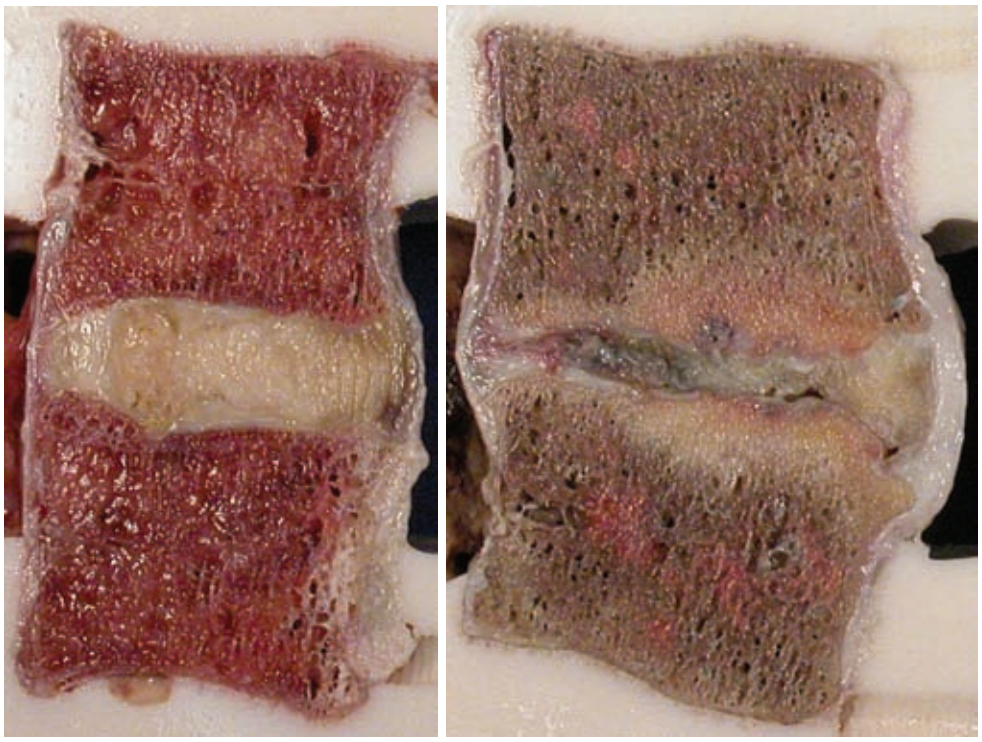

Figure II-20 Motion segment sections of higher degeneration grades: LWS 1136 L2-L3 was graded 3.5 and LWS 1123 L4-L5 was graded 5.0, respectively.

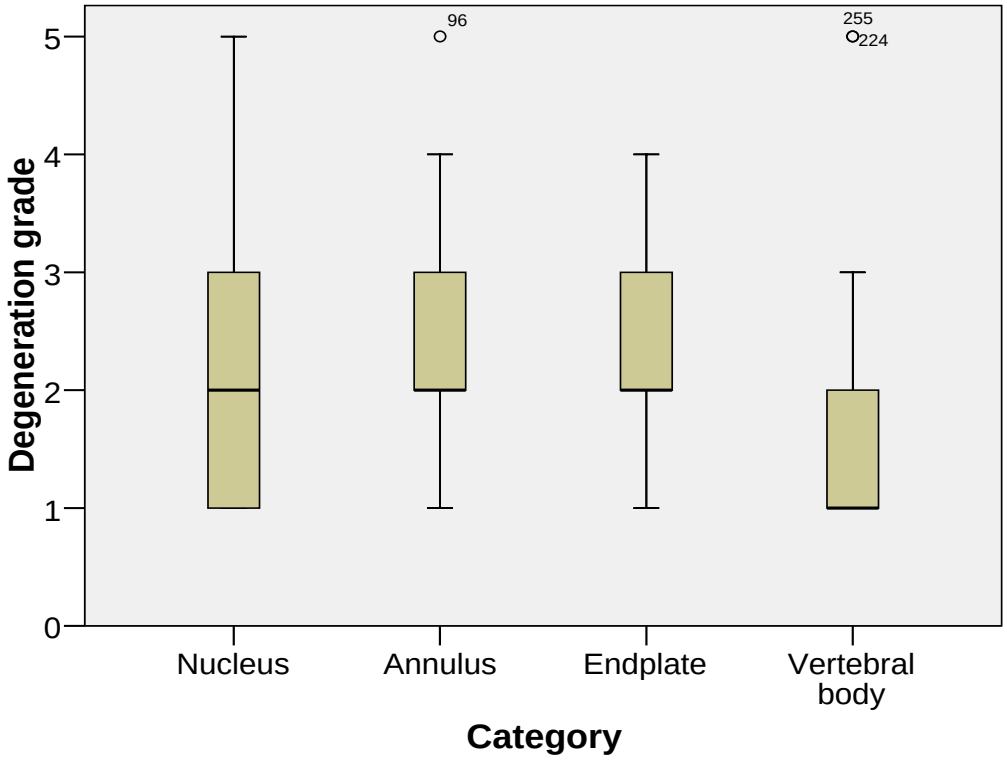

Figure II-21 Boxplots of disc degeneration grade, specimens tested in shear

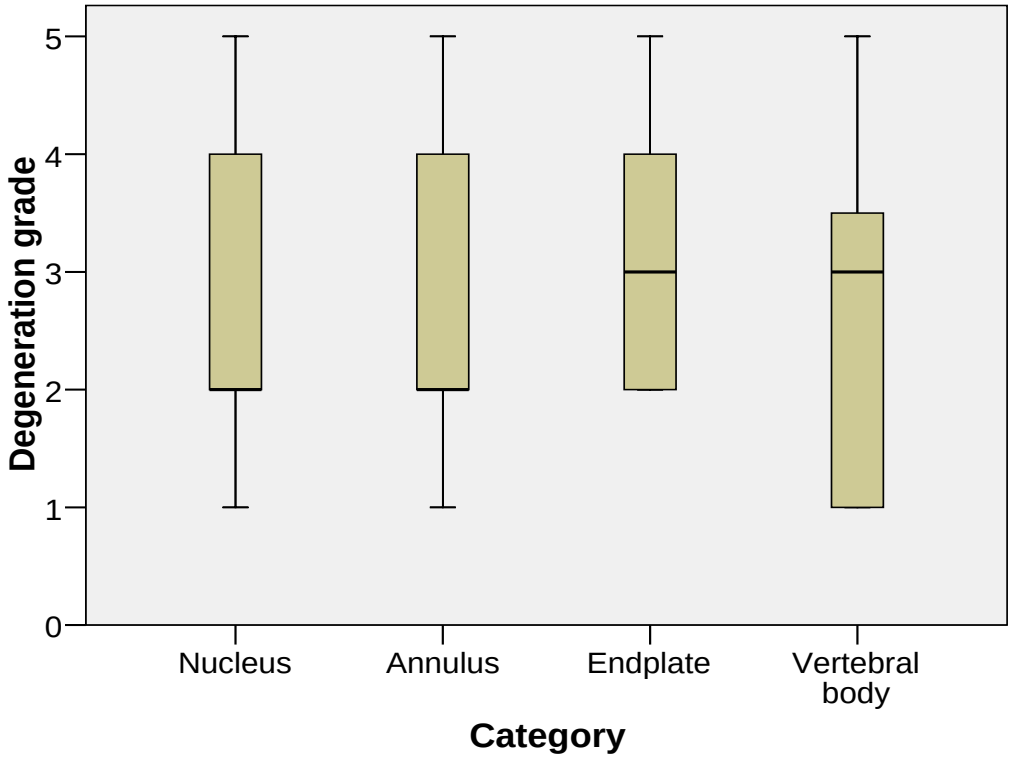

Figure II-22 Boxplots of disc degeneration grade, specimens tested in fatigue

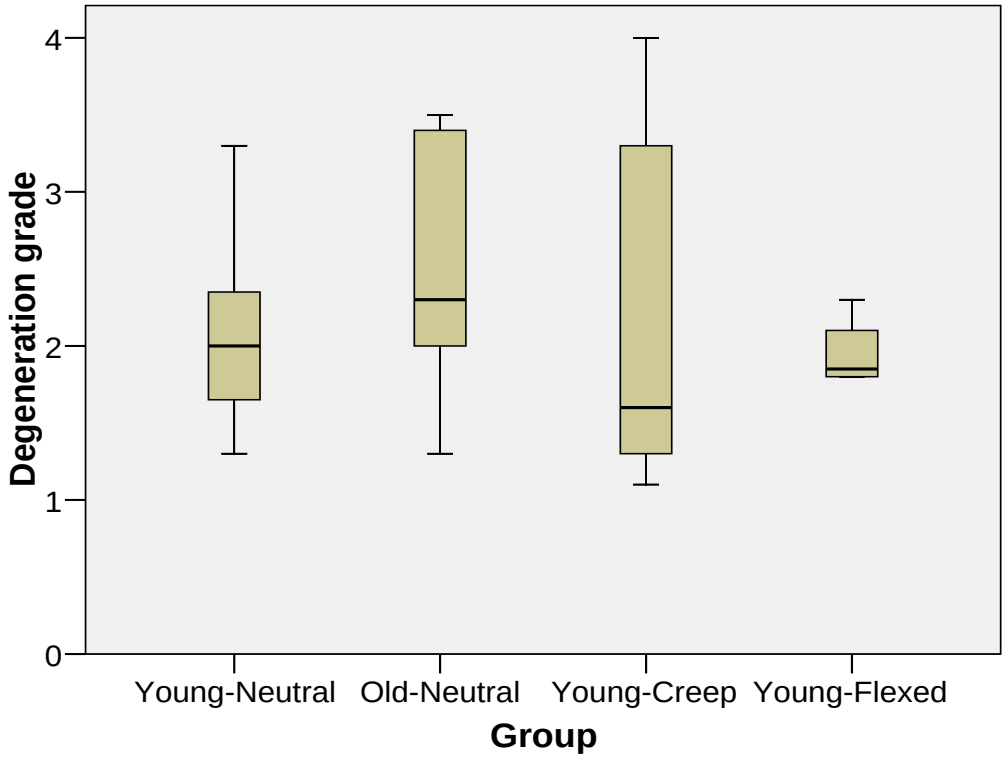

Figure II-23 Boxplots of total average disc degeneration grade for different testing groups, specimens tested in shear

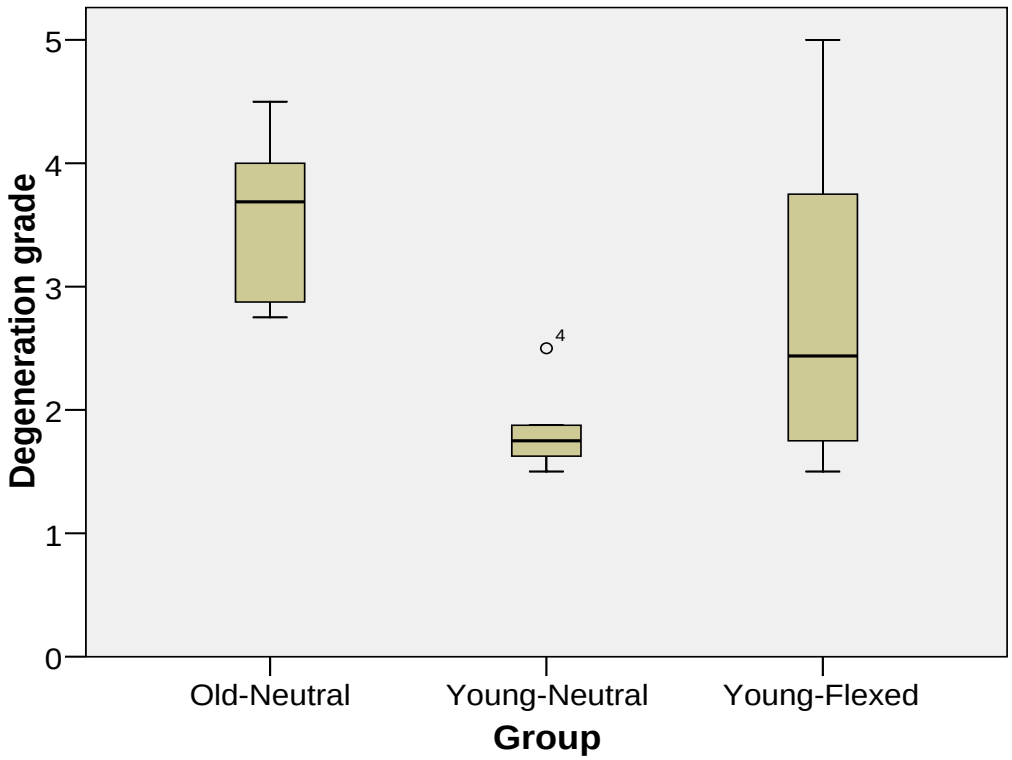

Figure II-24 Boxplots of total average disc degeneration grade for different testing groups, specimens tested in fatigue

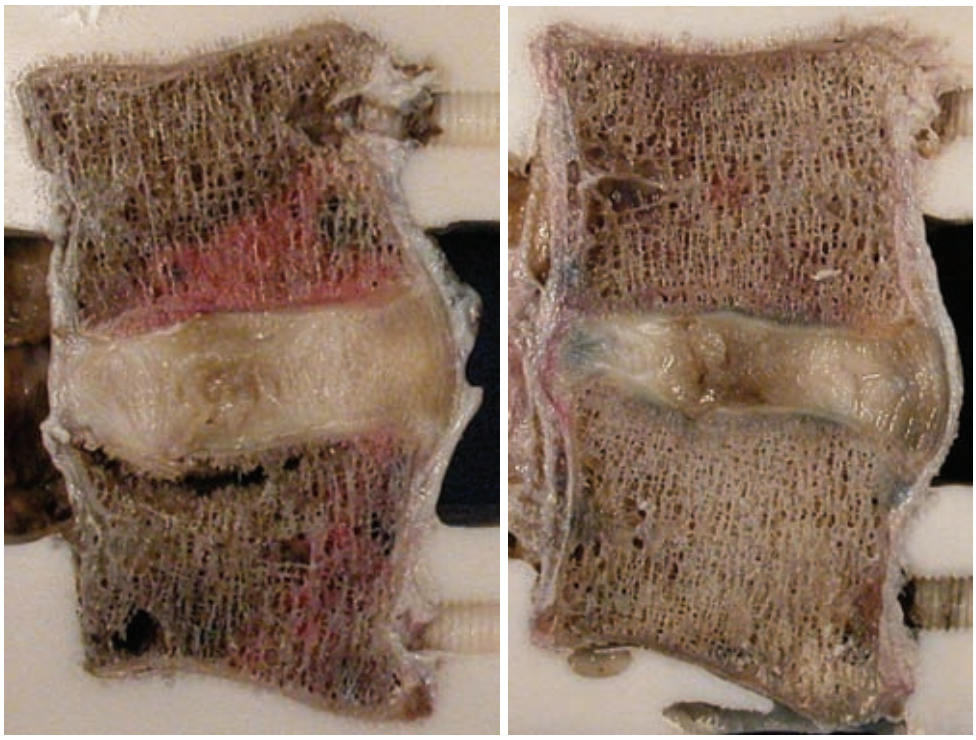

Figure II-25 Images of failed specimens tested in fatigue from the Old-Neutral group: LWS 1101 L4-L5 (grade 3.6) and LWS 1104 L4-L5 (grade 3.8), respectively

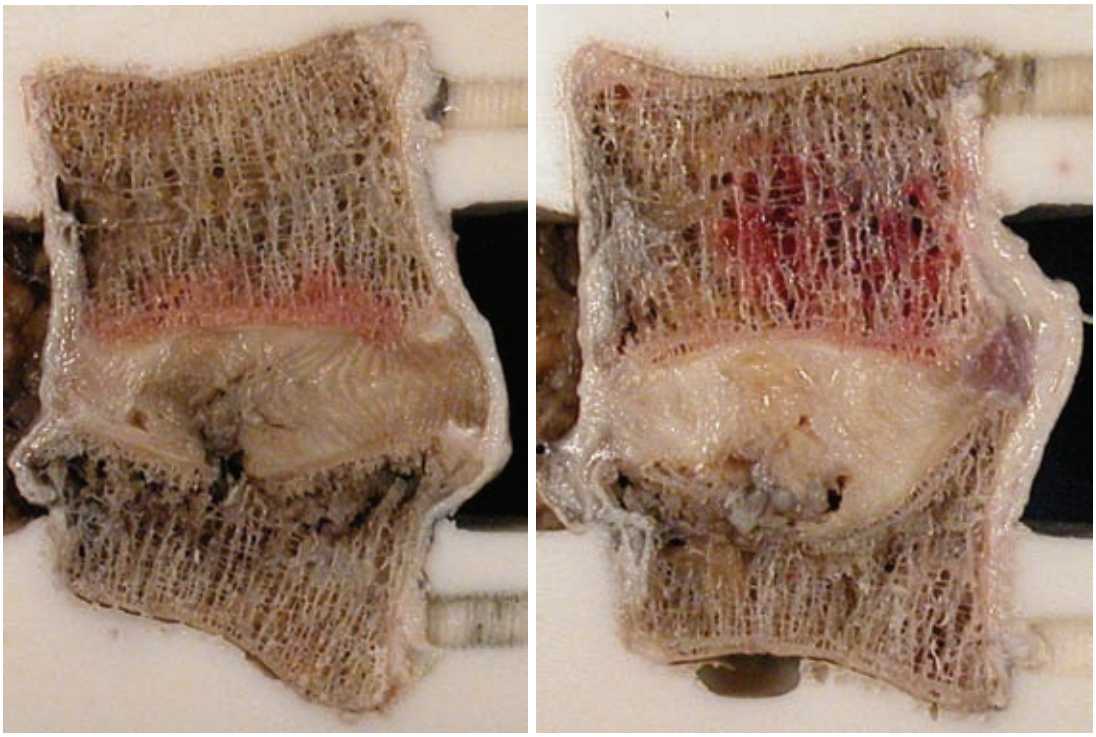

Figure II-26 Images of failed specimens tested in fatigue from the Old-Neutral group: LWS 1131 L4-L5 (grade 4.5) and LWS 1136 L4-L5 (grade 4.0), respectively

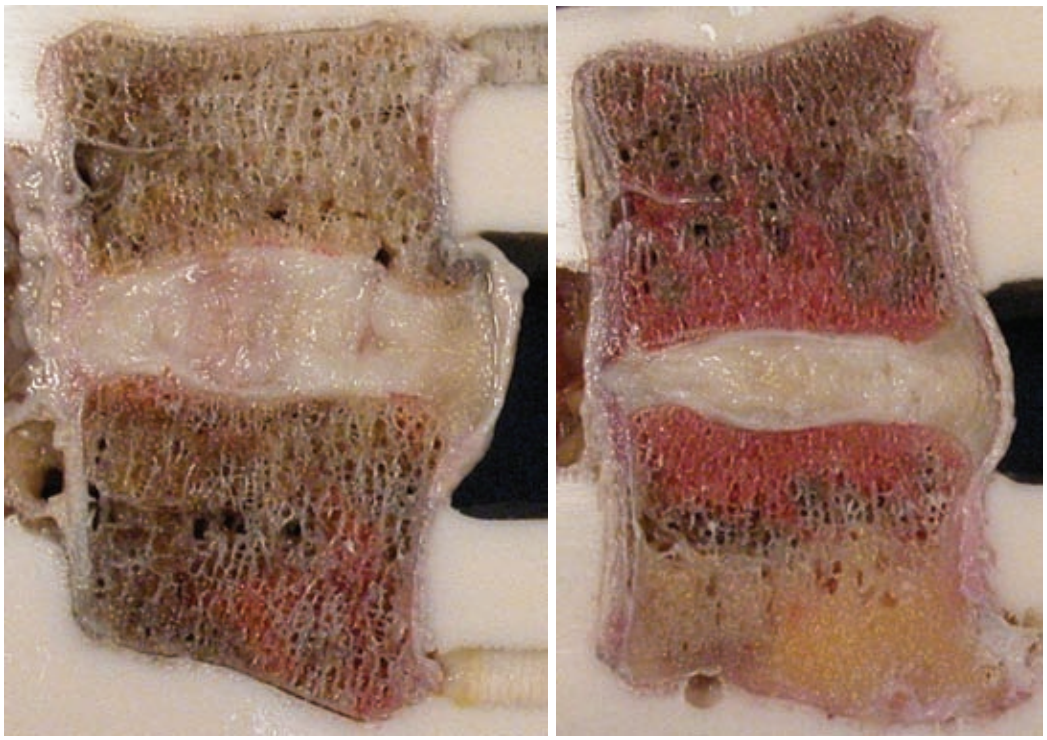

Figure II-27 Images of failed specimens tested in fatigue from the Young-Flexed group: LWS 1112 L4-L5 (grade 3.8) and LWS 1119 L4-L5 (grade 1.8), respectively

Table II-12 Thompson disc degeneration grade of L2-L3 motion segments tested in shear mode (NU: nucleus, AN: annulus, EP: endplate, VB: vertebral body)

LWS	Observer 1						Observer 2						Overall
	NU	AN	EP	VB	Max	Mean	NU	AN	EP	VB	Max	Mean	mean
0003	2	2	2	1	2	1.8	2	2	3	1	3	2.0	1.9
0004	2	2	2	1	2	1.8	1	2	3	1	3	1.8	1.8
0011	1	2	2	1	2	1.5	1	2	3	2	3	2.0	1.8
0012	2	3	3	2	3	2.5	2	2	4	2	4	2.5	2.5
0028	2	2	2	1	2	1.8	2	2	2	1	2	1.8	1.8
0033	1	2	2	1	2	1.5	1	1	2	1	2	1.3	1.4
0036	2	2	2	2	2	2.0	2	3	3	2	3	2.5	2.3
0052	1	1	2	2	2	1.5	1	2	3	2	3	2.0	1.8
1101	3	3	2	1	3	2.3	3	2	2	1	3	2.0	2.1
1104	3	3	3	2	3	2.8	3	2	3	2	3	2.5	2.6
1106	2	2	2	2	2	2.0	2	2	2	1	2	1.8	1.9
1107	2	2	3	2	3	2.3	3	3	2	2	3	2.5	2.4
1109	1	1	2	1	2	1.3	1	1	2	1	2	1.3	1.3
1110	4	4	3	3	4	3.5	4	3	4	2	4	3.3	3.4
1112	4	4	3	3	4	3.5	4	3	4	1	4	3.0	3.3
1116	1	1	1	1	1	1.0	1	1	2	1	2	1.3	1.1
1119	3	3	3	1	3	2.5	2	2	2	1	2	1.8	2.1
1120	3	3	3	1	3	2.5	2	2	3	1	3	2.0	2.3
1121	3	3	2	2	3	2.5	3	2	2	1	3	2.0	2.3
1122	2	2	3	2	3	2.3	2	2	3	2	3	2.3	2.3
1123	3	4	3	3	4	3.3	2	3	3	5	5	3.3	3.3
1124	2	2	2	1	2	1.8	2	2	2	1	2	1.8	1.8
1125	1	2	2	2	2	1.8	1	1	1	2	2	1.3	1.5
1126	1	1	2	1	2	1.3	1	1	2	1	2	1.3	1.3
1128	3	3	2	1	3	2.3	2	2	2	1	2	1.8	2.0
1130	3	3	2	1	3	2.3	2	2	2	1	2	1.8	2.0
1131	4	4	3	3	4	3.5	4	3	3	3	4	3.3	3.4
1132	1	2	2	1	2	1.5	1	1	2	1	2	1.3	1.4
1133	5	5	4	5	5	4.8	4	4	3	2	4	3.3	4.0
1134	3	3	2	3	3	2.8	2	2	2	1	2	1.8	2.3
1135	1	1	2	1	2	1.3	1	1	2	1	2	1.3	1.3
1136	4	4	3	3	4	3.5	4	3	4	3	4	3.5	3.5

Table II-13 Thompson disc degeneration grade of L4-L5 motion segments tested in fatigue mode (NU: nucleus, AN: annulus, EP: endplate, VB: vertebral body)

LWS	Observer 1						Observer 2						Overall
	NU	AN	EP	VB	Max	Mean	NU	AN	EP	VB	Max	Mean	mean
1101	4	4	4	3	4	3.8	4	3	4	3	4	3.5	3.6
1104	4	4	3	3	4	3.5	5	4	3	4	5	4.0	3.8
1106	1	1	2	1	2	1.3	1	2	2	3	3	2.0	1.6
1107	2	2	3	2	3	2.3	2	2	4	3	4	2.8	2.5
1108	3	3	3	3	3	3.0	2	2	3	4	4	2.8	2.9
1110	3	3	3	3	3	3.0	2	2	3	3	3	2.5	2.8
1112	3	3	4	5	5	3.8	4	4	2	5	5	3.8	3.8
1113	1	1	2	1	2	1.3	2	2	2	1	2	1.8	1.5
1119	2	2	2	1	2	1.8	2	2	2	1	2	1.8	1.8
1120	3	3	2	3	3	2.8	2	3	3	3	3	2.8	2.8
1123	5	5	5	5	5	5.0	5	5	5	5	5	5.0	5.0
1124	1	1	3	1	3	1.5	2	2	3	1	3	2.0	1.8
1125	2	2	2	1	2	1.8	2	3	3	2	3	2.5	2.1
1126	1	1	3	1	3	1.5	2	2	4	1	4	2.3	1.9
1131	4	4	4	4	4	4.0	5	5	5	5	5	5.0	4.5
1133	2	2	2	1	2	1.8	2	2	2	1	2	1.8	1.8
1135	1	1	2	1	2	1.3	2	2	2	1	2	1.8	1.5
1136	4	4	4	3	4	3.8	4	4	5	4	5	4.3	4.0

Part III Shear Experiments

Daniel M. Skrzypiec, Anke Klein, Felix Stahmer,
Michael M. Morlock, Klaus Püschel, Gerd Huber

1 Shear - Introduction

Lumbar spines are exposed to complex loading conditions with load amplitudes ranging above 2 kN during everyday activities. Their mechanical properties, such as stiffness, viscoelasticity and ultimate strength, are well known for axial loading conditions. However, little is known about the corresponding properties when spinal segments are exposed to anterior-posterior shear loads. It is unclear which structures in the human body are most affected by shear loading.

It is important to study these mechanical properties, however, because shear loads are considered to be a risk factor for lower back pain. In particular, whole-body vibrations during sitting postures in the workplace, such as those caused by large construction machines or fork-lifts, are currently in the focus of healthcare science. To account for this potentially dangerous work condition, regulations limiting the total amount of vibration exposure (2002/44/EG) have been established. However, those limits might be insufficient, as there is little experimental evidence considering the amount of vibration exposure (critical exposure) in the horizontal direction, which could cause failure of the human spine.

There are only a few studies investigating the effect of shear forces on the spine. These mainly use in vitro experiments as a source of information. Yingling and McGill (1999) investigated the mechanical behaviour of 56 porcine cervical motion segments exposed to anterior shear while pre-loaded with a compressive load of 300 N. They measured the contributions of the individual spinal structures by serial dissection. They gave results for the whole functional spinal unit, for a motion segment without posterior ligaments, and for a disc segment. It was shown that dynamic loading (load rate of 10,810 N/sec) as well as flexion of the motion segments (about 10°) increased the ultimate strength compared to quasi-static loading (load rate of 100 N/sec) or neutral postures, respectively. The ultimate strength of the disc reached up to 70 % of the shear resistance of complete functional spinal units. Despite the fact that the pars interarticularis were the primary site of failure and that the facets were not involved in the initial 2 mm of displacement, the posterior elements only bore 30% of the shear load. Furthermore, higher load rates caused endplate avulsion, specifically laterally close to the annulus.

Van Dieën et al. (2006) also used porcine lumbar motion segments in their investigation. They harvested 38 spines and dissected them into three functional spinal units (T13-L1, L2-L3, L4-L5). About one half of the specimens were used to investigate the differences between whole functional spinal units and disc segments only, while the other half were used to compare the effect of 10° flexion compared to a neutral position. In each subset, one third of the specimens were tested with a single overload while the others were exposed to cyclic loading with two different load levels (20% and 80% of the corresponding ultimate strength). All measurements

were performed in combination with a compressive pre-load of 1600 N. It was hypothesised that the ultimate strength of the functional spinal units in flexion would be lower than those in neutral position due to the increased load bearing of the intervertebral disc, which in this case is less protected by the posterior elements. However, flexion did not decrease the cycles to failure nor change the specimens' stiffness, but obviously the specimens without posterior elements failed earlier than the intact specimens. As long as the posterior elements were intact, no disc failure under cyclic loading was observed. This was also true for the severely flexed specimens.

Animal experiments furnish good insight into the possible failure mechanisms that could arise if spinal specimens are exposed to shear loads. They also provide reasonable starting values for human cadaveric spine experiments. However, absolute values measured in animal experiments are not representative for the situation in humans. Cripton et al. (1995) measured the ultimate strength of human lumbar functional spinal units (range L1-2 to L4-5) under shear load. They compared constrained and unconstrained segments without a compressive pre-load as well as constrained segments with two different levels of compressive pre-loads. Quasi-static (0.5 mm/s) and dynamic (50 mm/s) measurements were performed for all four groups. Without a compressive pre-load, constrained specimens could withstand an average failure load of 2776 N under quasi-static loading and 2894 N under dynamic loading. For the unconstrained case, the failure load decreased to 1292 N and 1767 N, respectively. The average ultimate strength of axially pre-loaded specimens under unconstrained quasi-static shear force was 1710 N and 2220 N under dynamic loading. These were the values for typical physiological axial loads (700 N). This strength changed to 1780 N and 1900 N in the dynamic case for very high compressive pre-loading (2200 N). Generally, the apophyseal joints failed first and the remaining disc still resisted 77% of the ultimate failure load after damage. An intrinsic problem with this test design was that the number of specimens within each group was rather small, rarely exceeding three specimens. Consequently, Cripton et al. could not distinguish between gender, age and spinal level. Furthermore, the age range was rather broad (35-71) and was not characteristic for people of working age, who are the main focus of this report.

Intraspinal forces caused by whole-body vibrations were estimated using a finite element model based on human anatomy (Seidel et al., 2008b). It was shown that positive dynamic peak force in shear direction at the L4-L5 level varied from 49 N to 324 N for forklift and harvester drivers, respectively. When the estimated maximum static shear force of 410 N is added to maximum dynamic loads, the shear force can exceed 700 N. Using the same models, white noise excitation with a magnitude of 1.8 ms^{-1} led to a similar shear load (64 N to 225 N) in segment L2-L3 (Hinz et al., 2008).

Previous research on human spines hardly addresses the influence of age, gender, and disc height loss due to creep on shear properties (Cripton et al., 1995; McGlashen et al., 1987; Lin et al., 1978). However, these factors play an important role when compressive forces are considered. It is known that the neural arch has to resist increasing loads with increasing age (Pollintine et al., 2004) and that disc height loss causes a load transfer from the discs to the neural arch (Adams et al., 1996). There is evidence that female spines have approximately 11% greater shear

force resistance when compared to male spines while doing the same activities (in vivo study, Marras et al., 2002).
The aim of the presented study was to determine the mechanical properties, such as stiffness and ultimate strength, of functional spinal units for specimens from male donors of working age. This was done for physiologically compressed lumbar human specimens. This data can serve as a basis for further studies, including the influence of repeated cycles.[1]

[1] The presented measurements were performed as an additional task, because during the Kick-off Meeting in Hamburg (09.10.2006) it was agreed to change the original project plan. Instead of the planned creep tests on the L2-L3 motion segments, studies on the ultimate shear strength of the segments appeared to be more promising, especially with regard to the new regulations.

2 Shear - Methods

The general test setup for each functional spinal unit consisted of an initial quasi-static anterior-posterior stiffness measurement followed by a single shear overload to determine the ultimate strength. Afterwards, the remaining stiffness was measured again by quasi-static load cycles. Together with this shear loading, physiological loading conditions in the axial direction were created. Details about the specimens and their preparation can be found in Part II.

The amount of axial compression was chosen based on the literature review. Duval-Beaupere (1987) expected 44 % of body weight for the vertebra at the L3 level. The mean axial load received was about 352 N (within the range of 269 N to 499 N). Andersson et al. (1984) studied spinal loading during different sitting activities. Based on their disc pressure measurement, loading from about 370 N to 530 N appeared to be appropriate. Specifically, 500 N were given for unsupported relaxed sitting. Furthermore, it was mentioned that sufficient time for creep (about three hours) has to be guaranteed so that the measurements will be performed while the specimens are in equilibrium. Gardner-Morse et al. (2004) performed non-destructive shear tests with pre-loads of 0 N, 250 N and 500 N. They hypothesised that the two load levels represent spinal loading for standing and sitting. In previous experiments performed by the authors (project F1899, Huber et al., 2005), a nearly linear correlation between nucleus pressure (p_{nuc}) and axial loading of the segment (F_{seg}) was found. The nucleus pressure in an L4-L5 segment can roughly be calculated as:

$$p_{nuc} = 0.1\,\mathrm{MPa} + 0.7\,\frac{\mathrm{MPa}}{\mathrm{N}} \cdot F_{seg} \quad . \qquad \text{(III-1)}$$

Using this equation and the findings of Wilke et al. (1999), who measured nucleus pressure of 0.46 MPa for unsupported relaxed sitting, segmental loading of 500 N appeared to be appropriate for the physiological loading.[2] However, the appropriate range for axial compression is broad. The two-fold loading of 1000 N would also lead to a physiological loading (0.8 MPa). Therefore, measurements with specimens preconditioned by the higher load were included in the test design as well.

2.1 Shear load application

For the experiment, high shear forces had to be applied while the specimens were under constant physiological compression. Therefore, the specimens were mounted in the test rig in an orientation similar to that in a supine position, i.e. with the superior-inferior axis horizontal and the anterior side of the specimen facing upwards. The superior vertebrae were mounted to the upper moveable attachment while the inferior vertebrae were attached to the fixed side of the test rig. In this way the

[2] The test rig discussed at the Kick-off Meeting in Hamburg (09.10.2006) turned out to be unusable for this study. We had planned to use the F1899 project's test rig again, but the truss-actuator design proved to be problematic, and therefore a new test setup had to be built. (We had assumed that the specimen could be rotated by 90° to allow the test rig hydraulic actuator to apply the shear load and the additional actuator on the truss to apply the axial compression. However, the truss-actuator had a force limit of 400 N, which was insufficient.)

vertical hydraulic actuator of the testing machine (Bionix, MTS, Eden Prairie, MN, USA) could apply the cyclic anterior-posterior shear load forces, and by moving further upwards, it could also generate the anterior shear load till failure (Figure III-1).

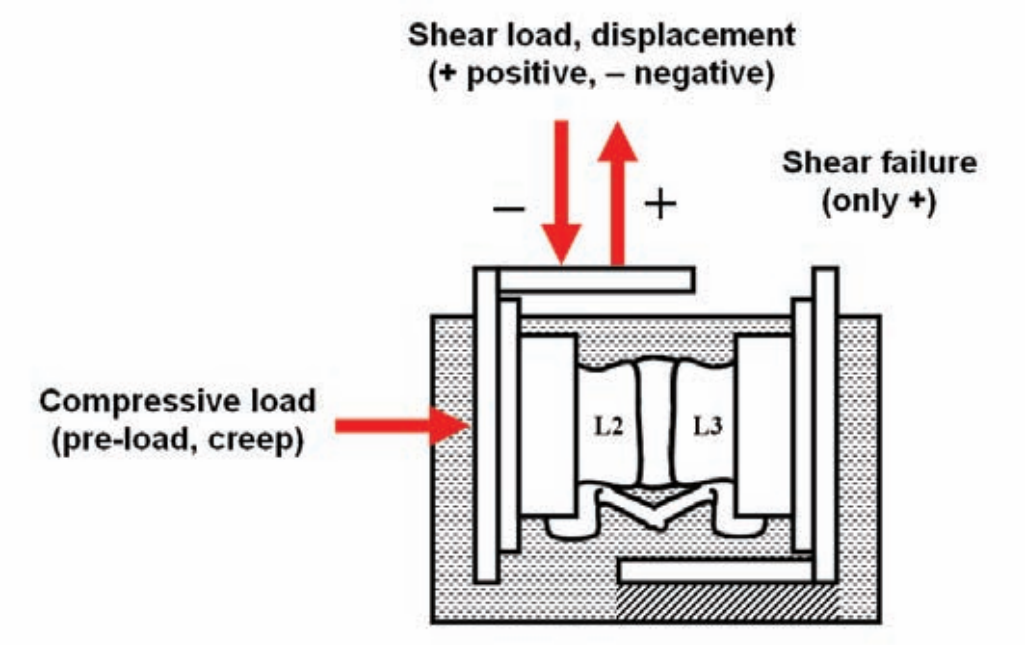

Figure III-1 Schematic view of the shear setup showing the specimen orientation and the corresponding loads

The two remaining translational degrees of freedom were unrestrained due to a 2D linear bearing allowing low-friction movements in both horizontal directions. This bearing was anterior-posterior and lateral with respect to the specimen orientation. The sturdy right-angled brackets for the attachment of the specimens were designed to remain rigid during the testing process (Figure III-2, Figure III-3), thus effecting a constrained mounting for the rotational degrees of freedom.

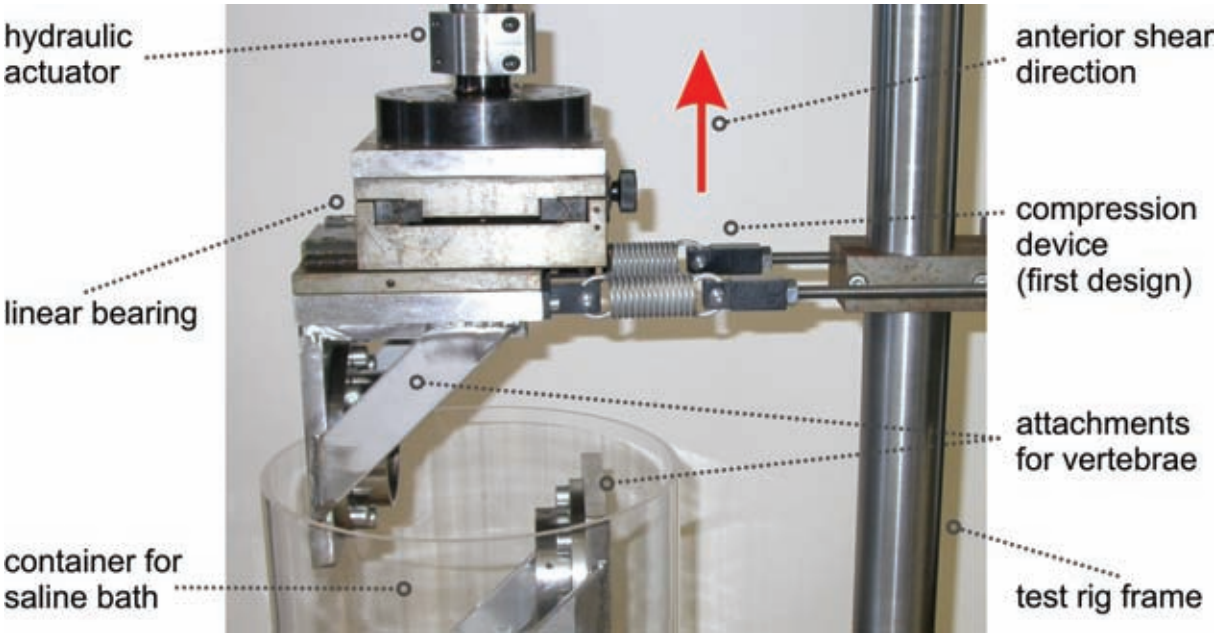

Figure III-2 First design of the shear test rig

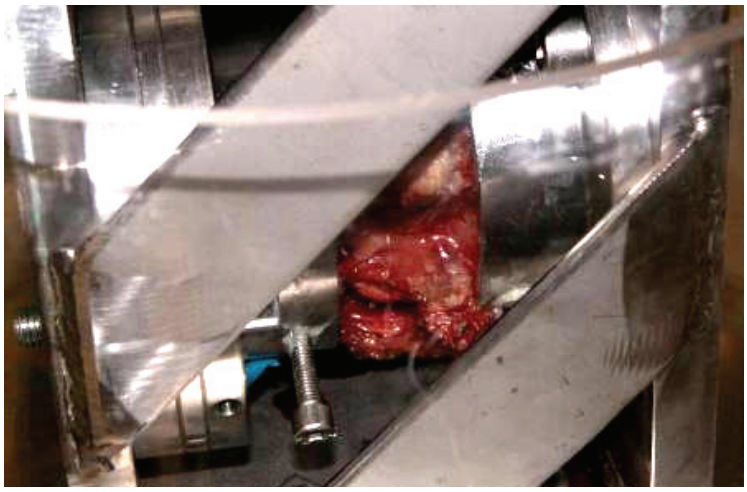

Figure III-3 Spinal specimens attached between the brackets (close-up)

On the fixed side at the bottom, the standard test rig load cell (axial-torsional load transducer, Model 662.10B-05, S/N V98547, MTS, Eden Prairie, MN, USA) and a sophisticated 6D load cell (Model 30031, Huppert, Herrenberg, Germany and carrier frequency amplifiers, Peekel Instruments GmbH, Bochum, Germany) were attached.

The axial compression was achieved by conservative systems applying a passive pre-load without a controlled actuator. The initial test apparatus was constructed with soft springs of combined stiffness of around 20 N/mm and a stretching device. These springs could be stretched by means of a threaded rod with a pitch of 1.5 mm until the required compressive load (measured by the load cell) was reached. The low stiffness of the springs was thought to allow approximately constant compressive conditions and to permit small manual adjustments during testing, thus compensating for the motion segment height loss. During pilot measurements, however, the compression force increased by almost 20% during the shear overload. This showed that the specimen's height changes exceeded the expected maximum value of 1 mm (Figure III-4). This undesirable axial height increase increased the length of the springs and resulted in the increased compressive load.

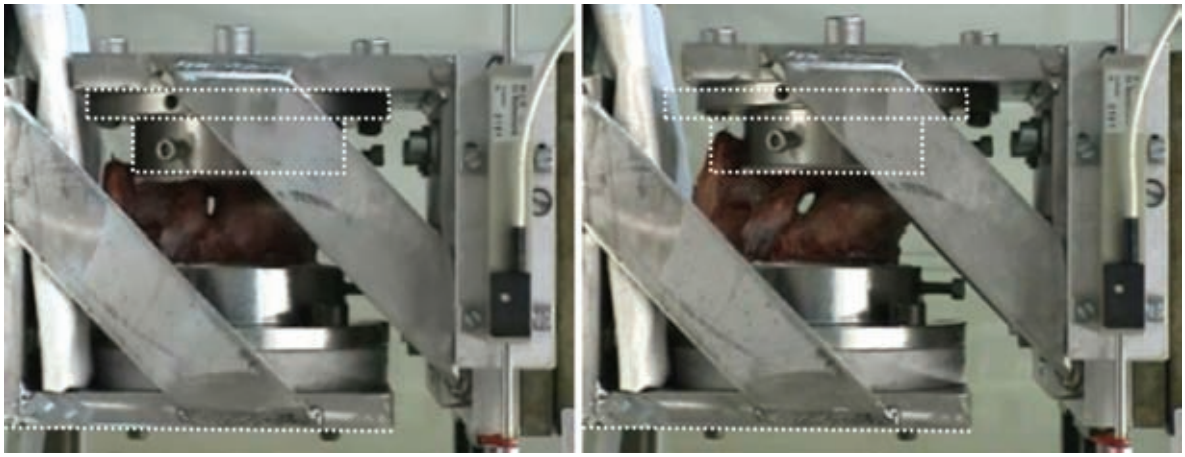

Figure III-4 Height changes during loading in anterior direction (rotated figures by 90° in comparison to previous figures, anterior on the right, superior at the top). Initial position of the specimen (left) and axial height increase during shear overloading (right) is shown.

Due to the available space, reduction of the spring stiffness and consequently elongation of the threaded rod was not possible. Therefore, the spring compressive pre-load system was replaced by a dead weight system (Figure III-5).

The dead weights were connected to the upper attachment of the specimen by means of strings. These strings were deflected by passing a low-friction nylon cable pulley. The linear bearing enabled the complete load transfer to the specimen. No bending moment was applied to the actuator of the hydraulic test rig. Furthermore, due to the long unguided length of the strings (linear bearing to guide pulley), changes of the load caused by alterations of the actuator height during the specimen loading were negligible.

The dead weight system enabled improved application of the compressive pre-load. During loading to shear failure, the compression of the specimen increased by only about 5%, which might be related to the friction within the linear bearing or to negligible dynamic effects.

Figure III-5 Compressive pre-load is applied with dead weights connected to the upper attachment of the specimen with strings.

To investigate the increase in the specimen height, a displacement sensor was attached to measure it. The sensor, which was oriented parallel to the compressive pre-load, is shown in Figure III-6. Its values were recorded via the analogue-digital converter of the hydraulic test system.

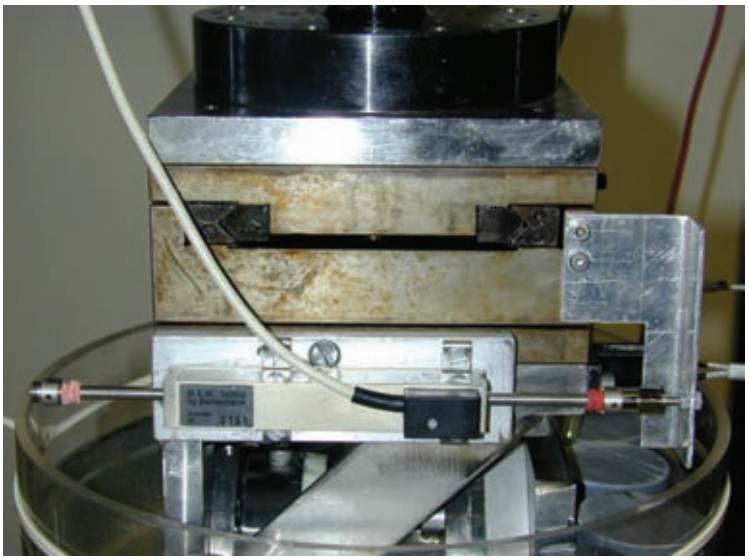

Figure III-6 Displacement sensor mounted parallel to the specimen's superior-inferior axes

The rig functioned well, but its reliability was strongly dependent on the mounting of the specimens. It was necessary to achieve the precise parallel orientation of the two potting cups relative to each other and to the horizontal mid-plane of the disc. Therefore, a previously used potting holder (Huber et al., 2005, F1899) was used. Furthermore, the fixture of the specimen within the potting mould was improved by the insertion of several wood screws into the vertebral body and the posterior elements (Figure III-7).

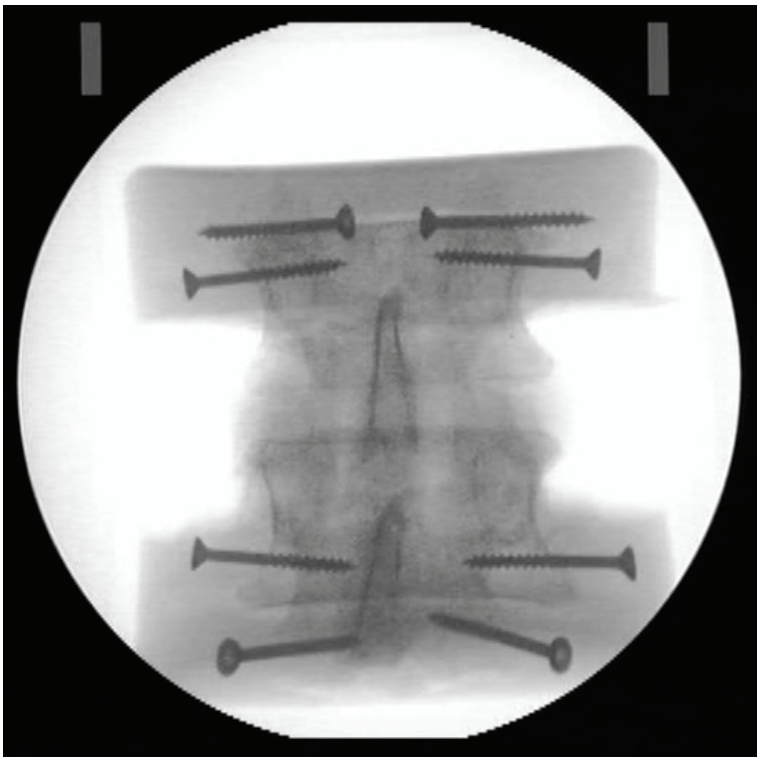

Figure III-7 Post-measurement X-ray image showing the position of the embedded screws

Measurements were performed with specimens immersed in a saline bath with a controlled temperature. The saline had almost physiological osmotic pressure (eight Ringer tablets per litre, Merck, Darmstadt, Germany). The constant temperature of 37°C was achieved with a custom-made temperature control system (Witt et al., 2007, see 0). This system comprises a PT100 temperature sensor (DIN EN 60751) with an in-head transmitter (Type 104, LKM electronic GmbH, Geraberg, Germany), a custom-made PC controller box, a roller pump (SR25, Rietschle Thomas Puchheim GmbH, Puchheim, Germany), and a heat exchange system (F6/B5, Haake Mess-Technik, Karlsruhe, Germany).

2.2 Shear test protocol

Four different groups of human lumbar functional spinal units were tested for anterior-posterior shear load stiffness and anterior shear ultimate strength. Those groups were called 'Young-Neutral', 'Old-Neutral', 'Young-Creep' and 'Young-Flexion'. The terms referred to the age of the donors. 'Young' stood for specimens from adult donors in the first decades of their working age, i.e. between 20 and 40 years old. 'Old' referred to specimens from donors at the end of their working age, i.e. between 50 to 60 years old. 'Neutral' described specimens tested in a neutral straight posture, potted into the holders without any kind of restriction forces. The term 'Creep' referred to specimens tested in the 'Neutral' manner, but the test protocol of those specimens was expanded by applying a long preconditioning period (1 hour) of constant axial load to enable axial creeping of the motion segment. The last group, 'Flexion', was also evaluated with the same test protocol, but the vertebrae were flexed by 5° each, so that the complete segment flexion was 10°. The first three groups mainly included L2-L3 segments from the same spines, the L4-L5 segments were harvested for the dynamic and fatigue experiments of this project.[3]

All segments beyond the six in the first two groups and all specimens in the 'Young-Flexion' group were derived from spines that either had damaged L4-L5 segments or from spines that had already been harvested for the F1899 project. It is assumed that thawing-freezing cycles have a bigger influence on mechanical properties than the length of storage time in the freezer. The aim of these additional tests was to give an idea of what to expect and also to expand the data bases.

After mounting the specimen to the materials testing machine, the bath container was filled with Ringer's solution and kept unloaded for 0.5 hours to bring the specimen to 37°C and equalise the temperature. First, all specimens were preconditioned by a compressive creep load of 500 N for 900 s.

Second, the anterior-posterior shear stiffness was determined while a compressive pre-load was still being applied (terminus: 'start'). This was done by loading the specimens up to +200 N (towards anterior), down to -200 N (towards posterior), and up to 0 N (towards anterior). This was repeated twice with the constant ramp load rate of 50 N/s (Figure III-8).

[3] These were the measurements that were a mandatory part of the F2059 project. Based on the commitment during the Kick-off Meeting, these measurements replaced the initially planned pure creep experiments.

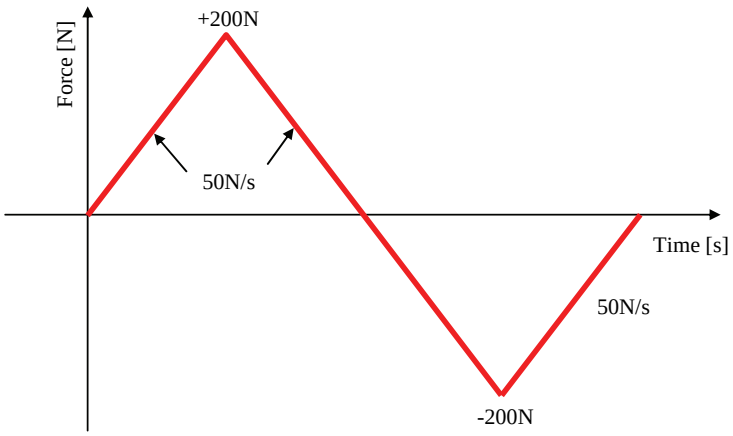

Figure III-8 Parameters of one ramp loading cycle for evaluation of shear stiffness

Third, a single cycle overload was applied to determine the ultimate strength of the specimens. This overload was achieved by a 15 mm anterior displacement of the superior vertebra, or for rigid specimens, by a maximum load of 6000 N instead. The displacement rate was chosen to be 0.5 mm/s, as was used earlier by Cripton et al. (1995). Again, a constant compressive pre-load of 500 N was applied.

Fourth, the anterior-posterior shear stiffness was determined again while the compressive pre-load was applied (terminus: ‘end’).

The only exception to this protocol concerned the ‘Young-Creep’ group. To allow creep prior to the ultimate strength test, the specimens were put under an axial compression force of 1000 N for 1 h. Additionally, the standard shear stiffness measurement was performed to protocol in order to detect any changes that might have occurred during the creep loading (terminus: ‘mid’). In these three stiffness measurements, solely the second load cycle was used for further analyses. Different characteristic values were investigated, but in this protocol mainly the peak-to-peak (PP) stiffness value, defined as the mean stiffness of the hysteresis curve from -200 N to +200 N, is given.

The ultimate strength in the single failure overload experiments was determined by the use of an automatic algorithm. The criterion was to detect the peak shear force prior to the occurrence of a 30 N drop in the load measurements.

3 Shear - Results

The harvested specimens closely matched the intended age range. The mean age between the three groups of young donors only differed by two years. The mean age of the group of old donors was more than 20 years older than that of the younger groups. The standard error of the four groups ranged from 1.7 to 2.8 years. Therefore, the three groups of young donors can be regarded as one age group while the fourth group is significantly older (Table III-1).

Table III-1 Complete overview of the L2-L3 specimens used in the shear test

	Flexion	Age [years]		N	Specimen ID
		Range	Mean ± STD		
Young-Neutral	0°	20 - 44	31.6 ± 9.0	12	1106, 1107, 1112, 1119, 1120, 1125, 1126, 1134, 0004, 0011, 0012, 0033
Old-Neutral	0°	48 - 64	54.3 ± 5.5	10	1101, 1104, 1109, 1110, 1121, 1122, 1128, 1130, 1131, 1136
Young-Creep	0°	22 - 38	29.8 ± 6.9	6	1116, 1123, 1124, 1132, 1133, 1135
Young-Flexed	10°	27 - 37	31.5 ± 4.2	4	0003, 0028, 0036, 0052

3.1 Shear stiffness results

The measured hysteresis showed the typical sigmoid shape. Consequently, the linear PP stiffness value used is only a rough estimation of the complex deformation-force behaviour of spinal specimens. The reversal point (lowest stiffness) does not necessarily have to be at the neutral position (no shear displacement or shear load, respectively). Figure III-9 shows an example with the reversal point at the posterior. However, the differences in stiffness both before and after the single overload appear to be sufficiently distinct to enable its exploration with the method used. Two examples of hysteresis are given in Figure III-9 and Figure III-10.

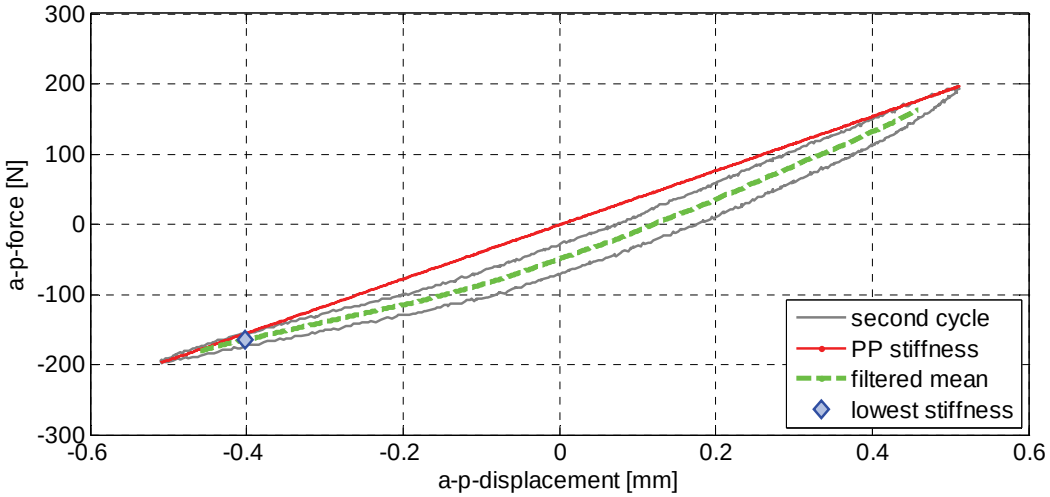

Figure III-9 Typical progressive hysteresis of specimen LWS 1116 prior to overloading

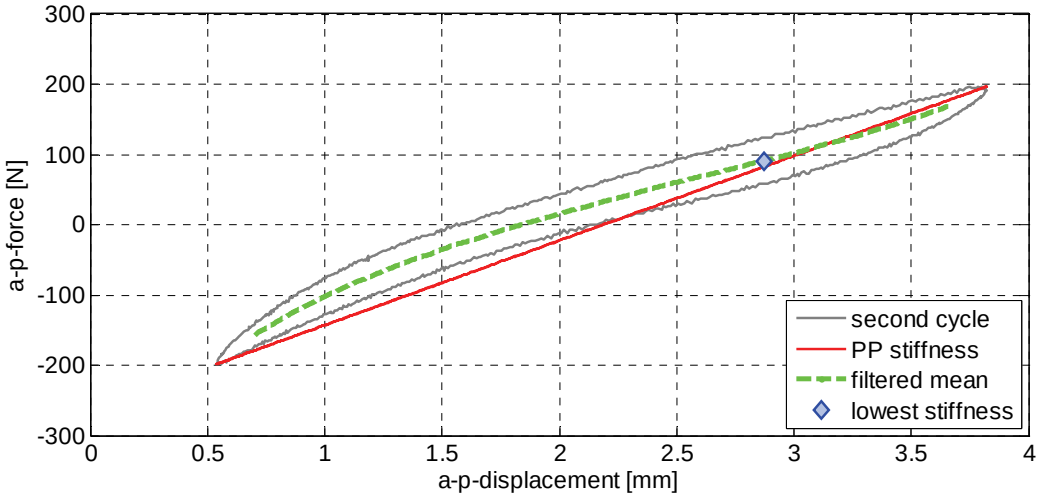

Figure III-10 Sigmoid hysteresis of specimen LWS 1122 after overloading, showing the typical rather low stiffness

The controller's functionality appears to have been largely sufficient. The mean and standard deviation of the actual force controlled loading for the 200 N amplitude command signal were 199 N ± 10 N (-203 N ± 10 N for the negative part). However, in the worst cases a controller error of 20% occurred. Consequently, higher numbers of cyclic repetitions have to be considered for further experiments.

The axial creep loading of 1000 N, which lasted for one hour, did not influence the specimen stiffness (Figure III-11). The mean PP stiffness decreased as little as 10% from its value prior to creep (419 N/mm) to that after creep (377 N/mm). Based on a Tamhane post-hoc test (no homogeneity of variance according to the Levene test), these differences are regarded as not significant ($p = 0.848$). Therefore, there is no evidence to distinguish between the stiffness before and after creep. Further analyses used the start value as a reference. However, there was a significant change in stiffness after overloading the specimens ($p = 0.004$).

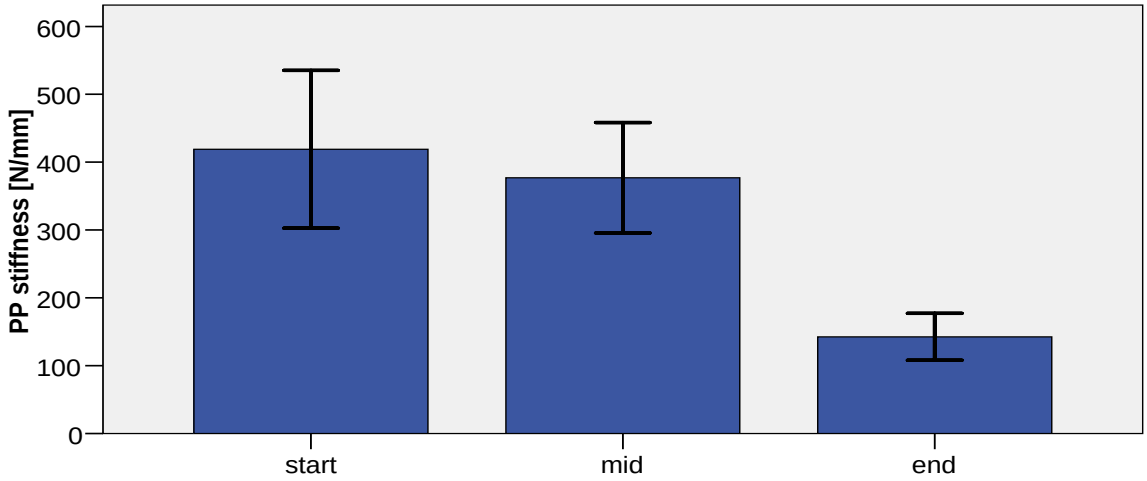

Figure III-11 PP stiffness of the six specimens in the 'Young-Creep' group. The mean PP stiffness (and 95% confidence interval) before and after creep (start and mid) as well as those after single overload (end) are shown.

For the four groups, the stiffness at the beginning of the measurements and after the overload was analysed using a univariate analysis of variance with two factors (group, order). It was found that the overload significantly decreased the PP stiffness by 61% ($p < 0.001$). However, no differences between the groups ($p = 0.583$) were discovered (power was poor: 0.179). In addition, the decrease in stiffness was similar for all four groups ($p_{interaction} = 0.860$; power was poor: 0.095). Results are summarised in Table III-2 and Figure III-12.

Table III-2 Descriptive statistics for PP stiffness

Group	Order	Mean [N/mm]	STD [N/mm]	N
Young-Neutral	start	446	101	12
	end	176	67	12
Old-Neutral	start	410	102	10
	end	176	63	10
Creep-Neutral	start	419	111	6
	end	142	33	6
Young-Flexed	start	408	96	4
	end	132	29	4
Total	start	425	99	32
	end	164	58	32

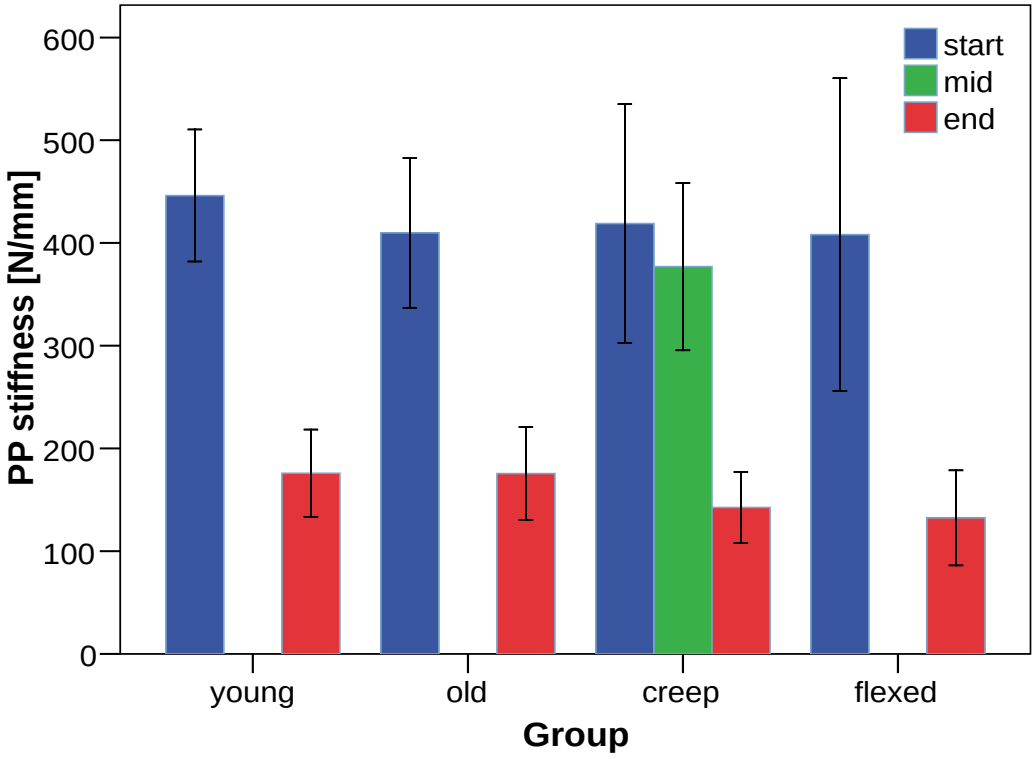

Figure III-12 Mean values and 95% confidence interval of all stiffness measurements

For further examination of the influence of age, only the specimens of the 'Young-Neutral' and 'Old-Neutral' groups were examined by means of regression analyses. However, no strong evidence was found either before or after the series of consecutive measurements that age influenced the PP stiffness (r^2_{kor} = 0.135; p = 0.052 and r^2_{kor} = -0.043; p = 0.722) of the functional spinal units (Figure III-13).

The small degree of explained variation is similar regarding the regression between the PP stiffness of the specimens before overload and the bone mineral density (BMD: r^2_{kor} = 0.146; p = 0.044) and also for regressions depending on the combinations of age and BMD (r^2_{kor} = 0.159; p = 0.74). However, at least for the regression of PP stiffness, depending on BMD, the influence appears to be significant.

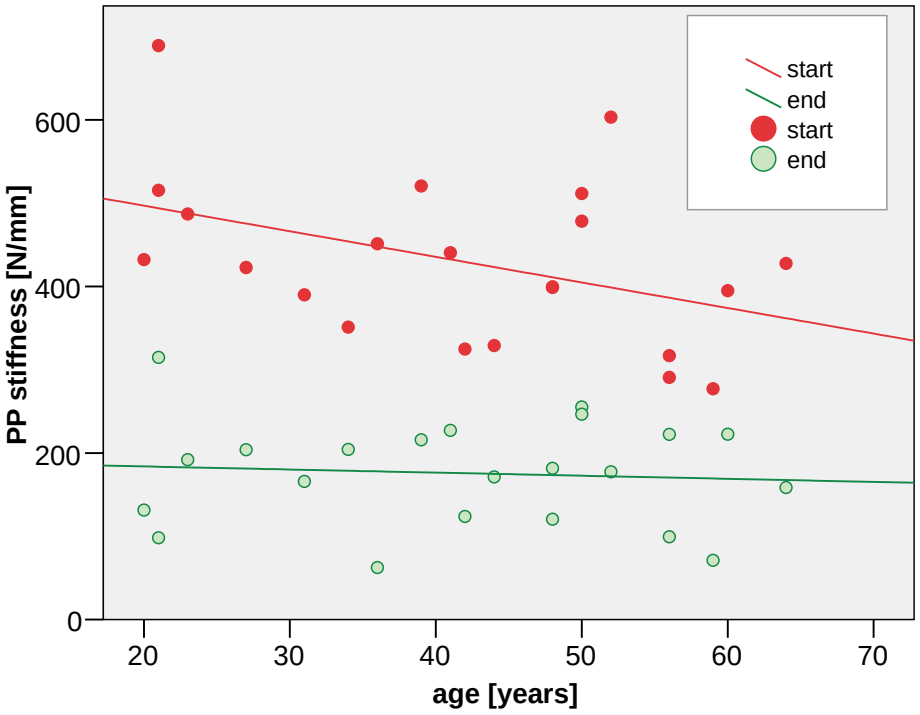

Figure III-13 Regression between PP stiffness and age for the specimens at the beginning and end of the consecutive measurements

3.2 Motion segment height increase

During the 15 mm shear overload tests, an increase in the height of the motion segment (Figure III-14) was observed. In the initial part of the shear displacement, all specimens showed a toe region. After the toe region (approximately 1.2 mm), the motion segment increased the height in all cases. Three parameters were chosen to describe this phenomenon (Figure III-14): total axial height increase Δh (Table III-3), initial shear displacement Lh5% at 5 % of the axial height increase (Table III-4), and shear force Fh5% corresponding to 5 % of the axial height increase (Table III-5).

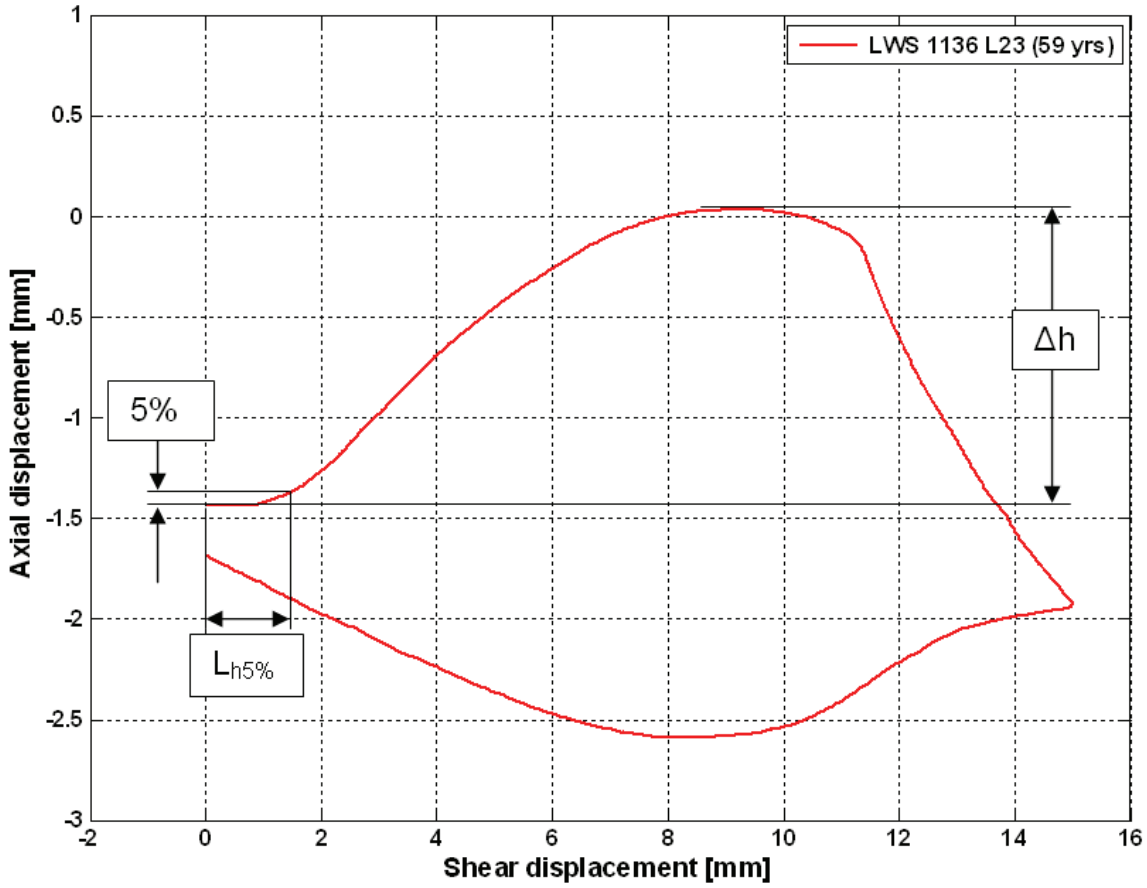

Figure III-14 Example of a height increase curve indicating parameters chosen for analysis (axial displacement does not start from zero as it includes the height decrease caused by the application of a 500 N compressive load)

The total axial height Δh of specimens in flexion increased the least during shear overload, but the difference did not reach significance ($p = 0.127$, Table III-3). Initial shear displacement Lh5% was the longest for specimens tested in flexion and differed significantly from 'Young-Neutral' and 'Old-Neutral' groups ($p < 0.05$, Table III-4), but was marginally non-significant for 'Young-Creep' group ($p = 0.054$). Shear force Fh5% was the biggest for specimens tested in flexion but this difference was not significant ($p = 0.111$, Table III-5).

Table III-3 Motion segment total axial height increase (Δh) during 15 mm shear overload

Group	Mean [mm]	STD [mm]	N
Young-Neutral	4.27	1.41	11
Old-Neutral	3.81	1.61	9
Creep-Neutral	3.78	1.07	6
Young-Flexed	2.31	0.52	4

Table III-4 Initial shear displacement ($L_{h5\%}$) at 5 % of axial height increase

Group	Mean [mm]	STD [mm]	N
Young-Neutral	1.20	0.28	11
Old-Neutral	1.17	0.25	9
Creep-Neutral	1.17	0.24	6
Young-Flexed	1.64	0.23	4

Table III-5 Shear force ($F_{h5\%}$) causing 5 % of axial height increase

Group	Mean [N]	STD [N]	N
Young-Neutral	624	187	11
Old-Neutral	585	108	9
Creep-Neutral	603	76	6
Young-Flexed	817	234	4

Three types of motion segment height change were observed. (I) The motion segment increased in height with increasing shear displacement up to a maximum, followed by a relative decrease in height at maximum shear displacement; see Figure III-15 (I). (II) The motion segment increased in height with increasing shear displacement up to a plateau; see Figure III-15 (II). (III) The axial displacement increased linearly with shear displacement; see Figure III-15 (III). The allocation within tested groups is shown in Table III-6. Specimens tested in flexion had the relatively largest numbers of type I and II curves.

Table III-6 Allocation of height increase curves amongst tested groups

Group	I	II	III
Young-Neutral	0	4	7
Old-Neutral	2	2	5
Creep-Neutral	0	3	3
Young-Flexed	2	2	0

When only types of curves were considered, the total height increase Δh was the largest in type III curves and this difference was significant ($p < 0.001$, Table III-7). The other parameters Lh5% and Fh5% did not show any significant differences ($p = 0.206$ and $p = 0.417$, respectively, Table III-7).

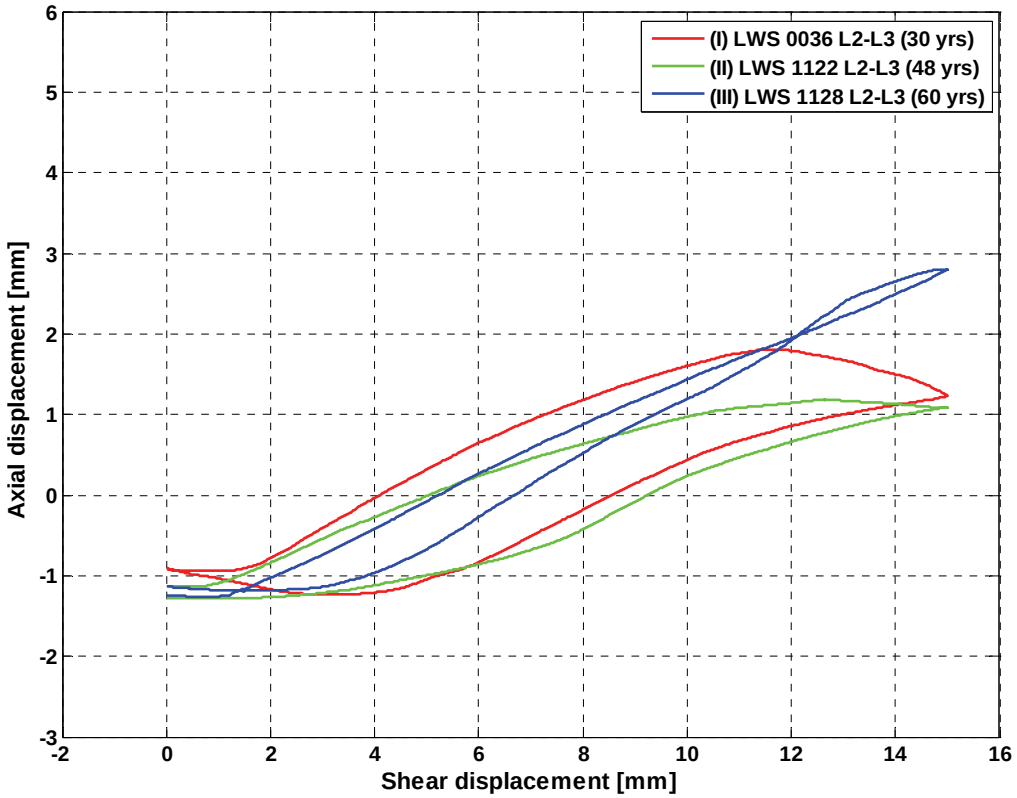

Figure III-15 Three types of curves of motion segment height change were observed during shear overload (axial displacement does not start from zero as it includes the height decrease caused by the application of a 500 N compressive load).

Table III-7 Parameters of disc height increase curves

Type	Δh [mm]	$L_{h5\%}$ [mm]	$F_{h5\%}$ [N]
I	2.23	1.51	700
II	2.73	1.28	675
III	4.95	1.14	586

3.3 Ultimate strength results

Examples of shear overload curves are shown in Figure III-16. The results of the ultimate strength test showed a trend of flex specimens having the greatest strength but did not show a clear picture of the differences between the other investigated groups. Figure III-17 shows a scatter plot of all single data points.

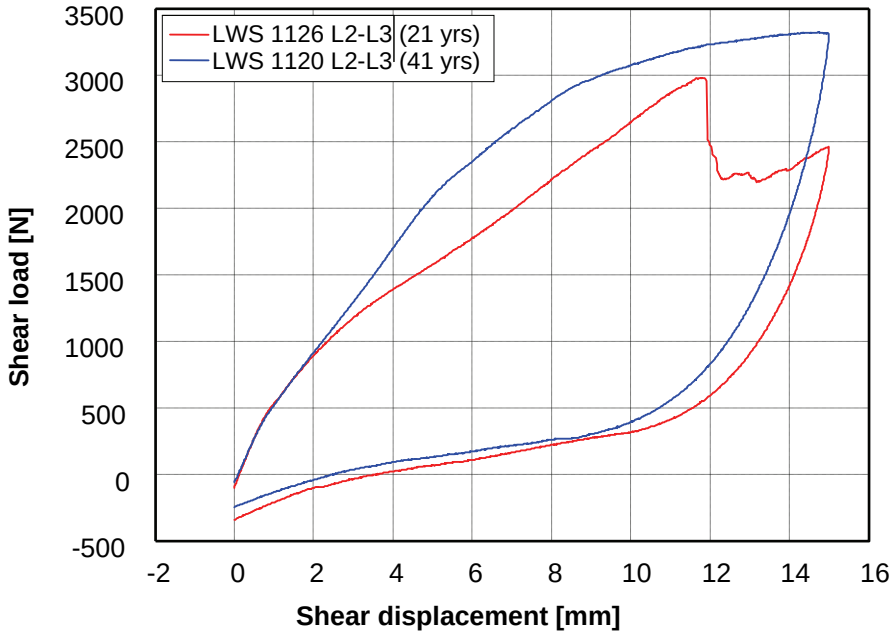

Figure III-16 Two examples of a load displacement curve recorded during shear experiments. The red curve indicates a specimen showing ultimate failure and the blue curve represents a specimen with only a marked decrease in stiffness.

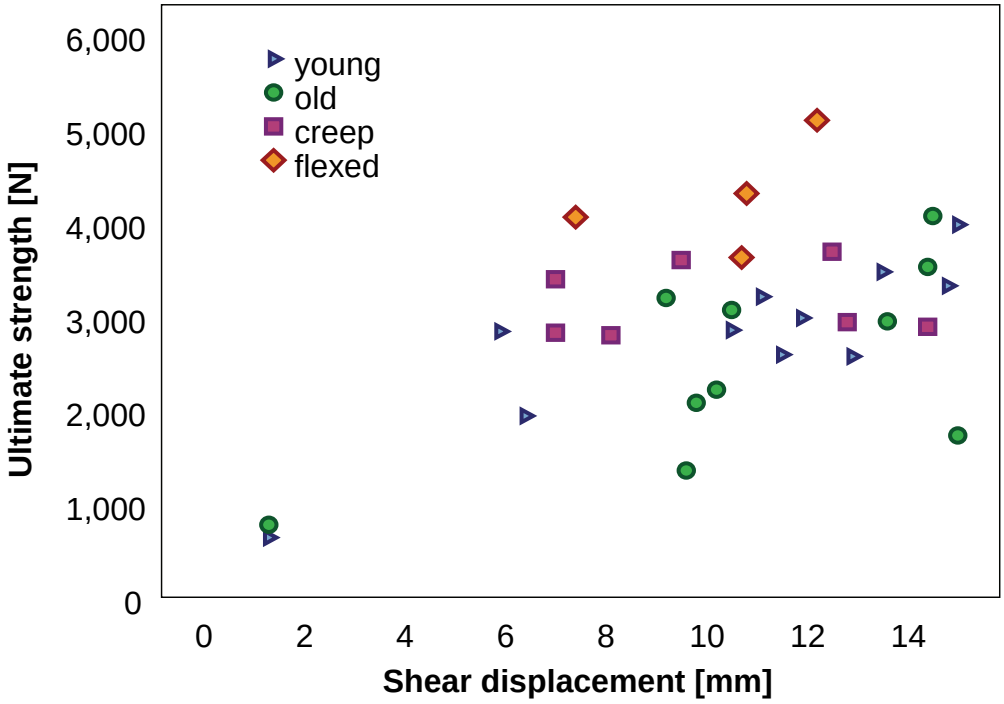

Figure III-17 Scatter plot of all measurements involved in this study

For specimens surviving an anterior-posterior displacement exceeding 14 mm, the 30 N drop criterion is not reliable, because the drop could have been caused by the backwards movement of the actuator after reaching 15 mm and not by ultimate

failure of the specimen. Therefore, the marker in Figure III-17 indicating ultimate failure around 15 mm does not necessarily indicate failure. A similar misinterpretation could have been caused at the beginning of the load ramp. Furthermore, imperfect controller settings or any kind of slip-stick in the system could have caused a small force drop at the beginning of the loading. Consequently, those specimens with detected failures before 2 mm of displacement or after 14 mm were excluded from further analyses. Therefore, the total number of specimens decreased from 32 to 23 (Table III-8).

Table III-8 Ultimate strength of the specimens in the four groups

Group	Mean [N]	STD [N]	N
Young-Neutral	2802	462	8
Old-Neutral	2471	717	6
Creep-Neutral	3105	364	5
Young-Flexed	4265	615	4
Total	3036	802	23

The specimens in the four groups showed significantly different failure loads ($p = 0.001$). Based on the Tukey post-hoc test, the ultimate strength of the specimens in 10° flexion is more than 37% higher than those of the others (vs. 'Young-Neutral' $p = 0.002$; vs. 'Old-Neutral' $p < 0.001$; vs. 'Young-Creep' $p = 0.025$). However, there were no differences between the other groups.

The specimens in neutral posture from the young donors and old donors did not exhibit a significant relation as a function of BMD (Figure III-18). There is a low correlation coefficient ($r^2_{corr} = 0.146$) that only follows a statistical trend ($p = 0.098$).

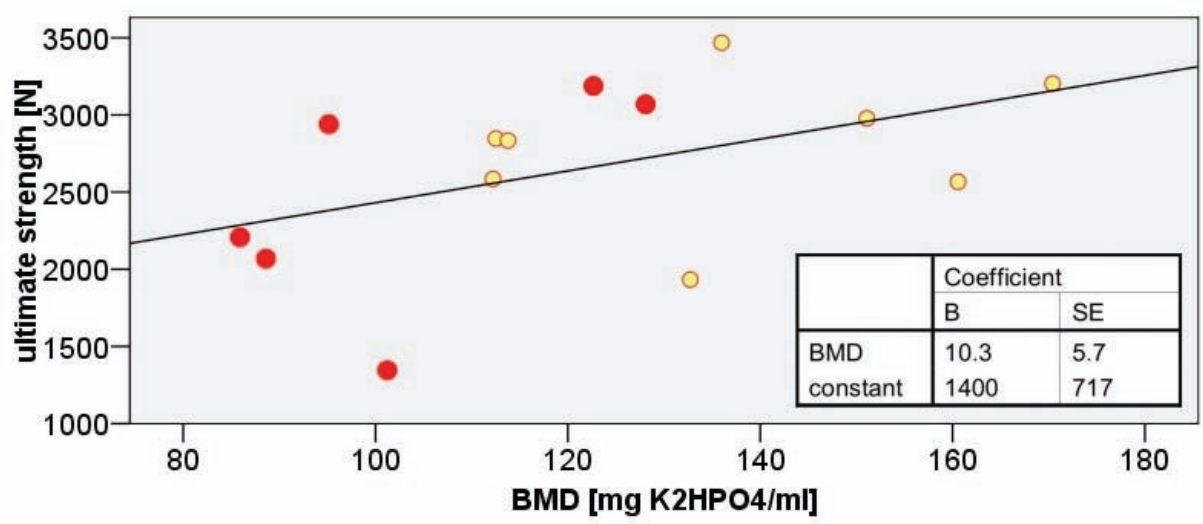

Figure III-18 Regression between BMD and ultimate strength. Red markers indicate the specimens from the 'Old-Neutral' group; the yellow markers represent the 'Young-Neutral' group.

4 Shear - Discussion

The observed differences between the investigated groups of spinal L2-L3 specimens are not as distinct as expected. In future studies it might be necessary to include further individual parameters to be used as covariates or to normalise the test data (e.g. size of specimen). In any case, the findings are only valid regarding the rather stiff and constrained boundary conditions used in this study. For the shear test, the rotational degrees of freedom were bounded, which differs from the in vivo situation.

Single overload decreases spinal stiffness by almost two thirds. The morphological overview supports the opinion that mainly the posterior structures (par interarticularis) are destroyed. However, regarding the rather high shear deformation of the specimen (sometimes almost 15 mm) until the single failure overload, the authors are not able to distinguish between the deformation of the specimen and the errors caused by the test design.

The ultimate shear forces recorded in this study are well above the shear peak forces in whole-body vibration estimated by Seidel et al. (2008). However, when the static maximum shear load is added, the resultant shear force can exceed 700 N.

Shear loading up to 1000 N did not cause ultimate failure in the tested specimens, but it is not clear if the neural structure would suffer injuries if exposed to this level of shear load in vivo.
The motion segments tested in 10° flexion showed an increase in shear resistance when compared to the other groups. This is similar to the reports for porcine motion segments reported by Yingling et al. (1999) but is opposite to the findings of Van Dieën et al. (2006).
There is small evidence that with increasing age and decreasing BMD, the stiffness of the spinal specimens and the ultimate strength decrease. However, the number of observations in this study was not sufficient to make a definitive statement.

The reason behind the motion segment height increase remains unclear. The chosen parameters did not differ much between the tested groups, but there was also no clear picture when the types of curves were considered. Additional experiments included in the appendix (Part VIII3, Height Increase) showed that the height increase was due to the unusual behaviour of the motion and disc segments and not caused by the test setup. Further analyses are required considering the geometry of the endplate and apophyseal joints, which might have been responsible for the height change.

Part IV Dynamic Experiments

Gerd Huber, Daniel M. Skrzypiec, Anke Klein,
Klaus Püschel, Michael M. Morlock

1 Dynamic - Introduction

Intervertebral discs show time-, loading-rate- and loading-magnitude-dependent mechanical behaviour. This is caused by the viscoelastic properties of the annulus fibrosus and nucleus pulposus matrix as well as by the poroelastic system, which is composed of intradiscal fluid passing through the matrix and endplate canals.

The most common consequence of this behaviour is the shrinkage of human body height during daily activities and its consequent expansion during bed rest (Broberg et al., 1993) or space flights (LeBlanc et al., 1994). With regard to isolated functional spinal units (FSUs), this effect was extensively investigated by analysing the creep or relaxation behaviour following step-like loading or deformation (e.g. Burns et al., 1984; Kaleps et al., 1984).

The mechanism that leads to creep or relaxation also influences the specimen's properties during dynamic loading. An analysis based on experimental creep curves showed that the specimen's compressive stiffness at 1 Hz loading significantly differs from quasi-static loading (Huber et al., 2003). Various other experiments have shown that the fully hydrated disc provides little resistance to compression at low loads and low loading rates. With more severe loading and at higher loading rates, the disc becomes stiffer. However, beyond a certain loading rate, the disc does not stiffen any further (Race et al., 2000). More specifically, it was shown that the stiffness of the disc did not differ for compressive loading rates of 90 N/s, 900 N/s and 9000 N/s. Koeller et al. (1986) performed axial dynamic compressive experiments on the thoraco-lumbar human intervertebral discs. The loads were sinusoidal, amounting to 950 N ± 450 N at 1 Hz. The energy ratio, which is defined as the ratio of hysteresis energy to energy input, was used to quantify the findings. The lumbar discs showed a decreasing energy ratio up to the middle of the third decade of human life (Koeller et al., 1986). After the age of 40, the energy ratio increases again. No correlation was found between biomechanical behaviour and disc degeneration.

Kasra et al. (1992) performed dynamic mechanical tests on human lumbar motion segments as well as FE analyses. It was found that the compliance magnitude decreases and the resonant frequency increases with a rising motion segment pre-load. The dynamic stiffness at 1 Hz frequency increases with higher compressive pre-loads, while the hysteresis decreases (Kasra et al., 1992). The FE model of the L3-L5 lumbar spine predicted that a spine exposed to vibrations would exhibit different behaviour in different spinal regions. The anterior region showed small vibration amplitudes, but the posterior regions showed large amplitudes, which suggests that they might be particularly susceptible to injury (Guo et al., 2005).

Comprehensive data on those combined effects and which also include values for young donors are demanded for work safety reasons, especially because the validity

of most FE models is still questionable. Furthermore, the dynamic response of FSUs to non-axial directed loading, especially anterior-posterior shear, is still relatively unknown. This is especially true with regard to interactions. For quasi-static tests it is known that the motion segments are on the order of five times more flexible in shear than in compression (Berkson et al., 1979). In one experiment a compressive pre-load of 2200 N resulted in a six-fold increase of that stiffness in shear (Janevic et al., 1991).

The purpose of this study was to investigate the influence of different types of loading (quasi-static and dynamic), different loading levels and amplitudes as well as different directions of loading (compressive and shear). The findings provide a better understanding of intervertebral disc behaviour under dynamic loading conditions and will help to improve FE models. As a consequence, it might enable the prediction of influence and mechanism of dynamic loading on spinal injury.

2 Dynamic - Methods

Eighteen human lumbar L4-L5 motion segments were used for the quasi-static and dynamic testing. They were divided into three groups each consisting of six specimens. The three groups were ‘Young-Neutral’, ‘Young-Flexed’ and ‘Old-Neutral’. The ‘Young’ groups were supposed to contain specimens between 20 and 40 years old (the first two decades of working age), and the ‘Old’ group was intended to contain specimens between 50 and 60 years old (the end of working age). Specimens tested in ‘Neutral’ posture were positioned in cups in a way that preserved the natural position from the dissection (no bending), whereas for specimens of the ‘Flexed’ group, each vertebra (upper and lower) was potted in cups in extension by 5°. Consequently, when the specimen was mounted on the testing machine, 10° of flexion was achieved. Further details about the specimens and their preparation can be found in Part II.

The specimens were tested on a modified hydraulic testing machine (MTS Bionix 858.2, MTS, Eden Prairie, MN, USA) capable of applying compression as well as shear loading. The modification consisted of an additional truss attached to the crosshead of the test rig. On this truss, a second actuator was attached (Figure IV-1) capable of applying a shear load (x-direction) to the specimen. The specimen was screwed to a moveable platform connecting the two actuators by means of elastic beams (no slip-stick effect) allowing movement in two axes (x and z). Further information about the design principles can be found in Huber et al. (2005).

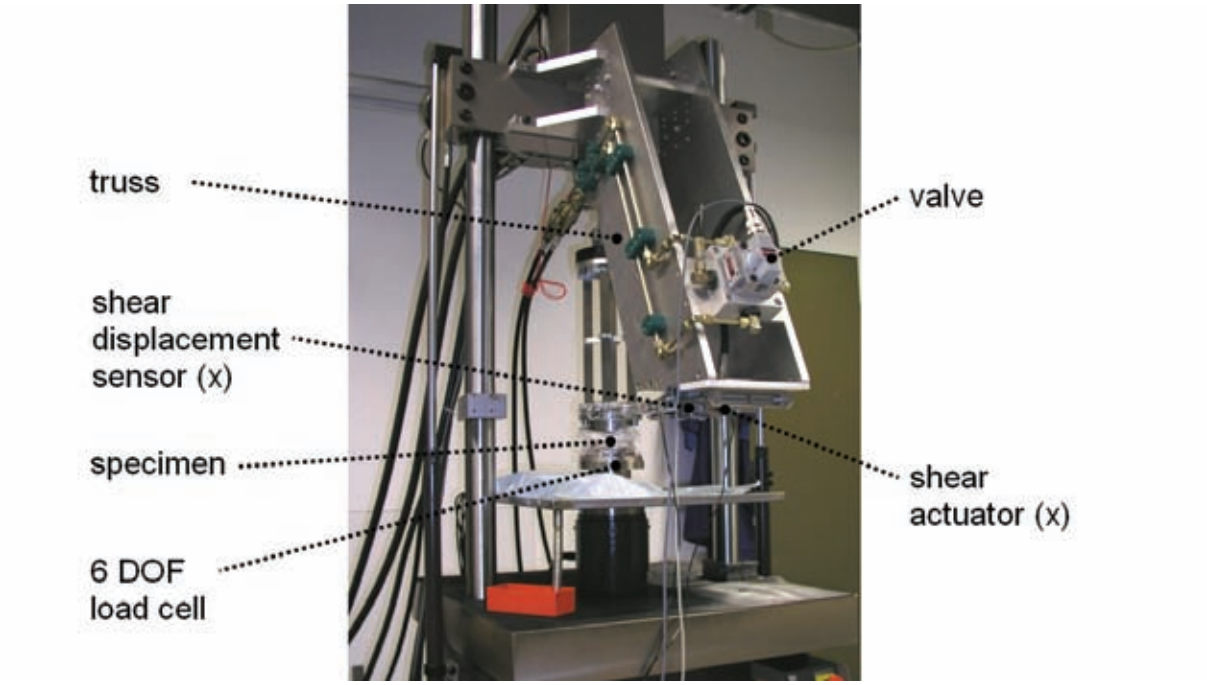

Figure IV-1 The modification of the test setup consisted of an additional truss with a shear actuator attached to the crosshead of the MTS.

In comparison to the previous study (Huber et al., 2005), the method of controlling the additional shear actuator (Type 120 10012-01, Hänchen, Ostfildern, Germany) was changed. In the present study the displacement sensor of the shear axis was connected to an I/O card that was integrated into the testing machine’s controller

system. The valve (Type G76-3012, S10JOGM4VPY, Moog, Böblingen, Germany) of the hydraulic cylinder was actuated by an integrated valve controller (Figure IV-2). This led to a simplified controlling system and allowed to record the data of the additional axis along with those of the standard axial axis.

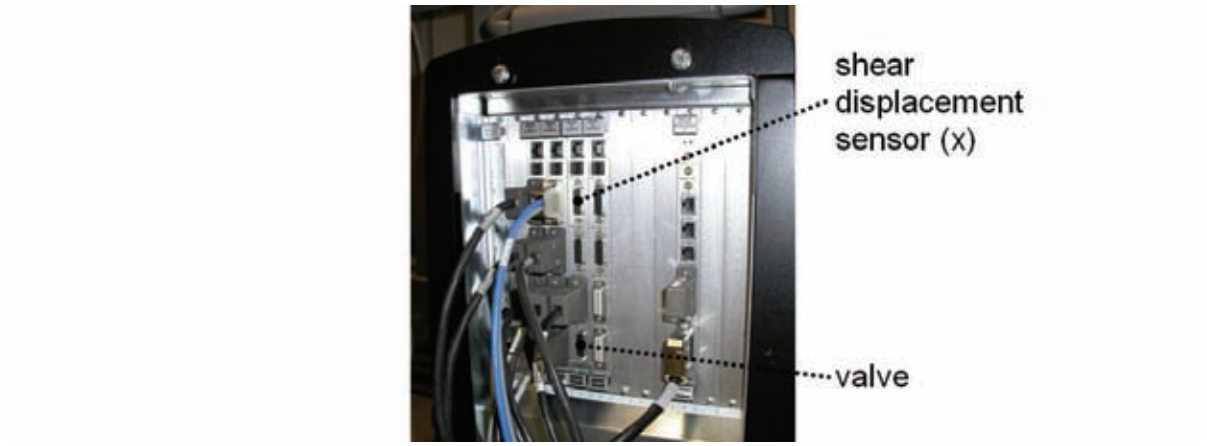

Figure IV-2 Slots for the connections of the valve and displacement sensor of the shear load axis to the controller (front view)

An additional six degree-of-freedom load cell (Huppert, Herrenberg, Germany) capable of measuring forces and moments in the three spatial directions was attached below the specimen. Force-controlled movement of the shear actuator was done based on the signal of this load cell. To verify this, strain gauges were applied on the two coupling elements between the shear actuator and the specimen. The load cell and the coupling strain gauges were connected to two synchronised carrier frequency amplifiers (Picas, Peekel Instruments, Bochum, Germany) and outputs from the amplifiers were connected to the test machine's controller analogue inputs (Figure IV-3).

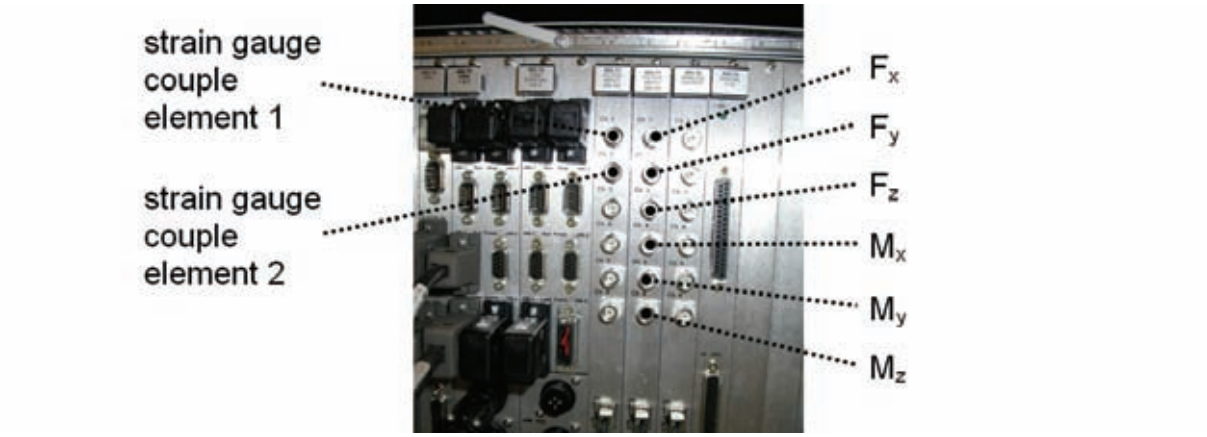

Figure IV-3 BNC connections of the analogue inputs of the loads and moments used for recording signals with the MTS controller (back view)

The test procedures were written using the user interface of the testing machine (Station Manager, version 4.0B 1978, MTS, Eden Prairie, MN, USA). During the quasi-static test, data acquisition was sampled at 5 Hz, and during the dynamic tests, it was sampled at 512 Hz.

The mechanical parameters test always started with quasi-static measurements (Table IV-1) followed by reference measurements (Table IV-2). During the dynamic measurements, e.g. ID 12, 12 frequency blocks were applied starting from 1 Hz with a step of 1 Hz up to 12 Hz. Each of the frequency blocks lasted 4 seconds plus 8 cycles (4 s + 8 c).

Table IV-1 Protocol of quasi-static measurements. Loading modes: constant (---), ramp from 0 N to maximum value and back (_/_) or ramp around offset value (-/\/-)

ID No.	Axial load					Shear load					Time
	Mode [-]	Offset [N]	Freq. [Hz]	Ampl. [N]	No. [-]	Mode [-]	Offset [N]	Freq. [Hz]	Ampl. [N]	No. [-]	[s]
01	_/_	-1000	0.005	-1000	2	---	0	/	/	/	400
02	_/_	-1000	0.005	-1000	2	---	200	/	/	/	400
03	_/_	-1000	0.005	-1000	2	---	-200	/	/	/	400
04	---	0	/	/	/	-/\/-	0	0.005	200	2	400
05	---	-1000	/	/	/	-/\/-	0	0.005	200	2	400
06	---	-2000	/	/	/	-/\/-	0	0.005	200	2	400
07	0					0					~300

Table IV-2 Protocol of reference measurements. Loading modes: constant (---), ramp from 0 N to maximum value and back (_/_) or sinus (~)

ID No.	Axial load					Shear load					Time
	Mode [-]	Offset [N]	Freq. [Hz]	Ampl. [N]	No. [-]	Mode [-]	Offset [N]	Freq. [Hz]	Ampl. [N]	No. [-]	[s]
01	_/_	-1000	0.005	-1000	2	---	0	/	/	/	400
12	~	-800	1-12	-550	12*(4s+8c)	---	0	/	/	/	73

After that, three sets of frequency-dependent measurements were applied in alternating order. The loading sets were compression load (Table IV-3), shear load (Table IV-4) and combined load (Table IV-5).

Table IV-3 Measurement protocol of compression set. Loading modes: constant (---) or sinus (~)

ID No.	Axial load					Shear load					Time [s]
	Mode [-]	Offset [N]	Freq. [Hz]	Ampl. [N]	No. [-]	Mode [-]	Offset [N]	Freq. [Hz]	Ampl. [N]	No. [-]	
08	~	-500	1-12	-200	12*(4s+8c)	---	0	/	/	/	73
09	~	-500	1-12	-400	12*(4s+8c)	---	0	/	/	/	73
10	~	-800	1-12	-200	12*(4s+8c)	---	0	/	/	/	73
11	~	-800	1-12	-400	12*(4s+8c)	---	0	/	/	/	73
12	~	-800	1-12	-550	12*(4s+8c)	---	0	/	/	/	73
13	~	-800	1-12	-700	12*(4s+8c)	---	0	/	/	/	73
14	~	-1100	1-12	-200	12*(4s+8c)	---	0	/	/	/	73
15	~	-1100	1-12	-400	12*(4s+8c)	---	0	/	/	/	73
16	~	-1100	1-12	-550	12*(4s+8c)	---	0	/	/	/	73
17	~	-1100	1-12	-700	12*(4s+8c)	---	0	/	/	/	73
18	~	-1100	1-12	-1000	12*(4s+8c)	---	0	/	/	/	73
07	0					0					~300

Table IV-4 Measurement protocol of shear set. Loading modes: constant (---) or sinus (~)

ID No.	Axial load					Shear load					Time [s]
	Mode [-]	Offset [N]	Freq. [Hz]	Ampl. [N]	No. [-]	Mode [-]	Offset [N]	Freq. [Hz]	Ampl. [N]	No. [-]	
19	---	-800	/	/	/	~	0	1-12	50	12*(4s+8c)	73
20	---	-800	/	/	/	~	0	1-12	125	12*(4s+8c)	73
21	---	-800	/	/	/	~	0	1-12	200	12*(4s+8c)	73
22	---	-800	/	/	/	~	+100	1-12	50	12*(4s+8c)	73
23	---	-800	/	/	/	~	+100	1-12	125	12*(4s+8c)	73
24	---	-800	/	/	/	~	+100	1-12	200	12*(4s+8c)	73
25	---	-800	/	/	/	~	+200	1-12	50	12*(4s+8c)	73
26	---	-800	/	/	/	~	+200	1-12	125	12*(4s+8c)	73
27	---	-800	/	/	/	~	+200	1-12	200	12*(4s+8c)	73
28	---	-800	/	/	/	~	-100	1-12	-50	12*(4s+8c)	73
29	---	-800	/	/	/	~	-100	1-12	-125	12*(4s+8c)	73
30	---	-800	/	/	/	~	-100	1-12	-200	12*(4s+8c)	73
07	0					0					~300

Table IV-5 Measurement protocol of combined loading sets. Loading modes: constant (---) or sinus (~)

ID No.	Axial load					Shear load					Time
	Mode [-]	Offset [N]	Freq. [Hz]	Ampl. [N]	No. [-]	Mode [-]	Offset [N]	Freq. [Hz]	Ampl. [N]	No. [-]	[s]
31	~	-800	1-12Hz	-700	12*(4s+8c)	---	+100	/	/	/	73
07	0					0					~300

The order of the three dynamic testing sets (axial, shear and combined) was alternated for each particular group separately. Therefore, the six specimens within each group were never tested in the same order of sets. The assignment of the six combinations of testing sets to the individual specimens is shown in Table IV-6. These alternations were used to ensure that the testing order had no influence on the evaluated frequency-dependent parameters. The reference measurements block was applied again at the end of the mechanical parameters test (Table IV-7).

Table IV-6 Overview of the specimen groups, block order and testing order of frequency-dependent measurements used in the mechanical parameters test (N: axial compression set, S: shear set, C: combined set)

Old-Neutral			Young-Neutral			Young-Flexed		
LWS	Order of sets	Test no.	LWS	Order of sets	Test no.	LWS	Order of sets	Test no.
1101	S N C	2	1106	S N C	3	1112	N S C	8
1104	N S C	1	1107	N C S	4	1113	N C S	5
1108	N C S	9	1124	C N S	15	1119	S C N	6
1110	S C N	11	1126	N S C	14	1120	C N S	7
1131	C N S	16	1133	S C N	12	1123	C S N	10
1136	C S N	18	1135	C S N	17	1125	S N C	13

Table IV-7 Protocol of reference measurements applied at the end of the mechanical parameters test. Loading modes: constant (---), ramp from 0 N to maximum value and back (_/_) or sinus (~)

ID No.	Axial load					Shear load					Time
	Mode [-]	Offset [N]	Freq. [Hz]	Ampl. [N]	No. [-]	Mode [-]	Offset [N]	Freq. [Hz]	Ampl. [N]	No. [-]	[s]
33 (01)	_/_	-1000	0,005	-1000	2	---	0	/	/	/	400
34 (12)	~	-800	1-12	-550	12*(4s+8c)	---	0	/	/	/	73

During the tests, the specimens were immersed in a Ringer solution bath at 37°C. The temperature was controlled by a custom-made temperature controller (details in Part VIII4). To prevent deterioration of specimens during long testing periods, an

antibiotic (Penicillin/Streptomycin, PAA, Austria, in a concentration of 10 ml/l) was added to the solution.
The parameters to analyse the cyclic measurement data were determined based on reference hysteresis curves that were calculated the following way (Matlab R2008a, MathWorks, Natick, MA, USA).

For the quasi-static measurements, this reference hysteresis was generated based on the measurements for the last complete loading cycle ending at the last local extremum. For axial measurements (ID 01 to ID 03 and ID 01 ref and ID 33), the testing time was 200 s to 400 s, while for shear loads (ID 04 to ID 06) it was 150 s to 350 s. To account for creep during the long cycle duration (200 s), the data were subjected to a linear detrend procedure, so that the two extrema were corrected to their average. Furthermore, fourth-order low-pass Butterworth filtering with a cut-off frequency of 0.5 Hz was used. This cut-off frequency is a hundred-fold higher than the measurement frequency and only serves to remove background noise. The approximately 1000 data points per hysteresis (200 s at 5 Hz) were reduced by a factor of 5 by applying a cluster procedure of the normalised hysteresis curves. In detail, a hierarchical cluster tree based on the unweighted centre of mass distance was used.

For the dynamic measurements, the reference hysteresis was generated in a similar manner. However, in contrast to the quasi-static case, the reference hysteresis was calculated based on the last four cycles of each frequency step (1 Hz to 12 Hz). Furthermore, no linear detrend procedure was needed. Filtering was also done by fourth-order low-pass Butterworth filtering. The cut-off frequency was 200 Hz in order to remove background noise. The 2048 to 171 data points that were collected within the four hysteresis curves (4 s to 0.33 s at 512 Hz) were clustered to 100 points.

For quasi-static as well as dynamic references, hysteresis curves, the same characteristic parameters describing this hysteresis, were calculated. Those were energy ratio and stiffness.

The energy ratio was calculated by dividing the hysteresis energy (area within the hysteresis curve, Figure IV-4) by the energy input (area below the loading part of the hysteresis, starting from the minimum force).

The area enclosed by the hysteresis was determined by a public domain function that is able to calculate the area within concave-shaped polygons (hullfit.m, Matlab function by Peter Wasmeier, p.wasmeier@bv.tum.de). This function uses piecewise linear sections between discrete data points and minimises the enclosed area. The minimisation is constrained by an additional factor which defines the ratio between the longest and shortest track sections. For this study, this optimisation factor was chosen to be 0.05.

The energy ratio becomes 1 for purely viscous material and 0 for purely elastic material. For viscoelastic materials, the ratio ranges between 0 and 1.

The stiffness is defined as the difference between minimum and maximum force (ΔF) divided by the difference between minimum and maximum displacement (Δd) (Figure IV-4).

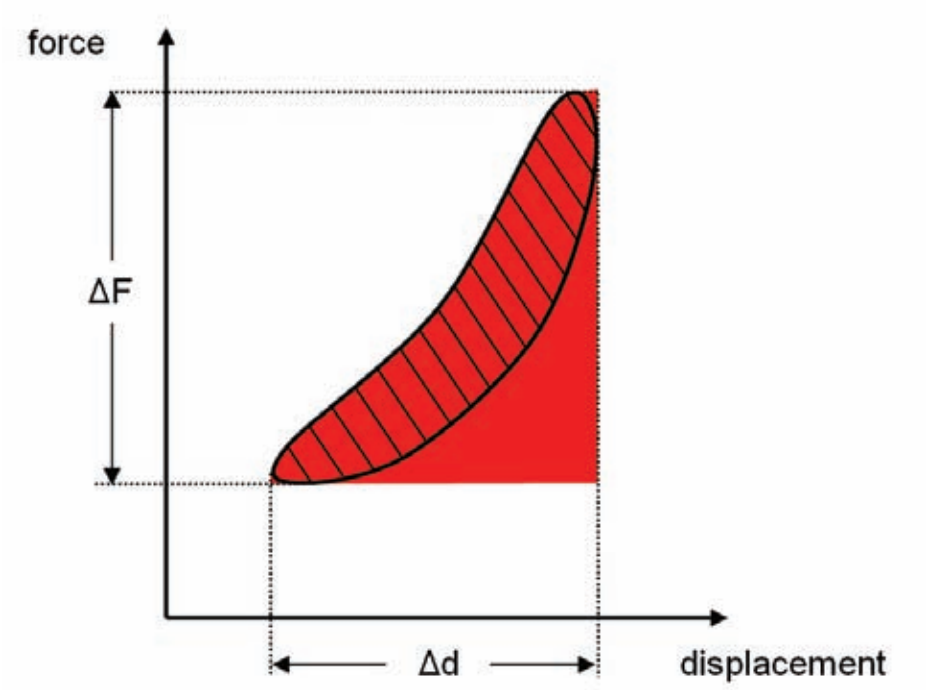

Figure IV-4 Explanation of mechanical parameters chosen for data analysis. The energy ratio is defined as the hysteresis (lined area) divided by the energy input (red area). Stiffness is defined as a ratio of ΔF to Δd.

3 Dynamic - Results

3.1 Quasi-static measurements

3.1.1 Quasi-static axial compression

The energy ratio was highest for the 'Young-Flexed' group (Figure IV-5). In that group, the additional shear load (ID 02 and ID 03) decreased the energy ratio as compared to the test without a shear load (ID 01). However, for the two other groups, 'Young-Neutral' and 'Old-Neutral', the ratio increased with the presence of a shear load. Statistical analysis showed that none of the groups or ID Nos. was significantly different.

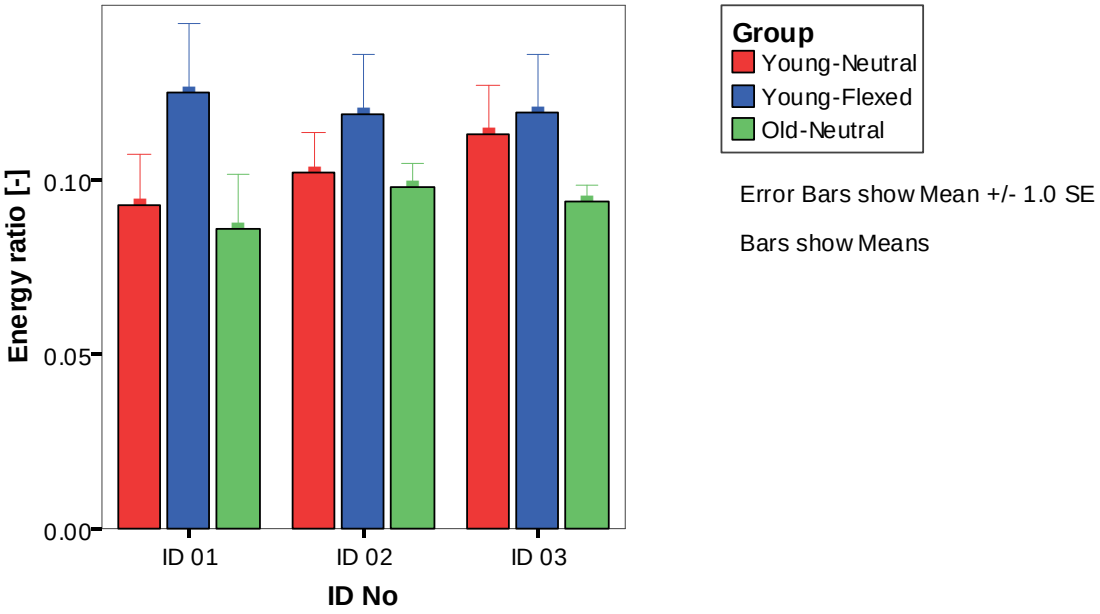

Figure IV-5 Energy ratio during quasi-static axial ramp loading (from 0 N up to 2000 N) with different shear loads (0 N, 200 N and -200 N)

The peak-to-peak stiffness in the quasi-static axial compression tests was always higher for axial loading without a shear load (Figure IV-6). When the shear load was applied, the stiffness decreased regardless of whether the shear load was positive or negative. These changes were statistically significant ($p < 0.001$). The highest stiffness values were observed for young specimens tested in flexion; this was significantly different from the other groups (Bonferroni test, $p < 0.001$). The groups 'Young-Neutral' and 'Old-Neutral' exhibited similar values.

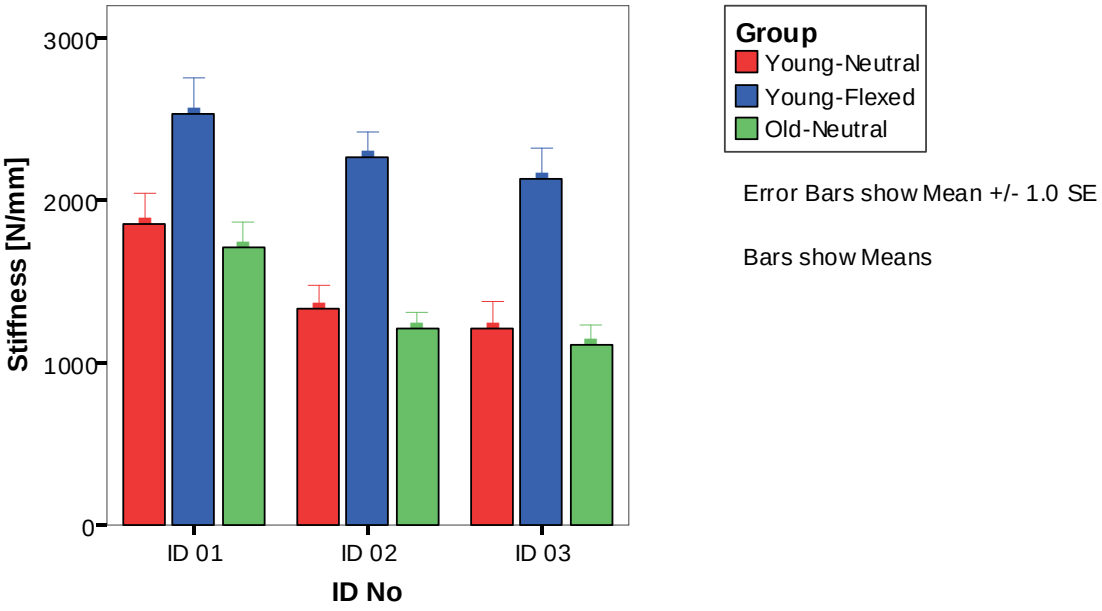

Figure IV-6 Stiffness during quasi-static axial ramp loading (from 0 N up to 2000 N) with different shear loads (0 N, 200 N and -200 N)

3.1.2 Quasi-static shear loading

The energy ratio in the shear ramp loading was smallest in the 'Young-Flexed' group (Figure IV-7), and this was significantly different from the two other groups (Bonferroni test, $p < 0.01$). The groups 'Young-Neutral' and 'Old-Neutral' showed a decreasing pattern with increasing compression load. On the other hand, the 'Young-Flexed' group showed an increasing pattern, although the differences in shear load due to increasing axial compression were not significant.

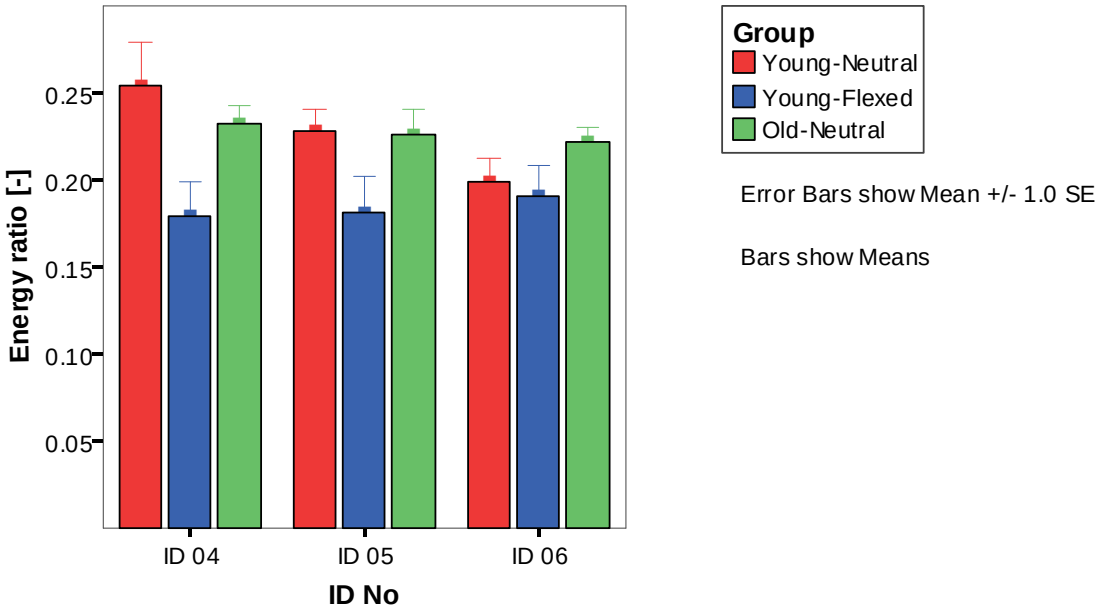

Figure IV-7 Energy ratio during quasi-static shear ramp loading with different axial compressive loads (0 N, -1000 N and -2000 N)

Stiffness in quasi-static shear ramp loading was smallest when there was no axial compressive load (Figure IV-8). An increasing axial compressive load caused a significant (Tamhane test, $p < 0.01$) increase in stiffness: 3.5 times at -1000 N and 4.9 times at -2000 N when compared to no compressive load for the specimens in the 'Young-Neutral' group. There was an overall statistical difference between the different groups ($p = 0.001$), but the Tamhane test did not show any particular group differences. Additionally, the interaction between the group and ID was significant ($p = 0.04$), indicating that there was a different effect of stiffness change (ID No.) within the different testing groups.

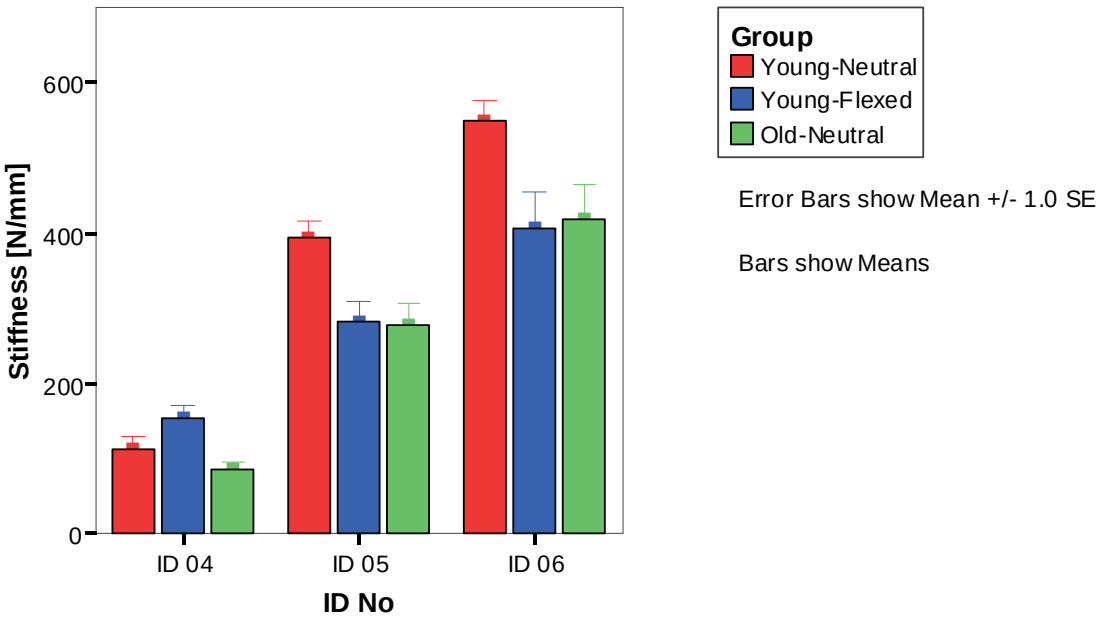

Figure IV-8 Stiffness during quasi-static shear ramp loading with different axial compressive loads (0 N, -1000 N and -2000 N)

3.2 Frequency-dependent measurements

One specimen (1104) belonging to the 'Old-Neutral' group had to be excluded from the dynamic data analysis. The measurement data obtained from this specimen exhibited an unstable controller setting from the testing machine, which led to poor control of the command values.

3.2.1 Dynamic axial compression

In all cases, the energy ratio had a tendency to increase with increasing testing frequency (Figure IV-9, Figure IV-10, Figure IV-11). For the groups 'Young-Neutral' and 'Young-Flexed', the energy ratio reached a slight maximum at 11 Hz frequency. The ratio was lowest for loading -1100 N ± 1000 N and highest for the loading groups with 200 N amplitudes. Generally, the values of the energy ratio were similar for the loading with the same amplitude despite the offset load.

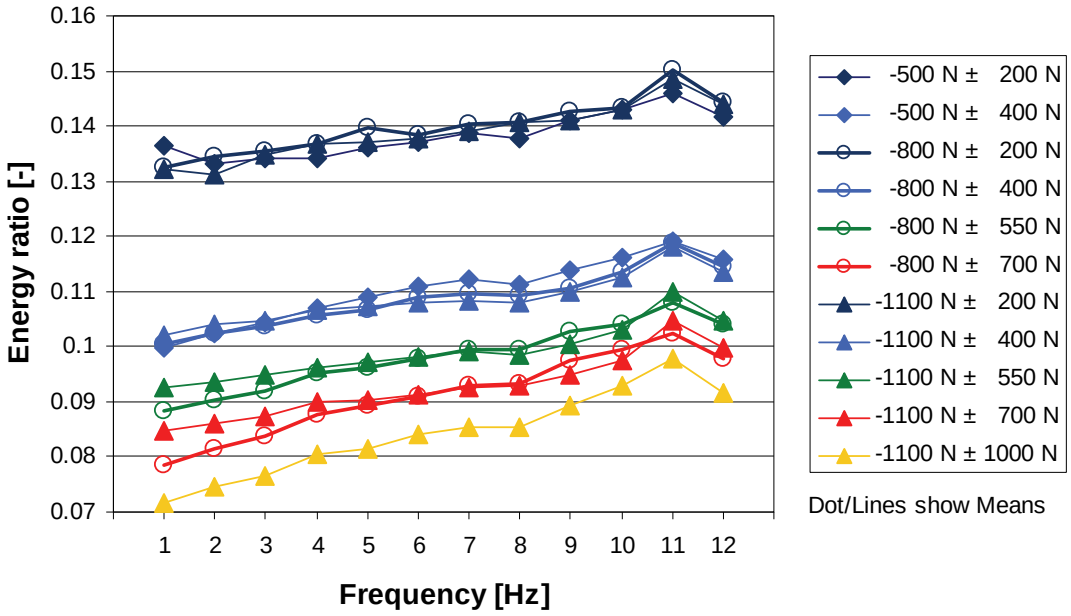

Figure IV-9 Energy ratio for the 'Young-Neutral' group during axial dynamic loading. The SEM was between 0.0023 and 0.0059.

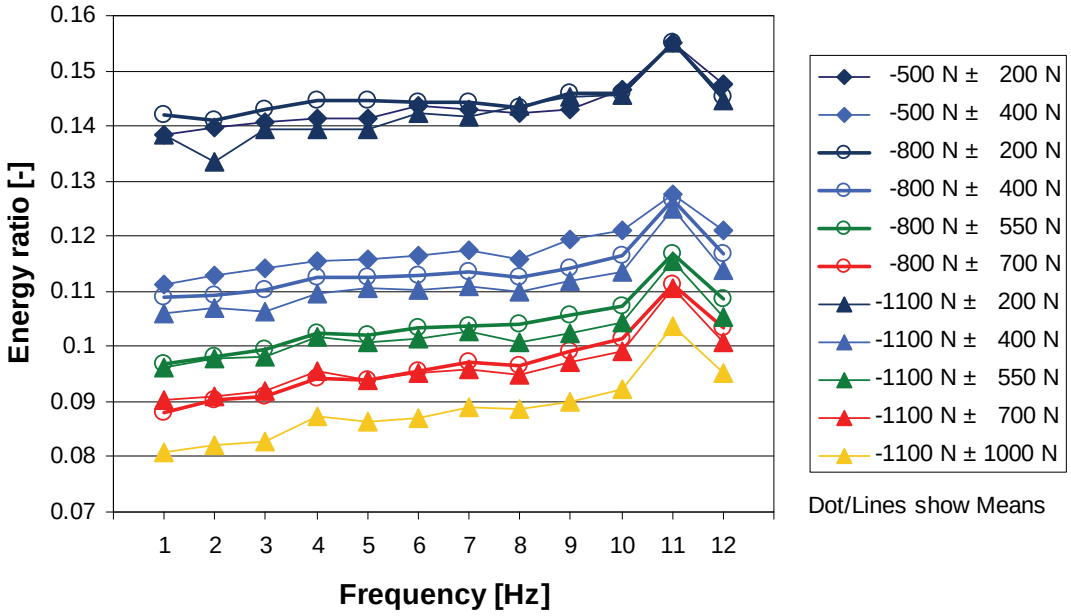

Figure IV-10 Energy ratio for the 'Young-Flexed' group during axial dynamic loading. The SEM was between 0.0038 and 0.013.

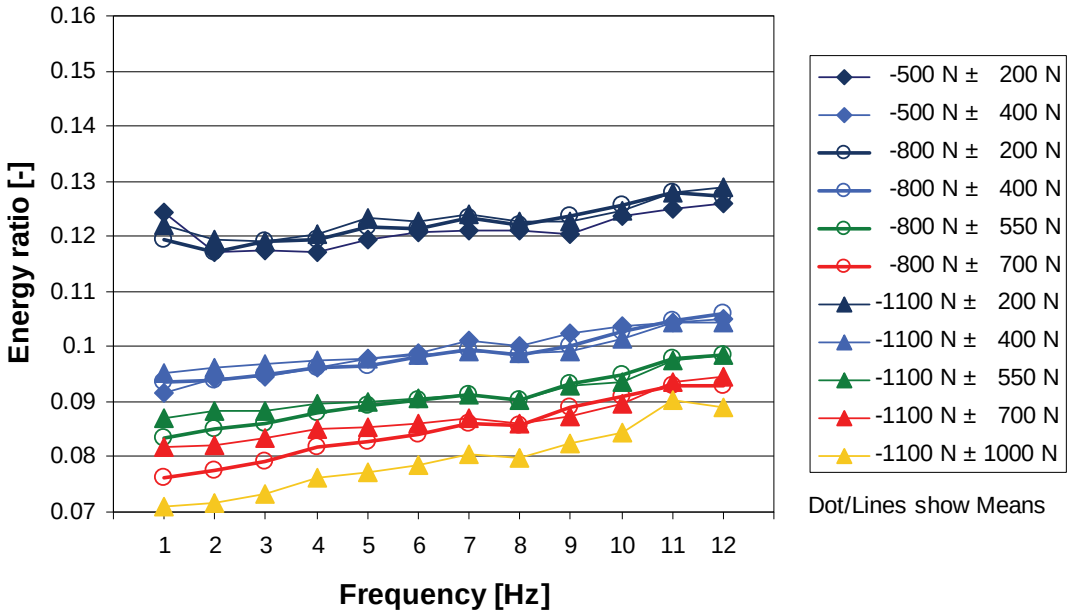

Figure IV-11 Energy ratio for the 'Old-Neutral' group during axial dynamic loading. The SEM was between 0.00054 and 0.013.

Stiffness showed an increasing trend with increasing testing frequency in all cases (Figure IV-12, Figure IV-13, Figure IV-14). The stiffness was lowest for loading -500 N ± 400 N and highest for loading -1100 N ± 200 N. Stiffness decreased with the increase of loading amplitude for the same offset loads. The 'Young-Flexed' specimens tended to be stiffer than those of the other two groups.

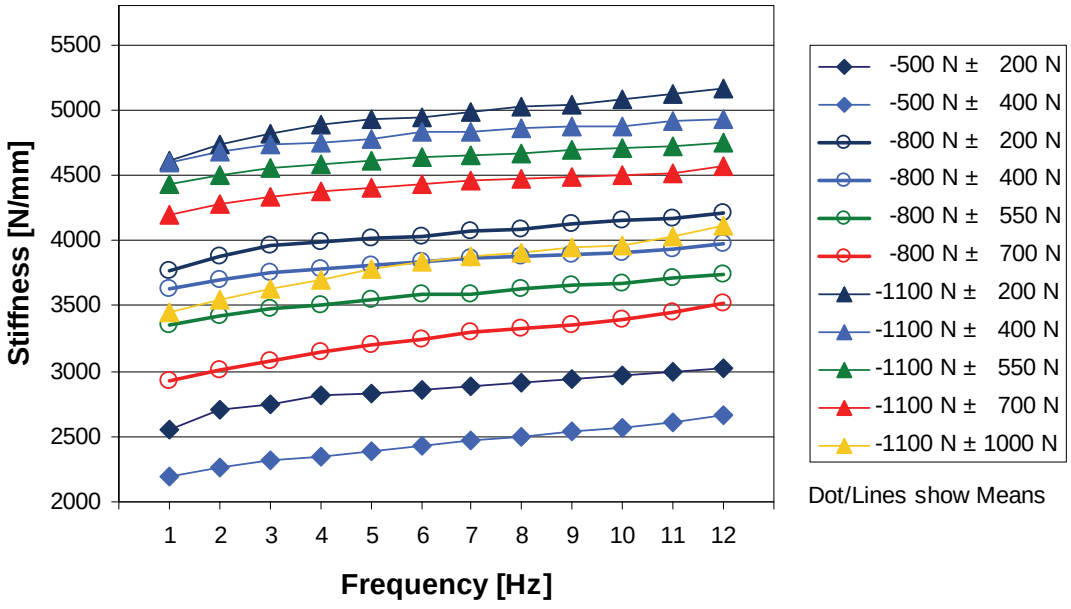

Figure IV-12 Stiffness for the 'Young-Neutral' group during axial dynamic loading. The SEM was between 286 and 365 N/mm.

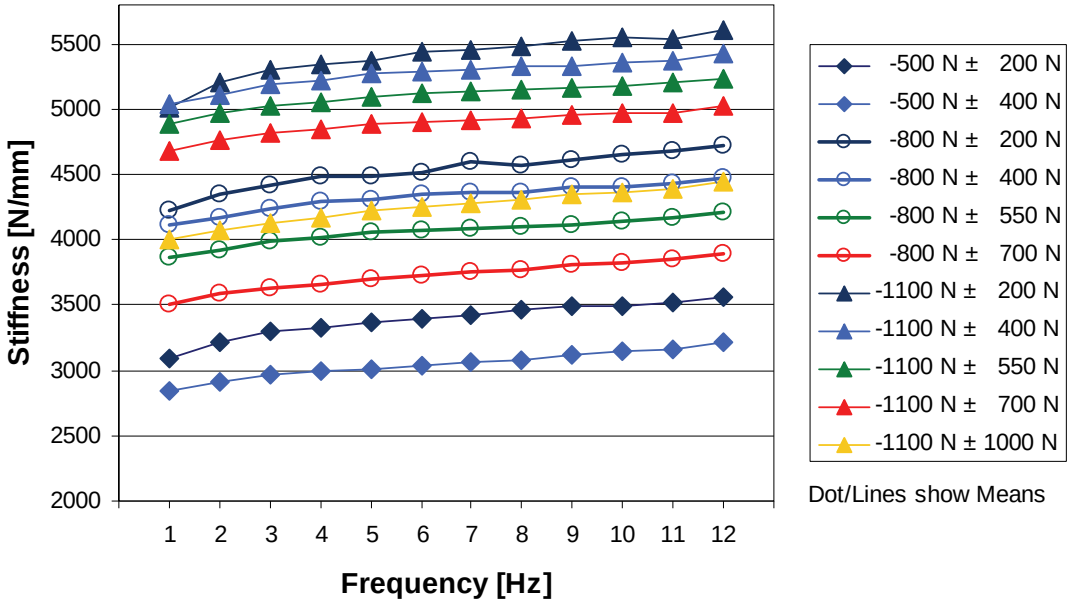

Figure IV-13 Stiffness for the 'Young-Flexed' group during axial dynamic loading. The SEM was between 281 and 467 N/mm.

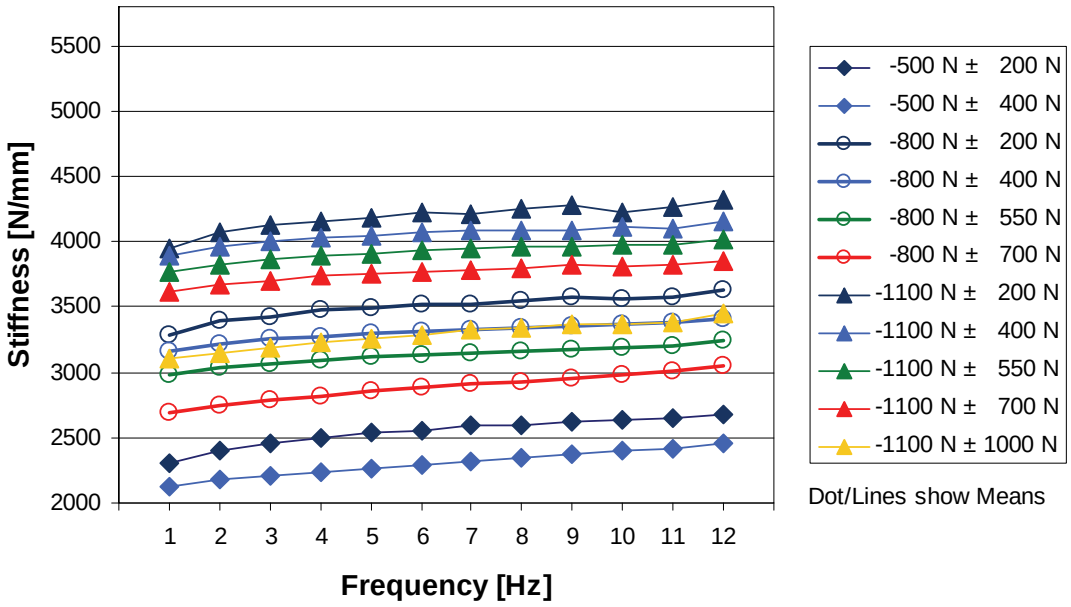

Figure IV-14 Stiffness for the 'Old-Neutral' group during axial dynamic loading. The SEM was between 192 and 330 N/mm.

3.2.2 Dynamic shear loading

The energy ratio showed an increasing trend with increasing testing frequency (Figure IV-15, Figure IV-16, Figure IV-17). The ratio did not appear to have any pattern. Data points were clustered together.

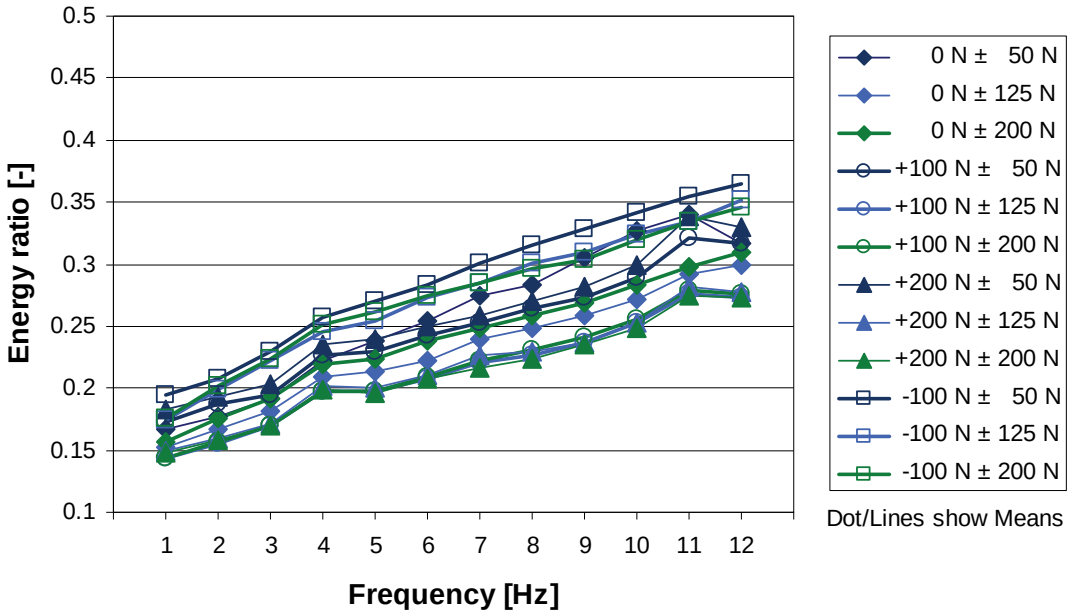

Figure IV-15 Energy ratio for the 'Young-Neutral' group during shear dynamic loading (constant axial compression 800 N). The SEM was between 0.0026 and 0.040.

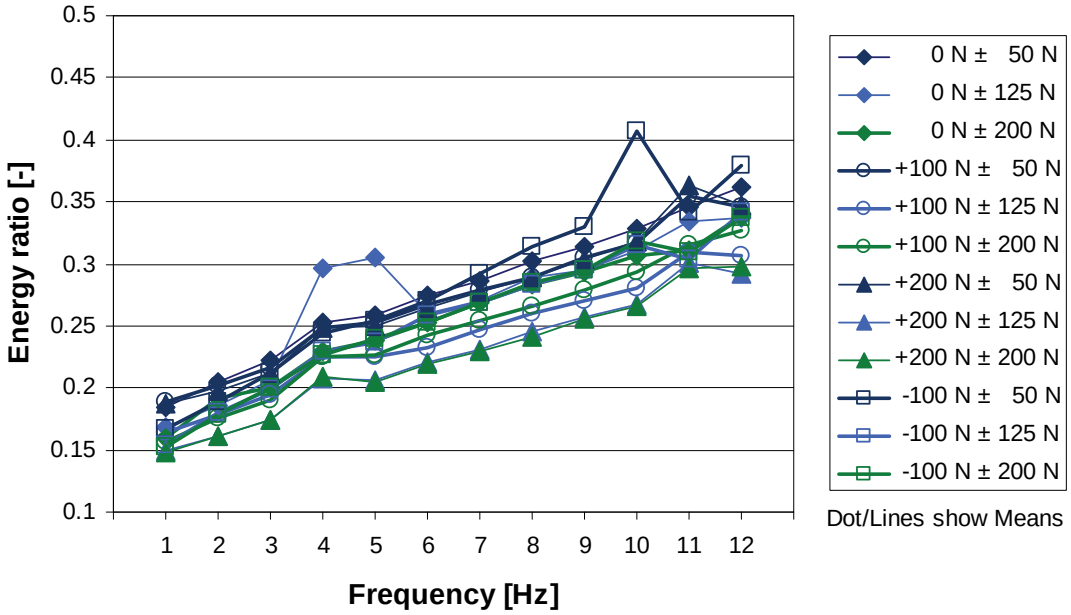

Figure IV-16 Energy ratio for the 'Young-Flexed' group during shear dynamic loading (constant axial compression 800 N). The SEM was between 0.0061 and 0.063.

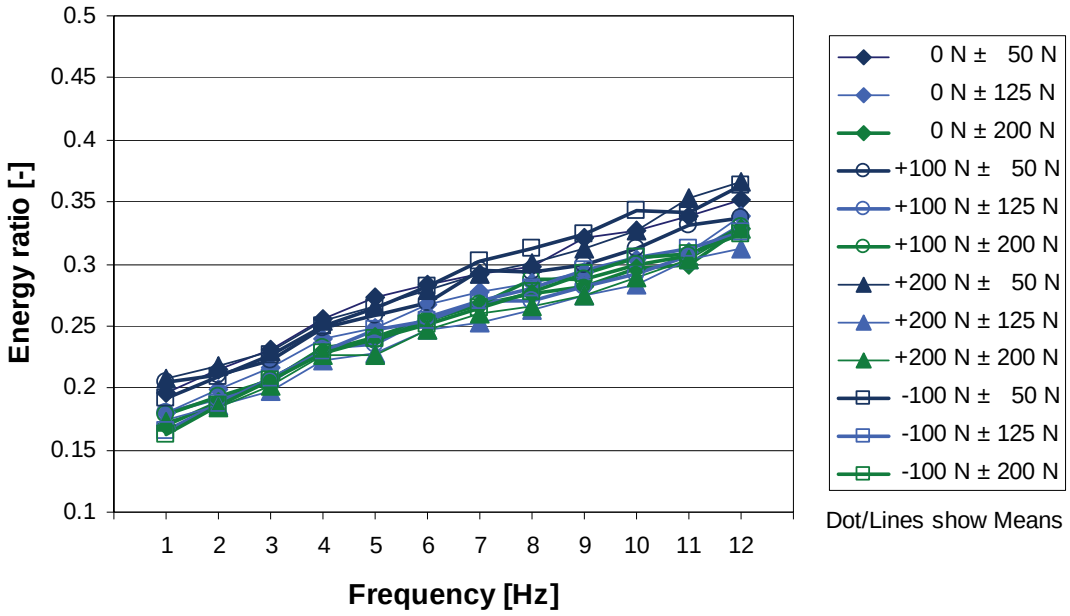

Figure IV-17 Energy ratio for the 'Old-Neutral' group during shear dynamic loading (constant axial compression 800 N). The SEM was between 0.0013 and 0.022.

Stiffness in all cases showed an increasing trend with increasing testing frequency (Figure IV-18, Figure IV-19, Figure IV-20). The stiffness was lowest for the loading group with an offset load of -100 N and highest for loading 200 N ± 50 N. A decrease in stiffness was observed with the increase of loading amplitude for the same offset loads. Specimens in the 'Young-Neutral' group tended to be stiffer than those of the other two groups.

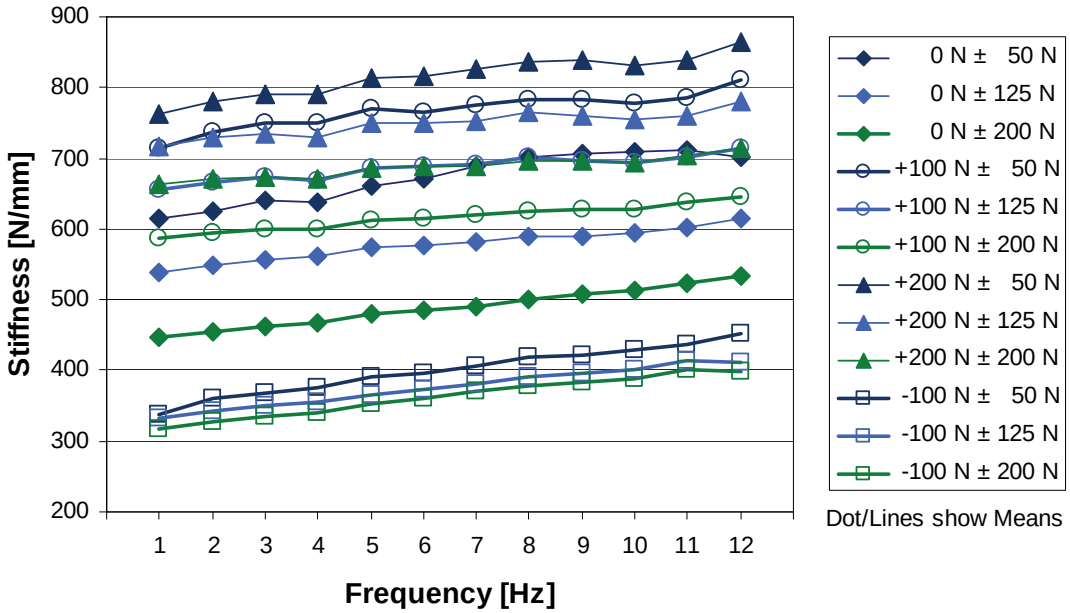

Figure IV-18 Stiffness for the 'Young-Neutral' group during shear dynamic loading (constant axial compression 800 N). The SEM was between 19 and 50 N/mm.

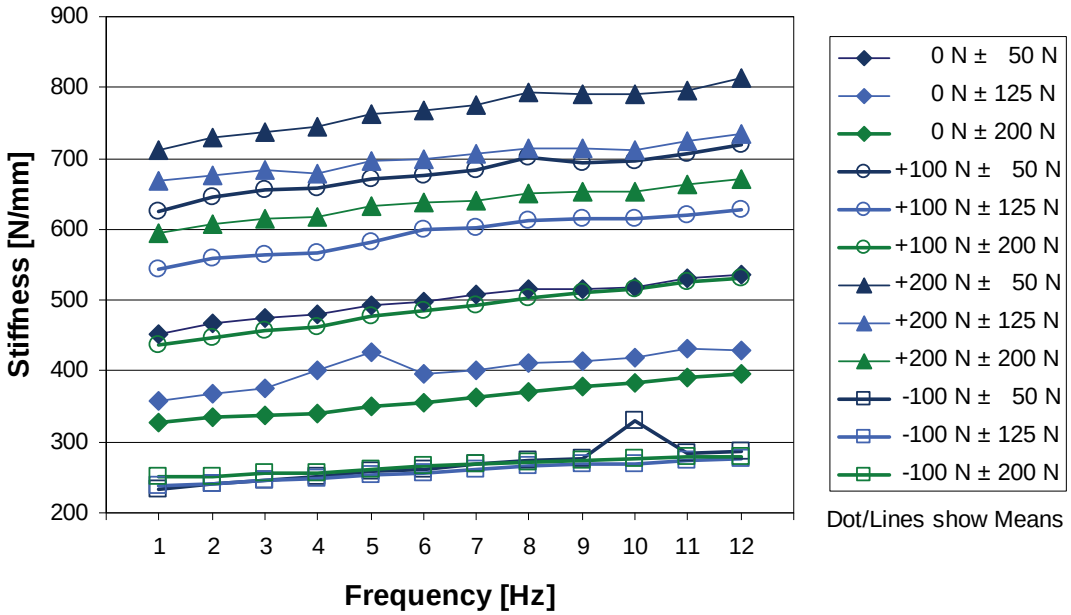

Figure IV-19 Stiffness for the 'Young-Flexed' group during shear dynamic loading (constant axial compression 800 N). The SEM was between 20 and 81 N/mm.

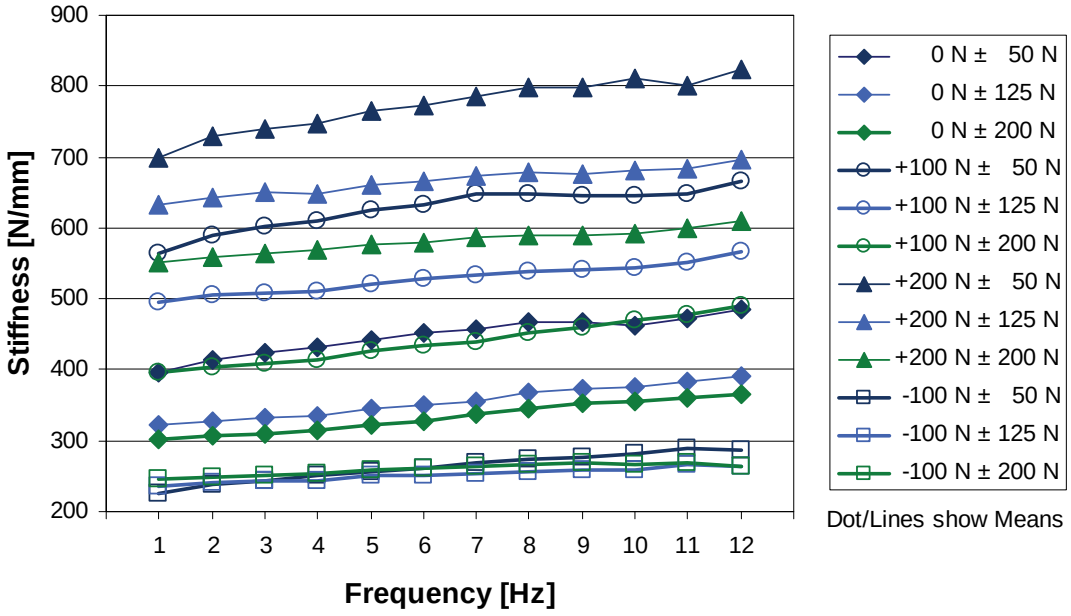

Figure IV-20 Stiffness for the 'Old-Neutral' group during shear dynamic loading (constant axial compression 800 N). The SEM was between 22 and 70 N/mm.

3.2.3 Dynamic combined loading

Generally, the energy ratio for dynamic axial loading without shear (ID 13) was smaller or equal when compared to the combined loading with additional anterior shear (ID 31). The energy ratio for combined loading (ID 31) was smaller for the 'Young-Neutral' group (Figure IV-21) than for the other groups (Figure IV-22, Figure IV-23). Furthermore, it exhibited the smallest difference when compared to similar axial loading without anterior shear (ID 13).

By mistake, the data sampling rate for the combined loading block (ID 31) was initially set too low. After the twelfth specimen, the rate was increased to the appropriate value. Therefore, only data from six specimens from different groups could be analysed (the number of specimens for each group is indicated under each graph).

The stiffness for combined loading (ID 31) was highest for the 'Young-Flexed' group (Figure IV-25). When compared to ID 13 without anterior shear, ID 31 had lower or equal stiffness Figure IV-24, Figure IV-26). For the 'Old-Neutral' group, the influence of the additional shear was the smallest.

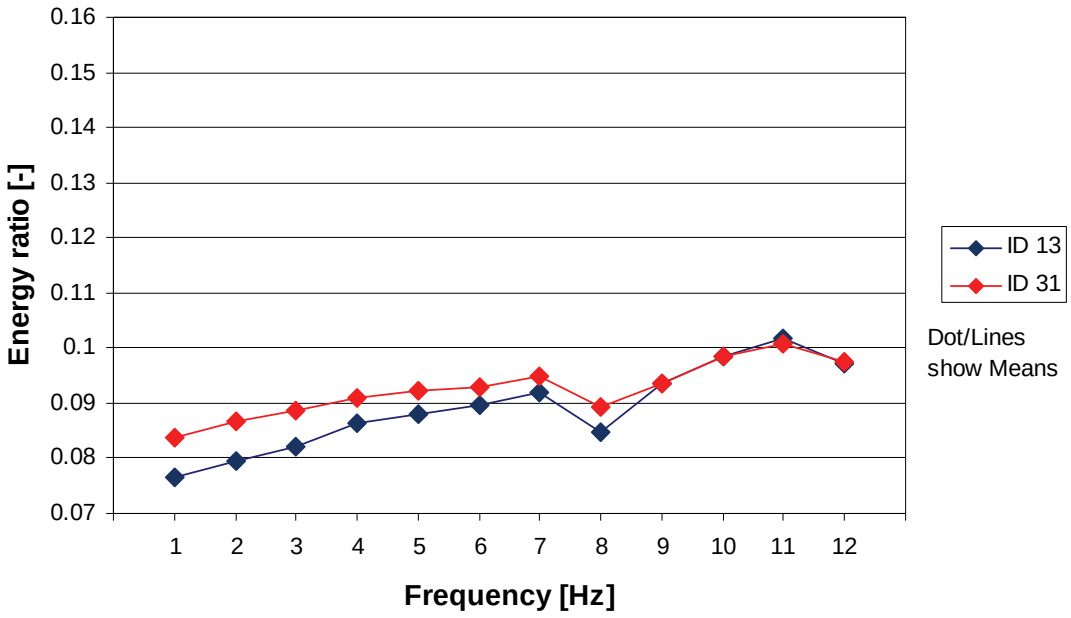

Figure IV-21 Energy ratio for the 'Young-Neutral' group during combined loading ID 31 (n = 3, axial offset -800 N, amplitude ±700 N, anterior shear +100 N) in comparison to ID 13 (the same axial loading, shear 0 N). The SEM was between 0.0036 and 0.0096 for ID 31 and between 0.0035 and 0.0055 for ID 13.

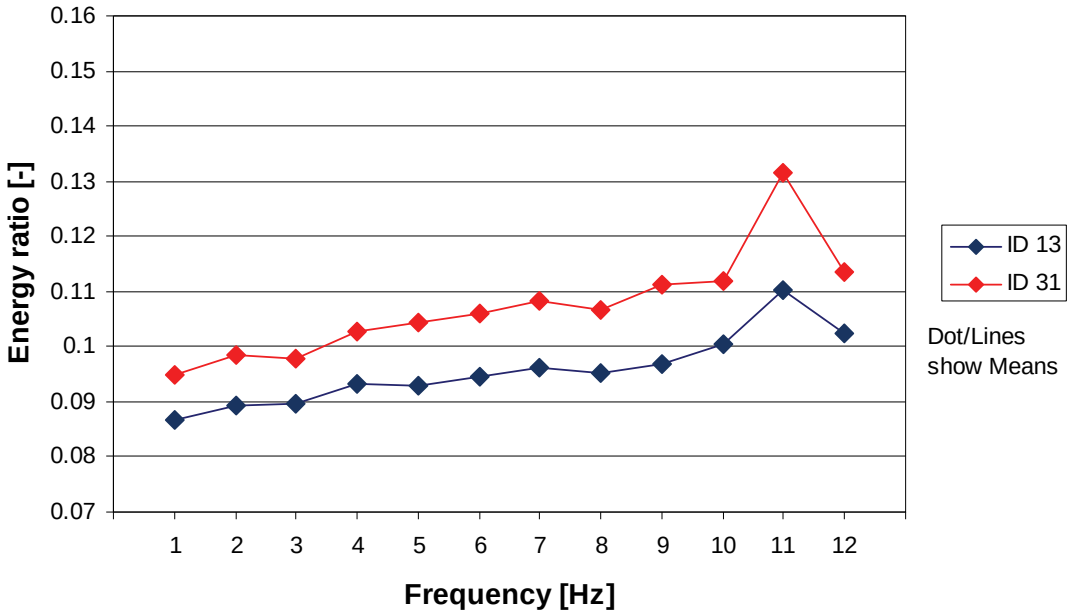

Figure IV-22 Energy ratio for the 'Young-Flexed' group during combined loading ID 31 (n = 1, axial offset -800 N, amplitude ±700 N, anterior shear +100 N) in comparison to ID 13 (the same axial loading, shear 0 N). The SEM was between 0.0058 and 0.0081 for ID 13.

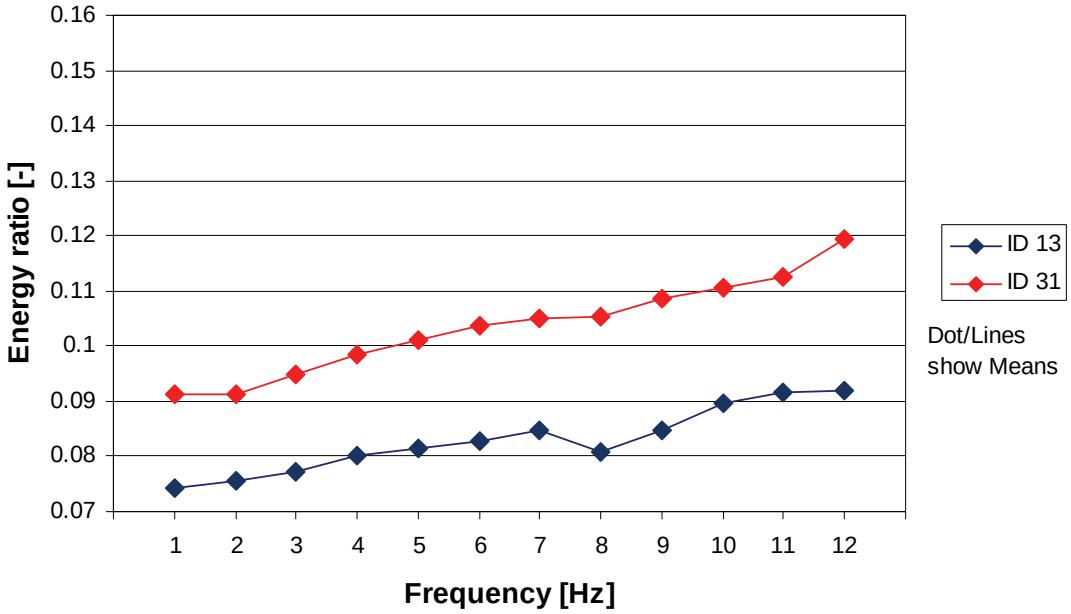

Figure IV-23 Energy ratio for the 'Old-Neutral' group during combined loading ID 31 (n = 2, axial offset -800 N, amplitude ±700 N, anterior shear +100 N) in comparison to ID 13 (the same axial loading, shear 0 N). The SEM was between 0.0040 and 0.0099 for ID 31 and between 0.0025 and 0.0041 for ID 13.

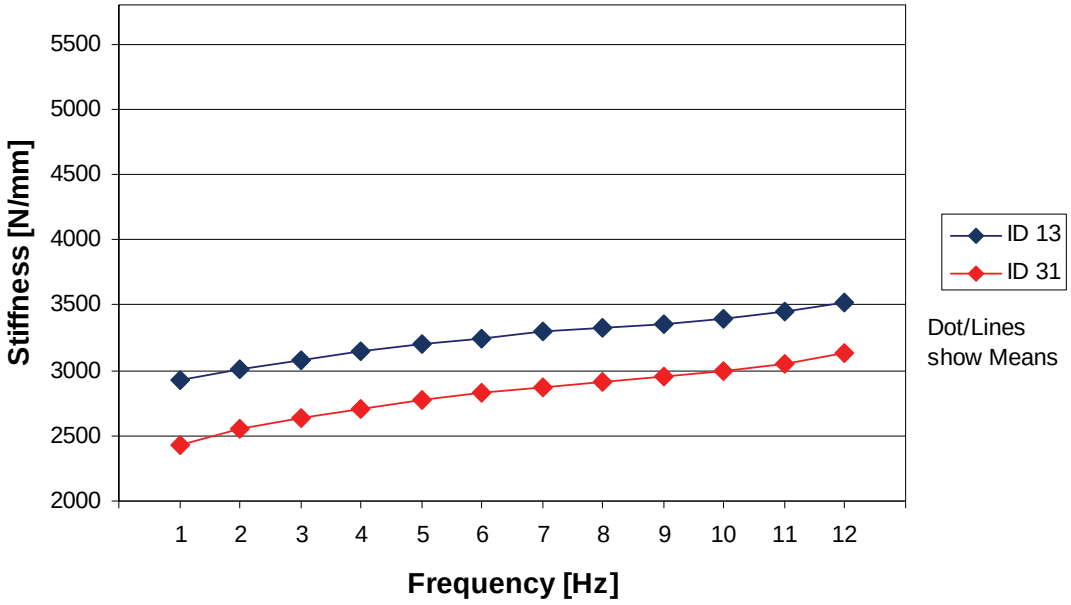

Figure IV-24 Stiffness for the 'Young-Neutral' group during combined loading ID 31 (n = 3, axial offset -800 N, amplitude ±700 N, anterior shear +100 N) in comparison to ID 13 (the same axial loading, shear 0 N). The SEM was between 168 and 287 N/mm for ID 31 and between 267 and 303 N/mm for ID 13.

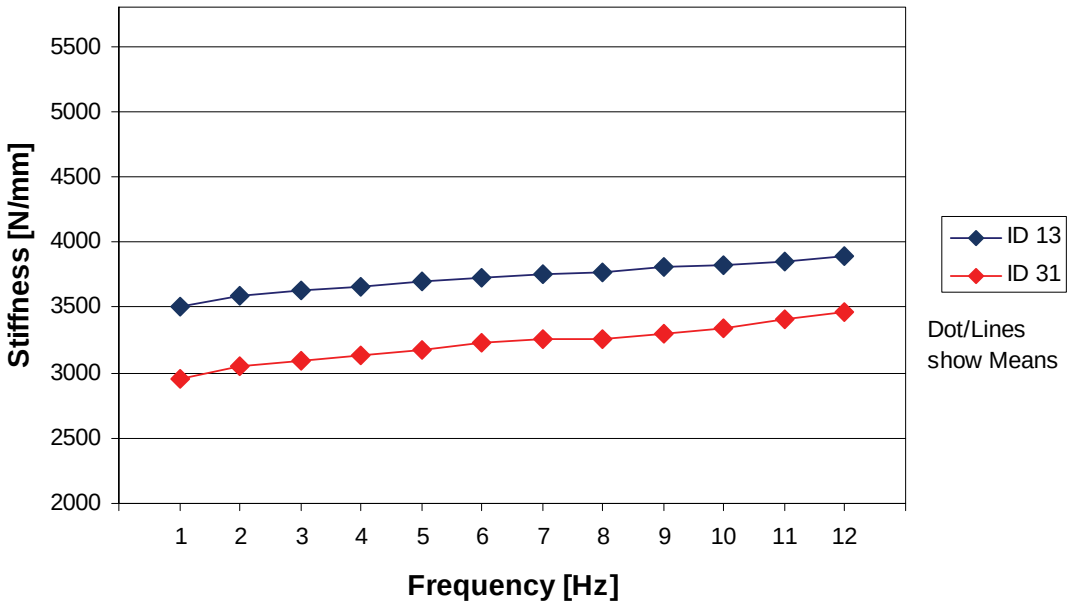

Figure IV-25 Stiffness for the 'Young-Flexed' group during combined loading ID 31 (n = 1, axial offset -800 N, amplitude ±700 N, anterior shear +100 N) in comparison to ID 13 (the same axial loading, shear 0 N). The SEM was between 313 and 333 N/mm for ID 13.

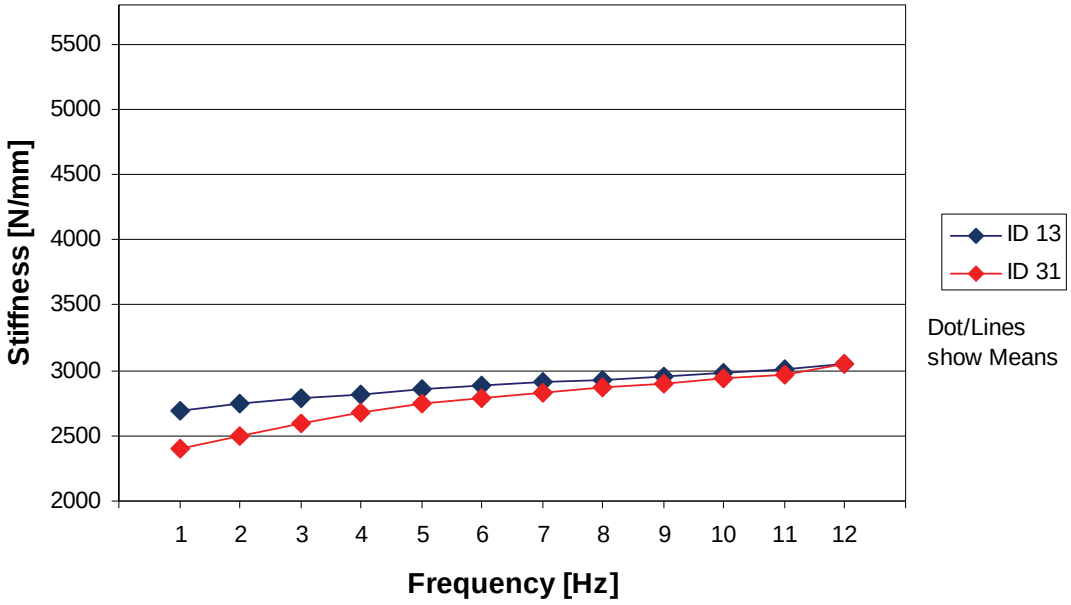

Figure IV-26 Stiffness for the 'Old-Neutral' group during combined loading ID 31 (n = 2, axial offset -800 N, amplitude ±700 N, anterior shear +100 N) in comparison to ID 13 (the same axial loading, shear 0 N). The SEM was between 431 and 655 N/mm for ID 31 and between 254 and 281 N/mm for ID 13.

3.3 Reference measurements

3.3.1 Quasi-static reference measurements

The energy ratio in the reference measurements (ID 01) was largest for the specimens in the 'Young-Flexion' group (Figure IV-27), and this was significantly different from the two other groups (Bonferroni test, $p < 0.01$). In that group the ratio decreased with each repetition of this test. The pattern for the other two groups was different, though. At ID 01 ref there was a decrease in the energy ratio, but at ID 33 it increased again. However, with regard to the repetition, the difference was not significant.

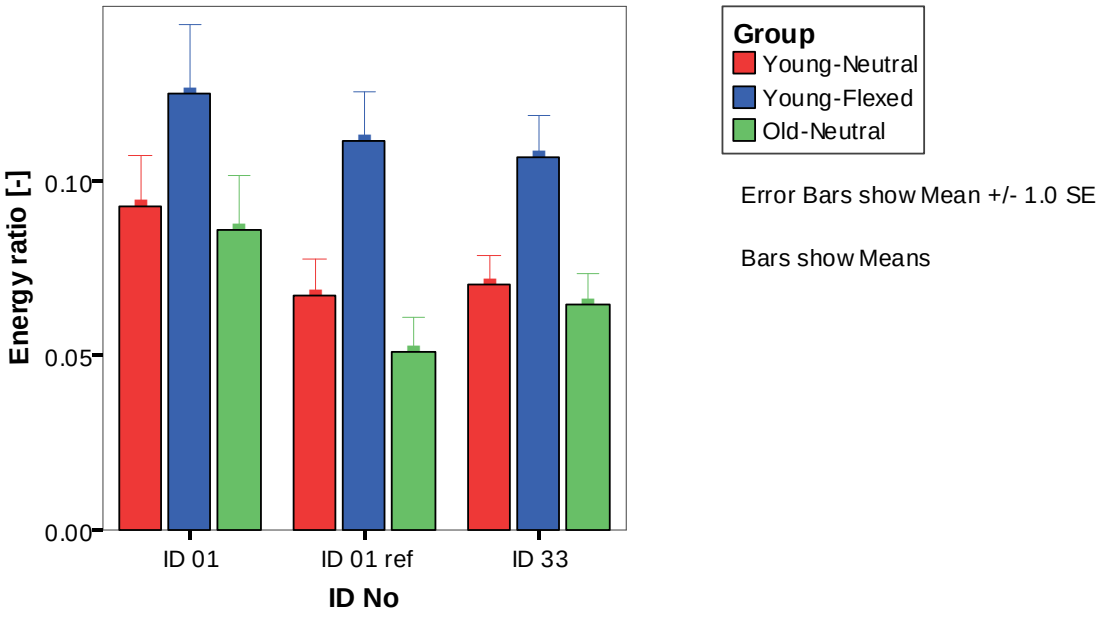

Figure IV-27 Energy ratio during quasi-static axial ramp loading (from 0 N up to 2000 N) in different periods of the mechanical parameters test

The stiffness in the initial measurements (ID 01) was largest for the young group of specimens tested in flexion (Figure IV-28); this was significantly different from the two other groups (Bonferroni test, $p < 0.001$). In all groups there was a trend of increasing stiffness with increasing repetition of the test, but this did not reach significance.

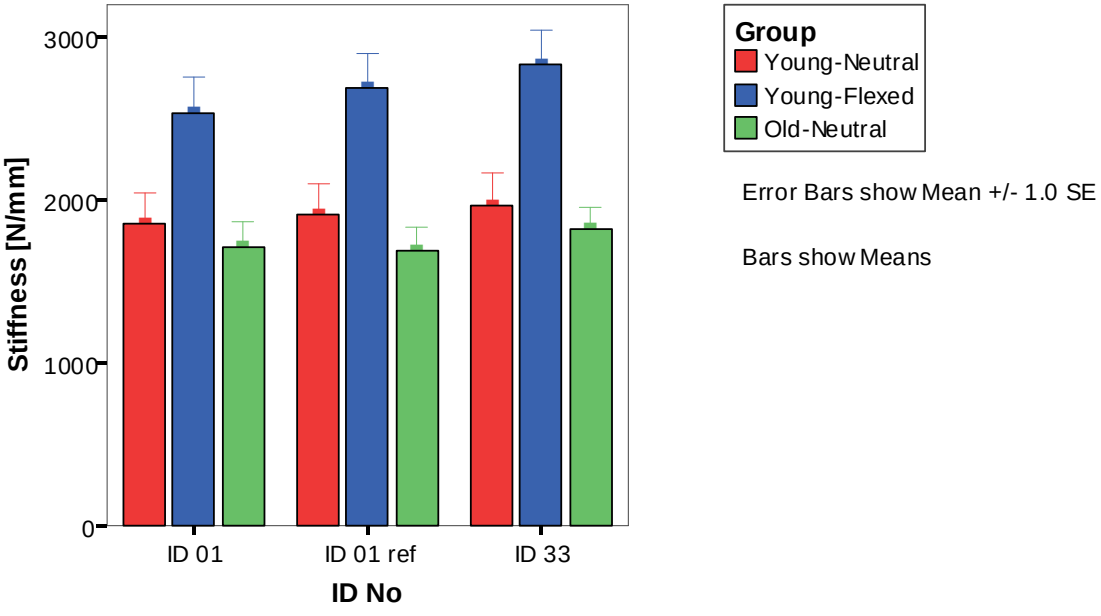

Figure IV-28 Stiffness during quasi-static axial ramp loading (from 0 N up to 2000 N) in different periods of the mechanical parameters test

3.3.2 Dynamic reference measurements

Dynamic reference measurements performed at three stages (ID No.) of the consecutive series of measurements exhibited small changes in energy ratio for all groups (Figure IV-29, Figure IV-30, Figure IV-31). For the three identical frequency-dependent reference measurements (ID 12 ref, ID 12 and ID 34), the changes were smallest for the 'Old-Neutral' group (Figure IV-31), but there were no significant differences between groups. There was a significant main effect of frequency on the energy ratio ($p < 0.001$, Greenhouse-Geisser correction). In comparison to the energy ratio at frequencies from 3 Hz to11 Hz, the energy ratio at a frequency of 1 Hz was significantly smaller ($p < 0.05$). The main effect of the ID No. on the energy ratio was significant ($p = 0.002$). The energy ratio of ID 12 ref was significantly larger than ID 12 (contrast, $p = 0.013$). The frequency within different IDs also had different effects on the energy ratio (frequency × stage interaction, $p < 0.001$).

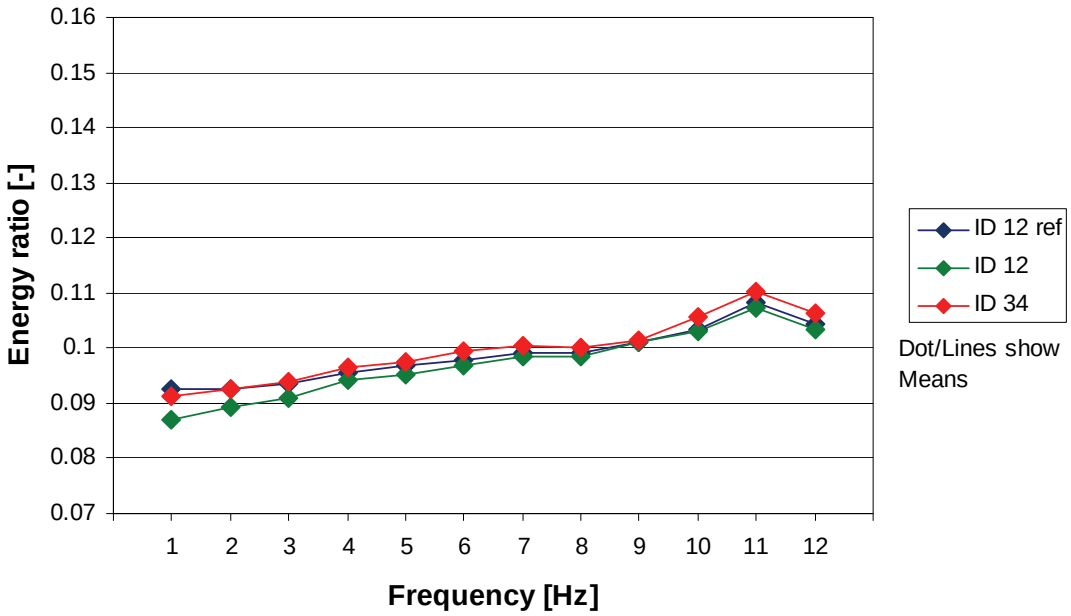

Figure IV-29 Energy ratio for the 'Young-Neutral' group during frequency-dependent measurements for axial loading (offset -800 N, amplitude ±550 N) in different periods of the mechanical parameters test. The SEM was between 0.0031 and 0.0050.

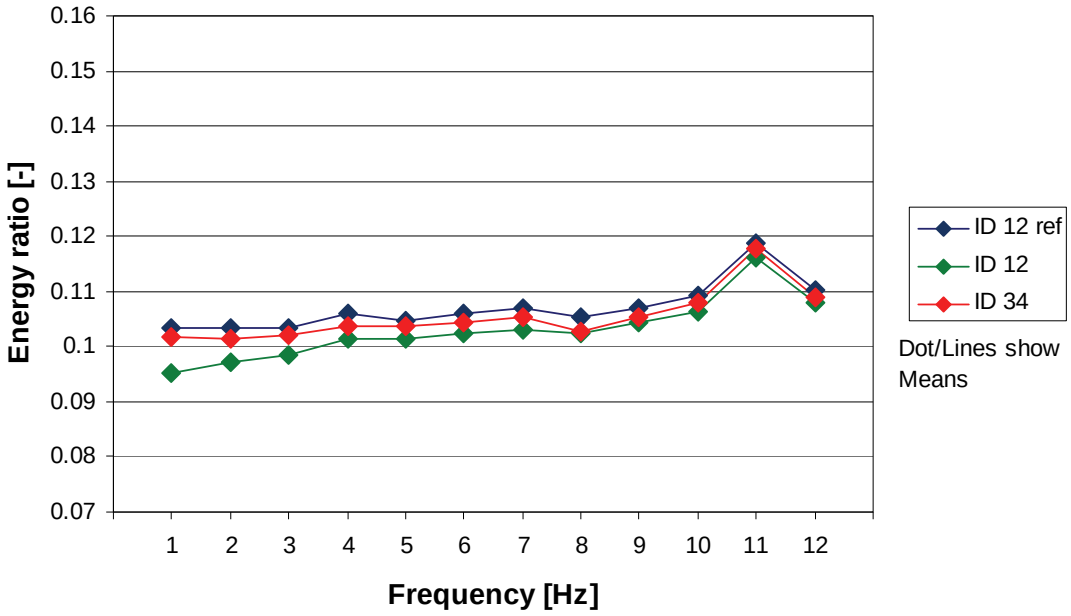

Figure IV-30 Energy ratio for the 'Young-Flexed' group during frequency-dependent measurements for axial loading (offset -800 N, amplitude ±550 N) in different periods of the mechanical parameters test. The SEM was between 0.0056 and 0.0090.

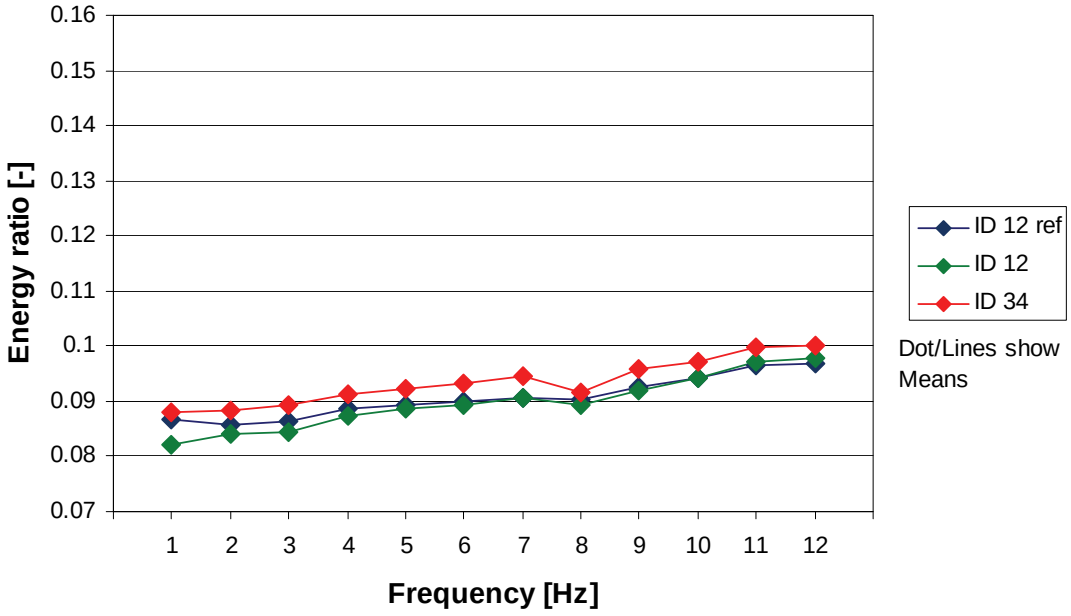

Figure IV-31 Energy ratio for the 'Old-Neutral' group during frequency-dependent measurements for axial loading (offset -800 N, amplitude ±550 N) in different periods of the mechanical parameters test. The SEM was between 0.0020 and 0.0056.

The stiffness for frequency-dependent reference measurements (ID 12 ref, ID 12 and ID 34) was highest for the 'Young-Flexed' group (Figure IV-33), although no

statistical differences between groups were observed. For all groups, the stiffness increased during consecutive measurements by as little as 0.6 % and by as much as 6 % (Figure IV-32, Figure IV-34). The main effect of frequency on stiffness was significant ($p < 0.001$, Greenhouse-Geisser correction). The stiffness for all frequencies was larger when compared to the stiffness at a frequency of 1 Hz (contrast, $p < 0.001$). Frequency and group interaction (frequency × group) was significant ($p = 0.009$, Greenhouse-Geisser correction). When compared to stiffness at a frequency of 1 Hz, the increase of stiffness at frequencies of 9, 10, 11 and 12 Hz was larger for the 'Young-Neutral' and 'Young-Flexed' groups than for the 'Old-Neutral' group (contrast, $p < 0.05$). The main effect of this stage of the experiment (ID No.) was significant ($p < 0.001$). Stiffness for ID 12 and ID 34 was significantly larger than for ID 12 ref (contrast, $p < 0.001$). The frequency within different IDs also impacted the stiffness differently (frequency × stage interaction, $p < 0.001$).

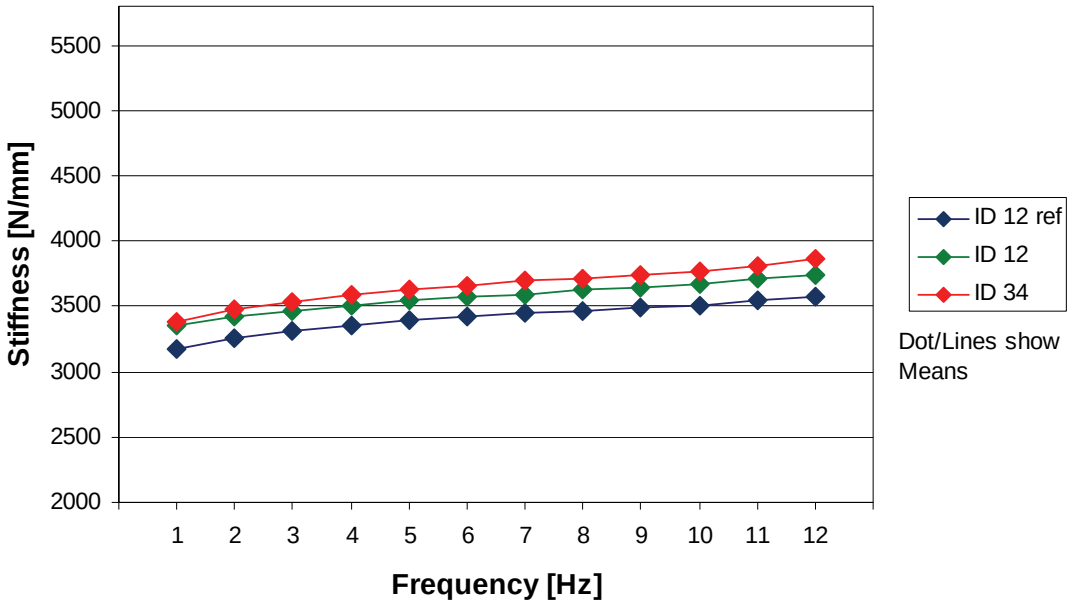

Figure IV-32 Stiffness for the 'Young-Neutral' group during frequency-dependent measurements for axial loading (offset -800 N, amplitude ±550 N) in different periods of the mechanical parameters test. The SEM was between 274 and 327 N/mm.

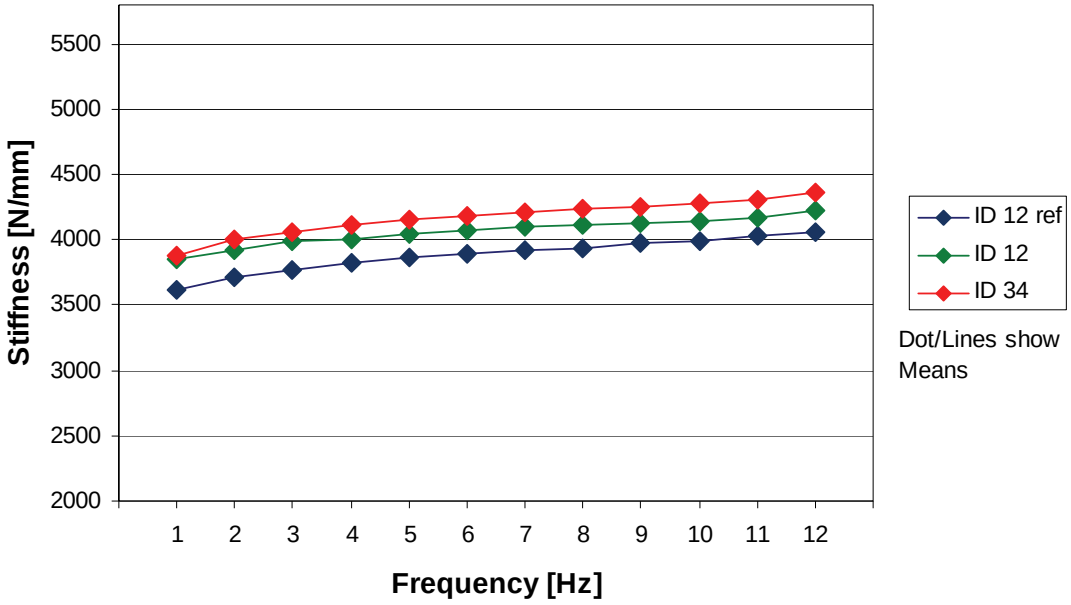

Figure IV-33 Stiffness for the 'Young-Flexed' group during frequency-dependent measurements for axial loading (offset -800 N, amplitude ±550 N) in different periods of the mechanical parameters test. The SEM was between 324 and 382 N/mm.

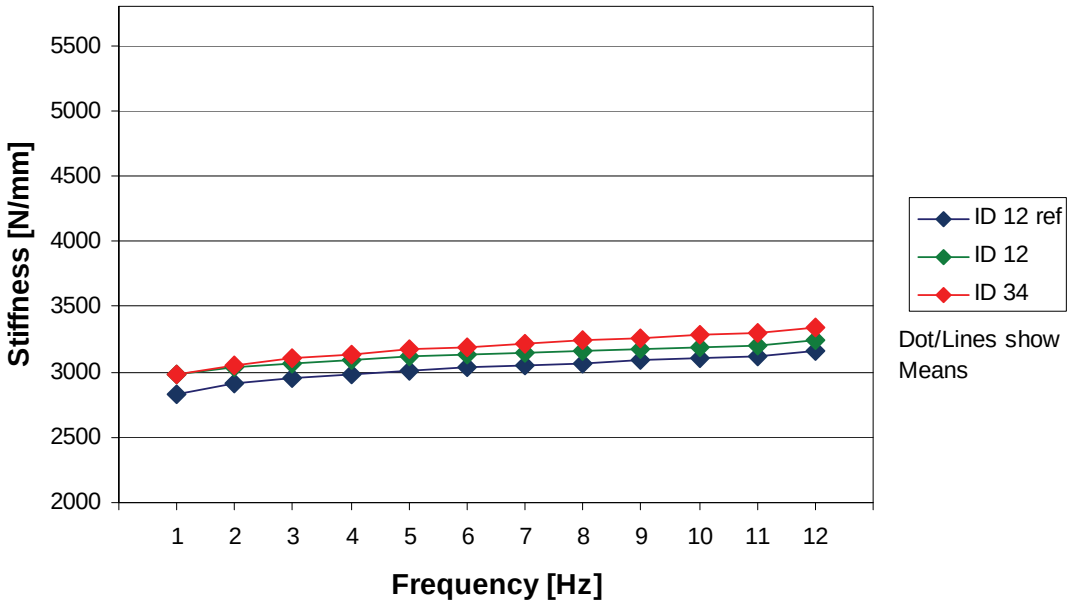

Figure IV-34 Stiffness for the 'Old-Neutral' group during frequency-dependent measurements for axial loading (offset -800 N, amplitude ±550 N) in different periods of the mechanical parameters test. The SEM was between 280 and 336 N/mm.

4 Dynamic - Discussion

Human lumbar motion segments exposed to different directions of loading (compressive or shear) with dynamic and quasi-static loading showed a variety of behaviours.

The energy ratio in the quasi-static shear tests was smallest for specimens of young donors tested in a flexed posture. This indicates that due to this posture, the specimens are less viscous in comparison to specimens in a neutral posture. It can be assumed that in flexion there would be less damping and this would result in an increased transmission of peak loads and vibrations.

The specimens' stiffness in the axial direction was highest when no additional shear load was present. Shear load decreased the axial stiffness regardless of the direction of this shear load (anterior or posterior). One could assume that the presence of an anterior shear load would load the apophyseal joints and increase stiffness. On the other hand, the shear load was only 200 N, which might not be enough to separate or bring the apophyseal joints together, but this does not explain the significant difference in axial stiffness. This finding is similar to the data presented by Huber et al. (2005). The mechanism that leads to this behaviour is still unclear.

The stiffness in the anterior-posterior shear direction increased with increasing axial compression load. It increased five-fold in comparison to the unloaded motion segment, when 2000 N of compression was applied. This finding is similar to Janevic et al. (1991). Flexion of the specimen led to higher values when compared to specimens tested in a neutral position. The compressive load had various effects on shear stiffness in the different groups. Initially, the shear stiffness was higher for the 'Young-Flexed' group than for the others. However, the shear stiffness increased more with increasing compressive load in the 'Young-Neutral' group than in the 'Young-Flexed' group. This discrepancy could be attributed to the position of the apophyseal joints. In the 'Young-Flexed' group the apophyseal joints were separated and the compressive load did not cause the joints to come into contact, whereas in the 'Young-Neutral' group the apophyseal joints were closer and the increased compressive load resulted in more contact between them, hence causing a greater increase in stiffness.

Quasi-static and dynamic tests showed a trend of increasing axial stiffness with repetition of the mechanical parameters tests.

The energy ratio of hysteresis obtained during the dynamic axial compression test rose with increasing test frequency. Similar values were observed for similar amplitudes regardless of differences in the applied offset load.

Dynamic axial and shear stiffness increased with increasing test frequency and decreased with increasing amplitude. This behaviour is similar to results presented by Huber et al. (2005). When the direction of the shear test is considered, the stiffness measured during cyclic loading with an offset load towards the anterior direction was higher than with offset loads towards posterior directions. It can be assumed that an offset load towards the anterior direction decreases the distance

between the apophyseal joint, hence increasing stiffness. The opposite happens when the offset load is directed towards the posterior.

Part V Modelling of Mechanical Response

Christoph Mischke, Daniel M. Skrzypiec,
Gerd Huber, Horst Peter Wölfel

1 Modelling - Introduction

Dynamic whole-body models of the human body allow the calculation of forces and displacements in various parts of the body and thus enable the evaluation of possible damage on a relative basis. In addition to whole-body models, there exist numerous models of parts of the human body. In order to estimate the risks of lower back pain as a consequence of whole-body vibrations, numerical models of both the human lumbar spine and lumbar spine motion segments have been developed. Most of these models represent an average geometry or might be adjustable to certain percentiles.

An overview of some of the older models can be found in Mischke et al. (2007). These can be used to predict aspects of comfort or health risks for one or different percentiles. In order to evaluate the individual health risks, it is necessary to develop partial or complete individual models.

To enable conclusions to be made about possible damage to individuals, the relevant stresses and strains must be taken into consideration. Because stresses and strains depend on geometry (amongst other factors), any numerical model for the purpose of patient-specific calculations must be individualised. A complete individual model is presented in Pfeiffer et al. (2007), who created an auto-meshed finite element (FE) model based on CT data and used it for their analysis. The advantage of this procedure is that it generates a highly individualised model that encompasses natural geometric asymmetries and other deformities. On the negative side, a great amount of time and effort is required for this method and the computational costs are significant. Moreover, auto-meshing requires the use of tetrahedron elements due to the non-isoparametric shapes of the vertebrae. The numerical behaviour of these elements is inferior compared to that of brick elements.

In the following chapters a partially individualised numerical model of a motion segment of the human lumbar spine (L4-L5) is presented (submodel). The model can be adjusted to individual lumbar spines using 23 geometric parameters. All parameters are based on individual CT data. The level of geometric individualisation is lower compared to completely individualised models, but on the other hand, individualisation using this method is faster and the computational costs of the analysis are lower as well. Furthermore, the numerical model consists of 8-node brick elements, which are numerically less critical than tetrahedral elements. The advantage of both individualisation methods is that CT data can be acquired both on in vitro and in vivo lumbar spines.

According to Griffin (2001), the submodel described in this study is an ‘effects model’ that represents one motion segment of the lumbar spine. It is an improvement of an existing submodel described by Mischke et al. (2007). Both models can be used to

calculate deformations, stresses and strains under different kinds of static or dynamic loads and they take individual geometric parameters into account. Data from in vitro experiments were used for the validation of both submodels. The advancement of the submodel presented here is a more sophisticated description of the annulus material; greater detail was necessary to account for the influence of combined loads (i.e. compression under shear load). Moreover, the validation of the model is now based on in vitro data of functional spinal units of older donors as well and also includes different flexion angles.

1.1 Numerical models of the lumbar spine in the literature

There are several three-dimensional FE models of the lumbar spine described in the literature that differ primarily in the number of modelled vertebrae. One model consists of a single vertebra (Pfeiffer et al., 2007), another comprises two vertebrae (Schmidt et al., 2007) and one consists of three vertebrae (Denozière et al., 2006). At the other end of the spectrum, two models comprise the whole lumbar spine from vertebra L1 to vertebra L5 (Rohlmann et al., 2006; Rochefort et al., 2005) and there is also one model that consists of all vertebrae from L1 to S1 (Shirazi-Adl, 2006).

Only three models offer geometries based on CT and/or MRT data of human lumbar spines (Shirazi-Adl, 2006; Schmidt et al., 2007; Pfeiffer et al., 2007). Of these, only one model allows for the individualisation of geometry (Pfeiffer et al., 2007) by directly meshing the geometry derived from the CT data. Therefore, this model is completely individualised.

In almost all of the above-mentioned models, the ligaments and the facet joints are modelled. The exception is the single vertebra model (Pfeiffer et al., 2007), which does not contain any soft tissues and no description of facet contacts.

Regarding the modelling of the intervertebral disc, the state of the art is a fibre-reinforced ground substance for the annulus and a liquid-filled cavity representing the nucleus.

The biggest limitation of the above-mentioned models is that they cannot be individualised, with the exception of the one consisting of a single vertebra without any soft tissues (Pfeiffer et al., 2007).

1.2 Objective of the study

Due to the limitations of existing models, the aim of this study was to establish a so-called ‘partially individualised’ finite element model of the lower human lumbar spine that consists of two vertebrae with state-of-the-art representation of the intervertebral disc. Moreover, the longitudinal ligaments and the facet joints are modelled. ‘Partially individualised’ means that the geometry of a reference model can be scaled on the basis of individual geometric parameters derived from CT data. The new model was validated on the basis of in vitro experiments. It was thereby investigated whether the experimental results of different individuals could be simulated with models that were based on the same set of material parameters but varied in terms of individual geometric parameters.

2 Modelling - Methods

The model of the vertebrae L4 and L5, including the connecting intervertebral disc and the longitudinal ligaments, consists of 4920 nodes (4972 elements) and was designed to closely imitate human anatomy. An examination of various levels of discreteness was performed during the development of an earlier version of the submodel (Hofmann et al., 2003).

The coordinate system was chosen in accordance with Figure V-1. A force in the negative z-direction results in axial compression of the lumbar spine; a force in the x-direction results in frontal shear. The FE model (Figure V-2) consists of the different components given in Table V-1. The properties of the ligaments can be found in the appendix.

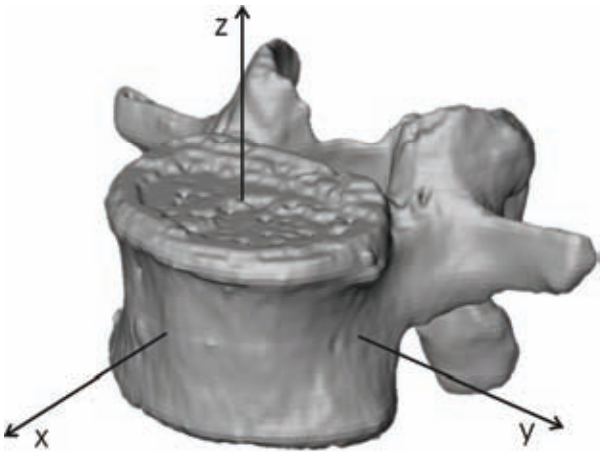

Figure V-1 Coordinate system of the numerical model

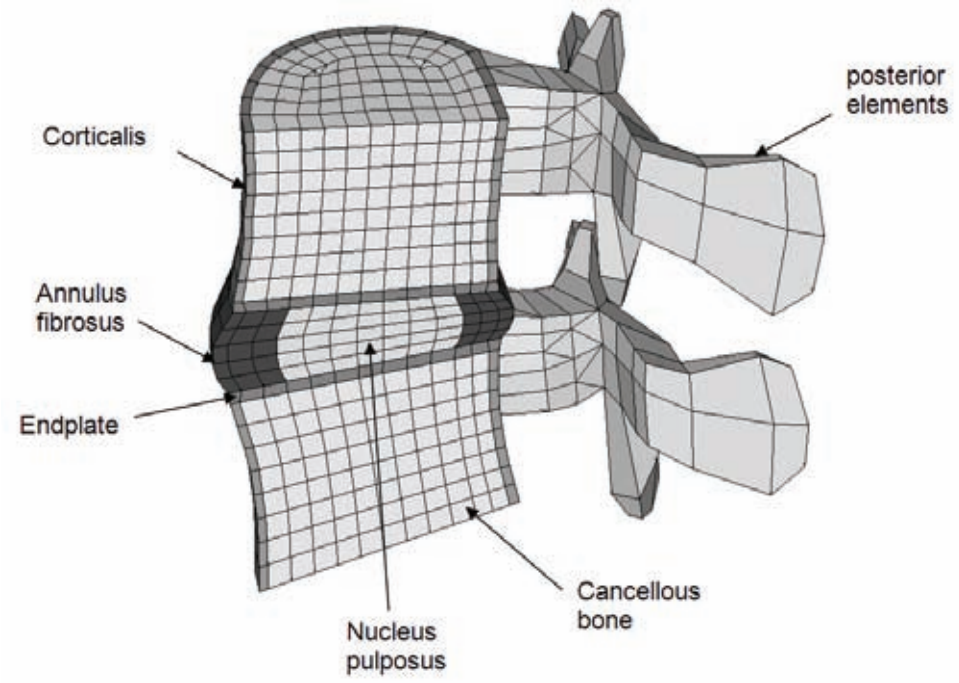

Figure V-2 Mid-sagittal virtual cut through the FE model (the modelled ligaments are not shown)

Table V-1 Material laws and parameters of the different components

Component	Material behaviour	Young's modulus [MN/m²]	v[-]	Shear modulus [MN/m²]
Cortical bone	isotropic	16500	0.3	(6346)
Cancellous bone	isotropic	100	0.2	(41.7)
Nucleus pulposus	viscoelastic, isotropic	0.105	0.35	(0.035)
Annulus fibrosus	transversal isotropic	E1=20.84 E2=20.84 E3= 2.0	0.3	G_{12}=3.47 G_{13}=5.40 G_{23}=5.40
Posterior elements	isotropic	10000	0.3	(3846.2)
Endplates	isotropic	23.8	0.4	(8.5)

2.1 Individualisation of geometry

The individualisation of the numerical model to the lumbar spines of all donors was made possible by the digital recording of the lumbar spines using computer tomography (CT). The CT data was processed using Amira software (Mercury Computer Systems, Inc., Berlin, Germany). Three-dimensional geometry models were created and measured for every lumbar spine based on CT slices.

The geometry of the FE model can be adapted using 23 parameters. Most of them are shown in Figure V-3. These parameters were obtained by measuring the three-dimensional geometric model created on the basis of individual CT data. The depth and width of each vertebra was measured on the top, in the middle and at the bottom (12 parameters). Because the FE model of each vertebra consists of 10 nodal planes, the planes between the top and the middle plane and between the bottom and the middle plane were adapted using linearised parameters. This procedure ensures that the outline of the vertebra is smooth and free from buckling. In addition, the ventral and distal height of each vertebra (4 parameters) and the distance between the vertebrae – at the front, in the middle and at the back of the lumbar spine (3 parameters) – as well as the depth and width of the posterior elements (4 parameters) were measured.

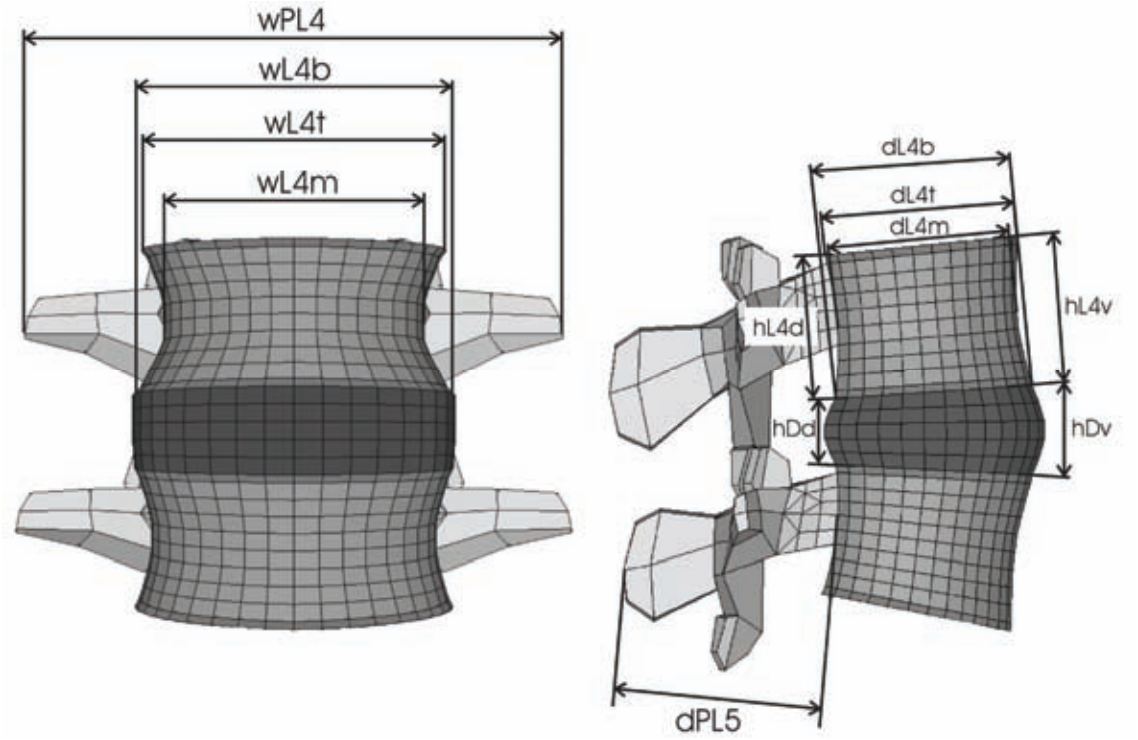

Figure V-3 Geometric parameters (apart from disc heights, each parameter shown refers to L4 and L5; disc height in the middle is not shown)

Concerning the individualisation process, the first step was to create a basic FE submodel that could be scaled in order to achieve the desired geometry. The measured data was loaded into the Matlab software. Matlab was then used to generate different 'command files' for HyperMesh software (Altair Engineering GmbH, Böblingen, Germany). Next, the individualisation process was automatically performed by HyperMesh on the basis of the command files.

A uniformly distributed load transmission was provided by the creation of a rigid plate on the top and at the bottom of the FE model. The experimental setup dictated that the submodel be constrained at the bottom, with the force applied on the top and the displacements calculated on the top as well. Moreover, the following degrees of freedom were constrained on the top: translation in the y-direction and the three rotational degrees of freedom.

2.2 Boundary conditions

The geometric boundary conditions that were active during the experimental tests were also transferred to the numerical model. The following figure shows the experimental setup scheme.

The functional spinal units (FSUs) were potted using a polymer (Figure V-5). The potted FSUs were then mounted in the testing machine. This procedure ensures that the forces are applied on the whole upper and lower planes of the FSUs and not only in isolated spots.

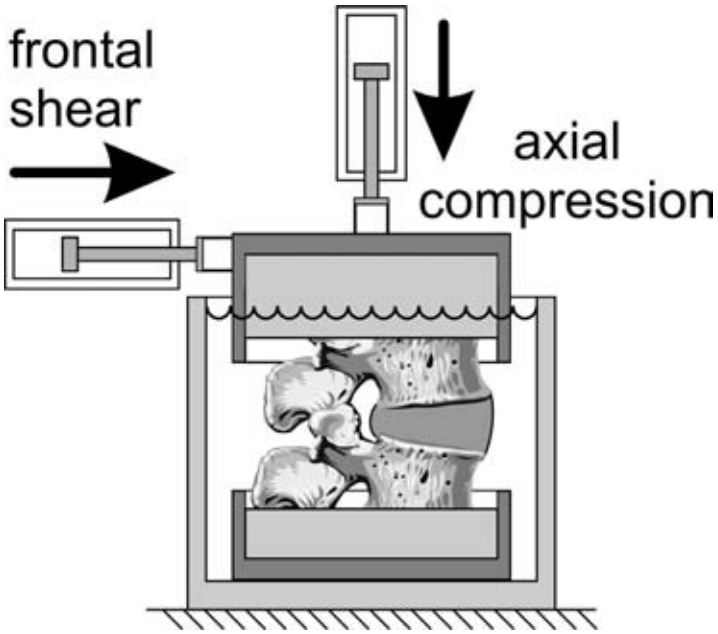

Figure V-4 Setup scheme (Huber et al., 2005)

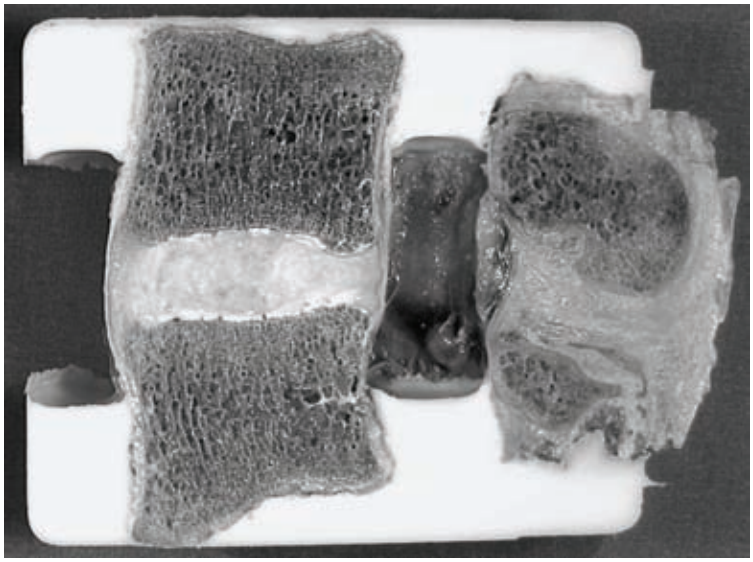

Figure V-5 LWS 0040 (L4-L5) after testing, sagittal plane (Huber et al., 2007)

To allow for realistic ambient conditions during the tests, the FSUs were surrounded by a physiological saline solution tempered at 37 °C. The lower pot was fixed in the testing machine in all six degrees of freedom, whereas the upper pot was only fixed in four directions (y, rotx, roty, rotz). Consequently, vertebra L4 could only move in the x- and z-directions.

First of all, the pots, the polymer and the FSUs were included in the model. The purpose of this pilot simulation was to investigate the influence of the stiffness of the polymer. The specification of the material parameters of the polymer proved to be particularly problematic in this case. The polymer chosen for potting is called RenCast® FC 53 Isocyanate / FC 53 Polyol and was applied with added filler. According to the manufacturer's declaration, this product has a bulk modulus K of 2400 MPa after hardening for seven days at room temperature and for 14 hours at

80 °C, respectively (RenShape Solutions, 2004). The bulk modulus K can be converted into the elastic modulus as follows (Szabó, 1964):

$$E = K \cdot (3 - 6 \cdot \nu) \quad . \tag{V-1}$$

Poisson's ratio ν has two extreme values for isotropic materials: $\nu = 0$ and $\nu = 0.5$, respectively. Using these values in the above-mentioned formula leads to a spread for the elastic modulus of E = 0 … 7200 MPa. Assuming a Poisson's ratio of $\nu = 0.3$, the elastic modulus is E = 2880 MPa. Using these parameters in the simulation and comparing this simulation with a simplified simulation without pots and polymer (the force is applied via rigid cover plates on the vertebrae, as can be seen in Figure V-6) showed no difference in the results for experiments ID 01 and ID 04. Even with an elastic modulus of E = 0.144 MPa ($\nu = 0.4$), there is hardly any discernible difference between the simulations (for example, the potted model is 0.02 % softer for quasi-static compression than the model with rigid plates).

The above-described assumption is necessary because a more accurate specification of the elastic modulus of the polymer is impossible. First of all, the hardening time affected the elastic modulus adversely. The time specified by the manufacturer could not be maintained because the FSUs had to be tested very soon after potting to reduce the risk of biological degradation. Moreover, not only the FSUs but also the polymer was surrounded by a physiological saline solution tempered at 37 °C, which exceeded the manufacturer's suggested range of 18 to 25 °C.

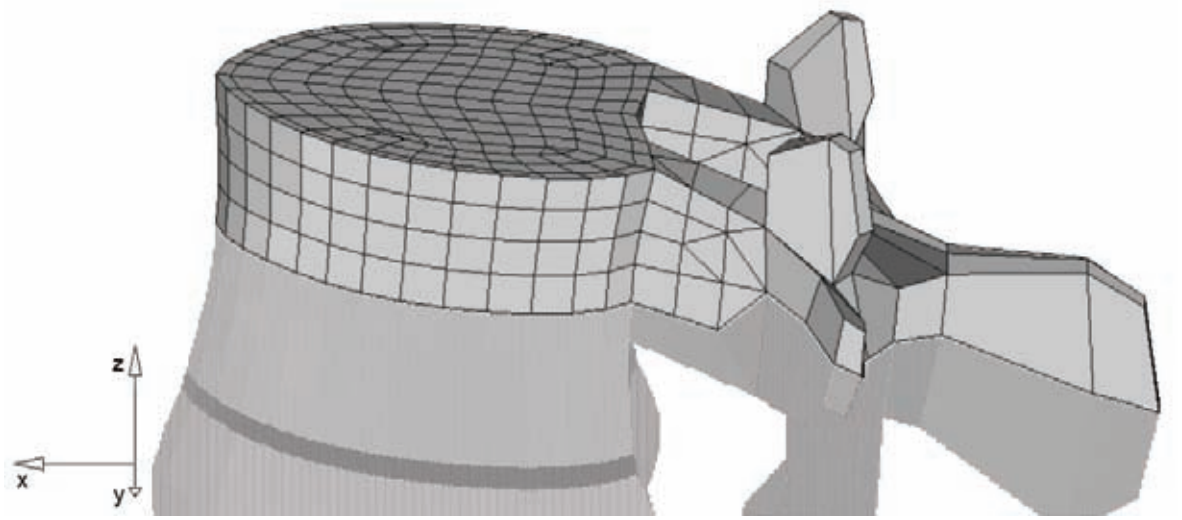

Figure V-6 Rigid cover plate of L4

The analyses specified allowed for using the simplified simulations with rigid cover plates when comparing the experimental results with the results of the numerical model. The dimensions of the rigid cover plates were chosen according to the boundary surface of the FSUs and polymer in the experiments. Each cover plate had a reference node on which the load was applied (upper plate) and which is constrained (lower plate), respectively. Modelling the pots and the polymer was not considered necessary.

2.3 Validation

The submodel had to undergo different validation steps according to the various experimentally investigated influencing factors. The complete set of in vitro experiments and the corresponding abbreviations can be found in the preceding chapter (**Part IV**) or in the appendix (**Part VIII1**). Of those measurements, six quasi-static in vitro tests and five dynamic measurements with a frequency range of 1 to 12 Hz were taken into account for the validation.

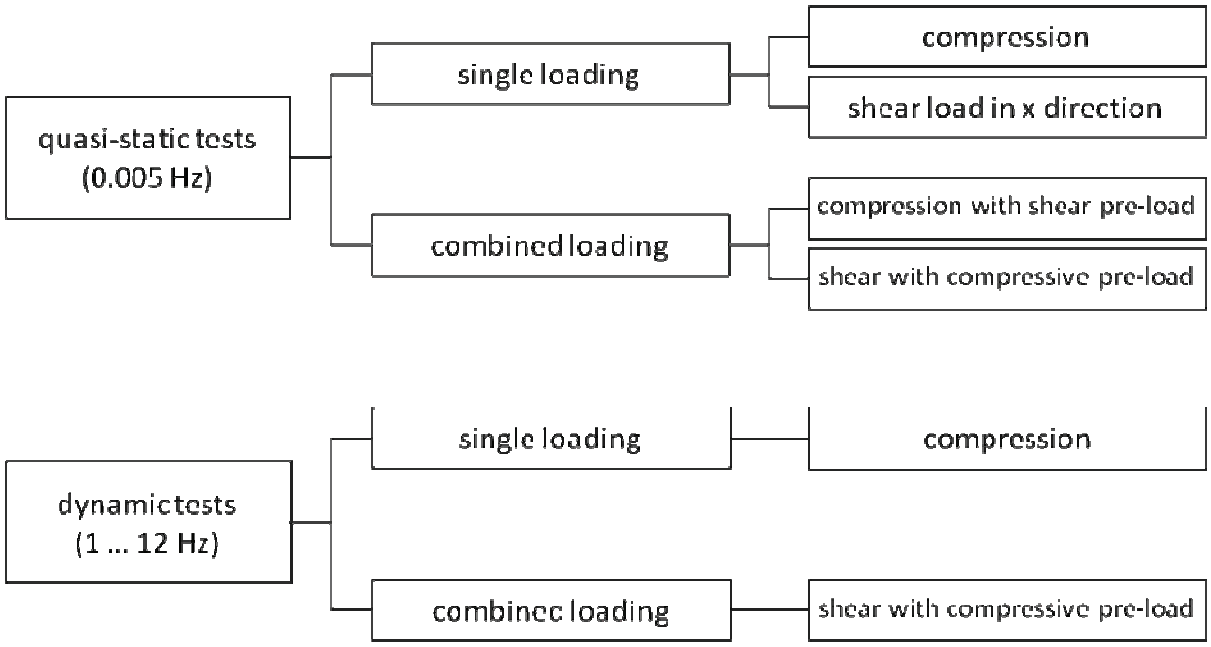

Figure V-7 Overview of performed in vitro experiments used for validation

Three quasi-static tests applied axial compression (z-direction) from 0 N to 2000 N. They differed with respect to the application of anterior-posterior shear (x-direction). No shear (ID 01), an anterior shear of 200 N (ID 02) or a posterior shear of -200 N (ID 03) was applied.

The following three measurements applied quasi-static cyclic anterior-posterior shear starting from 0 N to ±200 N. They differed in terms of the applied axial pre-load. No pre-load (ID 04), a -1000 N pre-load (ID 05) or a -2000 N pre-load (ID 06) was applied.

Three dynamic loadings with axial compression (z-direction) without shear differing in offsets and amplitudes were applied: -800 N ± 200 N (ID 10), 1100 N ± 200 N (ID 14) and -1100 N ± 1000 N (ID 18).

For two dynamic loadings, the cyclic loading was applied in the anterior-posterior shear direction (x-direction). In the axial direction a compression of -800 N was applied. The shear offset and amplitudes were 0 N ± 200 N (ID 21) and 100 N ± 200 N (ID 24).

2.3.1 Quasi-static validation

The validation of the quasi-static combined loading condition is a very challenging task, as shown by the first validation step performed in project F2028 (Mischke et al., 2007).

In Figure V-8 it can be seen that the compressive flexibility is highly dependent on the shear pre-load. Under a positive shear load (red curve), the compressive flexibility is more than two times higher compared to the loading condition without a shear load (blue curve). A negative shear load (green curve) increases the compressive flexibility even more. The displacement in the z-direction during pure shear loading shows that the functional spinal units expand in the z-direction. This can be seen in Figure V-9. Because of this expansion the lumbar spines are more flexible in the z-direction under combined loading than under single compression loading.

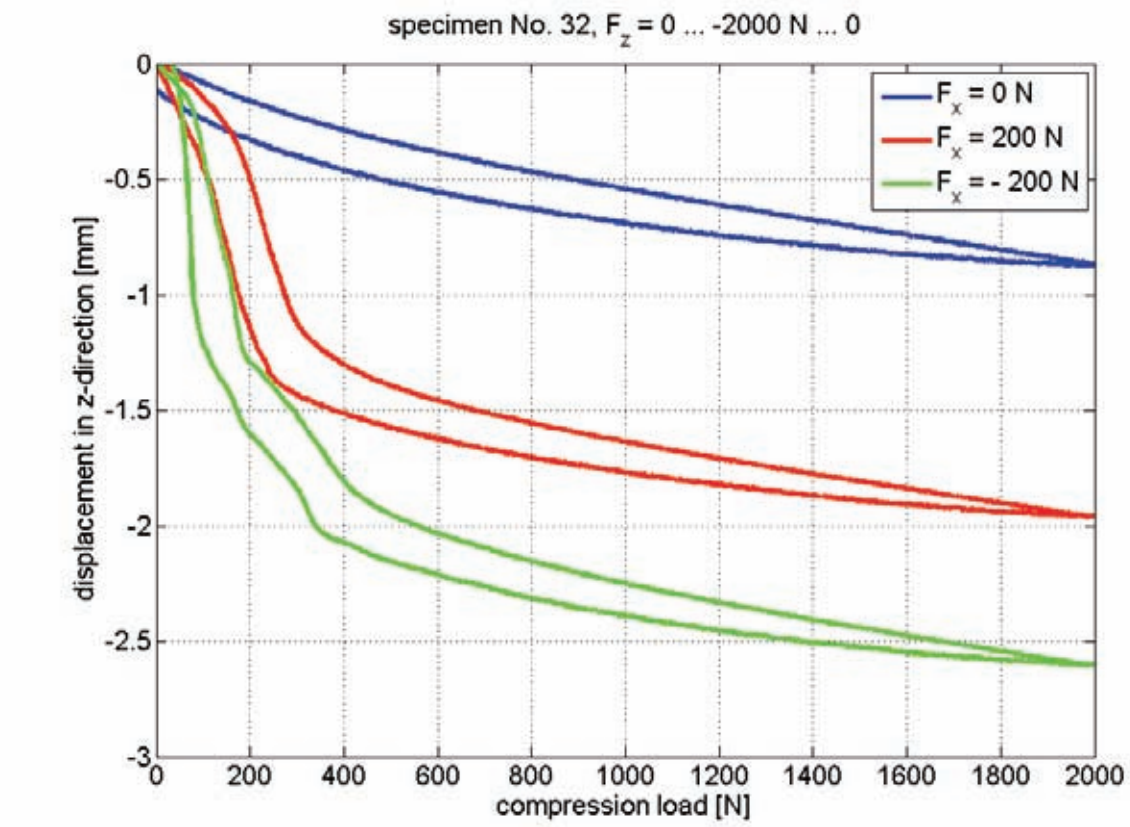

Figure V-8 Results of experiments ID 01, ID 02 and ID 03 for lumbar spine LWS 0032 (measurements from Huber et al., 2005)

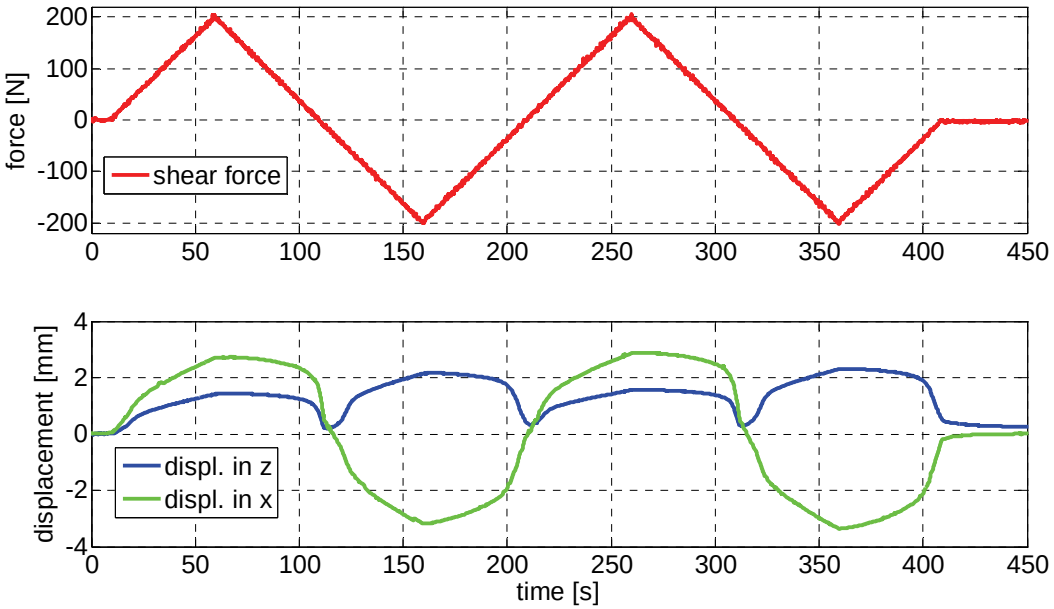

Figure V-9 Displacement in x- and z-directions under pure shear load – ID 04, LWS 0032 (measurements from Huber et al., 2005)

Two main factors could be responsible for this phenomenon: the intervertebral disc and the facet joints. The influence of the intervertebral disc was discovered during the testing of a functional spinal unit without the posterior elements, and therefore without the influence of the facet joints.

The behaviour of the functional spinal unit shown in Figure V-9 is representative for all of the other tested lumbar spine segments in project F1899. In order to implement this behaviour in the submodel, a numerical model solely of the intervertebral disc was created. With the aid of this disc model, the following influencing factors were analysed:

- material laws and material parameters for the annulus
- spring elements in the annulus (modelling of the fibres)
- shape of the endplates.

2.3.1.1 Material laws and material parameters

In the reference submodel (Mischke et al., 2007), the annulus was modelled as hyperelastic isotropic material with spring elements (representing the fibres) connecting the adjacent endplates. However, this approach is unsuitable for describing the behaviour shown in Figure V-9.

Another approach was tested using a simple FE model of a brick first. There are some materials, mostly polymer foams, which have a negative Poisson's ratio ($-1 < \nu < 0$). Stretching these so-called 'auxetic' materials in one direction makes them thicker in perpendicular directions. This phenomenon is shown in Figure V-10

for an isotropic material. Under shear load (Figure V-10, lower line), a small undesired decrease in height can be observed.

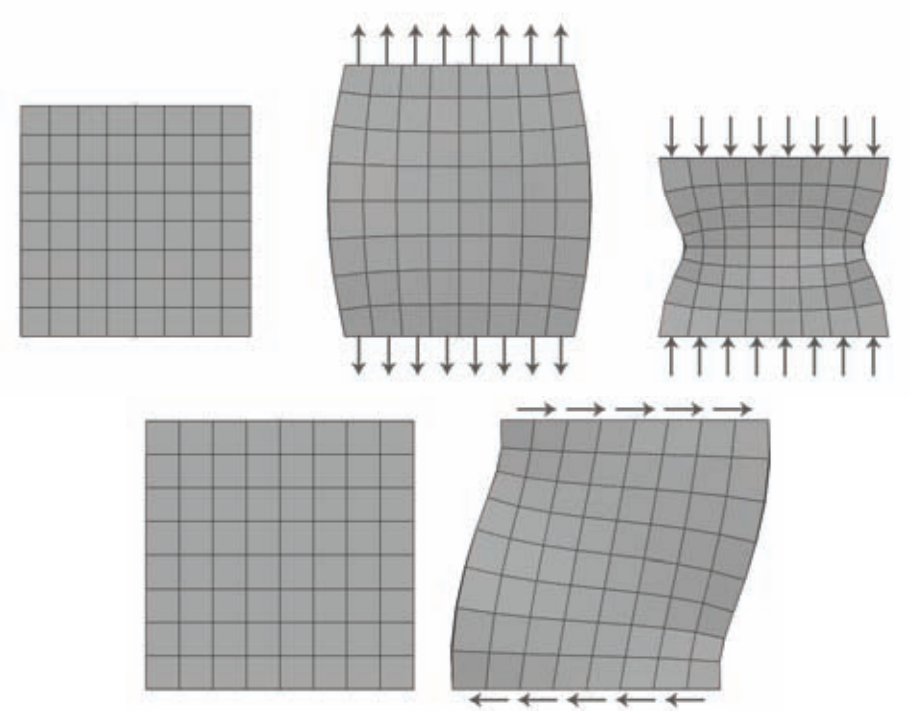

Figure V-10 Behaviour of test model with auxetic material (isotropic)

Using orthotropic (instead of isotropic) auxetic materials and different material parameters in the three translational degrees of freedom would not have led to the desired results either because shear stress does not induce strain in either isotropic or orthotropic materials. Consequently, anisotropic material was used to define the annulus, as this is the only material description that implies a correlation between shear stress and strain.

2.3.1.2 Modelling of the fibres

The annulus fibrosus can be described as a fibre-reinforced matrix; fibres are arranged concentrically around the nucleus pulposus. The fibres criss-cross and connect the endplates of two adjacent vertebrae (Figure V-11).

Figure V-11 Interbred fibres connecting the endplates of two vertebrae (Kummer, 2005)

Figure V-12 displays the implementation of the above-mentioned fibre structure in the numerical model of the functional spinal unit.

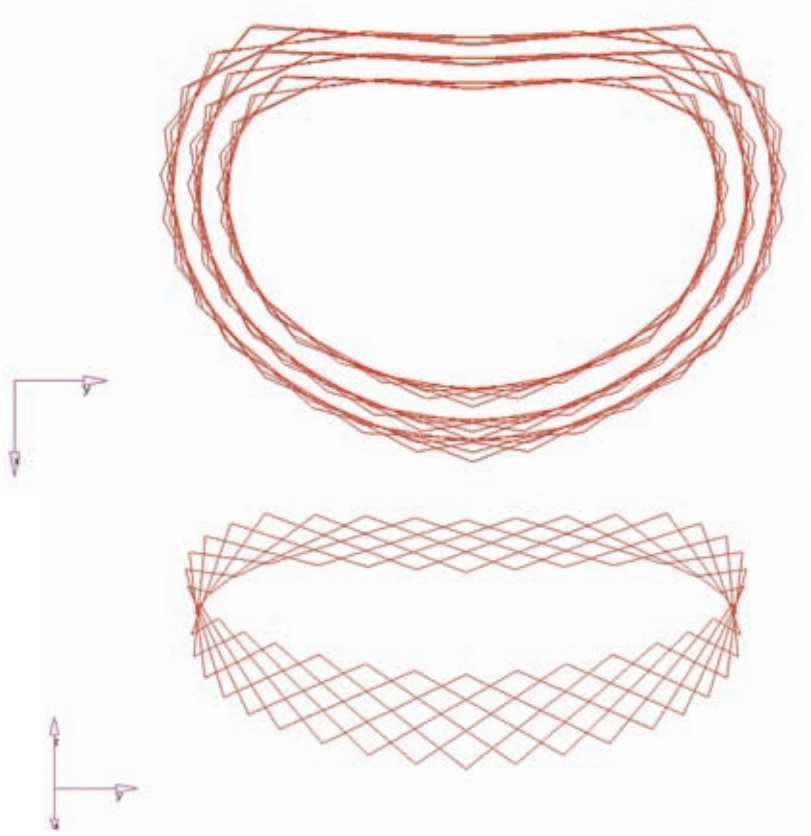

Figure V-12 Modelling of the fibres (above: 3 layers; below: 1 layer)

The experiments showed that there is a pressure of 0.5 to 1.8 bar in the nucleus pulposus of the unstressed functional spinal units. Amongst other things, the variation of the pressure depends on health aspects and the posture of the donors after dying. The counterforce that compensates the resulting force of the pressure inside the nucleus pulposus is induced by the fibres. Consequently, the fibres are pre-stressed.

The application of the intervertebral disc model shows that the pre-stressed fibres play an important role in the above-mentioned behaviour of the functional spinal units under shear load (expansion in the z-direction).

2.3.1.3 Shape of the endplates

The third influencing factor, after the material laws/parameters and the modelling of the fibres, is the shape of the endplates. Up to now, the endplates were modelled as planar areas, which do not conform to human anatomy. For a more detailed description of the geometry, one additional geometric parameter was measured compared to the reference submodel (Mischke et al., 2007): the distance between the vertebrae in the middle of the endplates. This information allows the endplates to be modelled with a domed shape (Figure V-13).

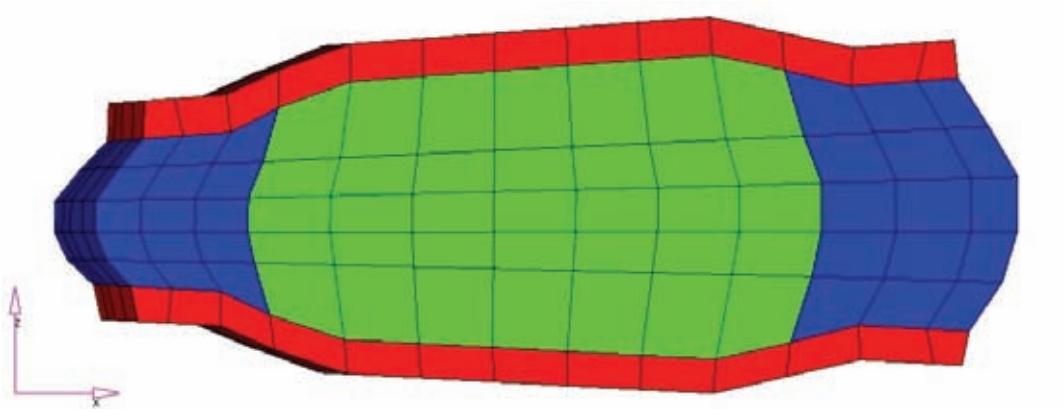

Figure V-13 Intervertebral disc with domed shape (sagittal plane)

2.3.1.4 Conclusion of quasi-static validation

The attempt to implement the above-mentioned behaviour (increasing softness in the z-direction under the shear pre-load) in the numerical model did not satisfy expectations. Work on this specific problem will not continue because the new experiments (project F2069) did not show this behaviour to such extent as can be seen in Figure V-14.

One reason for the higher compressive flexibility of the FSUs under the shear pre-load is their expansion in the z-direction when force in the x-direction is applied. A higher expansion in the z-direction as a result of a pre-load is equivalent to a higher degree of compressive flexibility. The comparison shows the expansion in the z-direction under the shear pre-load. However, it can be seen that the expansion in the z-direction declines in the new experiments; comparison of the green curves: u_z project F1899 (old experiments) and u_z project F2069 (new experiments). Nevertheless, the described behaviour can still be recognised in the new experiments but cannot be implemented in the numerical model.

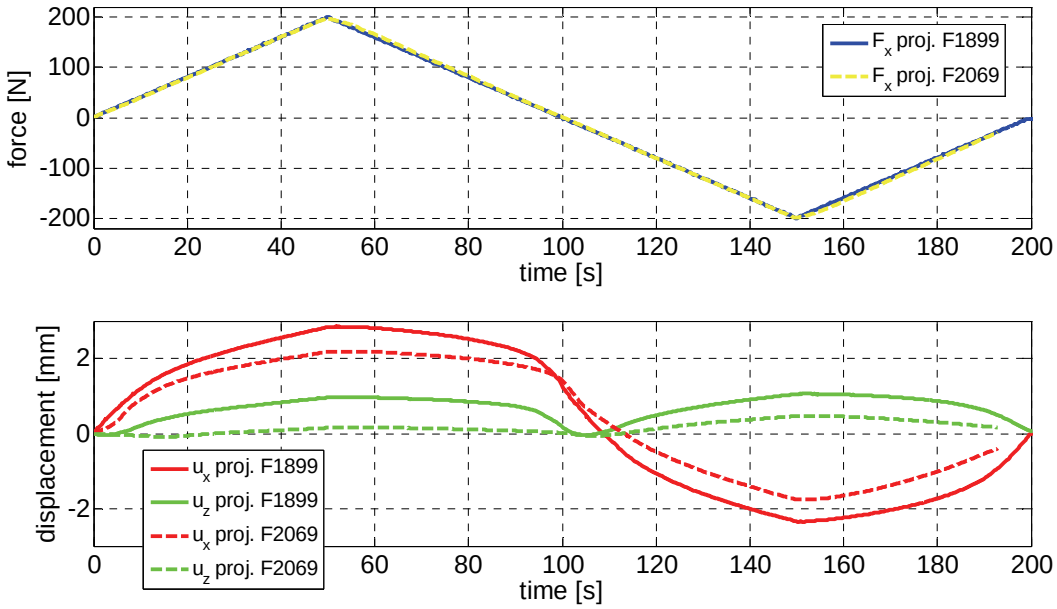

Figure V-14 Comparison of averaged results of experiments ID 04 between the two projects F1899 (solid lines) and F2069 (dashed lines)

2.3.2 Dynamic validation

As can be seen in Figure V-15, there is a distinct difference in amplitude when comparing quasi-static and dynamic results for experiments in the z-direction (shown here for lumbar spine LWS 0032).

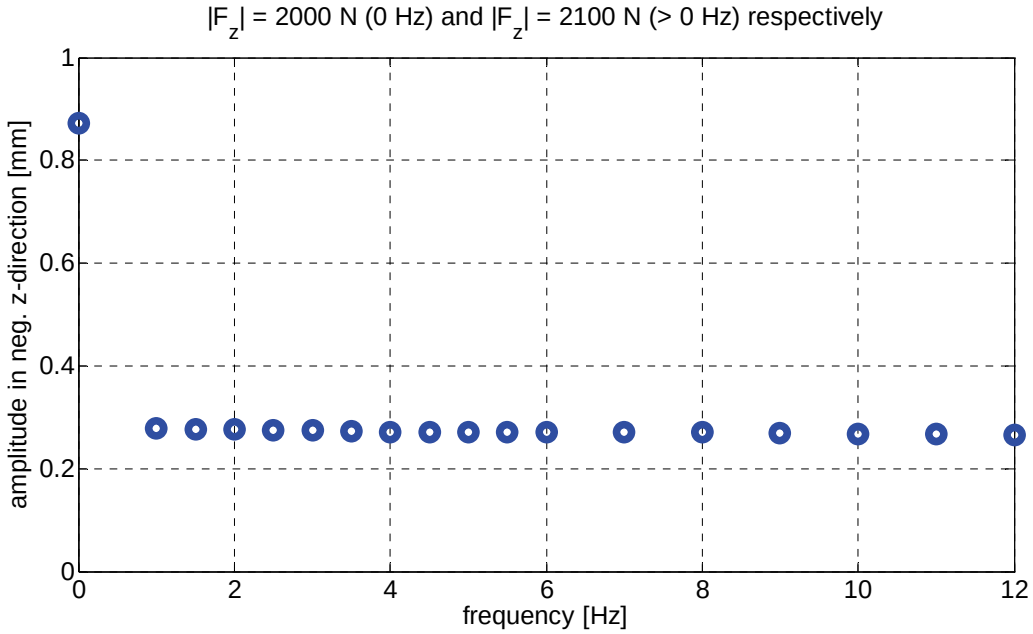

Figure V-15 Comparison between quasi-static and dynamic results of experiments ID 01 and ID 18, LWS 0032 (measurements from Huber et al., 2005)

In the range between 1 and 12 Hz, only slight changes in amplitudes can be observed. To account for the difference between quasi-static and dynamic behaviour, the modelling of the reference submodel (Hofmann et al., 2003) had to be optimised. The damping parameters of the nucleus exert a dominating influence on the dynamic simulation results compared to the damping coefficients of the other components of the model. Consequently, the viscoelastic description of this part of the reference submodel was modified, which led to a better performance of the model for dynamic load cases.

2.4 Influence of age

In this project, the experimental results of six functional spinal units of older donors were compared to the results of twelve FSUs of young donors, which were the subject of the former project F1899. This comparison is shown in the following figures for six different functional spinal units from donors who were close to the 50th male percentile (Table V-2). For the comparison, an additional parameter was introduced: the so-called 'referenced disc height', which is the average disc height divided by the average endplate area of L4 and L5. The endplate area is calculated using the measured width and depth, assuming that the endplate shape is elliptical.

Table V-2 Anthropometric data of the donors

LWS	Age	Body mass	Body height	BMI	Disc height			Referenced disc height
					Aver.	Max.	Min.	
	[yrs]	[kg]	[m]	[kg/m²]	[mm]	[mm]	[mm]	[1/m]
0032	38	79	1.74	26.1	09.9	12.1	6.5	1.555
0045	31	73	1.84	21.6	12.7	15.3	8.7	1.927
1101	56	65	1.74	21.5	11.3	12.9	8.9	1.933
1107	36	75.7	1.74	25.0	10.2	12.2	7.3	1.713
1131	56	73	1.65	26.8	10.2	12.0	6.7	1.443
1135	22	73.8	1.74	24.4	11.3	13.3	7.5	1.948

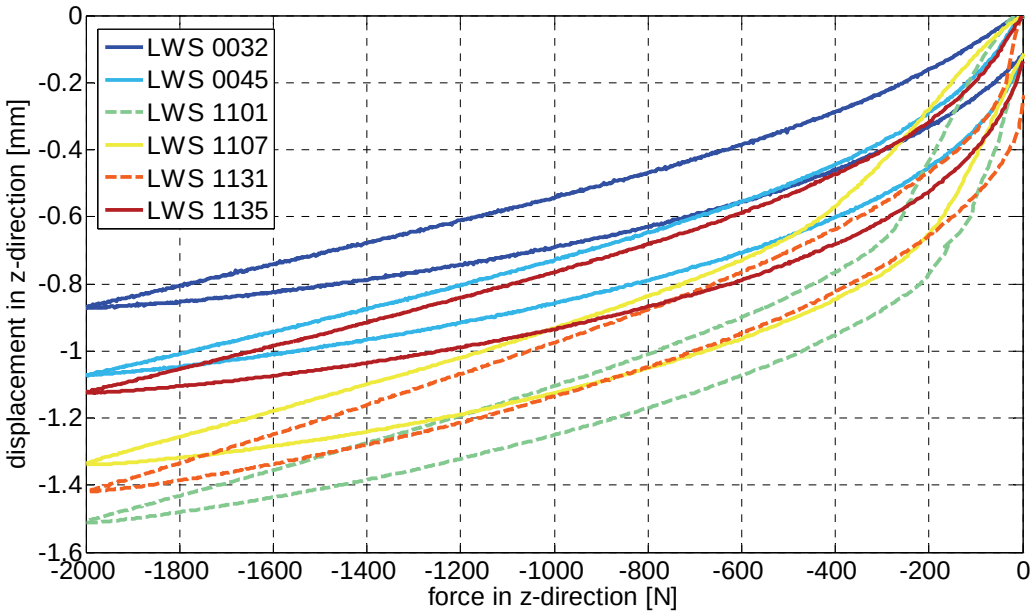

Figure V-16 Experimental data of test ID 01 (dashed lines: old donors)

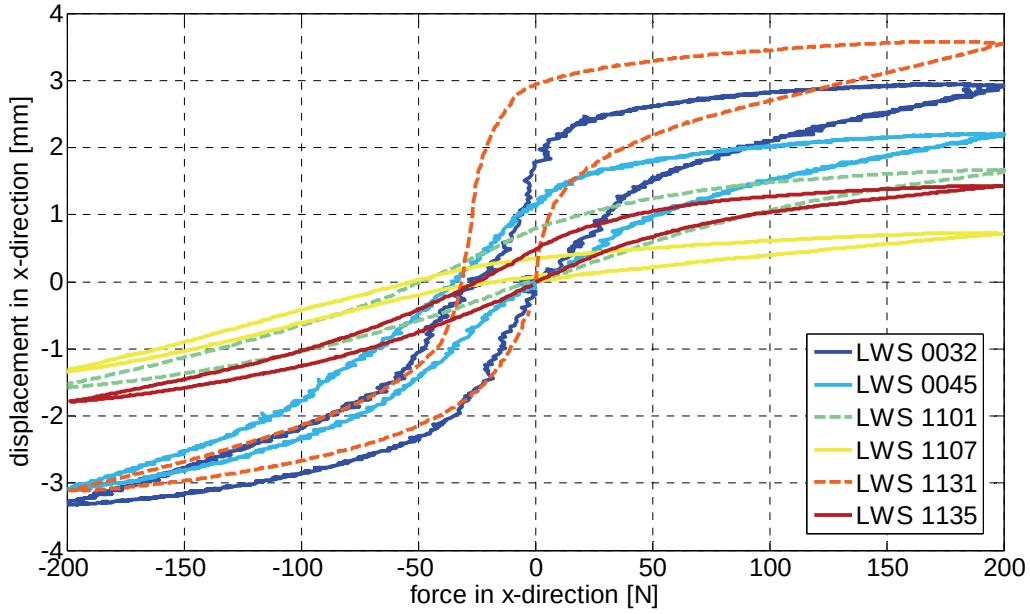

Figure V-17 Experimental data of test ID 04 (dashed lines: old donors)

No general correspondence between the quasi-static behaviour and the influencing factors of age, BMI or (referenced) disc height could be found. For example, the influence of age on the hysteresis of young and old donors with similar anthropometric data can be seen in
Figure V-16 and Figure V-17. Compared to the hysteresis of younger donors (solid lines), the FSUs of the old donors (dashed lines) showed softer behaviour during quasi-static compression (
Figure V-16). However, this was not the case under quasi-static shear load (Figure V-17). One specimen from the old donors exhibited stiff behaviour during shear experiments while the other one showed a rather soft behaviour compared to the young donors. Therefore, the experiments did not provide any clear evidence that

age can directly be used as a determining factor when looking at a specimen's or model's general multi-axial stiffness.

2.5 Influence of flexion

After the influence of age, the influence of flexion was studied as well. Six of the 18 FSUs were tested after the application of a flexion angle of 5° to each vertebra (for a total flexion of 10°, Table V-3). The influence of this parameter is displayed in the following figures.

It can be seen that the flexion of the FSUs leads to stiffer behaviour under compression if the comparison includes the referenced disc height. However, this was not the case under shear load. LWS 1107 (yellow line) indicates that factors other than geometric parameters influence the relation between force and displacement as well. LWS 1107 shows the stiffest behaviour in test ID 04, but in test ID 01 it is the second softest FSU. A possible explanation could be the effects of ligaments and facet joints, which also have to be taken into account with respect to individualisation.

Table V-3 Anthropometric data of the donors (flexed LWS 1112 and LWS 1113)

LWS	Age	Body mass	Body height	BMI	Disc height			Referenced disc height
					Aver.	Max.	Min.	
	[yrs]	[kg]	[m]	[kg/m²]	[mm]	[mm]	[mm]	[1/m]
1101	56	65	1.74	21.5	11.3	12.9	8.9	1.933
1107	36	75.7	1.74	25.0	10.2	12.2	7.3	1.713
1112	20	63.3	1.74	20.9	11.5	13.7	8.4	2.124
1113	21	75.9	1.75	24.8	09.3	10.9	6.5	1.801
1135	22	73.8	1.74	24.4	11.3	13.3	7.5	1.948

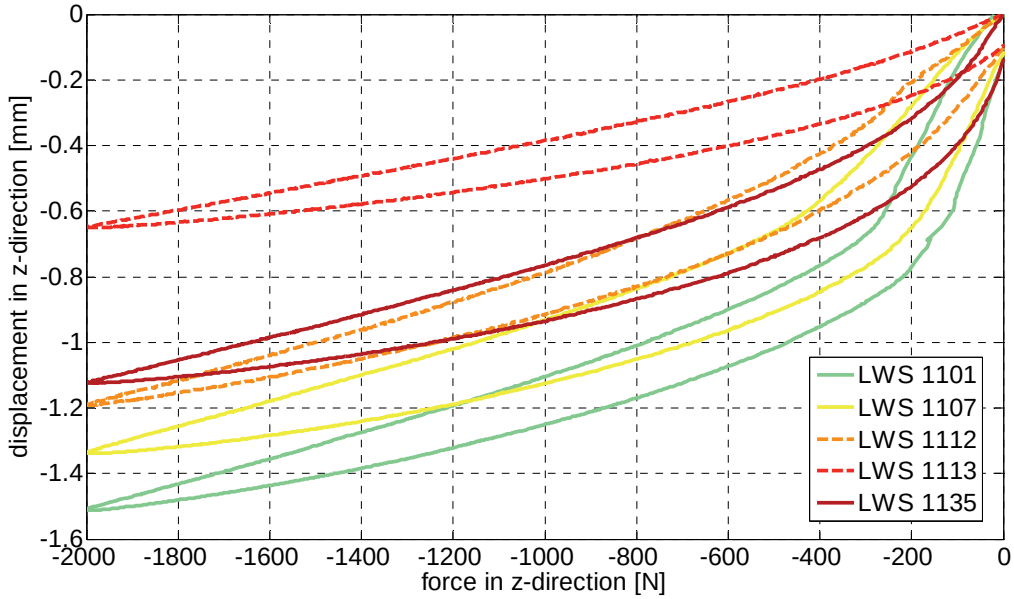

Figure V-18 Experimental data of test ID 01 (dashed lines: flexed FSUs)

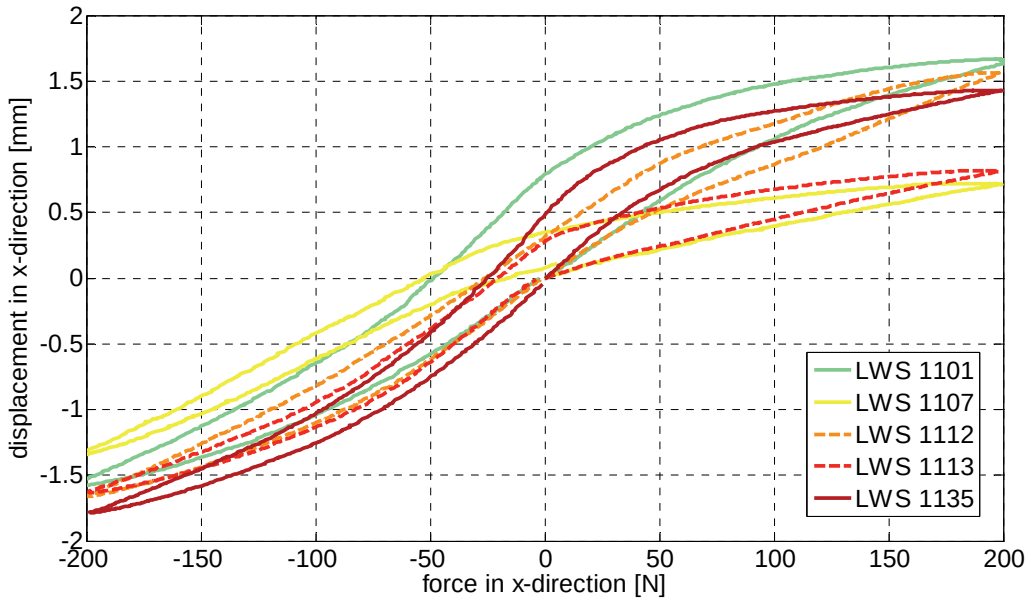

Figure V-19 Experimental data of test ID 04 (dashed lines: flexed FSUs)

3 Modelling - Results

For the presentation of the results, the experimentally identified force-displacement curves of three different FSUs are compared to the numerically calculated curves.

3.1 Quasi-static results

3.1.1 Experiment ID 01

For a quasi-static compressive load from 0 N to -2000 N without a pre-load, all simulation results were close to the target FSU (LWS 1135). Geometric individualisation led to only minor differences between the calculated curves.

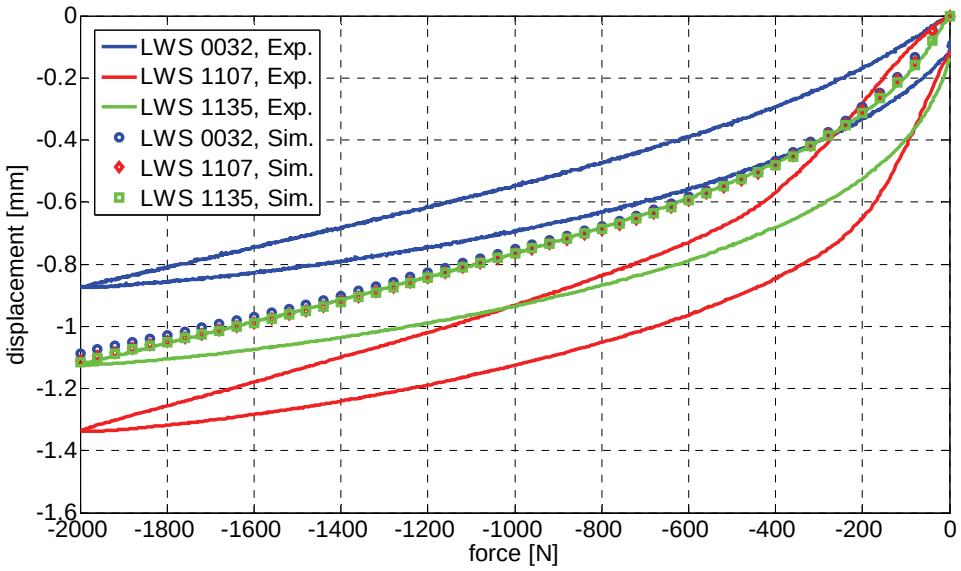

Figure V-20 Comparison of quasi-static compression results without pre-load for young donors

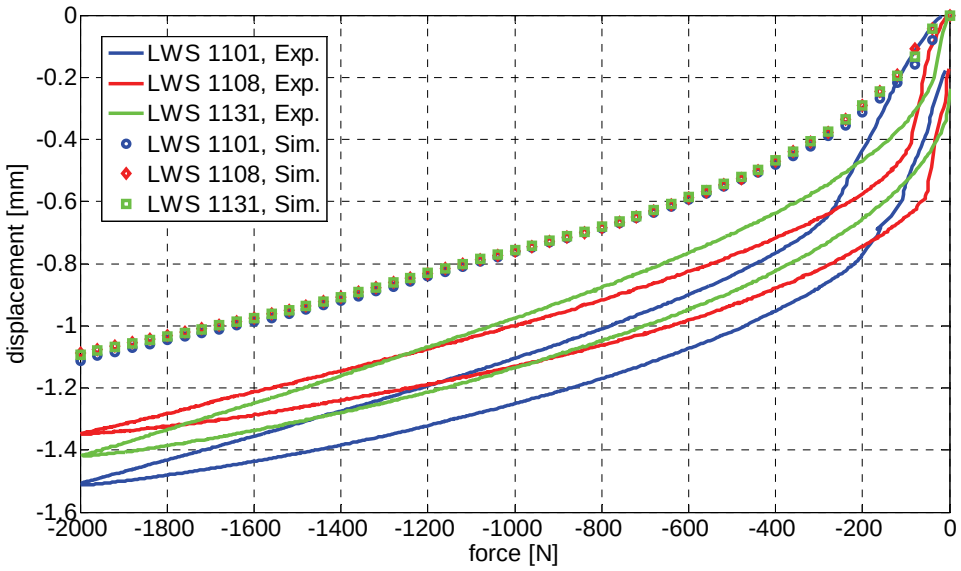

Figure V-21 Comparison of quasi-static compression results without pre-load for old donors

3.1.2 Experiment ID 04

For a quasi-static anterior-posterior shear (± 200 N) without a pre-load, all simulation results were again quite close to the target FSU (LWS 1135). Geometric individualisation led to only minor differences between the calculated curves.

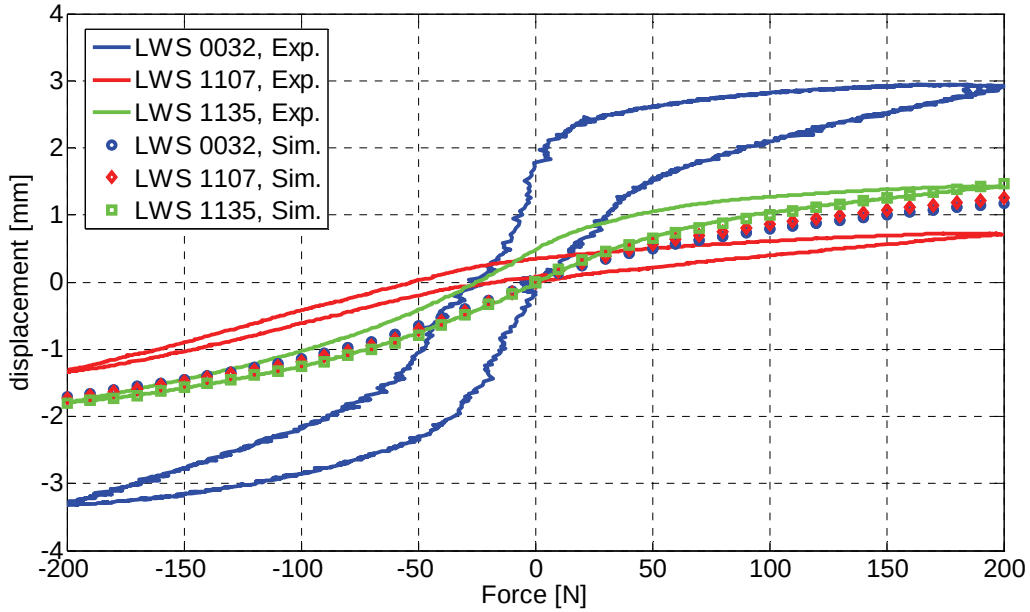

Figure V-22 Comparison of quasi-static shear load results without pre-load for young donors

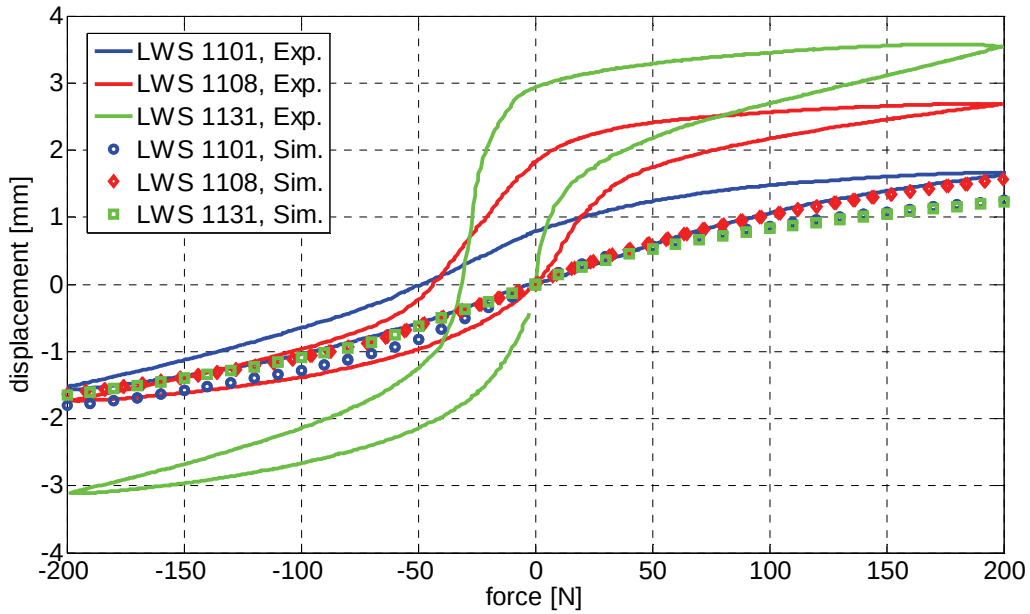

Figure V-23 Comparison of quasi-static shear load results without pre-load for old donors

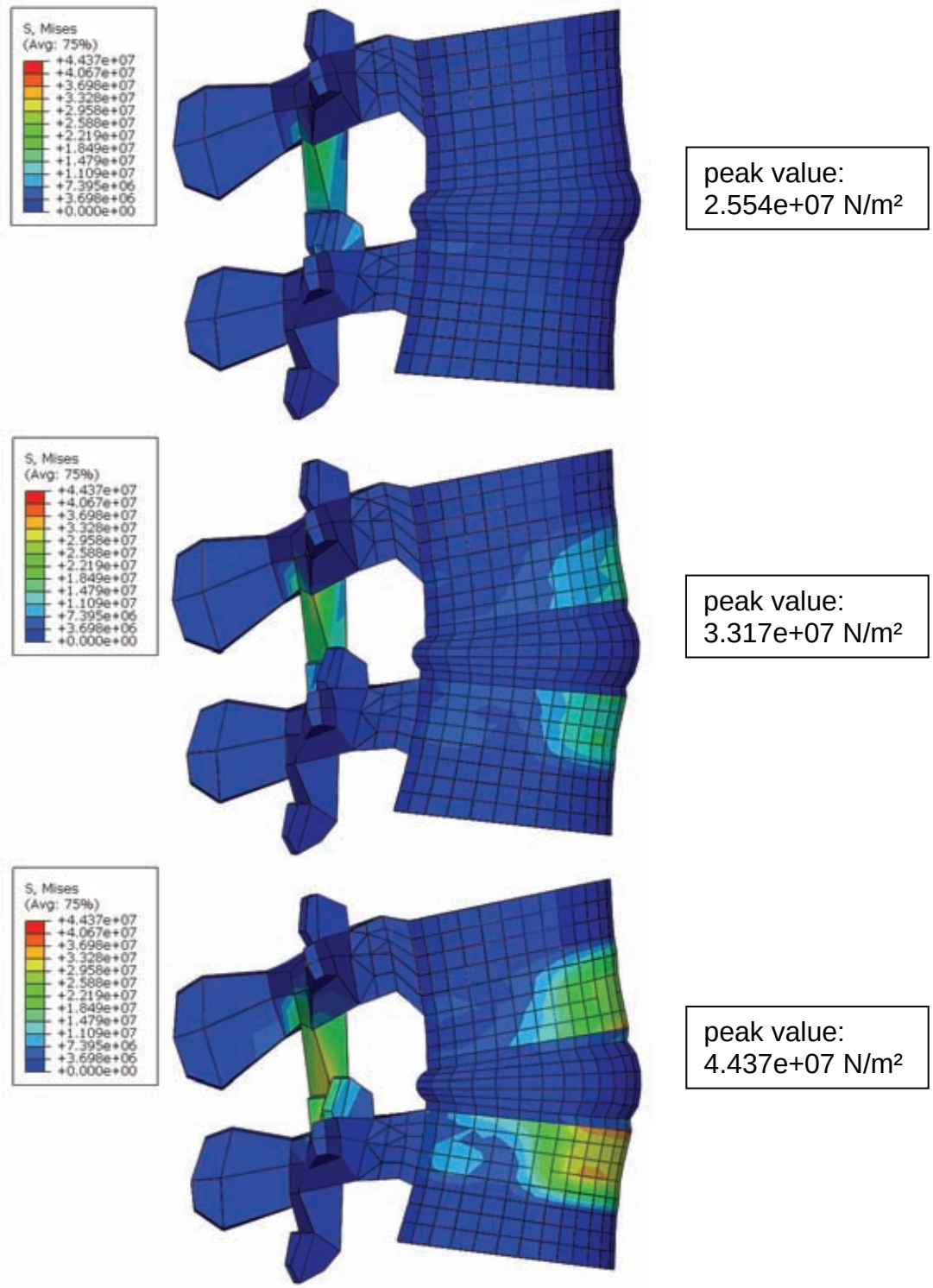

Figure V-24 Comparison of neutral posture (above) and flexed (middle 4° and below 6°) model (ID 04)

The increase of the flexion angle led to noticeably higher peak values of von Mises stress as well as to a change in stress distribution. The stress increase can be seen not only in the posterior elements in the area around the facet joints but also in the anterior region of the lumbar vertebrae.

3.1.3 Experiment ID 05

For quasi-static anterior-posterior shear (±200 N) with a compressive pre-load of -1000 N, the experimental results were quite close to each other and so were the simulation results. The experimental results show a stiffer behaviour of the FSUs than do the simulation results.

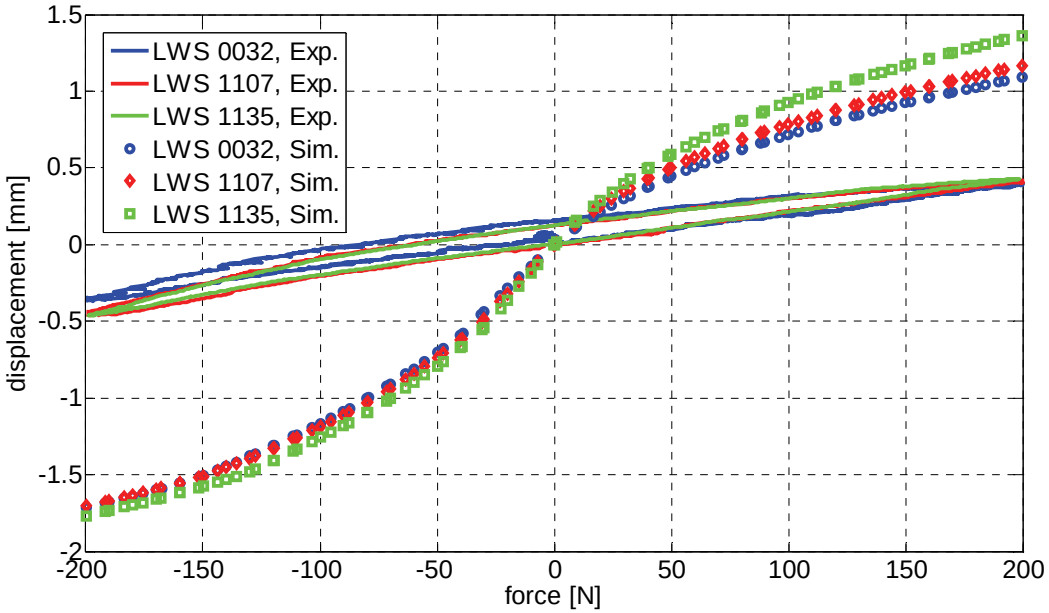

Figure V-25 Comparison of quasi-static shear load results with compressive pre-load for young donors

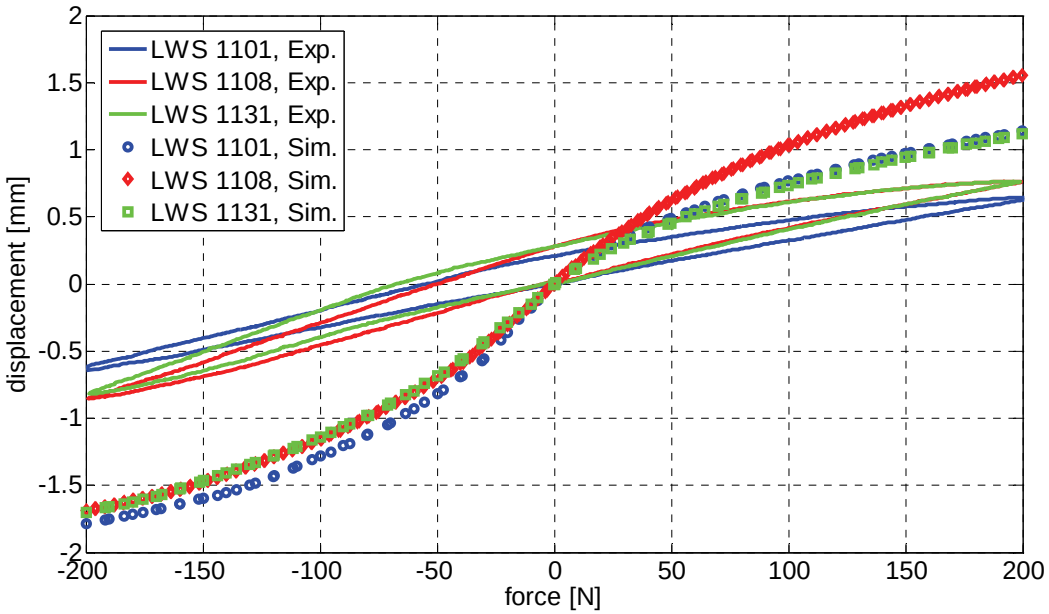

Figure V-26 Comparison of quasi-static shear load results with compressive pre-load for old donors

3.2 Dynamic results

3.2.1 Experiment ID 10

For dynamic compression of ±200 N with a compressive offset load of -500 N, the simulation of the overall behaviour for young donors was closer to the experimental data than for the older donors. The measured amplitudes exceeded the numerically calculated ones by up to 35% for old donors.

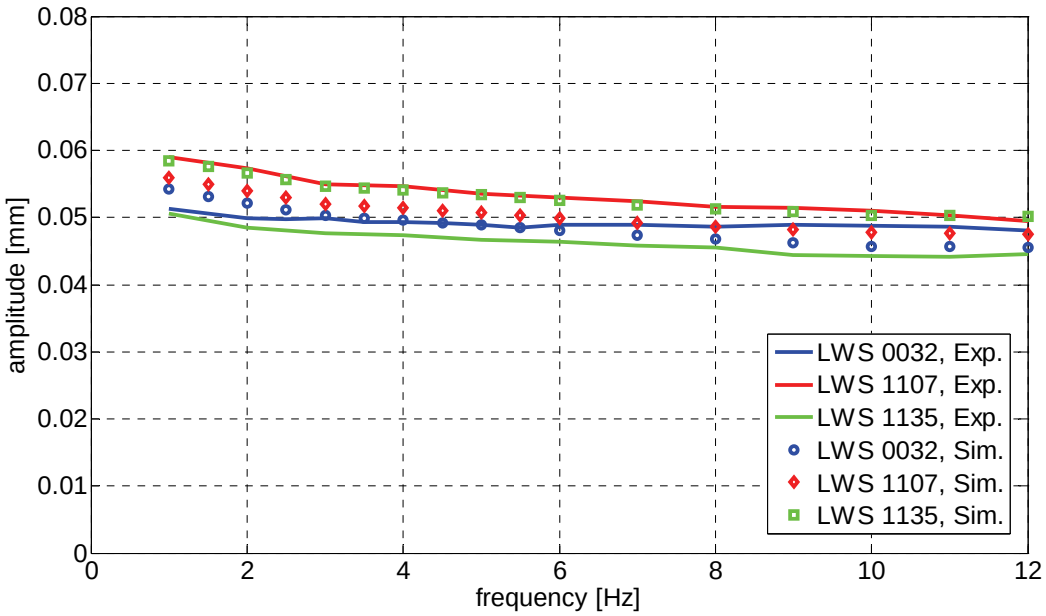

Figure V-27 Comparison of dynamic compression with compressive pre-load of 800 N for young donors

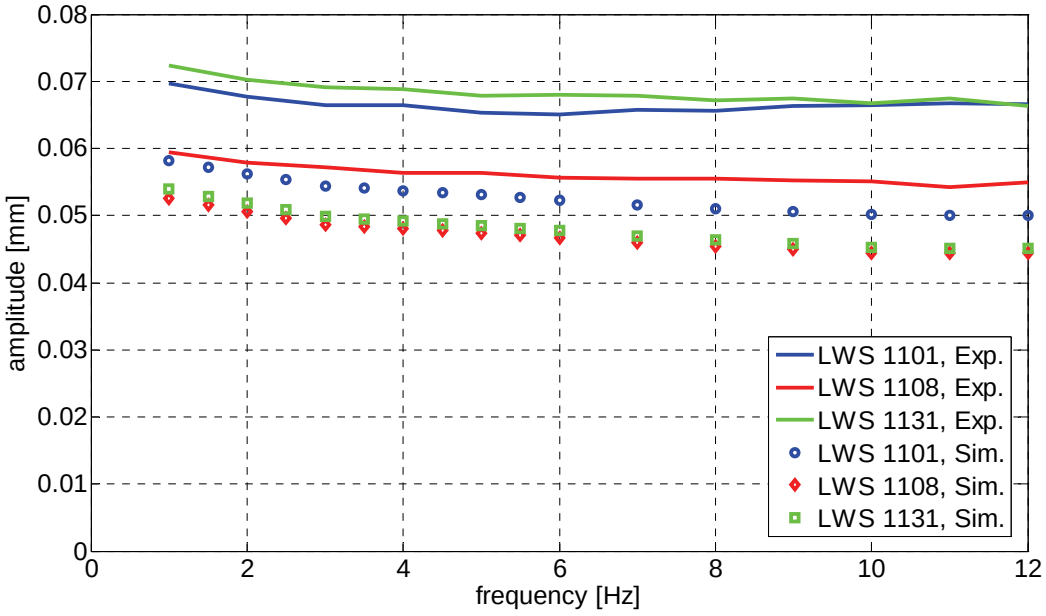

Figure V-28 Comparison of dynamic compression with compressive pre-load of 800 N for old donors

3.2.2 Experiment ID 14

For dynamic compression of ±200 N with a compressive offset load of -1100 N, the simulation of the overall behaviour for old donors was closer to the experimental data than for the young donors. The numerically calculated amplitudes exceeded the measured ones by up to 41% for young donors.

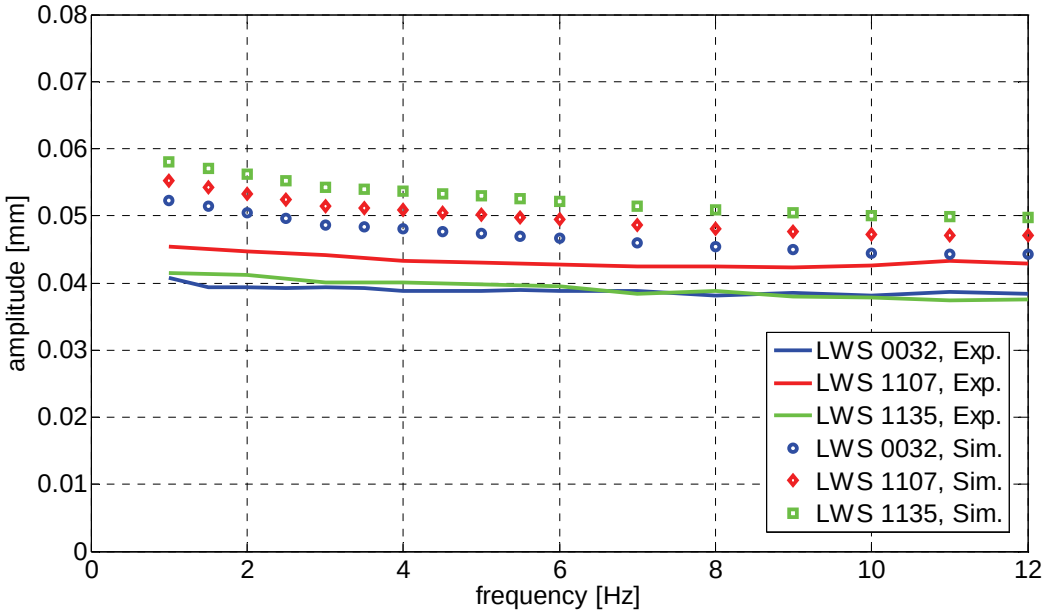

Figure V-29 Comparison of dynamic compression with compressive pre-load of 1100 N for young donors

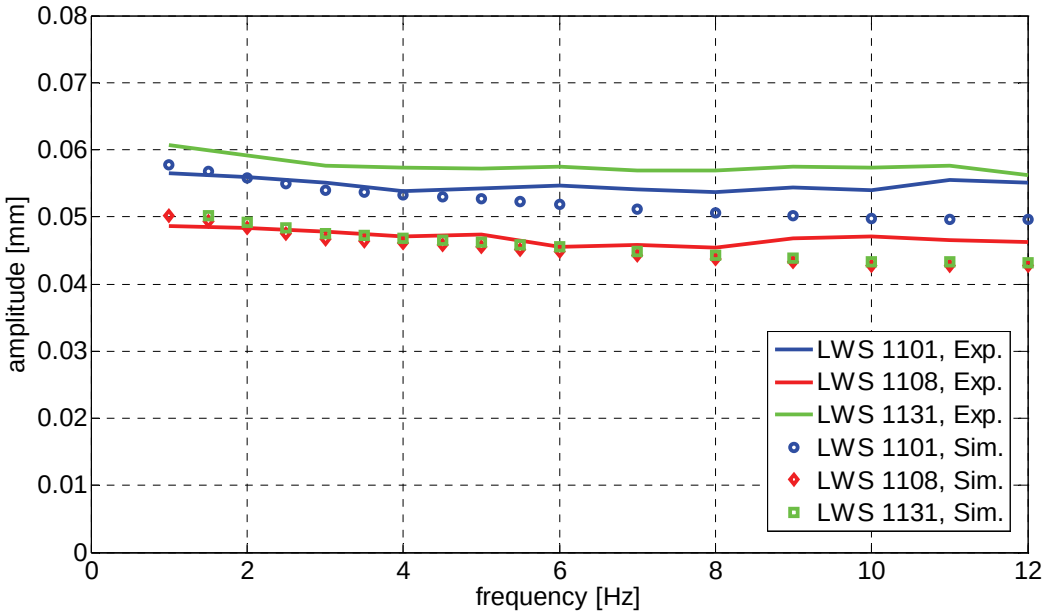

Figure V-30 Comparison of dynamic compression with compressive pre-load of 1100 N for old donors

3.2.3 Experiment ID 21

For anterior-posterior shear (±200 N) without an anterior offset load and constant axial compression (-800 N), the simulation of the overall behaviour for young donors was closer to the experimental data than for the older donors. The measured amplitudes exceeded the numerically predicted ones by up to 160% for old donors.

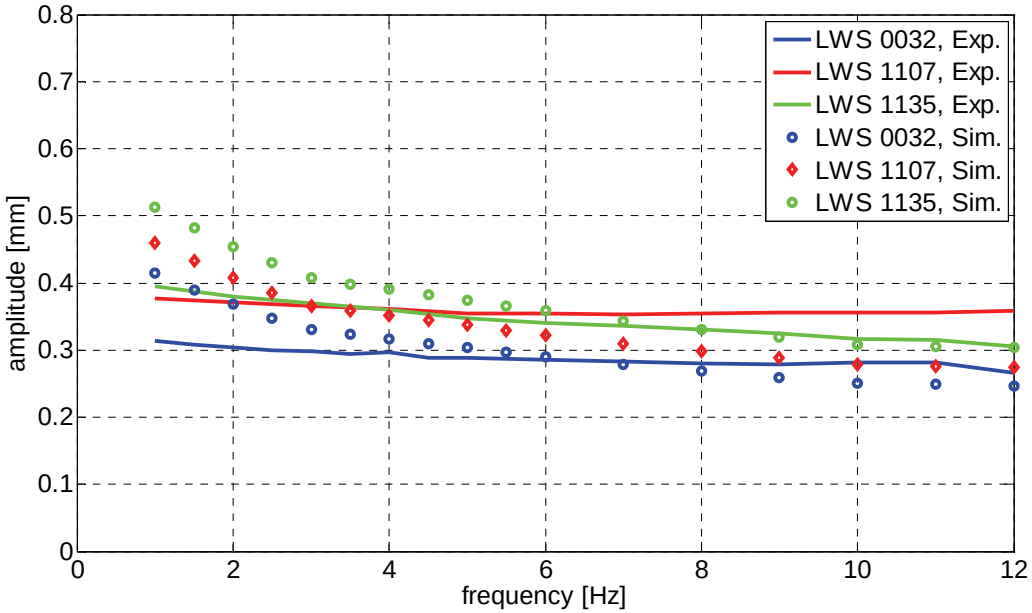

Figure V-31 Comparison of dynamic shear load with compressive pre-load of 800 N for young donors

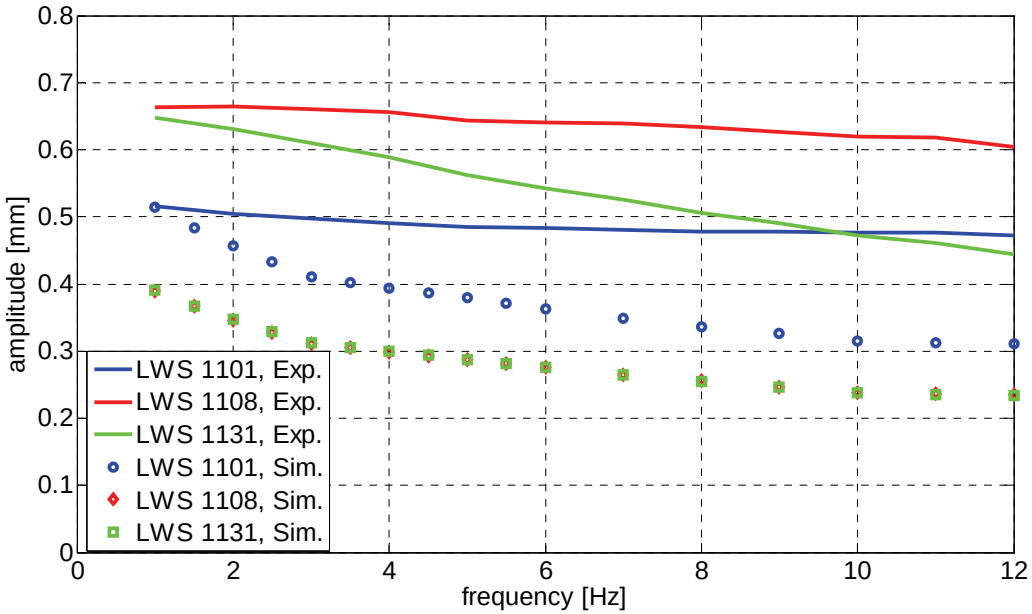

Figure V-32 Comparison of dynamic shear load with compressive pre-load of 800 N for old donors

3.2.4 Experiment ID 24

For anterior-posterior shear (±200 N) with an anterior offset load (100 N) and constant axial compression (-800 N), the simulation of the overall behaviour for young donors was closer to the experimental data than for the older donors. The measured amplitudes exceeded the numerically predicted ones by up to 109% for old donors.

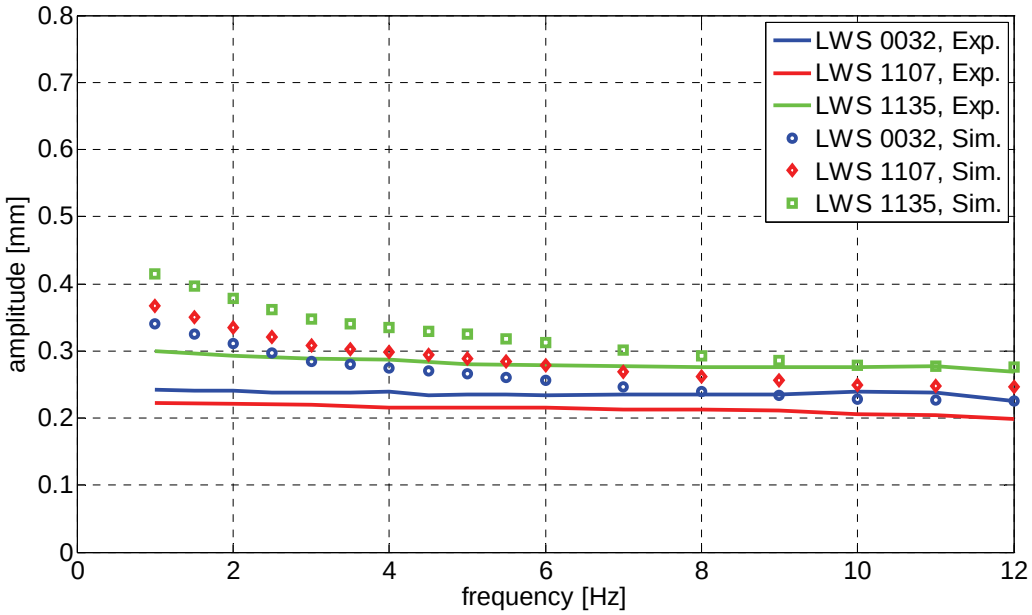

Figure V-33 Comparison of dynamic shear load with compressive pre-load of 800 N for young donors

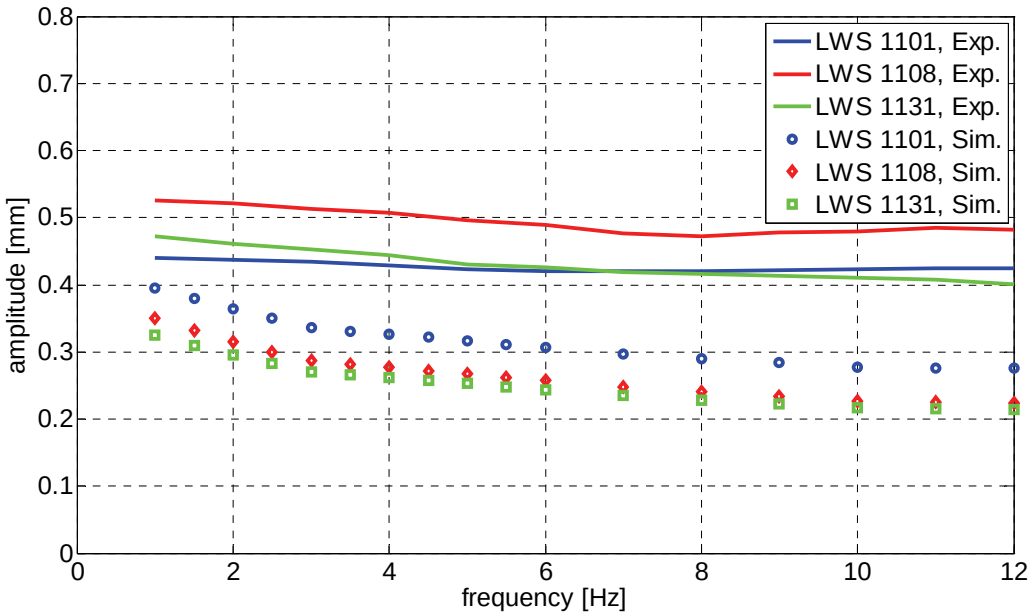

Figure V-34 Comparison of dynamic shear load with compressive pre-load of 800 N for old donors

3.3 Influence of posture

The loading of the lumbar spine strongly depends on the posture, which is shown in the following figures. For two sitting postures (upright and bent forward, Figure V-35), the resulting strain components under identical compressive loads are calculated.

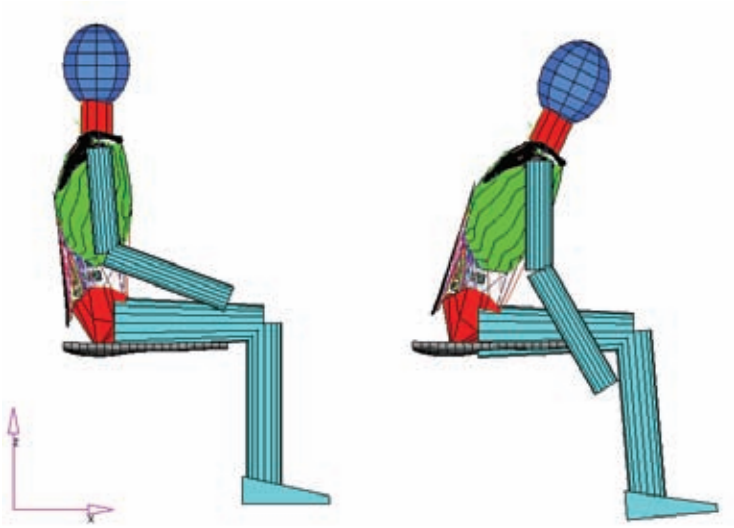

Figure V-35 Upright (left) and bent-forward (right) posture

In the whole-body model (Hofmann et al., 2003), the bent-forward posture leads to a rotation of the intervertebral disc between L4 and L5 (Figure V-35) and to a slightly reduced flexion angle for this region of the lumbar spine. L4 rotates by nearly 0.5° relative to L5 around the y-direction. The geometric change caused by bending forward was assigned to the model of the lower lumbar spine and different simulations were carried out. As a consequence, the distribution and the peak value of the global elastic strain in the intervertebral disc changed (Figure V-36). For example, in the bent-forward position, the peak value increased by 26% for load case ID 04.

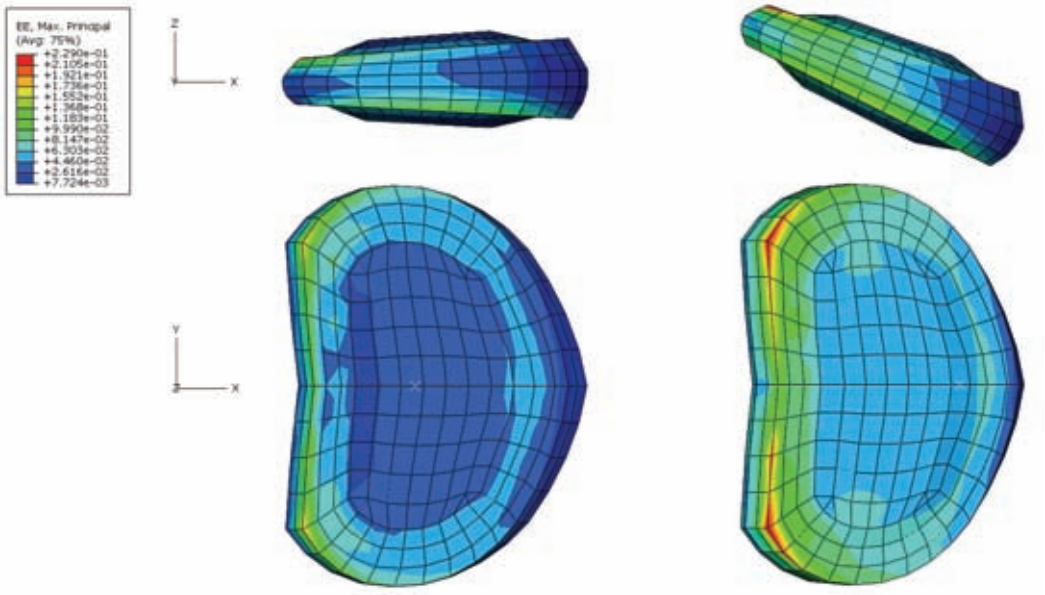

Figure V-36 Global elastic strain in the intervertebral disc for upright (left) and bent-forward (right) posture

3.4 Comparison of the old and new submodels

Figure V-37 serves to exemplify the advancements of the new submodel regarding the simulation results. Geometric differences led to slightly different simulation results. These differences in geometry cannot be accounted for using the old submodel. However, it can be seen that the differences in the experimental tests are still larger than in the simulation. This indicates that material parameters should be individualised as well.

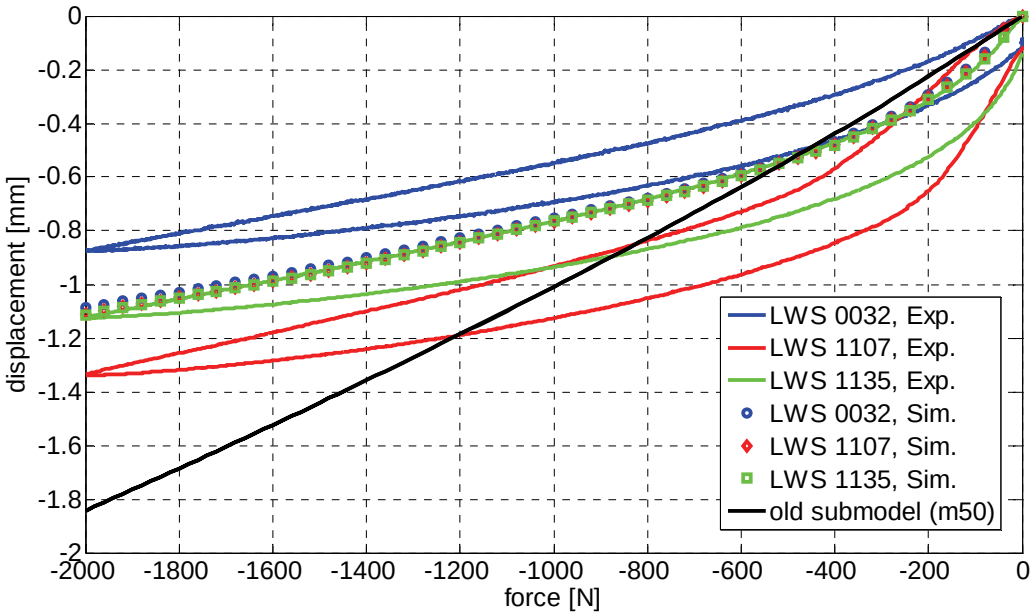

Figure V-37 Comparison of the new submodel and the old submodel (m50) with the experimental data for experiment ID 01

4 Modelling - Discussion and Conclusion

When using a numerical model of the lumbar spine, it is important to clarify exactly what the model is intended to predict. Is the objective of the application a statement concerning an individual or a particular group of people (e.g. the 50th percentile)?

This study has shown that a patient-specific simulation of both quasi-static and dynamic in vitro experiments is a challenging task. Accurate results require a highly individualised model of the lumbar spine.

Quasi-static, uni-axial loading
Even for rather simple load cases (ID 01: compression, ID 04: shear load), the results of the numerical simulations indicate that geometric individualisation is necessary but not sufficient for calculating the responses of different specimens under distinct load cases. Accurate results can only be achieved for the target FSU (LWS 1135). Geometric individualisation does not seem to be adequate for calculating the individual results of the different FSUs tested.

Quasi-static, combined loading
A compressive pre-load (e.g. ID 05) led to a stiffer behaviour of the FSUs. The numerical model stiffened only slightly under compressive pre-load. Consequently, the simulation of quasi-static combined load cases (ID 05 and ID 06) did not turn out satisfactorily.

Dynamic loading
For some dynamic simulations the results were quite close to the experimental data. But there were also FSUs with up to a 160 % difference in the amplitudes between the simulations and the experimental tests. This emphasises the fact that taking individual geometry into account alone is not enough to produce accurate simulation results.

Age
The experimental results do enable conclusions to be drawn about the influence of age (equivalent to a loss of bone mineral density) on the quasi-static or dynamic force-displacement behaviour. A reduction of the bone density parameter in the numerical model did not lead to a change in the simulation results. However, the reduced fracture strength for the FSUs of old donors should be implemented in the calculation of individual health risks.

Flexion
The influence of flexion is shown in chapter 0. With increasing flexion angle, there was a distinct difference between the peak values of the von Mises stress of the flexed model and the model simulating specimens in a neutral posture: the loading of the vertebrae increased. This indicates that flexion has a great deal of influence on the stress values and stress distribution of the lumbar spine.

Advancements of the new submodel
The objective of this study was to establish a numerical model of the lower human lumbar spine that could be geometrically individualised and is validated with in vitro experiments. These conditions are met by the model presented here. Moreover,

there is no model in the literature with comparable possibilities for individualisation combined with such extensive validation to date.

In spite of geometric individualisation, the simulation results of the new model are still not able to completely describe the experimentally shown specimen behaviour. This important result leads to the conclusion that individual material parameters and individual descriptions of the facet joints should be taken into account as well. However, there are still many advancements in the new model compared to the one proposed by Hofmann et al. (2003):

- geometric individualisation using 23 parameters (old submodel: two parameters)
- new annulus modelling (fibre-reinforced ground substance)
- validation of the numerical results on the basis of experimental data of human FSUs.

Geometric individualisation is an important prerequisite for the validation of the material parameters. The intervertebral disc of the old submodel for the 50^{th} percentile was much too thick, so the model demonstrated an overly soft force-displacement behaviour for quasi-static and dynamic compressive loads. The improvement for the quasi-static compressive load case is described in chapter 0.

Although not all of the simulations of load cases were satisfactory, it has to be mentioned that in almost every load case the new submodel produced better results than the old model. The new annulus modelling with pre-stressed spring elements representing the fibres is now closer to human anatomy and also accounts for the intradiscal pressure, which can be measured even in unloaded FSUs.

Part VI Fatigue Experiments

Gerd Huber, Daniel M. Skrzypiec, Anke Klein
Helge Paetzold, Klaus Püschel, Michael M. Morlock

1 Fatigue - Introduction

Human spines are exposed to dynamic loads during everyday activities. Especially at the workplace, these dynamic loads might be rather high due to the increased usage of machines along with increased specialisation, which can lead to longer periods of similar physical stress within the daily working routine. Therefore, the duration of the exposure to these loads might last for a reasonable portion of each day, and consequently, the exposure adds up over one's lifetime and exerts a cumulative effect. In particular, vibrations combined with constrained sitting postures are regarded as a risk factor for disc degeneration and endplate failure. Workers who operate large construction machinery, forest harvesters and forklifts are prominent examples for workers especially exposed to these potentially harmful postures. Another consequence of the increased usage of machines is that the physical constitution of workers in western societies is continually worsening due to the lack of regular exercise. One indication of this is that the mean body mass index has increased, which is of course not solely caused by using machines. This decreased constitution might cause reduced muscle protection and stiffening of the trunk during exposure to dynamic loads.

To prevent extensive loading and diminish the associated risks, the cumulative amount of exposure to vibrations should be limited according to regulations and recommendations (2002/44/EG; ISO 2631-1, 1997; ISO 2631-5, 2004). The scientific basis for these recommendations is scant, however. For example, little is known about the effect of external vibration loads transmitted from the seat to the body on the internal relative loads within spinal structures. Even less is known about different postures and intra-individual differences of human bodies in general and specifically differences in spinal structures. The main reason for this is that in vivo studies in humans are rarely possible. The experiments would either be too harmful for the potential subjects or they can only be performed on injured persons, such as e.g. experiments with instrumented cages or fixators (Rohlmann et al., 2001; Wilke et al., 2001b).

However, it is important to become aware of this external-internal transfer mechanism in order to understand the mechanism of disc degeneration and other kinds of spinal injuries. This could improve the appraisal of occupational accidents, enable the determination of implant duty cycles and spur the development of future treatments or implants as well as improve prophylaxis in the workplace and in private life.

To close this gap, numerical whole-body models have been developed to examine the behaviour of spinal columns exposed to different types of vibration while sitting in different postures (VIBRISK, FIOSH). However, capturing the anatomical complexity and including all relevant active and passive elements within the load chain is still

challenging and even the improved models will on principle be unsuitable for determining the fatigue characteristics of spinal segments. Fatigue behaviour of functional spinal units (FSUs) has been determined in vitro (Brinckmann et al., 1988), but mainly for donors in the upper range of working age or after retirement (n = 70, 51±18 yrs). Furthermore, the numbers of cycles to failure were small (N < 5000), partly due to the high load used. In a recent study (Huber et al., 2006), the FSUs of younger donors (n = 30, 33±6 yrs) were shown to fail during 100,000 load cycles only if this loading with a high physiological load (peak-to-peak: 0-2 kN) coincided with pure bone mineral density (BMD).

The aim of this in vitro study was to investigate how specimen posture and vertebral characteristics like age, BMD and endplate size might be used to determine the fatigue strength of spinal specimens.

The hypothesis for this study is based on a recent publication (Seidel et al., 2008a). The number of cycles to failure (N_K) is thought to be related to the maximal failure load (Fmax) within a single overload experiment in the following way:

$$N_K = \left(\frac{F_{max} - F_{mean}}{0.5 \cdot F_{peak-to-peak}} \right)^6 \quad . \qquad \text{(VI-1)}$$

The given equation is a simplified version of the original one. It is only valid for cyclic loads with a constant mean load (F_{mean}) and a constant peak-to-peak load ($F_{peak\text{-}to\text{-}peak}$). For more complex loading conditions, the contributions of different consecutive load cycles are summed up (Figure VI-1).

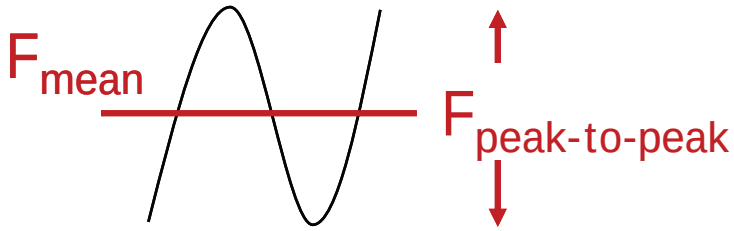

Figure VI-1 Parameters used for the equation to determine the fatigue strength

Obviously, it is not possible to measure both the cycles to failure in a fatigue experiment and the single failure overload (or ultimate strength, respectively) with the same specimens. Therefore, an established equation for the maximal failure force (Brinckmann et al., 1989) was used. This equation is based on the endplate area (AREA) and the bone mineral density (BMD):

$$F_{max} = 0.32\,kN + 0.00308 \cdot BMD \cdot AREA \cdot \frac{kN}{\frac{mg}{ml} K_2HPO_4 \cdot cm^2} \quad . \qquad \text{(VI-2)}$$

Combining these two equations leads to a simple relation with one combined input (BMD · AREA) and one output value (N_K). The values c_i represents constants adding the parameters of the equation for the ultimate strength and the cyclic loading:

$$N_k = (c_1 + c_2 \cdot BMD \cdot AREA)^6 \quad . \qquad \text{(VI-3)}$$

As an alternative non-invasive method, the ultimate strength might also be predicted based on the age of the donors (AGE). The use of X-rays could therefore be omitted. This is not of interest for in vitro studies, but important with regard to in vivo investigations. Several regressions were published in a meta-study (Seidel et al., 1998) and one of them (STEEP) is similar to that incorporated into the Annex of ISO 2631-5 (2004). In the original publications stresses are given, but in the context of this study forces are more appropriate. Therefore, the equations are given with an additional product (AREA) representing the endplate area. First, one with a low gradient (LOW):

$$F_{max} = \left(-0.037747 \ \frac{MPa}{years} \cdot AGE + 5.106713 \ MPa \right) \cdot AREA \qquad \text{(VI-4)}$$

and second, one with a steep gradient (STEEP):

$$F_{max} = \left(-0.067184 \ \frac{MPa}{years} \cdot AGE + 6.765024 \ MPa \right) \cdot AREA \quad . \qquad \text{(VI-5)}$$

Individual ultimate force can be calculated by the donors age and the corresponding endplate area. For an age of 56, the predicted ultimate strength is similar for both equations. The ultimate strength at this age will be about 3 MPa for both equations. Because of the different slopes, the strength of a specimen from a 20 year old donor will be 4.4 MPa for the LOW equation and 5.4 MPa for the STEEP one. With the given hypothesis for the prediction of cycles to failures, the following equation arises (the variable k_i represents constants):

$$N_k = \left(k_1 + k_2 \cdot AREA + k_3 \cdot AGE \cdot AREA\right)^6 \quad . \qquad \text{(VI-6)}$$

For further group wise analyses, the mean AREA is calculated out of the average of the superior L5 endplate and the inferior L4 endplate of all 18 specimens in this part (16.7±3.1 cm²). The ultimate force at the age of 56 for a mean AREA will be about 5 kN for both equations. Because of the different slopes, the strength of a specimen from a 20 year old donor will be 7.3 kN for the LOW equation and 9 kN for the STEEP one.

2 Fatigue - Methods

Lumbar spinal specimens (L4-L5) were used for this study. Three groups of six specimens each were investigated. The groups were ‘Young-Neutral’, ‘Young-Flexed’ and ‘Old-Neutral’. The term ‘Flexed’ indicates specimens that were tested in a rigid 10° flexed posture. For the ‘Young’ groups it was intended to include specimens from donors between 20 and 40 years old while the ‘Old’ group was supposed to cover donors between 50 and 60. With regard to actual retirement ages in Europe (60-67 years), the latter group represents people in the second half of their working lives while the other two groups comprise adult workers at the beginning of their working lives. Taking into account the current life expectancy of about 80 years for western European males (OECD 2009), ‘Young’ and ‘Old’ should be seen as relative terms. Further details about the specimens and their preparation can be found in Part II.

The specimens were exposed to 300,000 cycles of sinusoidal axial compression (5 Hz, peak-to-peak: 0-2 kN). Using numerical whole-body vibration models combined with in vivo vibration measurements, this peak-to-peak load was determined to act on the lumbar spine while driving forwarders without cargo (Seidel et al., 2008b). Furthermore, preliminary tests showed that this load leads to nucleus pressures of approximately 1.4 MPa, which resembles a load of the upper physiological range (Wilke et al., 1999). The height of the load and the remained pressure is consistent with loading situations described for in vitro measurements elsewhere (e.g. McMillan et al., 1996).

Prior to cyclic fatigue loading, quasi-static and dynamic load cycles were applied in order to determine the mechanical parameters of the FSUs (~90 min). Care was taken not to damage the specimens during these measurements, which also served as preconditioning. Details about these measurements can be found in the appendix (Part VIII1).

A modified hydraulic testing machine (MTS Bionix 858.2, MTS, Eden Prairie, MN, USA) was used as a test rig. The modification consisted of an additional horizontal shear actuator which was attached to an aluminium truss (Figure VI-2) on the front side of the crosshead of the hydraulic testing machine. The shear force actuator and the vertical test rig actuator were connected with the specimen holder by leaf springs instead of the more commonly used joints and sliders. In addition to the shown configuration, additional stiffing beams were mounted between the truss and the test machine.

Forces were measured by strain gauges on the coupler and a load cell below the fixed specimen flange. Target force values for the shear actuator were specified using the analogue-digital converter of the hydraulic test system, which also realised the data acquisition. For the fatigue measurements, the anterior-posterior shear actuator enabled unrestricted movements in that direction. The remaining translational degree of freedom was restrained, as were the rotational degrees of freedom. Further information about the design principles can be found elsewhere (Huber et al., 2005).

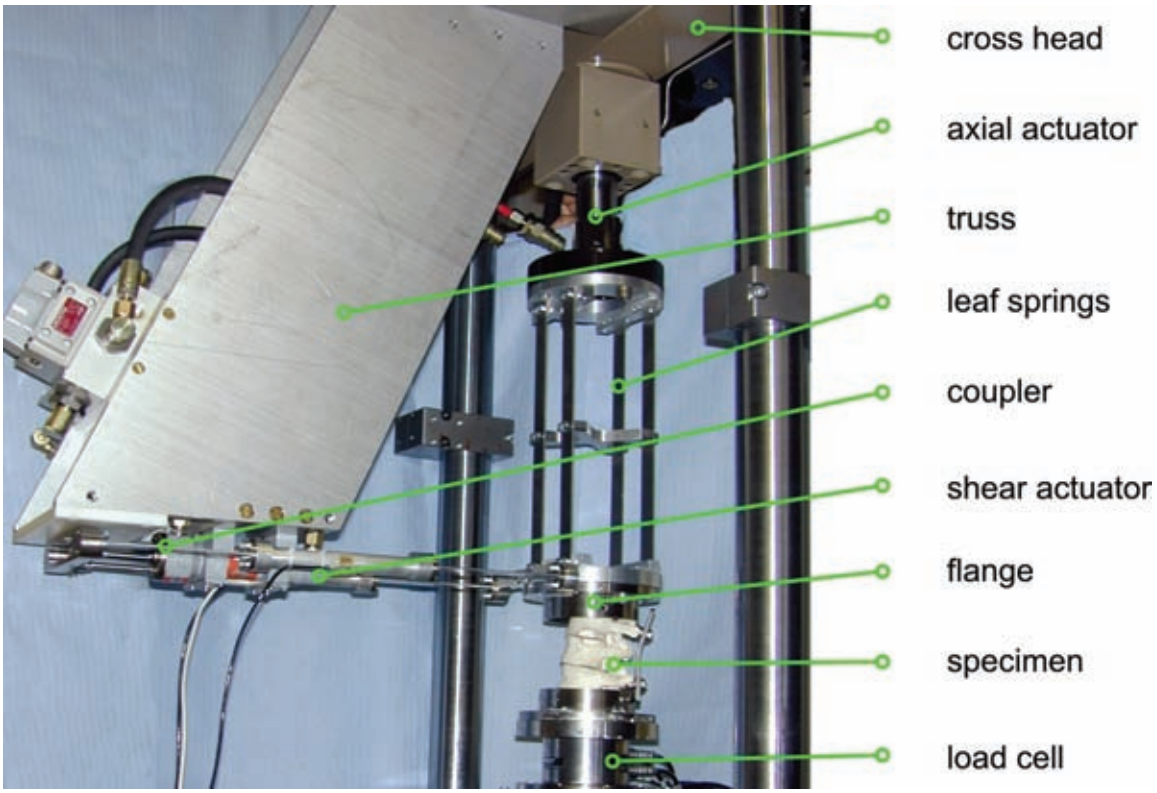

Figure VI-2 Modification of the standard test rig

During the long-term fatigue measurements (~18 h), biological degeneration within the 37°C Ringer solution test environment was minimised by adding Penicillin/Streptomycin (PAA, Austria). Specimen height loss was continuously recorded. Unsteadiness in the creep curve was taken as a specimen failure (cycles to failure).

3 Fatigue - Results

The BMD of the specimens in the three groups was broadly distributed (Table VI-1, Table VI-2). The standard deviations ranged from 10 to 25% of the corresponding mean values. The BMD values between the FSUs of the 'Old-Neutral' and the 'Young-Flexed' groups were significantly different (Bonferroni post-hoc test, $p = 0.041$). The endplate areas between groups did not differ.

Table VI-1 Group characteristics (n = 6 per group)

		Old-Neutral		**Young-Flexed**		**Young-Neutral**	
		Mean	**STD**	**Mean**	**STD**	**Mean**	**STD**
AGE	years	53.5	3.8	30.5	8.3	29.0	7.1
BMD	mg K_2HPO_4 per ml	117.0	28.8	161.8	29.2	152.8	15.4
AREA	cm^2	17.8	3.1	16.7	3.7	15.6	2.1

Table VI-2 Overview of the L4-L5 specimens used in the fatigue test

Old-Neutral			**Young-Neutral**			**Young-Flexed**		
LWS	**AGE**	**Day of testing**	**LWS**	**AGE**	**Day of testing**	**LWS**	**AGE**	**Day of testing**
1101	56	20.06.07	1106	23	27.06.07	1112	20	11.09.07
1104	48	10.05.07	1107	36	05.07.07	1113	21	10.07.07
1108	50	19.09.07	1124	34	18.12.07	1119	39	07.08.07
1110	52	11.10.07	1126	21	13.12.07	1120	41	22.08.07
1131	56	07.01.08	1133	38	07.11.07	1123	35	26.09.07
1136	59	19.02.08	1135	22	31.01.08	1125	27	05.12.07

In Figure VI-3 the creep curve of a specimen that did not fail within 300,000 cycles is visible. It shows the typical decrease of specimen height. Figure VI-4 shows the same data if a logarithmic timescale is used. In contrast Figure VI-5 shows the creep curve of a specimen that failed after fewer than 2000 cycles. The curves are not continuous, because stiffness measurements interrupted the fatigue experiments. The curves show the complete load cycles. In fact, the width of the line is the amplitude of the cyclic loading.

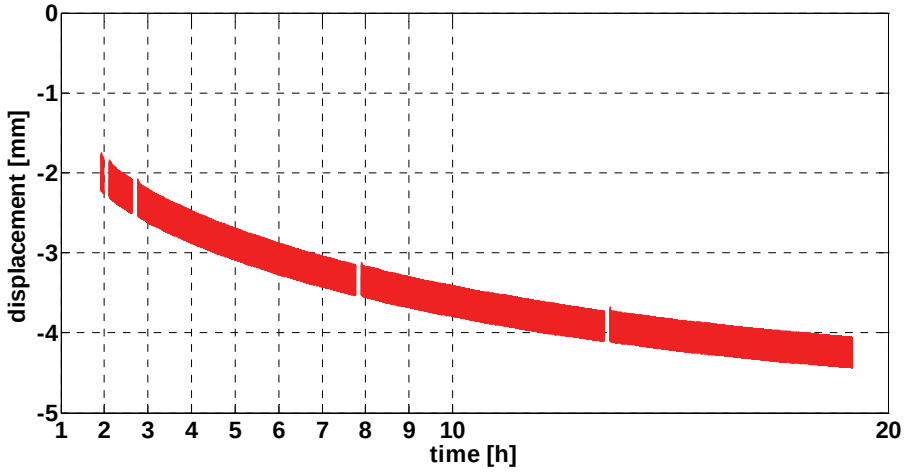

Figure VI-3 Creep curve of a specimen that did not fail

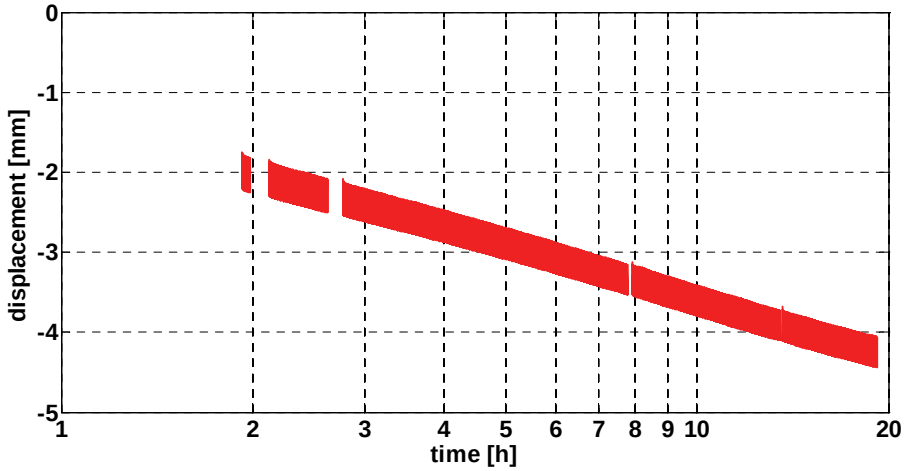

Figure VI-4 Creep curve of a specimen that did not fail (logarithmic timescale)

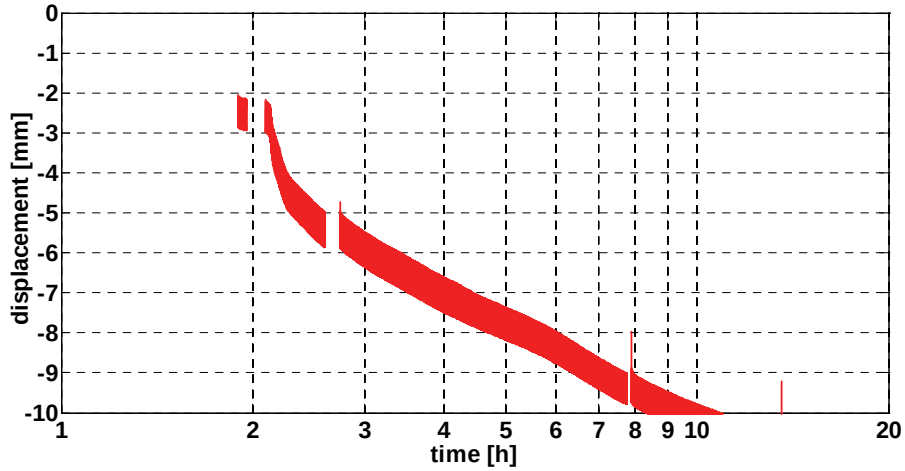

Figure VI-5 Creep curve of a specimen that failed after fewer than 2000 cycles (logarithmic timescale)

Unsteadiness in the creep curves was clearly noticeable. Two investigators came to almost the same results for cycles to failure (Figure VI-6). The slope of regression was 1 and the coefficient of variation was $r^2 > 0.99$.

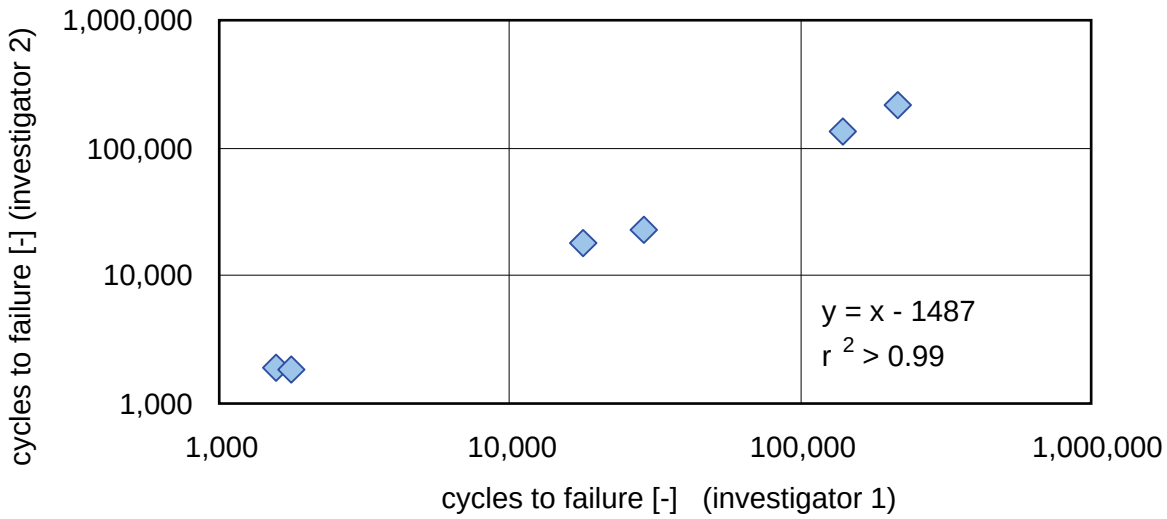

Figure VI-6 Determined number of cycles to failure by two investigators

Altogether, 6 of 18 specimens failed in this study. In the 'Neutral' posture, none of the 'Young' specimens failed during the test period, while four of the 'Old' specimens (those with low BMD) failed. In the flexed posture, two of the young specimens failed during the test period. Mainly failures of the vertebral body were observed (Table VI-3).

Table VI-3 Spinal characteristics and cycles to failure for failed specimens

		Old-Neutral				**Young-Flexed**	
		1104	**1101**	**1131**	**1136**	**1112**	**1119**
AGE	[years]	48	56	56	59	20	39
AREA	[cm²]	16.6	14.9	17.4	15.8	13.5	14.0
BMD	[mg K_2HPO_4 per ml]	99.9	114.7	88.3	88.8	136.4	205.8
Cycles	[x 1000]	28.9	18.0	1.6	1.8	140.0	215.6

In most of the cases when specimens were identified as failed, the failure could be observed in a post-testing X-ray image as well as during the Thompson classification. The first exception was observed for the youngest specimen in the 'Old-Neutral' group, where no bony fracture was found in the X-ray, but a small endplate fracture combined with disc delamination was observed during the morphological Thompson grading of the dissected specimen (LWS 1104, Figure VI-7). The second exception was observed for one of the specimens tested in the flexed position. Neither the X-ray nor morphological grading could spot any signs of failure (LWS 1119, Figure VI-8). Furthermore, CT scans of the specimens LWS 1104, LWS 1112 and LWS 1119, which were performed after testing and Thompson grading, did not lead

to other findings. In the cases of LWS 1104 and LWS 1119, no other bony damage was found. For LWS 1112, the failure of the caudal endplate of LWS 1112 was also observed (Figure VI-9).

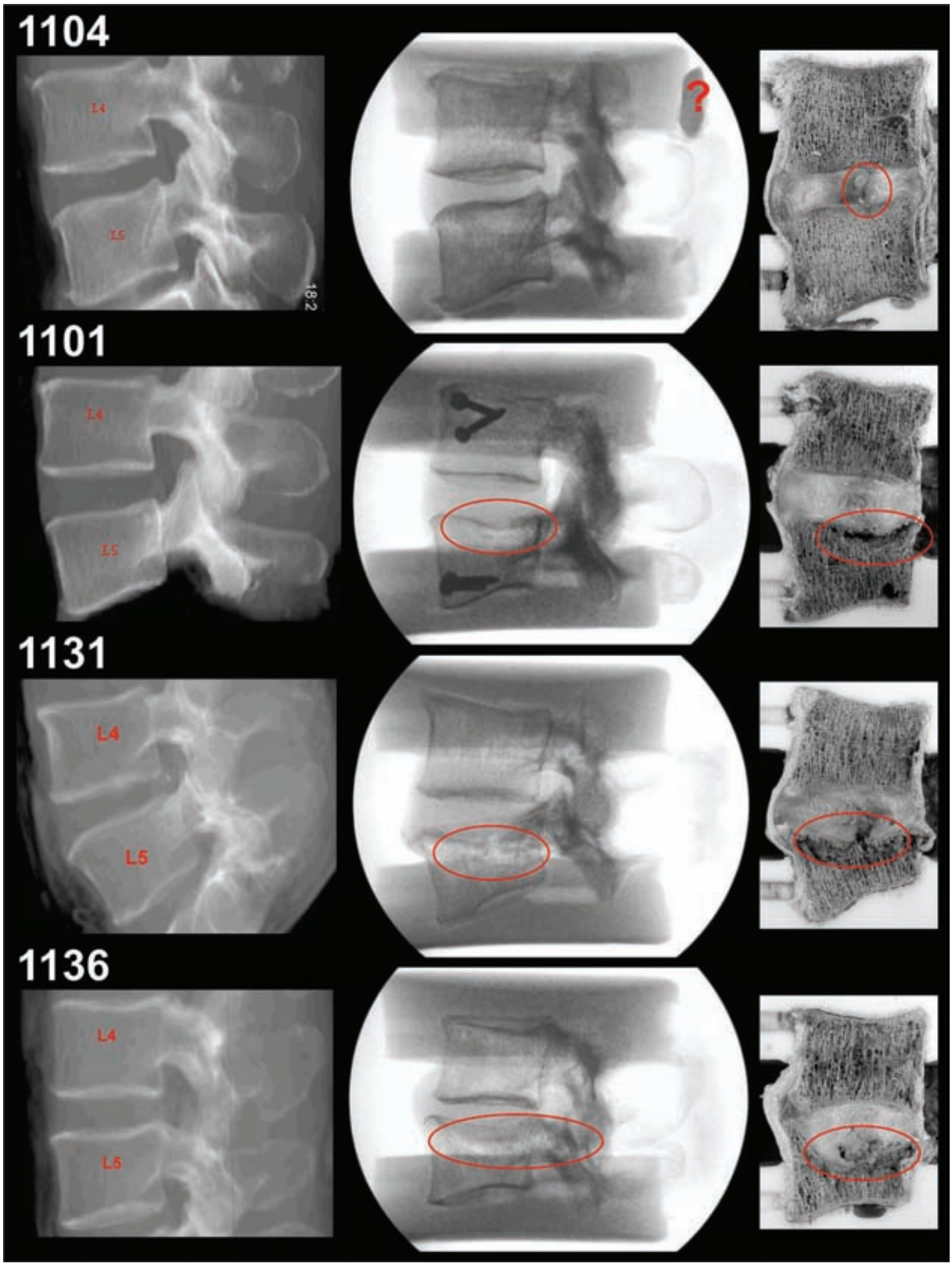

Figure VI-7 Comparison between pre-testing CT projection, post-testing X-ray and dissected specimen of the four failed specimens of the 'Old-Neutral' group

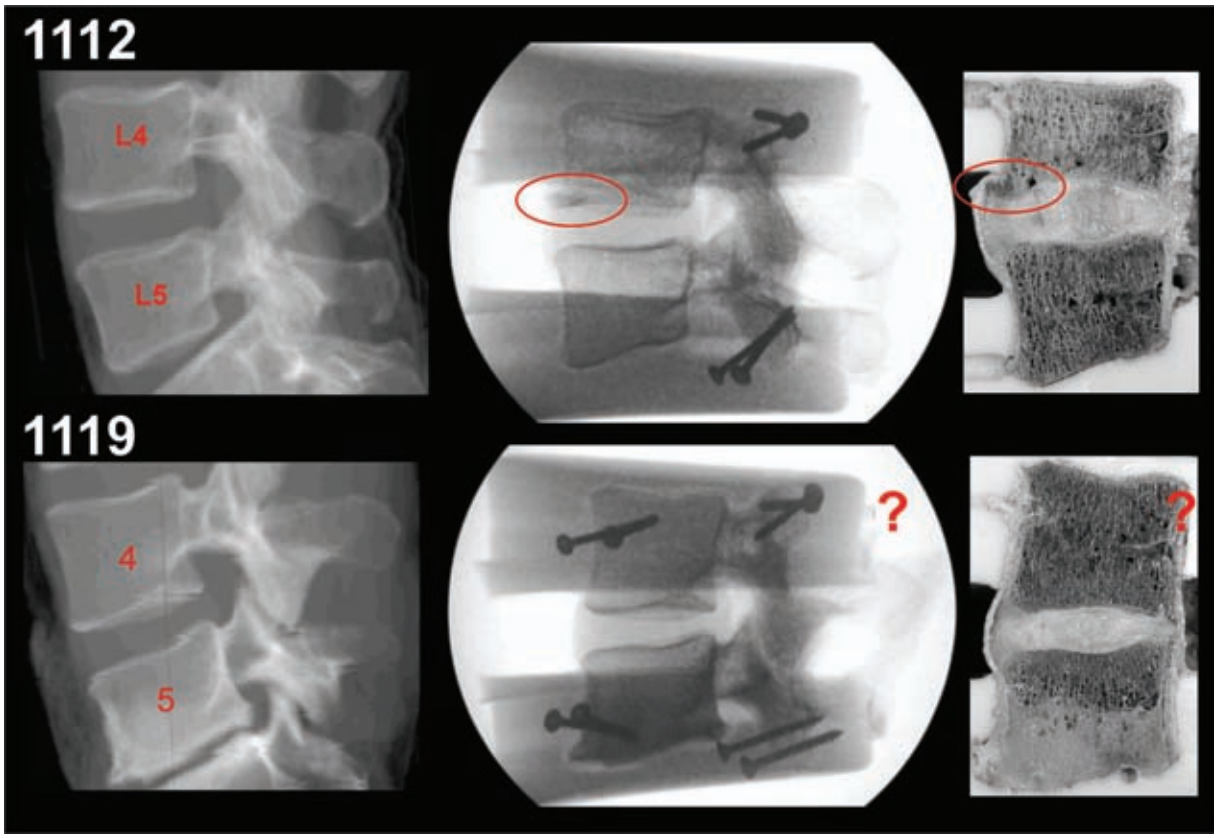

Figure VI-8 Comparison between pre-testing CT projection, post-testing X-ray and dissected specimen of the two failed specimens of the 'Young-Flexed' group

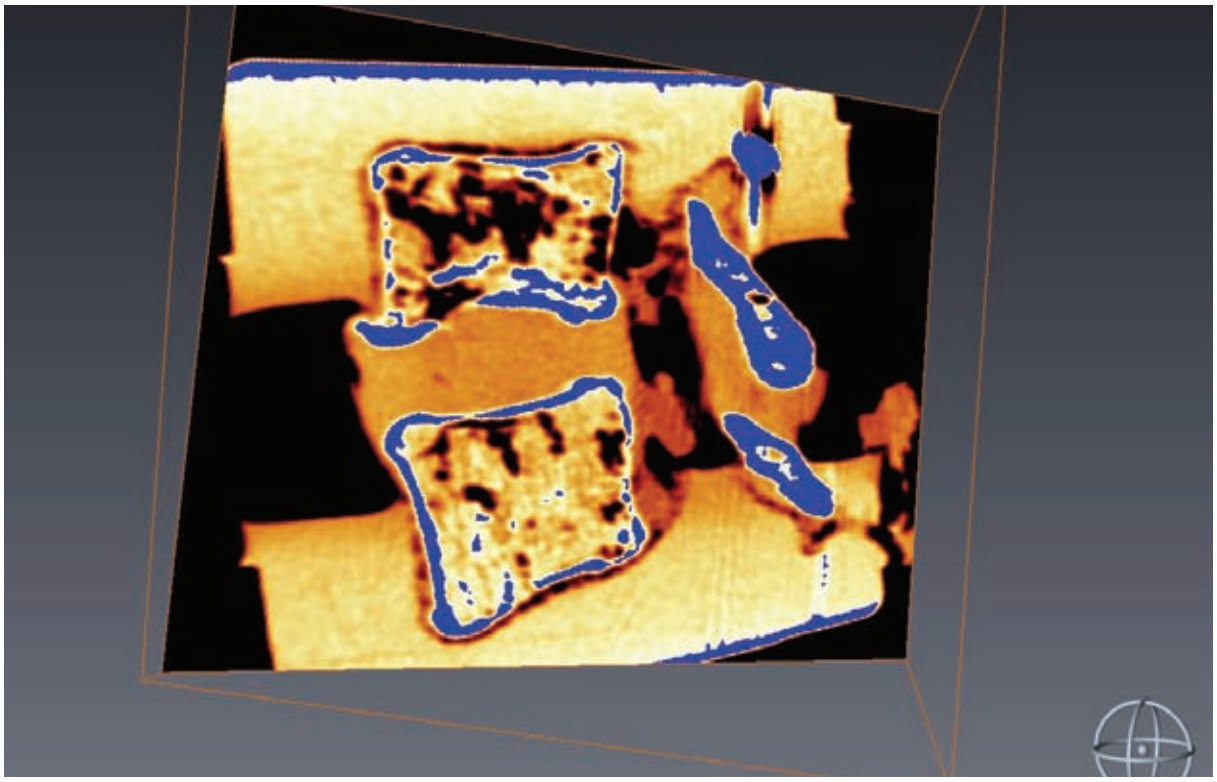

Figure VI-9 CT scan of specimen LWS 1112 (after testing and Thompson grading). The blue areas identify regions with HU values above 400. The caudal endplate of L4 appears to be broken.

In the following three diagrams, the cycles to failure of the specimens with regard to different independent values are given (Figure VI-10, Figure VI-11 and Figure VI-12). Those are AGE, BMD and the product of AREA and BMD (see Introduction). For the three following diagrams, open markers represent specimens which did not fail during testing; filled markers indicate failed specimens. Results from three specimens of the F1899 project are also shown. Those three specimens were loaded similarly to the specimens in this study and did not fail within 100,000 cycles.

In Figure VI-10 the dotted lines represent the hypothesised failure curves for the STEEP and the LOW relation between age and ultimate strength. Both curves are calculated using the mean endplate area of the specimens (16.7 cm^2). In the case of STEEP, a confidence interval is also given. This interval is representing the limits of variation, if the area is increased or decreased by one standard deviation (3.1 cm^2), respectively. In Figure VI-12 the hypothesised line is more individual, because each specimens proper AREA and BMD was used to calculate the abscissa value.

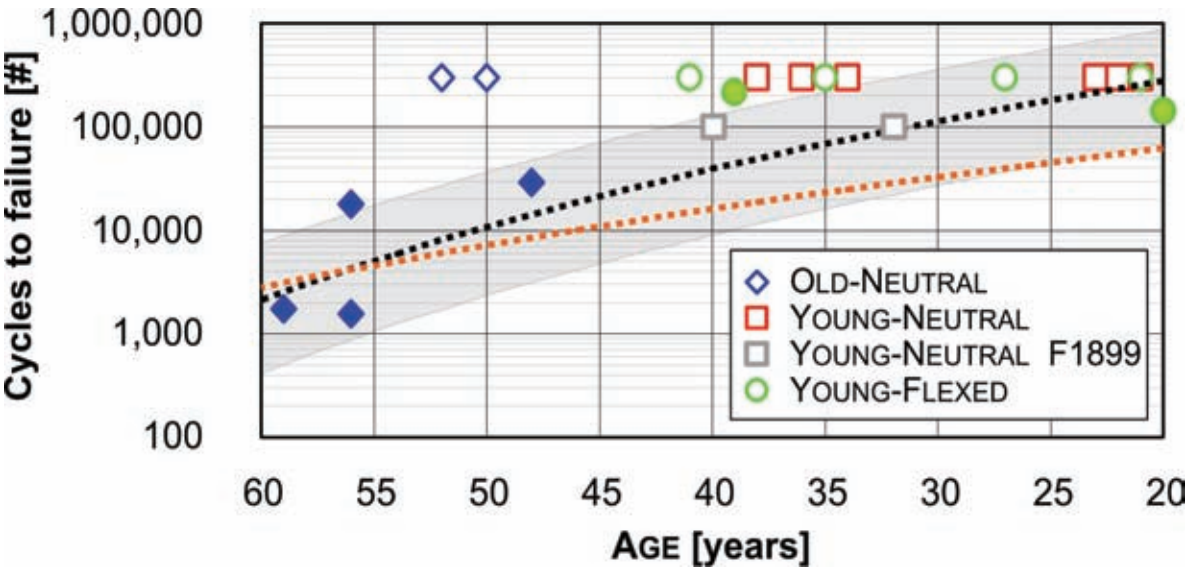

Figure VI-10 Cycles to failure vs. donor's age for the different groups. Open markers represent specimens which did not fail during testing. The dotted lines represent the hypothesised failure curves (STEEP: black; LOW: orange). For STEEP a confidence interval is given in grey (plus/minus one standard deviation for AREA). Only two markers for the three measurements of F1899 are seen because two donors were the same age.

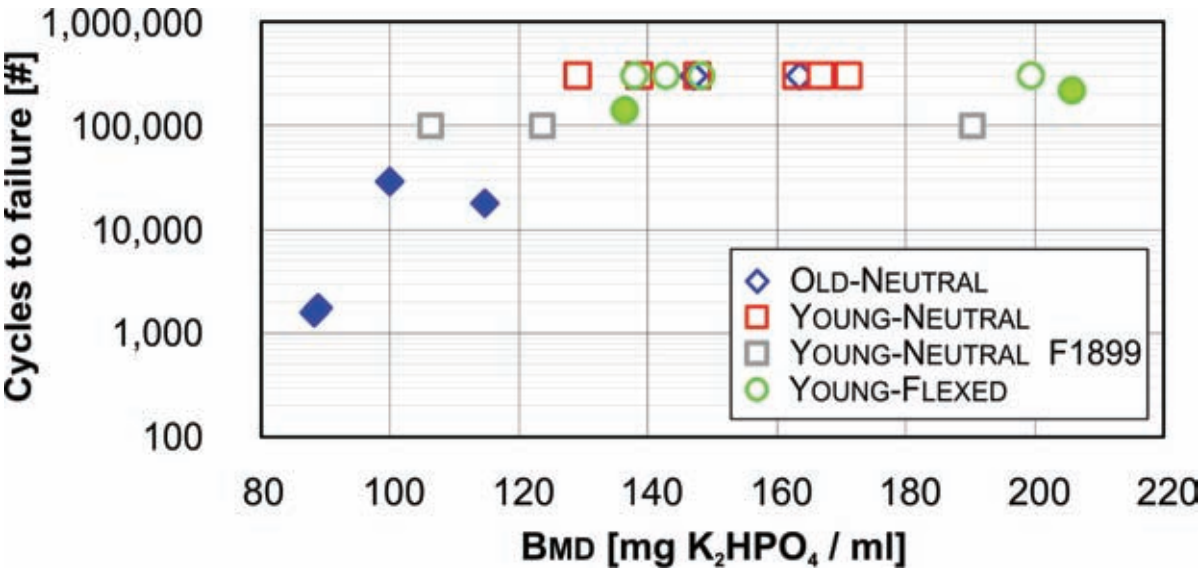

Figure VI-11 Cycles to failure vs. BMD for the different groups. Open markers represent specimens that did not fail during testing.

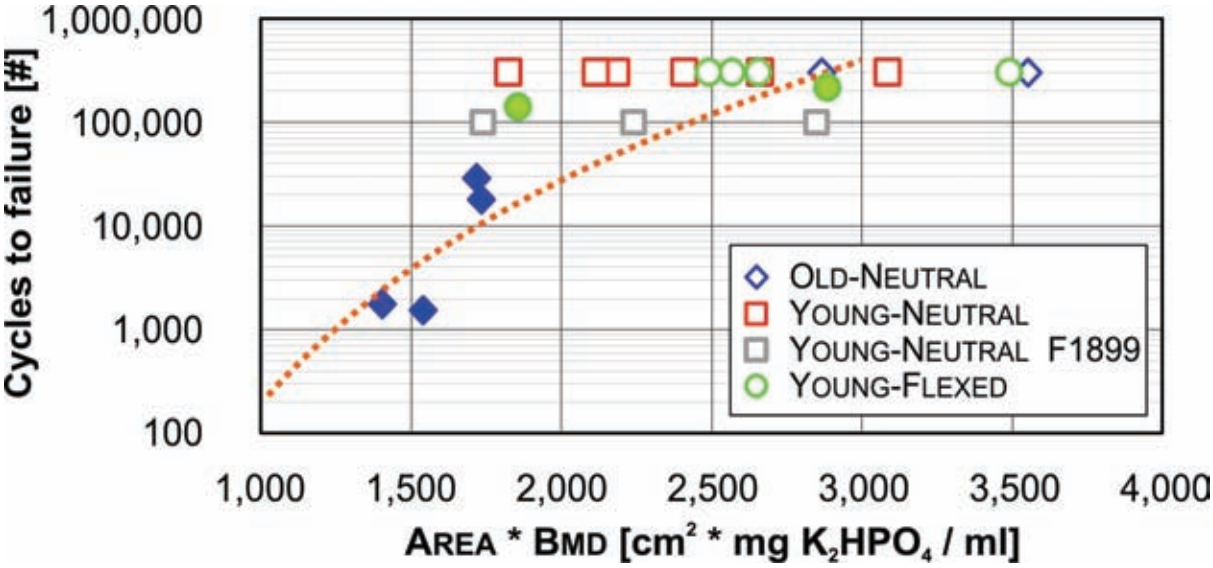

Figure VI-12 Cycles to failure vs. characteristic value (AREA * BMD) for the different groups. Open markers represent specimens that did not fail during testing. The dotted line represents the hypothesised failure curve.

4 Fatigue - Discussion

The resistance of young specimens against fatigue load was unexpectedly high, but specimens from donors in the second half of working age (‘Old’) with low BMD failed if exposed to high physiological loads. Here, a linear relationship ($r^2 = 0.74$) between cycles to failure (log scale) and the characteristic mechanical value (AREA * BMD) appears appropriate. However, this curve cannot be extrapolated to higher BMD values and is, as mentioned, only supported by four measurements. Only two of the young specimens in the flexed posture failed. One of those (LWS 1112) with low BMD fit into the relationship derived for the specimens from older donors, whereas the second failed young specimen (LWS 1119) did not. Therefore, the influence of flexion remains unclear. However, examinations of the latter specimen did not spot any clear failure. Therefore, it is rather likely that in this case the identification of fatigue failure based on the creep curve was not adequate.

The three-fold increase of load cycles compared to the F1899 project (Huber et al., 2005) and the inclusion of specimens from old donors did not lead to the expected high increase in failed specimens compared to the former project. The increase in loading was still to low to induce a higher failure rate.

In vitro testing only roughly mimics the in vivo situation, so the results cannot be directly transferred to the in vivo situation. The influence of constraints such as the potting or the reduced degree of freedom could lead to increased failure strength. However, the product of AREA and BMD (which decreases with age) might be usable to predict fatigue strength. From the authors’ point of view, additional efforts have to be made to improve knowledge about the ultimate strength of specimens from young donors. Furthermore, additional studies are required to extend knowledge about fatigue strength. Nevertheless, it has been demonstrated that with regard to fatigue strength and consequently with regard to whole-body vibration injuries, age and individual characteristics, such as endplate area, should be considered.

Part VII Point of view

Gerd Huber, Daniel M. Skrzypiec, Helmut Seidel
Barbara Hinz, Christoph Mischke, Michael M. Morlock

This study was undertaken within the general framework of research promoted by the German FIOSH (Seidel et al., 1998, 2005, 2008a, 2008b; Hinz et al., 2008) and aims to elaborate an improved health risk assessment for whole-body vibration. Improvements in risk assessment are only possible, if external excitation-reaction-relations, internal force-strain-relations and strain-failure-relations of the internal structures are brought together. The most promising way is the development and application of numerical models based on in vivo measurements, taking into account the in vitro determined structural stiffness and strength of the anatomical structures. This model based approach should be executed on a whole-body- and on a functional-units-scale. Due to its complexity, it is not surprising, that the final goal of the general framework has not been completed yet. The high variations expected and observed in the in vitro and in vivo experiments with human specimens and subjects, the high number of loading directions, magnitudes and frequencies as well as the nonlinear behaviour of the tissue are limiting the principle of superposition with regard to load magnitudes and different loading directions, such increasing the number of measurements required.
Over the past years however, the German FIOSH, the Institute for Structural Dynamics in Darmstadt and the Institute of Biomechanics in Hamburg, achieved big progress in all three topics mentioned. An important example is the herewith completed project F2069 which enlarged the knowledge about modelling of individualized functional spinal units based on prominent geometrical scaling factors, delivered outstanding shear strength limits and dynamic material properties and showed the dependency of fatigue failure on age and individual properties like geometry and bone mineral density. An intrinsic phenomenon with research projects as the present one is its self-preservative nature; questions answered by research lead to new questions. Alike in this study several findings were unexpected and could not be readily explained. Moreover, some findings require the need for further investigations. In the following, the most important findings made during the F2069 project are summarized and commented.

Shear loading up to 1000 N did not cause ultimate failure in the tested specimens. The majority of specimens failed at loads around 2000 N to 4000 N. The failure mode is unclear. For a few specimens the x-ray based analyses showed failure of the posterior elements, but it is likely that mainly failures of soft tissues occurred. This single overload experiment however, has to be seen with regard to the dynamic cyclic loading with high loading peaks that are expected to occur. In literature shear peak loads exceeding 700 N were predicted, when static and dynamic effects are combined (Seidel et al., 2005). Shear forces exceeding 30 percent of the ultimate strength have been supposed as potential cause of shear fatigue failure (McGill et al., 1998). The shear ultimate strength measured in this study is giving a first indication about spinal shear load capacity, but additional in vitro studies of shear fatigue loading are strongly recommended, to elucidate if repeated load cycles of shear in a range experienced by operators of heavy machines will lead to fatigue

failure of bony structures as well as discs. For those measurements the influence of superposed axial loading is of special interest, because reduced axial compression is supposed to increase shear strain (Seidel et al. 2008b).

The evaluation of mechanical shear properties showed that initial peak-to-peak shear stiffness was lowest for Young-Flexed specimens. This is probably caused by the separation of apophyseal joints, when only disc and ligaments are resisting shear forces. However, when the shear ultimate strength is considered, the resistance to shear force was the largest for the flexed specimens. This inconsistency and also the thereby observed axial height increase during shear overload are unclear effects. Further FE studies including fluid movements should be applied. The apophyseal joints might partly contribute to the effects especially under large shear loads, but the height increase was also observed in isolated disc segments. The incorporation of shear loading to health risk assessment, e.g. in ISO 2631-5, is not yet possible, since its contribution to vibration-associated injury remains unclear.

A clear influence of frequency on stiffness and energy ratio was observed for frequencies ranging from quasi-static to dynamic (up to 12 Hz). If only dynamic loading is considered, the differences might be not relevant. In complex whole-body vibration models it might be appropriate, to model the behaviour with frequency independent stiffness and damping. The measured dynamic stiffness itself will affect all modelling done so fare. In an iterative process, the new data might improve the quality of whole body models and lead to better predictions of the internal forces on the spine. However the increasing energy ratio with rising frequency, or in other words, the higher energy dissipation in the disc might increase the probability of cumulative injury. In future studies, this question could be addressed by repeating the compressive fatigue experiments with 10 Hz loading frequency instead of 5 Hz used in this study.

The improvement in modelling spinal specimens' behaviour showed that the geometrical individualisation of FE models partly improves the prediction of specimen's in vitro behaviour. Moreover, the choice of a reasonable amount of scaling factors can replace the complex modelling of every single individual anatomy and might make individual models easy to handle. The inclusion of fluid movements and the influence of apophyseal joints, the interaction of nucleus soft tissue and the rather rigid and strictly oriented disc fibres have to be further investigated. In order to understand the respective contribution of the apophyseal joints and the lumbar discs to the mechanical behaviour of the intact functional spinal unit, consecutive experiments with specimens before and after removal of the posterior elements should be performed and replicated with numerical simulations.

Fatigue experiments in neutral posture with specimens belonging to the older group lead to vertebrae failures if bone mineral density was low (4 out of 6 specimens). The results of fatigue experiments of young specimens tested in flexion were inconsistent. During the experiments two specimens showed signs of failure within 300.000 cycles. The vertebrae of one of those specimens had very low mineral density which fits with the findings for older donors. The other specimen was difficult to classify into the failed specimens group since the change in creep behaviour was rather small and neither the post testing CT nor the morphological grading did indicate any signs of failure. There is still no strong evidence, that the failure rate is increased during

fatigue loading of flexed specimens in vitro. On the other hand, epidemiological data and model calculations suggest increased back pain for people working in awkward postures for a long duration of time (e.g. heavy duty bridge crane, helicopter pilots, certain heavy earth-moving equipment). Increased compressive stiffness was observed for the flexed specimens in the in vitro experiments. It is most likely that this increased stiffness also changes the failure mode. This was already shown in in vitro experiments determining ultimate strength. Granhed et al. (1989) pointed out, that flexion led to a rather wedged shape failure mechanism. However, the 10° flexed position in the present study represents unsupported sitting at L4-L5 level (Andersson et al., 1979), but not bending forward. This fits with the observation that the ultimate compressive strength measurements did not show significant differences between failure loads for specimens flexed up to 9° and in neutral posture (Adams et al., 1994). This might indicate that an increased failure rate will occur in vitro if the flexion angle during in vitro testing is increased, but moderate flexion, as during seating, might not be a crucial risk factor. It is also unclear if the neutral orientation of vertebral specimens after harvesting, freezing and preparation can really be assumed to represent “normal” standing. This should be clarified.

The ISO 2631-5 accounts for axial compression only and determines workers individual load capacitance based on measurements of the ultimate quasi-static compression strength depending on age. For a given dynamic axial stress the numbers of load cycles to reach a risk factor of 100% can be calculated. The result is very much dependent on the exponent that is used in the equation to sum up the equivalent dose. In the ISO 2631-5 this exponent is 6. This solitary part of the ISO 2631-5, Annex A, describing the relation between fatigue and ultimate strength, can be compared to the fatigue experiment presented in this study, if a mean vertebral reference area is assumed (16.7 cm^2). For typical young donors, the load cycles to failure where clearly above the predicted relation, but the prediction used in this ISO overestimated the strength of three specimens with low bone mineral density and small endplate size. Two specimens are belonging to the group of older donors, one to the group of flexed specimens. For the presented in vitro study however, it is not possible to incorporate the load cycles that the donors accumulated during lifetime. The new findings do not show a clear indication to revise the recommendation of the ISO 2631-5 in this special point of deriving fatigue strength from ultimate strength. It appears however, that bone mineral density and some geometrical measures would be even more capable for the risk assessment, if available.

With regard to the isolate topic of spinal strength, some basic questions in risk assessment are still open. No guideline or experiment justifies the proper cycle-counting algorithms to reduce a spectrum of real stochastic vibration load cycles into a set of simple load reversals in order to make their injury potential comparable (e.g. Rainflow-counting algorithm). Moreover, it is not yet clear if load offset or load cycle amplitude is the most prominent factor for spinal fatigue failure or if it is simply a matter of loading peaks. Vertebral fatigue strength knowledge exceeding the findings of this report is rare. All those open questions lead to the recommendation that further experiments and modelling with the major loading directions (anterior-posterior shear and axial compression) should be conducted.

The preceding projects (F1899, F5162, F2028) together with this study (F2069) made validated methods in risk assessment accessible, but as pointed out, further

fundamental work likewise the already started F2059 project to support and enlarge methods and knowledge will be needed. Such results could help to advance risk assessment and contributes to an improved health care for workers exposed to whole-body vibration and shocks.

Part VIII Appendix

1 Mechanical Parameters

Several loading conditions were applied to the 18 L4-L5 FSUs. In this appendix they are listed with corresponding identification numbers (ID). The required parameters are given for axial load and shear load. Movements in the remaining four degrees of freedom were restricted.

Three different loading modes were used: a constant load (---), a ramp from 0 N to maximum value and back (_/_) and a ramp around an offset value (-/\/-). For those modes the respective offset, frequency, amplitude and numbers of cycles are given.

1.1 Quasi-static measurements

For quasi-static measurements, FSUs were loaded with ascending and descending compression loads from 0 to 2000 N with a cycle duration of 200 s, both with and without the influence of shear loads.

A constant shear load was applied in the anterior (+200 N) and posterior (-200 N) directions during the cyclic loading in the axial direction (ID 01 and ID 02). A cyclic shear load (ID 04 to ID 06) from -200 N to +200 N was applied with 4 N/s (cycle duration of 200 s) in combination with three compression values (0 N, 1000 N, 2000 N).

Table VIII-1 Quasi-static measurements (conditioning). Loading modes: constant (---), ramp from 0 N to maximum value and back (_/_) or ramp around offset value (-/\/-)

ID No.	Axial load [N]					Shear load [N]					Time
	Mode	Offset	Freq.	Ampl.	No.	Mode	Offset	Freq.	Ampl.	No.	
01	_/_	-1000	0.005 Hz	-1000	2	---	0	/	/	/	400s
02	_/_	-1000	0.005 Hz	-1000	2	---	200	/	/	/	400s
03	_/_	-1000	0.005 Hz	-1000	2	---	-200	/	/	/	400s
04	---	0	/	/	/	-/\/-	0	0.005 Hz	200	2	400s
05	---	-1000	/	/	/	-/\/-	0	0.005 Hz	200	2	400s
06	---	-2000	/	/	/	-/\/-	0	0.005 Hz	200	2	400s
07	0					0					~5 min

High subsidence effects occur in unloaded motion segments, and despite long cycle durations, viscoelastic effects are expected (Huber et al., 2001). Therefore, two complete cycles were performed, but only the second one was used for analysis. Quasi-static measurements also served as preconditioning of the specimen for the following measurement blocks.

1.2 Reference measurements

Reference measurements were performed after quasi-static measurements and before and during fatigue measurements. This was done in order to investigate how different loading modes affected the quasi-static and dynamic parameters at different stages of the experiment. The total time of reference experiment was approximately 8 min. This reference block was used, under different ID numbers, during fatigue loading.

Table VIII-2 Reference measurements. Loading modes: constant (---), ramp from 0 N to maximum value and back (_/_) or sinus (~)

ID No.	Axial load [N]					Shear load [N]					Time
	Mode	Offset	Freq.	Ampl.	No.	Mode	Offset	Freq.	Ampl.	No.	
01	_/_	-1000	0.005 Hz	-1000	2	---	0	/	/	/	400s
12	~	-800	1-12 Hz	-550	12*(4s+8c)	---	0	/	/	/	73s

1.3 Frequency-dependent measurements

Frequency-dependent measurements were carried out with sinusoidal loads at frequencies in the relevant range for occupational medicine (1 Hz-12 Hz).

1.3.1 Axial compression

Cyclic axial compression was done for three different offset loads (500 N, 800 N, 1100 N) with five different amplitudes (200 N, 400 N, 550 N, 700 N, 1000 N). Shear force was maintained at 0 N.

Table VIII-3 Measurement process for compression load. Loading modes: constant (---) or sinus (~)

ID No.	Axial load [N]					Shear load [N]					Time
	Mode	Offset	Freq.	Ampl.	No.	Mode	Offset	Freq.	Ampl.	No.	
08	~	-500	1-12 Hz	-200	12*(4s+8c)	---	0	/	/	/	73s
09	~	-500	1-12 Hz	-400	12*(4s+8c)	---	0	/	/	/	73s
10	~	-800	1-12 Hz	-200	12*(4s+8c)	---	0	/	/	/	73s
11	~	-800	1-12 Hz	-400	12*(4s+8c)	---	0	/	/	/	73s
12	~	-800	1-12 Hz	-550	12*(4s+8c)	---	0	/	/	/	73s
13	~	-800	1-12 Hz	-700	12*(4s+8c)	---	0	/	/	/	73s
14	~	-1100	1-12 Hz	-200	12*(4s+8c)	---	0	/	/	/	73s
15	~	-1100	1-12 Hz	-400	12*(4s+8c)	---	0	/	/	/	73s
16	~	-1100	1-12 Hz	-550	12*(4s+8c)	---	0	/	/	/	73s
17	~	-1100	1-12 Hz	-700	12*(4s+8c)	---	0	/	/	/	73s
18	~	-1100	1-12 Hz	-1000	12*(4s+8c)	---	0	/	/	/	73s
07	0					0					~5 min

For every frequency step there was a time of 4 s, followed by 8 complete cycles. Transient effects should have been low during the last cycles. Measurement took about 13 min, followed by a recovery period of 5 min.

1.3.2 Shear loads

For measurements at dynamic shear loads in anterior-posterior directions, four mean values (0 N, 100 N, 200 N, -100 N) were combined with three different amplitudes (50 N, 125 N, 200 N). Measurements with a cyclic sinusoidal shear load were performed with a constant axial pre-load of 800 N. For each of the twelve frequency steps, a time of 4 s, followed by 8 measuring cycles, was applied. This should have allowed transient effects to die away. The measurement took about 15 min.

Table VIII-4 Measurement process for shear loading tests. Loading modes: constant (---) or sinus (~)

ID No.	Axial load [N]					Shear load [N]					Time
	Mode	Offset	Freq.	Ampl.	No.	Mode	Offset	Freq.	Ampl.	No.	
19	---	-800	/	/	/	~	0	1-12 Hz	50	12*(4s+8c)	73s
20	---	-800	/	/	/	~	0	1-12 Hz	125	12*(4s+8c)	73s
21	---	-800	/	/	/	~	0	1-12 Hz	200	12*(4s+8c)	73s
22	---	-800	/	/	/	~	+100	1-12 Hz	50	12*(4s+8c)	73s
23	---	-800	/	/	/	~	+100	1-12 Hz	125	12*(4s+8c)	73s
24	---	-800	/	/	/	~	+100	1-12 Hz	200	12*(4s+8c)	73s
25	---	-800	/	/	/	~	+200	1-12 Hz	50	12*(4s+8c)	73s
26	---	-800	/	/	/	~	+200	1-12 Hz	125	12*(4s+8c)	73s
27	---	-800	/	/	/	~	+200	1-12 Hz	200	12*(4s+8c)	73s
28	---	-800	/	/	/	~	-100	1-12 Hz	-50	12*(4s+8c)	73s
29	---	-800	/	/	/	~	-100	1-12 Hz	-125	12*(4s+8c)	73s
30	---	-800	/	/	/	~	-100	1-12 Hz	-200	12*(4s+8c)	73s
07	0					0					~5 min

1.3.3 Combined loads

A harmonic compression load (mean value 800 N, amplitude 700 N) was also applied in combination with a constant shear force of 100 N. Settling time and measurement cycles were chosen in accordance with previous measurements. Measurement time was 1 min. After frequency-dependent measurements, the specimen was kept without a load for 5 min.

Table VIII-5 Measurement report showing the measurement process for combined loading tests. Loading modes: constant (---) or sinus (~)

ID No.	Axial load [N]					Shear load [N]					Time
	Mode	Offset	Freq.	Ampl.	No.	Mode	Offset	Freq.	Ampl.	No.	
31	~	-800	1-12 Hz	-700	12*(4s+8c)	---	+100	/	/	/	73s
07	0					0					~5 min

1.4 Fatigue

To determine fatigue strength of motion segment L4-L5, a constant load of 1000 N and amplitude of 1000 N were applied on 18 specimens. The number of load cycles was about $3*10^5$ cycles at a frequency of 5 Hz. The resulting measurement time was 17.5 hours. Minimum and maximum values of deformation were recorded and controlled continuously. Cyclic fatigue loading was interrupted after 1000, 10,000, 100,000, 200,000 and 300,000 cycles according to the above-mentioned reference measurements. During these measurements the shear load was maintained at 0 N.

Table VIII-6 Measurement process for fatigue loading tests. Loading modes: constant (---), ramp from 0 N to maximum value and back, sinus (~) or long-term loading (~~~)

ID No.	Axial load [N]					Time
	Mod.	Offset	Freq.	Ampl.	Cycles	
33 (01)	_/_	-1000	0.005 Hz	-1000	2	400s
34 (12)	~	-800	1-12 Hz	-550	12*(4s+8c)	73s
37	~~~	-1000	5 Hz	-1000	1000	200s
38 (01)	_/_	-1000	0.005 Hz	-1000	2	400s
39 (12)	~	-800	1-12 Hz	-550	12*(4s+8c)	73s
42	~~~	-1000	5 Hz	-1000	9000	30min
43 (01)	_/_	-1000	0.005 Hz	-1000	2	400s
44 (12)	~	-800	1-12 Hz	-550	12*(4s+8c)	73s
47	~~~	-1000,	5 Hz	-1000	90,000	300min
48 (01)	_/_	-1000	0.005 Hz	-1000	2	400s
49 (12)	~	-800	1-12 Hz	-550	12*(4s+8c)	73s
52	~~~	-1000,	5 Hz	-1000	100,000	333min
53 (01)	_/_	-1000	0.005 Hz	-1000	2	400s
54 (12)	~	-800	1-12 Hz	-550	12*(4s+8c)	73s
57	~~~	-1000,	5 Hz	-1000	100,000	333min
58 (01)	_/_	-1000	0.005 Hz	-1000	2	400s
59 (12)	~	-800	1-12 Hz	-550	12*(4s+8c)	73s

2 Parameters of the Ligaments

This section is giving the non-linear properties of the ligaments used in the FE model. Modelled ligaments were anterior and posterior longitudinal ligaments, ligamentum flavum, interspinous and supraspinous ligaments and finally the facet capsulary ligaments. The implementation in the FE model bases on the dissertation of Buck (1997). A more detailed description of the ligaments can be found there.

2.1 Anterior longitudinal ligament

This ligament was modelled as five fibres, each with seven sections (bottom section = Section 1, top section = Section 7).

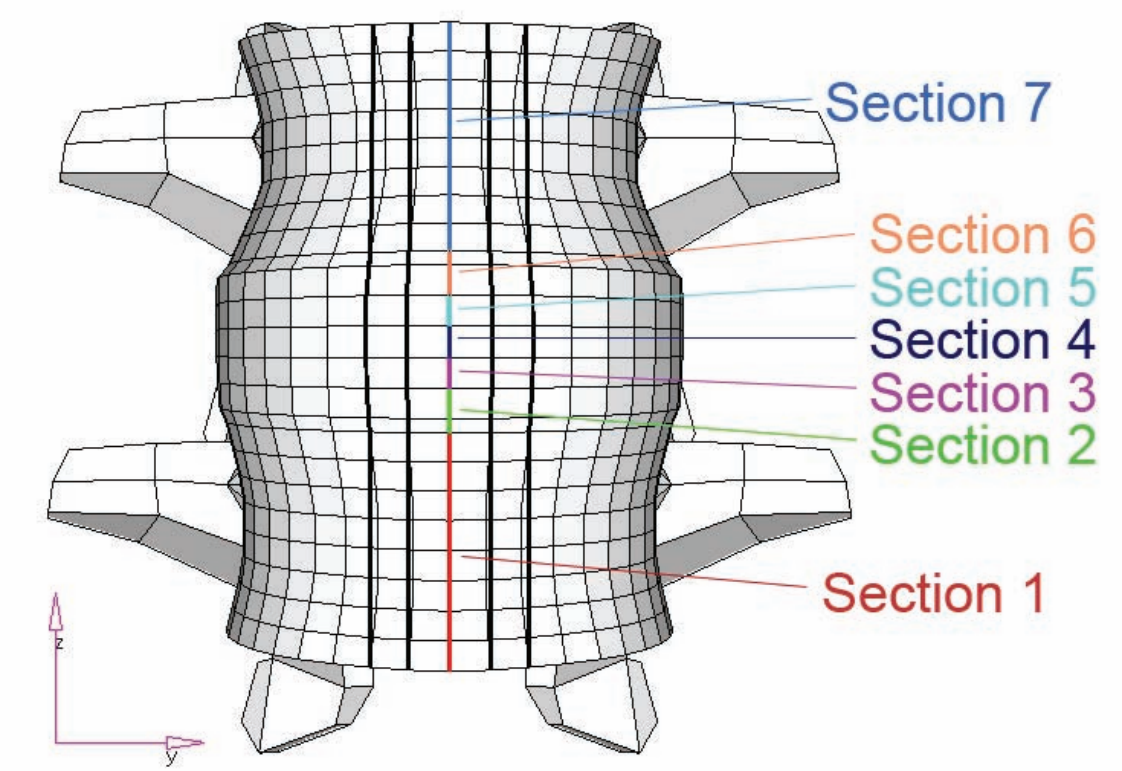

Figure VIII-1 Fibres of the anterior longitudinal ligament

Table VIII-7 Parameters of the middle fibre of the anterior longitudinal ligament

Force [N]	Relative displacement (strain) [%]						
	Section 1	Section 2	Section 3	Section 4	Section 5	Section 6	Section 7
1.000000	0	0	0	0	0	0	0
2.647051	0.179653	0.034852	0.027167	0.027652	0.027034	0.037612	0.179653
12.329239	0.359307	0.069704	0.054333	0.055303	0.054069	0.075224	0.359307
41.990464	0.538960	0.104560	0.081500	0.082955	0.081103	0.112835	0.538960
137.876665	0.718614	0.139407	0.108670	0.110606	0.108140	0.150447	0.718614

Table VIII-8 Parameters of the lateral interior fibres of the anterior longitudinal ligament

Force [N]	Relative displacement (strain) [%]						
	Section 1	Section 2	Section 3	Section 4	Section 5	Section 6	Section 7
1.000000	0	0	0	0	0	0	0
5.294101	0.178833	0.034519	0.026734	0.027185	0.026614	0.037160	0.178833
24.658478	0.357667	0.069039	0.053468	0.054370	0.053228	0.074320	0.357667
83.980929	0.536500	0.103560	0.080202	0.081555	0.079842	0.111480	0.536500
275.753330	0.715334	0.138077	0.106940	0.108740	0.106460	0.148640	0.715334

Table VIII-9 Parameters of the lateral exterior fibres of the anterior longitudinal ligament

Force [N]	Relative displacement (strain) [%]						
	Section 1	Section 2	Section 3	Section 4	Section 5	Section 6	Section 7
1.000000	0	0	0	0	0	0	0
2.647051	0.177347	0.034118	0.026142	0.026534	0.026030	0.036572	0.177347
12.329239	0.354694	0.068235	0.052285	0.053069	0.052061	0.073145	0.354694
41.990464	0.532042	0.102350	0.078427	0.079603	0.078091	0.109720	0.532042
137.876665	0.709389	0.136470	0.104570	0.106140	0.104120	0.146289	0.709389

2.2 Posterior longitudinal ligament

This ligament was modelled as five fibres, each with seven sections (bottom section = Section 1, top section = Section 7).

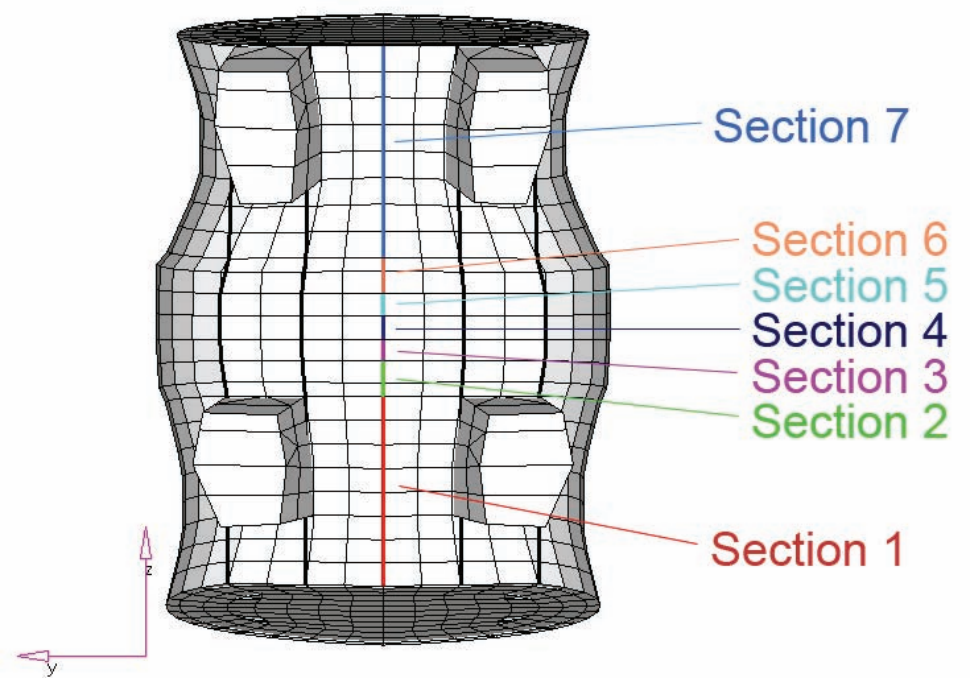

Figure VIII-2 Fibres of the posterior longitudinal ligament

Table VIII-10 Parameters of the middle fibre of the posterior longitudinal ligament

Force [N]	Relative displacement (strain) [%]						
	Section 1	Section 2	Section 3	Section 4	Section 5	Section 6	Section 7
1.000000	0	0	0	0	0	0	0
2.514597	0.160851	0.031769	0.019584	0.020002	0.019569	0.030985	0.160851
15.193746	0.321703	0.063538	0.039169	0.040004	0.039138	0.061970	0.321703
69.589427	0.482555	0.095308	0.058753	0.060006	0.058707	0.092955	0.482555
311.304591	0.643407	0.127076	0.078338	0.080008	0.078277	0.123939	0.643407

Table VIII-11 Parameters of the lateral interior fibres of the posterior longitudinal ligament

Force [N]	Relative displacement (strain) [%]						
	Section 1	Section 2	Section 3	Section 4	Section 5	Section 6	Section 7
1.000000	0	0	0	0	0	0	0
5.029193	0.159858	0.031824	0.019456	0.019919	0.019466	0.030945	0.159858
30.387491	0.319716	0.063647	0.038912	0.039839	0.038933	0.061890	0.319716
139.178853	0.479574	0.095471	0.058369	0.059758	0.058399	0.092835	0.479574
622.609183	0.639432	0.127294	0.077825	0.079677	0.077865	0.123780	0.639432

Table VIII-12 Parameters of the lateral exterior fibres of the posterior longitudinal ligament

Force [N]	Relative displacement (strain) [%]						
	Section 1	Section 2	Section 3	Section 4	Section 5	Section 6	Section 7
1.000000	0	0	0	0	0	0	0
2.514597	0.159238	0.032151	0.019441	0.019941	0.019475	0.031169	0.159238
15.193746	0.318477	0.064301	0.038883	0.039881	0.038949	0.062337	0.318477
69.589427	0.477715	0.096452	0.058324	0.059822	0.058424	0.093506	0.477715
311.304591	0.636954	0.128602	0.077765	0.079762	0.077899	0.124674	0.636954

2.3 Ligamentum flavum

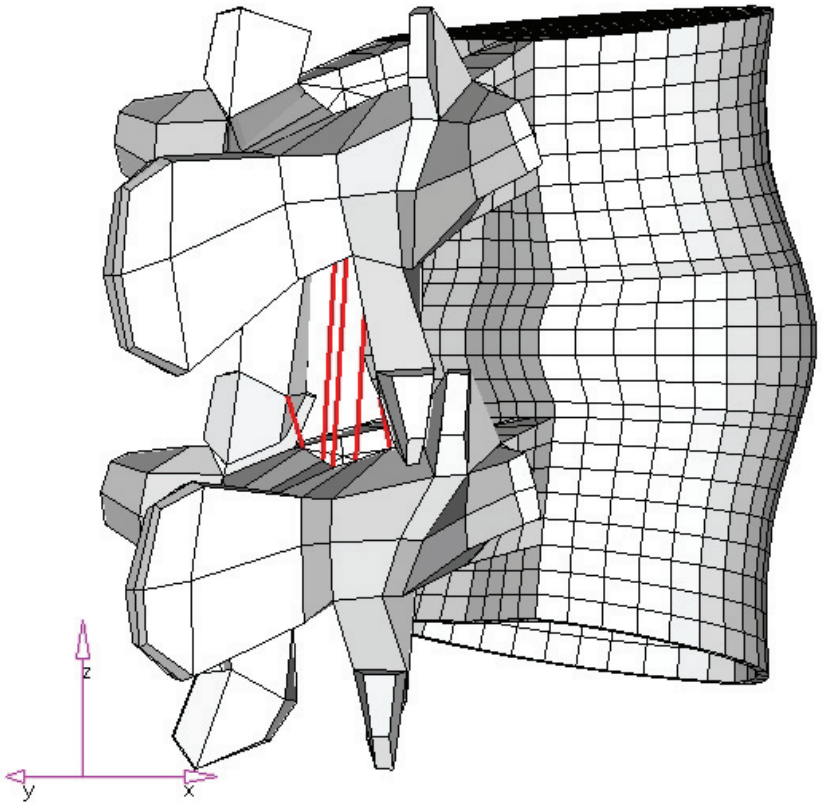

Figure VIII-3 Fibres of the ligamentum flavum

Table VIII-13 Parameters of the fibres of the ligamentum flavum

Middle fibre		Lateral interior fibres		Lateral exterior fibres	
Force [N]	**Relative displacement (strain) [%]**	**Force [N]**	**Relative displacement (strain) [%]**	**Force [N]**	**Relative displacement (strain) [%]**
1.000000	0	0	0	0	0
0.523084	0.068622	1.046168	0.068622	0.523084	0.068622
2.446445	0.137244	4.892889	0.137244	2.446445	0.137244
8.370826	0.205866	16.741650	0.205866	8.370826	0.205866
27.620550	0.274488	55.241100	0.274488	27.620550	0.274488

2.4 Interspinous ligament

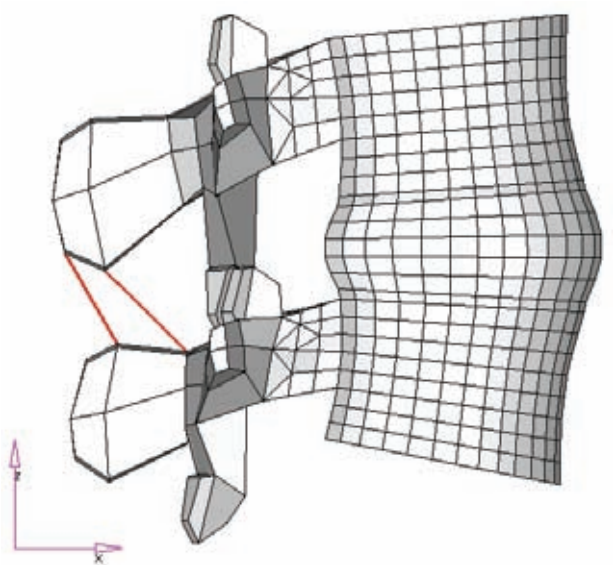

Figure VIII-4 Interspinous ligament

Table VIII-14 Parameters of the interspinous ligament (same values for both fibres)

Force [N]	Relative displacement (strain) [%]
1.000000	0
2.377079	0.314350
10.923480	0.428701
36.641820	0.543051
118.405100	0.657402

2.5 Supraspinous ligament

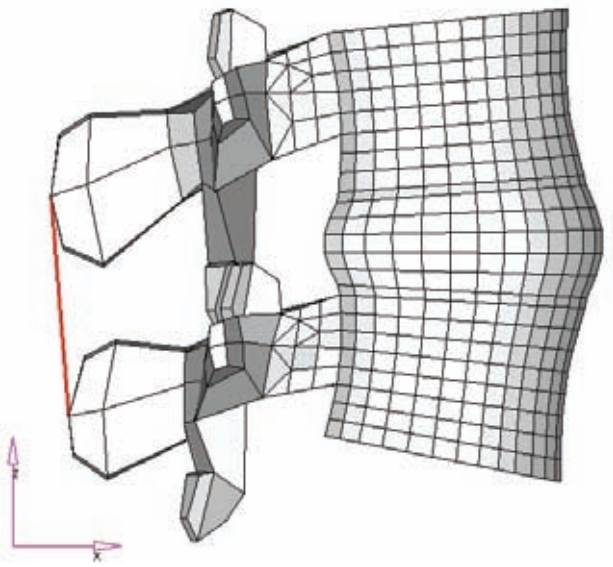

Figure VIII-5 Supraspinous ligament

Table VIII-15 Parameters of the supraspinous ligament

Force [N]	Relative displacement (strain) [%]
1.000000	0
11.172230	0.461947
38.439370	0.723895
93.860980	0.985842
216.315000	0.01247790

2.6 Facet capsulary ligament

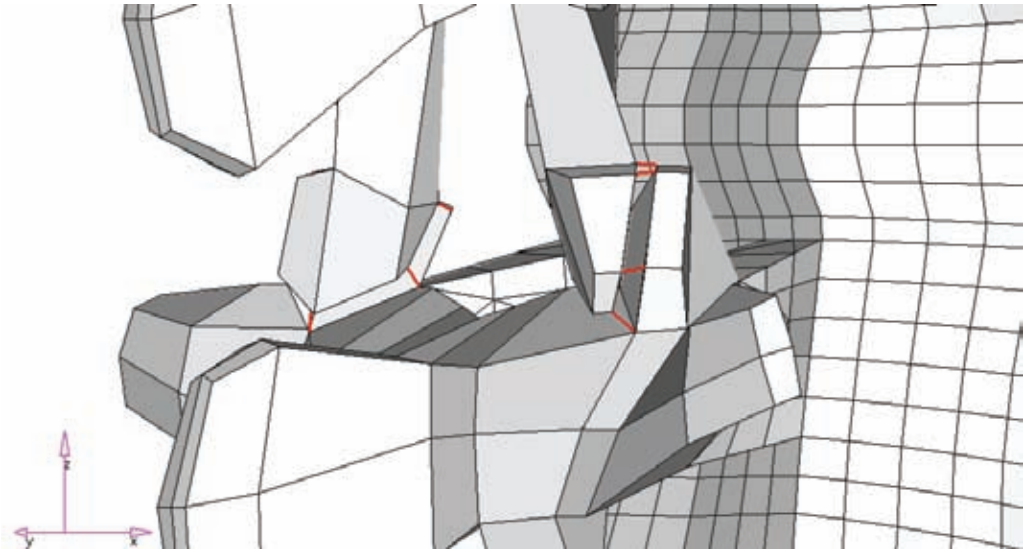

Figure VIII-6 Fibres of the facet capsulary ligament (six fibres for each facet joint)

Table VIII-16 Parameters of the fibres of the facet capsulary ligament (same values for all fibres)

Force [N]	Relative displacement (strain) [%]
0.000000	0
0.698969	0.082294
4.012882	0.164587
17.335540	0.246881
72.984640	0.329175

3 Height Increase

As mentioned in Chapter III, an increase in the height of the motion segment during shear overload was observed. This phenomenon did not appear to be greatly affected by age, posture or creep in motion segments. It was assumed that either the apophyseal joints or the setup arrangement was responsible for this behaviour. To investigate if this behaviour would be affected by the lack of apophyseal joints, disc segments (from levels L2-L3 and L4-L5) were tested in the same way as described in Chapter III, in neutral posture. To address the second issue, the setup arrangement, a rubber specimen was tested in shear, in neutral posture; if the setup arrangement was problematic, then a height increase should have been observed in the rubber specimen.
The results of the additional experiments are shown in Figure VIII-7. It can be seen that the disc specimens exposed to shear displacement showed an increase in height with increased shear displacement. On the other hand, the rubber specimen showed a decrease in height with increased shear displacement.

It can be concluded that the observed increase in the height of the motion segments and disc segments with increased shear displacement is a property of those specimens and not caused by the setup arrangement. However, it is not clear which mechanism is responsible for the increase.

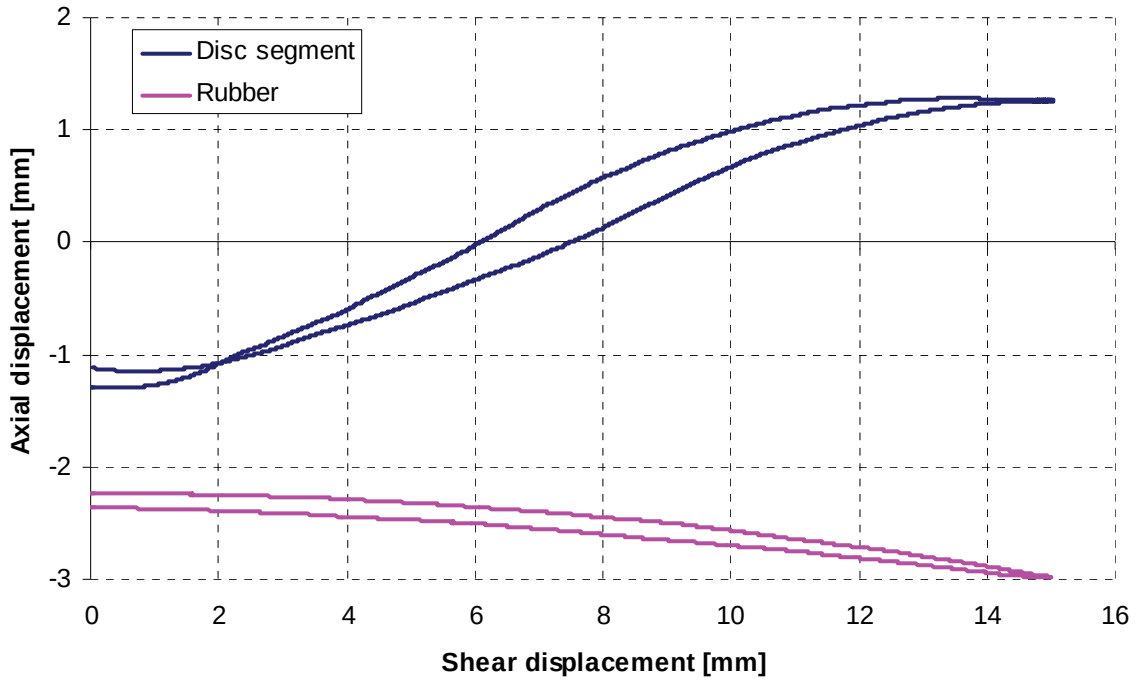

Figure VIII-7 Example of axial height changes for disc segments and rubber specimens exposed to shear displacement (axial displacement does not start from zero as it includes the height decrease caused by the application of a 500 N compressive load)

4 Temperature Controller

To perform experiments with human lumbar segments under in vivo conditions, a tempered water bath is typically used to keep the specimens humid and warm in order to avoid unwanted changes in their mechanical behaviour. Accurate water bath temperature regulation requires a control circuit. Therefore, temperature data collection, data processing and corresponding temperature adjustment is needed.

In preliminary studies, commercially available systems for the temperature control of water baths were evaluated. Since the control parameters were found to be insufficient in terms of their adaption time and accuracy, an improved system was developed (master thesis; Witt, 2007). Besides the control of the water bath temperature, this device was designed to simultaneously control several parameters of the testing environment. It thus allowed correspondence with a wide variety of sensor and actor types. Additionally, adaptation of the controller layout to the individual needs of each parameter was set as an input requirement. To reduce hardware costs, this device uses the serial interface (RS-232, following DIN 66020, 66021 and 66259) to communicate, which is a standard hardware component of commonly used personal computers and thus minimises hardware expenses. Control loops of environmental parameters in biomechanical experiments demand a relatively low clock rate so that a predetermined transfer rate can easily be achieved by the serial interface.

The architecture of the measurement and control device follows the diagram below Figure VIII-8.Four sensor ports and four actuator ports can be controlled simultaneously by one central personal computer via a microcontroller.

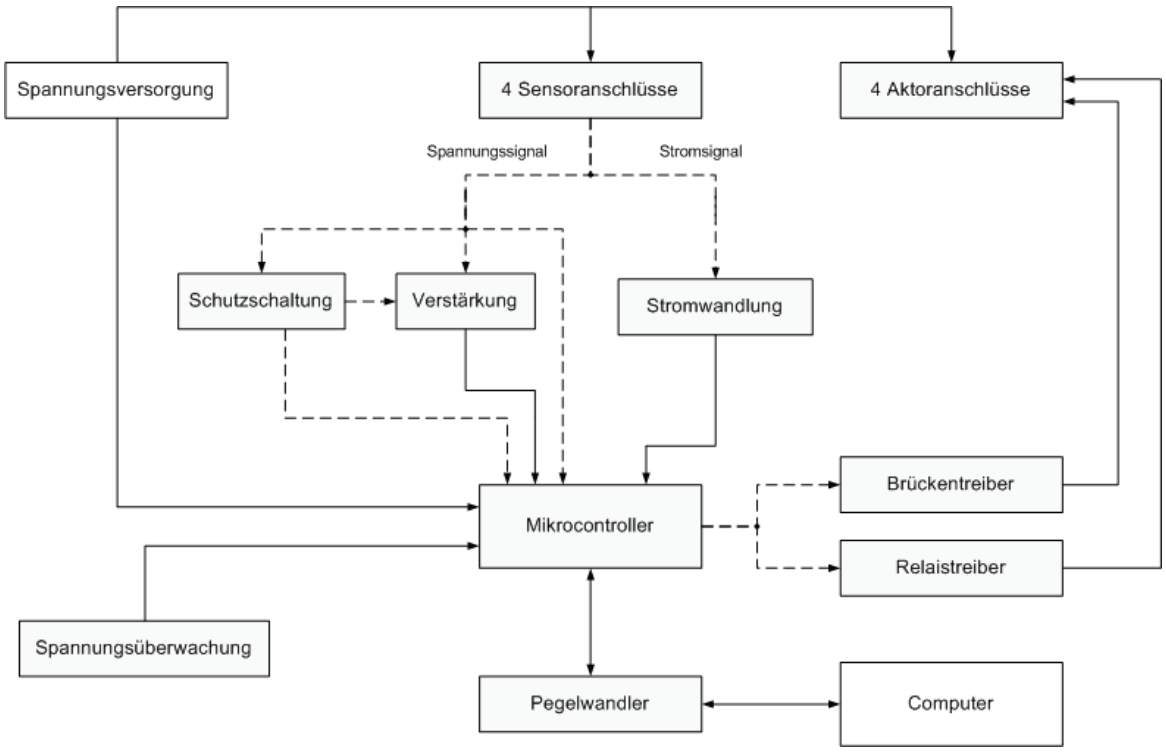

Figure VIII-8 Architecture of the measurement and control device

4.1 Microcontroller

An Atmel ATmega16 8 bit microcontroller was used for data acquisition and actuator control and for communication with the personal computer. The microcontroller was programmed using a STK-500 developing board and is equipped with an external quartz-type clock-pulse generator which provides reliable timing (8 MHz) even during raised temperature variations. A reference voltage supply unit provides 5 V to allow utilisation of transistor-transistor logic (TTL) sensors, which provide 0-5 V signal outputs. Due to a downstream-implemented multiplexer, 8 input channels can be handled and A/D-converted simultaneously with a resolution of 4.9 mV (10 bit). For communication, USART is used, which personal computers generally provide. If the supplied voltage under-runs the operational voltage of the microcontroller (4.5V), a TL7705 fuse-bit (STMicroelectronics, Geneva, Switzerland), which is used as a voltage monitor, restarts the system. The restart can also be initiated manually. Collected data are internally analysed and sent to the computer passing a level converter to achieve an RS-232-compatible data format.

4.2 Sensor signal

Generally, the design of the microcontroller is optimised for commonly used TTL sensors. To expand the number of usable sensor types, a protective circuit consisting of three units was implemented to the signal input. Unit 1 contains a first-order low-pass filter to handle high-frequency signals. Unit 2 contains two Schottky diodes, which adjust the voltage level of different sensor types to the desired level. Unit 3 secures the microcontrollers from overvoltages of up to 24 V.

If required, four operational amplifiers OP295 (Analog Devices, Norwood, MA, USA) enhance the signals to an optimised level by a factor of two or four. To allow the usage of sensors to induce a current signal, the signal has to be converted into a voltage signal that can be processed by the microcontroller. An IC chip RCV420 (Texas Instruments, Dallas, TX, USA) converts the commonly provided current of 4-20 mA into a 0-5 V signal.

4.3 Actuator control

Actuators can either be driven using a dual full-bridge driver or relay-type driver. The dual full-bridge driver L298 (STMicroelectronics, Geneva, Switzerland) provides 50 V output voltage and can be controlled using the pulse-width modulation (PWM) signal allocated by the microcontroller. Alternatively, relays can be switched to provide input signals for successive circuit units.

A LPT46 power supply (ASTEC) provides 5 V, 12 V and 24 V to the actuators and the sensors as well as to the microcontroller. LED control lamps ensure proper connection of applied sensors and actuators. An inside view of the measurement and control box as well as the exterior view can be seen in Figure VIII-9 and Figure VIII-10.

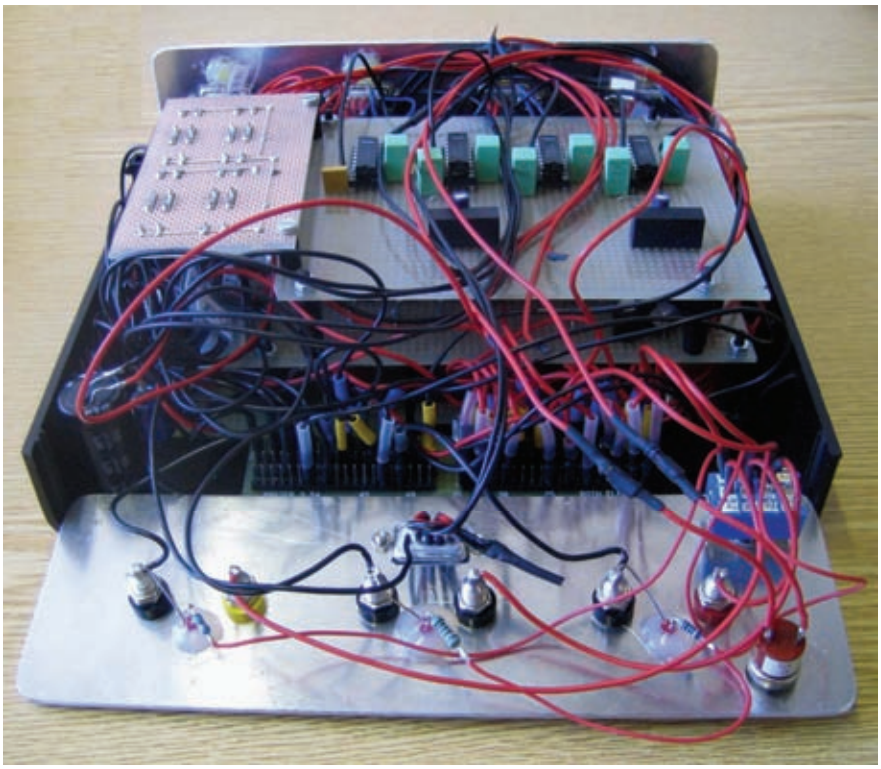

Figure VIII-9 Inside view of the measurement and control box

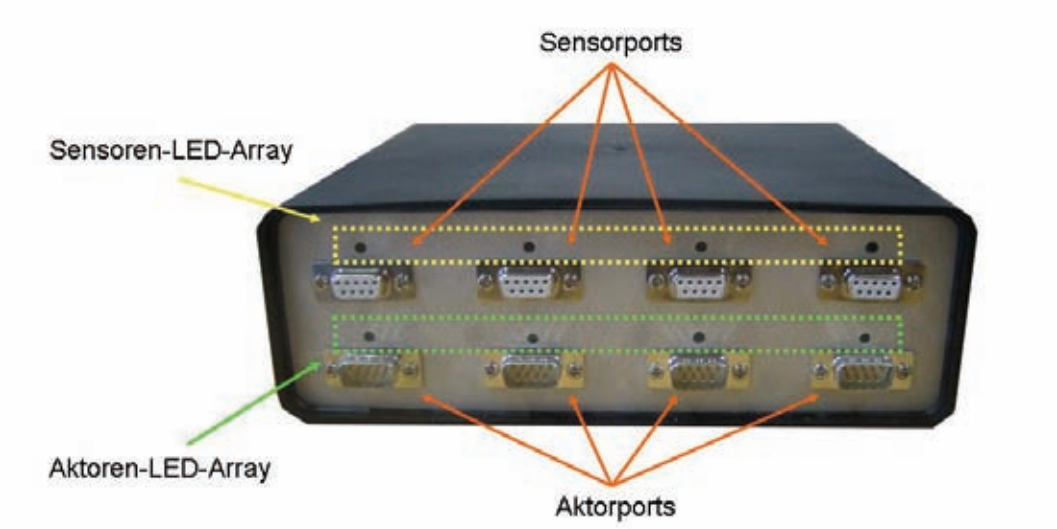

Figure VIII-10 Ports and telltale lamp on the back side of the measurement and control box

4.4 Software

After starting the control device, the microcontroller uploads standard libraries and embeds input and output functions as well as defines handling conventions for exchanged data strings. Each port is initiated automatically and data exchange conditions are defined. In an infinite loop, data strings are alternately received by and sent to the personal computer. Data from the computer contain commands for the actuators and data sent to the computer contain measured data from the sensors.

4.5 User interface

In a user interface (Matlab, Mathworks), sensor ports and actuator ports can be defined and monitored. The character of the sensors (current or voltage) and the corresponding type of actuator control (relay or PWM) can be chosen as well as the design of the closed loop including the circuit parameters. The default control loop designs are P, PI or PID controller, but customised controller designs can be embedded. The calibration data of the sensors can be loaded from Excel sheets, collected data can be saved to file and former measurements can be uploaded for further investigation.

4.6 Conclusion

The above-demonstrated device is an all-purpose functional system that can be used for multi-channel data collection and to control various kinds of sensors and actuators. The usage of the serial interface allows any personal computer to be used without any additional hardware. The user interface makes monitoring and influencing the control functions easy. As long as the dynamics of the controlled states do not exceed the data rate of the serial port, this system provides a reliable, easy-to-adapt and low-budget tool for all kinds of biomechanical experiments. This has been proven in various studies in the Biomechanics Section of the TUHH during the last few months.

5 Nucleus Pressure

Measurements of spinal nucleus pressure are beneficial for interlinking loads applied during in vitro studies with those occurring in vivo (Nachemson, 1966; Wilke, 2001). In a former in vitro study (FIOSH project F1899, Huber et al., 2005) such measurements were successfully performed. For axial compression, the relation between pressure increase and force changes accounts for about 0.6 to 0.7 MPa/kN.

However, the high number of 100,000 cycles applied for each specimen during that study led to a high failure rate for the sensors used (needle pressure transducer, Gaeltec Ltd, Isle of Skye, Scotland). Consequently, it was hard to distinguish between special effects due to disc anatomy or disc mechanics and sensor failure.

In order to detect possible problems, a device was assembled to control the reliability of pressure transducers before and after mechanical testing to ensure that long-lasting cyclic loading did not have a significant effect on the pressure results obtained. This device consists of a hydraulic cylinder (maximum pressure 11 bar) to which a digital manometer (MAN SD, KOBOLD Messring GmbH, Hofheim/Taunus, Germany) is attached. The accuracy class of this reference digital manometer was 0.5.

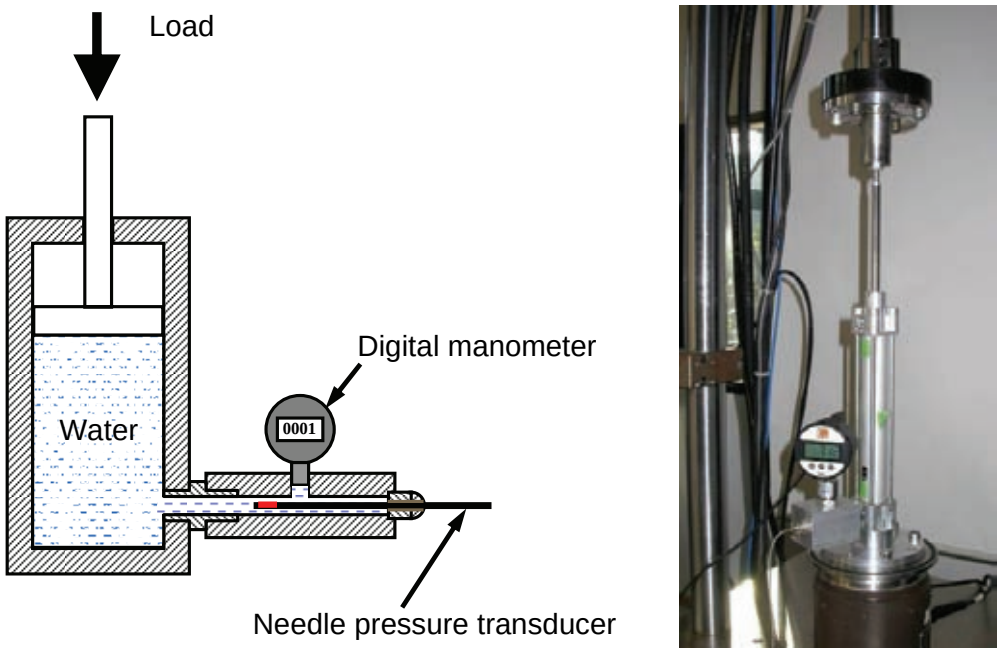

Figure VIII-11 Setup of the calibration device for the needle pressure transducers

The water-filled calibration device was mounted on a hydraulic material testing machine (MTS Bionix, MTS, Eden Prairie, MN, USA). The digital manometer and the needle pressure transducer were both connected to the analogue digital converter of the testing machine to enable simultaneous recording of both sensors. The applied forces led to fluid pressure ranging from 0 to 10 bar. Measurements were repeated twice.

Within the investigated pressure range there was very good agreement (linear coefficient 0.98, r^2>0.99) between the pressure recorded by the needle pressure

transducer and that measured by the digital manometer. The first and second measurements showed the same behaviour.

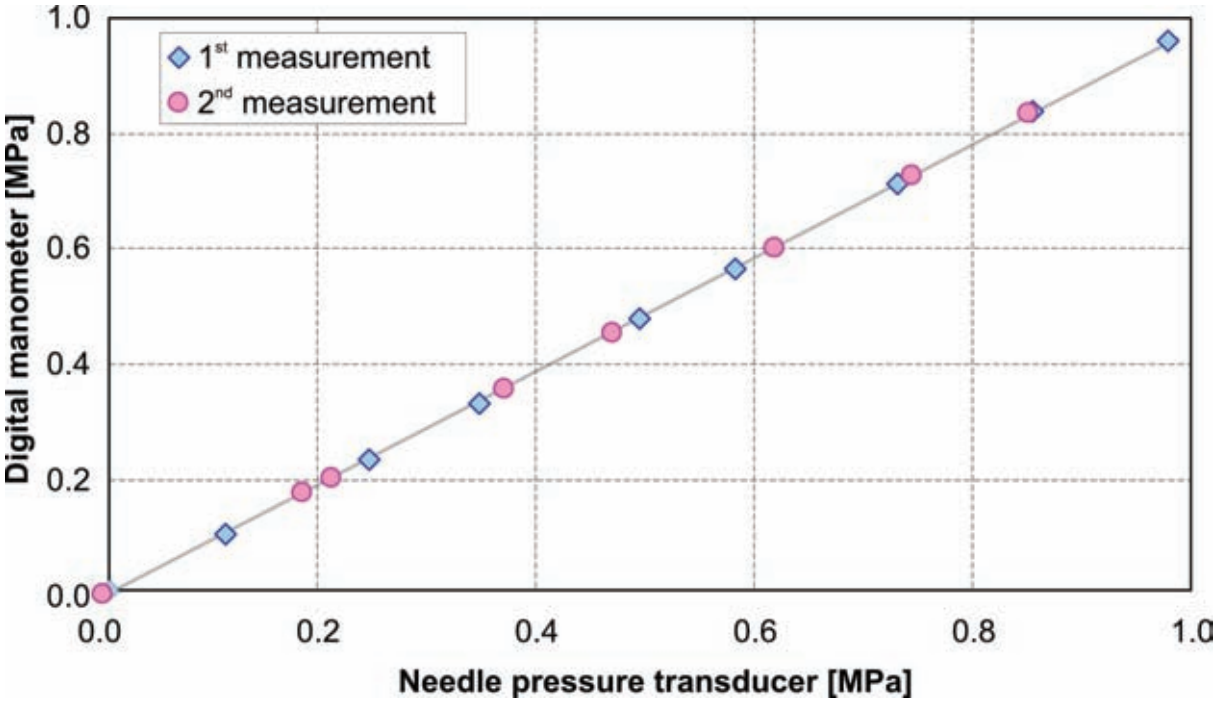

Figure VIII-12 Repeated measurements showed excellent linear correlation between the manometer and needle transducer.

The described device was used to control the needle transducer before and after the first measurements with L4-L5 functional spinal segments. It was thereby realised that the sensors were not able to withstand the three-fold increase in the number of cycles mandatory for this study. Referring to the elective usage of pressure sensors, this part of the study was aborted.[4]

[4] The decision was taken in agreement with the representatives of the FIOSH and was documented in the 4th Interim Report submitted on 16 August 2007.

6 Corresponding Publications

During the period of the presented project, the following articles and conference contributions were made based on project data. This was done in accordance with the interests of the Federal Institute for Occupational Safety and Health (FIOSH), which requested broad publishing of the project results.

6.1 Articles and monographs

Huber, G., Skrzypiec, D., Klein, A., Püschel, K., Morlock, M.M., High Cycle Fatigue Behaviour of Functional Spinal Units, Industrial Health Journal, submitted

Seidel, H., Pöpplau, B.M., Morlock, M.M., Püschel, K., Huber, G., The size of lumbar vertebral endplate areas – Prediction by anthropometric characteristics and significance for fatigue failure due to whole-body vibration, International Journal of Industrial Ergonomics 38: 844–855, 2008

Huber, G., Paetzold, H., Püschel, K., Morlock, M.M., Experimentelle Daten zur Validierung von Finite Elemente Modellen für dynamische Belastungen, VDI-Berichte Nr. 2002, Humanschwingungen Auswirkungen auf Gesundheit - Leistung - Komfort, VDI Wissensforum IWB GmbH, VDI Verlag Düsseldorf, 249-264, 2007

Mischke, C., Wölfel, H.P., Einfluss individueller Geometrie auf die Ergebnisse eines numerischen Modells der unteren Lendenwirbelsäule – Vergleich zwischen Simulationsergebnissen und experimentellen Daten; VDI-Berichte Nr. 2002, Humanschwingungen Auswirkungen auf Gesundheit - Leistung - Komfort, VDI Wissensforum IWB GmbH, VDI Verlag Düsseldorf, 265-276, 2007

Huber, G., Paetzold, H., Püschel, K., Morlock, M.M., Verhalten von Wirbelsäulensegmenten bei dynamischer Belastung, Schriftenreihe der Bundesanstalt für Arbeitsschutz und Arbeitsmedizin, Fb 1062, Wirtschaftsverlag NW, Berlin, 2005

6.2 Conference proceedings

Huber, G., Skrzypiec, D., Klein, A., Püschel, K., Morlock, M.M., High Cycle Fatigue Behavior of Functional Spinal Units, 4th International Conference on Whole Body Vibration Injuries, Montréal, Canada, June 2009

Mischke, C., Huber, G., Skrzypiec, D., Wölfel, H.P., Typical Variations in Spinal Geometry Strongly Influences the Mechanical Behaviour of Lumbar Spines – A combined In Vitro and Finite Element Study, 4th International Conference on Whole Body Vibration Injuries, Montréal, Canada, June 2009

Huber, G., Skrzypiec, D., Klein, A., Püschel, K., Morlock, M.M., Welchen Einfluss hat Alter und Körperhaltung auf die Ermüdungsfestigkeit von Bewegungssegmenten?, 6. Jahrestagung der Deutschen Gesellschaft für Biomechanik, Münster, May 2009

Huber, G., Skrzypiec, D., Klein, A., Püschel, K., Morlock, M.M., Does Age and Flexion Reduce the High Cycle Fatigue Behavior of Functional Spinal Units?, 54th Annual Meeting of the Orthopaedic Research Society, Las Vegas, February 2009

Morlock, M., Huber, G., Methods in Biomechanics – an overview, Conference on Orthopaedic & Implant Biomechanics, ISIC, New Delhi, India, November 2008

Huber, G., Skrzypiec, D., Klein, A., Paetzold, H., Püschel, K., Morlock, M.M., Bone mineral density may determine high cycles fatigue behaviour of Functional spinal Units, 16th congress of the European society of biomechanics, Luzern, July 2008

Skrzypiec, D., Klein, A., Stahmer, F., Seidel, H., Morlock, M.M., Huber, G., Shear load sharing in the human lumbar spine, 16th Congress of the European Society of Biomechanics, Luzern, July 2008

Huber, G., Paetzold, H., Püschel, K., Morlock, M.M., Experimentelle Daten zur Validierung von Finite Elemente Modellen für dynamische Belastungen, AGMT-Vortragsreihe „Biomedizinische Technik heute“, HAW, Hamburg, June 2008

Huber, G., Pöpplau, B., Seidel, H., Paetzold, H., Püschel, K., Morlock, M.M., Erlauben anthropometrische Maße Rückschlüsse auf Größe und Steifigkeit von Bewegungssegmenten?, Workshop der Bundesanstalt für Arbeitsschutz und Arbeitsmedizin: Vorstellung neuer Ergebnisse der Vibrationsforschung und ihrer Relevanz für die Praxis, Berlin, November 2007

Skrzypiec, D., Klein, A., Stahmer, F., Seidel, H., Morlock, M. M., Huber, G., Bewegungssegmente unter Schub. In-vitro Versuche an lumbalen Bewegungssegmenten von männlichen Spendern, Workshop der Bundesanstalt für Arbeitsschutz und Arbeitsmedizin: Vorstellung neuer Ergebnisse der Vibrationsforschung und ihrer Relevanz für die Praxis, Berlin, November 2007

Huber, G., Skrzypiec, D., Paetzold, H., Püschel, K., Morlock, M.M., Jung und Alt - Unterschiede in den mechanischen Eigenschaften von Bewegungssegmenten, Workshop der Bundesanstalt für Arbeitsschutz und Arbeitsmedizin: Vorstellung neuer Ergebnisse der Vibrationsforschung und ihrer Relevanz für die Praxis, Berlin, November 2007

Skrzypiec, D., Paetzold, H., Morlock, M.M., Huber, G., Änderung der Schwingungsdämpfung von Bewegungssegmenten der Lendenwirbelsäule in Abhängigkeit von Größe und Dauer der dynamischen Belastung, Workshop der Bundesanstalt für Arbeitsschutz und Arbeitsmedizin: Vorstellung neuer Ergebnisse der Vibrationsforschung und ihrer Relevanz für die Praxis, Berlin, November 2007

Mischke, C., Huber, G., Wölfel, H.P., Einfluss der Individualisierung auf die Simulationsergebnisse eines numerischen Modells der unteren LWS für verschiedene Belastungsfälle, Workshop der Bundesanstalt für Arbeitsschutz und Arbeitsmedizin: Vorstellung neuer Ergebnisse der Vibrationsforschung und ihrer Relevanz für die Praxis, Berlin, November 2007

Huber, G., Paetzold, H., Püschel, K., Morlock, M.M., Experimentelle Daten zur Validierung von Finite Elemente Modellen für dynamische Belastungen, Humanschwingungen Auswirkungen auf Gesundheit - Leistung - Komfort, VDI Tagung Dresden, October 2007

Mischke, C., Wölfel, H.P., Einfluss individueller Geometrie auf die Ergebnisse eines numerischen Modells der unteren Lendenwirbelsäule – Vergleich zwischen Simulationsergebnissen und experimentellen Daten; Humanschwingungen Auswirkungen auf Gesundheit - Leistung - Komfort, VDI Tagung Dresden, October 2007

Skrzypiec, D., Paetzold, H., Morlock, M.M., Huber, G., The Effect of Magnitude and Duration of Dynamic Loading on Viscoelastic State of Male Human Lumbar Motion Segments, Deutscher Kongress für Biomechanik, Brüggemann und Niehoff (Hrsg.), Köln, March 2007

Huber, G., Pöpplau, B., Seidel, H., Paetzold, H., Püschel, K., Morlock, M.M., Können die Größe und Steifigkeit von Bewegungssegmenten der Wirbelsäule anhand anthropometrischer Maße abgeschätzt werden? Deutscher Kongress für Biomechanik, Brüggemann und Niehoff (Hrsg.), Köln, March 2007

Mischke, C., Huber, G., Morlock, M.M., Wölfel, H.P., The Influence of Individual Geometry on the Results of a Numerical Model of the Lumbar Spine – Experimental Data and Simulation, 5th World Congress of Biomechanics 2006, Munich, Germany, July 29th - August 4th, Journal of Biomechanics, 39 (S1), 2006

Paetzold, H., Huber, G., Morlock, M.M., The Influence of Dynamic Load Level and Loading Amplitude on the Creep Behavior of Functional Lumbar Spinal Units, 52nd Annual Meeting of the Orthopaedic Research Society, in Chicago, Illinois, March 2006

Huber, G., Paetzold, H., Ito, K., Morlock, M.M., Moistening of Spinal Specimens during Dynamic In-Vitro Measurement, 3rd International Conference on Whole-Body Vibration injuries, Nancy, France, June 2005

Mischke, C., Huber G., Michael, M. M., Wölfel H.P., Validating a numerical model of the lumbar spine with in vitro experiments, 3rd International Conference on Whole-Body Vibration Injuries, Nancy, France, June 2005

Rosenau, E., Paetzold, H., Morlock, M.M., Huber, G., Investigation of Strain Gauge Bonding for Moistened In-Vitro Measurements, 3rd International Conference on Whole-Body Vibration injuries, Nancy, France, June 2005

Paetzold, H., Morlock, M.M., Huber, G., Mechanical Properties of Spinal Specimens during Fatigue Testing, 3rd International Conference on Whole-Body Vibration injuries, Nancy, France, June 2005

Huber, G., Vollmer, M., Sellenschloh, K., Morlock, M.M., A new setup for dynamic in vitro testing of spinal specimen in two degrees of freedom, 14th European Society of Biomechanics Conference, ‘s-Hertogenbosch, Netherlands, July 2004

6.3 Bachelor and master theses

Jung, J.: Erstellung und Anwendung eines vollständig individuellen FE-Modells der unteren menschlichen Lendenwirbelsäule, Bachelor Thesis, supervisor Mischke, Fachgebiet Strukturdynamik, TU Darmstadt, 2008

Matthaei, A., Vorhersage der Dauerfestigkeit von Bewegungssegmenten der Wirbelsäule anhand von in-vivo messbaren Parametern, Bachelor Thesis, supervisor Huber, September 30th, 2008

Witt F., Ein modulares System zur Datenaufnahme und differenzierten Regelung niederfrequenter Prozesse mittels serieller Schnittstelle, Diplomarbeit, supervisor Huber, March 30th, 2007

Pöpplau, B., Korrelation anthropometrischer Parameter mit lumbalen Endplattenflächen und den mechanischen Eigenschaften angrenzender Bandscheiben, Kleine Studienarbeit, supervisor Huber, June 14th, 2006

7 Affiliation

TUHH Hamburg University of Technology
Institute of Biomechanics
Denickestraße 15, 21073 Hamburg, Germany

Gerd Huber	(Dr.-Ing.)
Arne Hothan	(Dipl.-Ing.)
Anna Matthaei	(B.Sc.)
Michael M. Morlock	(Prof. Dr.)
Helge Paetzold	(Dipl.-Ing.)
Berry Pöpplau	(Dipl.-Ing.)
Annelie Rehmer	(Dipl.-Ing.)
Kay Sellenschloh	(Dipl.-Ing.)
Daniel M. Skrzypiec	(Ph.D.)
Felix Stahmer	(Dr. med.)
Matthias Vollmer	(Dipl.-Ing.)
Florian Witt	(Dipl.-Ing.)

Darmstadt University of Technology
Department of Structural Dynamics
Petersenstraße 30, 64287 Darmstadt, Germany

Christoph Mischke	(Dipl.-Ing.)
Horst Peter Wölfel	(Prof. Dr.)

University Medical Center Hamburg-Eppendorf
Department of Legal Medicine
Martinistraße 52, 20246 Hamburg, Germany

Birol Aydin	(Dr. med.)
Anke Klein	(Dr. med.)
Klaus Püschel	(Prof. Dr.)
Nadine Wilke	(Dr. med.)

University Medical Center Hamburg-Eppendorf
Diagnostic and Interventional Radiology Department and Clinic
Martinistraße 52, 20246 Hamburg, Germany

Harald Ittrich	(Dr. med.)

Federal Institute for Occupational Safety and Health
Nöldnerstraße 40-42, 10317 Berlin, Germany

Barbara Hinz	(Dr. rer. nat.)
Helmut Seidel	(Dr. med.)

Part IX Literature

Adams, M.A., McNally, D.S., Chinn, H., Dolan, P., Posture and the compressive strength of the lumbar spine, Clinical Biomechanics, 9 (1): 5-14, 1994

Andersson, G., Murphy, R., Ortengren, R., Nachemson, A., The influence of backrest inclination and lumbar support on lumbar lordosis, Spine, 4(1):52-58, 1979

Andersson, G.B.J., Chaffin, D.B., Pope, M.H., Occupational Biomechanics of the Lumbar spine. In: Pope MH, Frymoyer JW, Andersson G, eds. Occupational Low Back Pain. New York: Praeger, 39-70, 1984

Berkson, M.H., Nachemson, A., Schultz, A.B., Mechanical properties of human lumbar spine motion segments – Part II: Responses in compression and shear; influence of gross morphology. Journal of Biomechanical Engineering, 101: 53-7, 1979

Bovenzi, M., Rui, F., Negro, C., D'Agostin, F., Angotzi, G., Bianchi, S., Bramanti, L., Festa, G.L., Gatti, S., Pinto, I., Rondina, L., Stacchini N., An epidemiological study of low back pain in professional drivers, Journal of Sound and Vibration, 298: 514-539, 2006

Brinckmann, P., Biggemann, M., Hilweg, D., Fatigue fracture of human lumbar vertebrae, Clinical Biomechanics, 3 (S1):1-23, 1988

Brinckmann, P., Biggemann, M., Hilweg, D., Prediction of the compressive strength of human lumbar vertebrae, Spine, 14 (6): 606-610, 1989

Broberg, K., Slow deformation of intervertebral disc. Journal of Biomechanics, 26(4-5):501-512, 1993

Buck, B., Ein Modell für das Schwingungsverhalten des sitzenden Menschen mit detaillierter Abbildung der Wirbelsäule und Muskulatur im Lendenbereich, Dissertation, Shaker Verlag, 1997

Buck, B., Pankoke, St., Wölfel, H.P., Lateralsymmetrisches Modell der Lendenwirbelsäule zur Berechnung dynamischer Bandscheibenkräfte (Schlußbericht). Bremerhaven; Wirtschaftsverlag NW, Schriftenreihe der Bundesanstalt für Arbeitsschutz und Arbeitsmedizin Dortmund/Berlin, Forschung FB 770, 1997

Burns, M., Kaleps, I., Kazarian, L., Analysis of compressive creep behavior of the vertebral unit subjected to a uniform axial loading using exact parametric solution equations of kelvin-solid models - Part 1. Human intevertebral joints. Journal of Biomechanics, 17(2):113-130, 1984

Cripton, P., Berleman, U., Visarius, H., Begeman, P.C., Nolte, L.P., Prasad, P., Response of the lumbar spine due to shear loading, Wayne State University, Injury Prevention Through Biomechanics, Symposium Proceedings, 111-126, 1995

Denozière, G., Ku, D.N., Biomechanical comparison between fusion of two vertebrae and implantation of an artificial intervertebral disc, Journal of Biomechanics, 39, 766-775, 2006

Dhillon, N., Bass, E.C., Lotz, J.C., Effect of frozen storage on the creep behavior of human intervertebral discs, Spine, 26 (8): 883-887, 2001

van Dieën J.H., van der Veen, A., van Royen, B.J., Kingma, I., Fatigue Failure in Shear Loading of Porcine Lumbar Spine Segments, Spine, 31 (15): E494–E498, 2006

DIN 33402-2, Ergonomics – Human body dimensions – Part 2: Values, 2005

Directive 2002/44/EC, European Parliament and Council of 25 June 2002 on the minimum health and safety requirements regarding the exposure of workers to the risks arising from physical agents (vibration), sixteenth individual Directive within the meaning of Article 16(1) of Directive 89/391/EEC, Official Journal of the European Communities July 2002:L177/13-L177/19.

Duval-Beaupere, G., Robain, G., Visualization on full spine radiographs of the anatomical connections of the centres of the segmental body mass supported by each vertebra and measured in vivo, International Orthopaedics, 11:261-269, 1987

Gardner-Morse, M.G., Stokes, I.A.F, Structural behavior of human lumbar spinal motion segments, Journal of Biomechanics, 37: 205–212, 2004

Gleizes, V., Viguier, E., Féron, J.M., Canivet, S., Lavaste, F., Effects of freezing on the biomechanics of the intervertebral disc, Surg Radiol Anat, 20 (6): 403-7, 1998

Granhed, H., Jonson, R., Hansson, T., Mineral content and strength of lumbar vertebrae. A cadaver study, Acta orthopaedica Scandinavica, 60 (1): 105-9, 1989

Griffin, M.J., A comparison of standardized methods for predicting the hazards of whole-body vibration and repeated shocks. Journal of Sound and Vibration 215 (4): 883-914, 1998

Griffin, M.J., The validation of biodynamic models, Clinical Biomechanics, 16 (S1): 81-92, 2001

Griffin, M.J., Minimum health and safety requirements for workers exposed to hand-transmitted vibration and whole-body vibration in the European Union; a review. Journal of Occupational and Environmental Medicine, 61: 387–397, 2004

Grunendahl, A., Beitrag zur numerischen Simulation des sitzenden Menschen zur Beurteilung der Auswirkungen von Ganzkörperschwingungen, Dissertation, RWTH Aachen, 2004

Guo, L.X., Teo, E.C., Lee, K.K., Zhang, Q.H., Vibration characteristics of the human spine under axial cyclic loads: effect of frequency and damping. Spine, 30(6):631-7, 2005

Hinz, B., Menzel, G., Blüthner, R., Seidel, H., Transfer functions as a basis for the verification of models – variability and restraints. Clinical Biomechanics, 16 (S1): S93-S100, 2001

Hinz, B., Seidel, H., Hofmann, J., Menzel, G., The significance of using anthropometric parameters and postures of European drivers as a database for finite-element models when calculating spinal forces during whole-body vibration exposure, International Journal of Industrial Ergonomics, 38: 816-846, 2008

Hofmann, J., Pankoke, S., Wölfel, H.P., Individualisierbares Finite-Elemente-Modell des sitzenden Menschen zur Berechnung der Beanspruchungen bei Vibrationsanregung in verschiedenen Raumrichtungen und Stoßanregung an einer Reihe von Körperstellen – Ganzkörpermodell und Submodell der unteren Lendenwirbelsäule (Schlussbericht), Herausgeber: Bundesanstalt für Arbeitsschutz und Arbeitsmedizin (Fb 994), Wirtschaftsverlag NW / Verlag für neue Wissenschaft GmbH, Dortmund / Berlin / Dresden, 2003

Huber, G., Linke, B., Morlock, M.M., Ito, K., The influence of in vitro testing method on measured intervertebral disc characteristics, Spinal Implants: Are we evaluating them appropriately?, ASTM STP 1431, Editor: M. N. Melkerson, S. L. Griffith, und J. S. Kirkpatrick, ASTM International: 101-113, 2003

Huber, G., Paetzold, H., Püschel, K., Morlock, M. M., Verhalten von Wirbelsäulensegmenten bei dynamischer Belastung, Schriftenreihe der Bundesanstalt für Arbeitsschutz und Arbeitsmedizin, Fb 1062, Wirtschaftsverlag NW, Berlin, 2005

Huber, G., Paetzold, H., Püschel, K., Morlock, M. M., Experimentelle Daten zur Validierung von Finite Elemente Modellen für dynamische Belastungen, VDI-Berichte Nr. 2002, Humanschwingungen Auswirkungen auf Gesundheit - Leistung – Komfort, VDI Wissensforum IWB GmbH, VDI Verlag Düsseldorf, 249-264, 2007

ISO 2631-1, International Standard. Mechanical vibration and shock – Evaluation of human exposure to whole-body vibration – Part 1: General requirements. Second edition, corrected and reprinted 1997-07-15. Geneva: International Organization for Standardization; 1997

ISO 2631-5:2004(E), Mechanical vibration and shock – Evaluation of human exposure to whole-body vibration – Part 5: Method for evaluation of vibration containing multiple shocks. Geneva: International Organization for Standardization; 2004

Janevic, J., Ashton-Miller, J.A., Schultz A.B., Large compressive preloads decrease lumbar motion segment flexibility. Journal of Orthopaedic Research, 9(2):228-36, 1991

Kaleps, I., Kazarian, L., Burns, M., Analysis of comprehensive creep behaviour of the vertebral unit subjected to a uniformal axial loading using exact parametric solution equations of kelvin-solid models - Part 2. Rhesus monkey intevertebral joints. Journal of Biomechanics, 17(2):131-136, 1984

Kasra, M., Shirazi-Adl, A., Drouin, G., Dynamics of human lumbar intervertebral joints. Experimental and finite-element investigations. Spine, 17(1):93-102, 1992

Koeller, W., Muehlhaus, S., Meier, W., Hartmann, F., Biomechanical properties of human intervertebral discs subjected to axial dynamic compression-influence of age and degeneration. Journal of Biomechanics, 19(10):807-16, 1986

Kummer, B., Biomechanik, Form und Funktion des Bewegungsapparates, Deutscher Ärzte-Verlag Köln, 2005

LeBlanc, A.D., Evans, H.J., Schneider, V.S., Wendt, R.E. 3rd, Hedrick, T.D., Changes in Intervertebral Disc Cross-Sectional Area with Bed Rest and Space Flight. Spine, 19 (7):812-7, 1994

Lin, H.S., Liu ,Y.K., Adams, K.H., Mechanical response of the lumbar intervertebral joint under physiological (complex) loading, Journal of Bone and Joint Surgery Am., 60: 41-55, 1978

Marras, W.S., Davis, K.G., Jorgensen, M., Spine Loading as a Function of Gender, Spine, 27 (22): 2514–2520, 2002

Matthaei, A., Vorhersage der Dauerfestigkeit von Bewegungssegmenten der Wirbelsäule anhand von in-vivo messbaren Parametern, Bachelor Thesis, supervisor Huber, 2008

McGILL S.M., NORMAN R.W., YINGLING V.R., WELLS R.P. and NEUMANN P., Shear Happens! Suggested guidelines for ergonomists to reduce the risk of low back injury from shear loading**.** Presented at: The 30th Annual Conference of the Human Factors Association of Canada (HFAC), Mississauga, Ontario, Canada, 157-161, 1998

McGlashen, K.M., Miller, J.A.A., Schultz, A.B., Anderson, G.B.J., Load Displacement Behavior of the Human Lumbo-sacral Joint, Journal of Orthopaedic Research, 5:488-496, 1987

McMillan, D.W., McNally, D.S., Garbutt, G., Adams, M.A., Stress distributions inside intervertebral discs: the validity of experimental ‘stress profilometry’, Proceedings of the Institution of Mechanical Engineers. Part H, Journal of Engineering in Medicine, 210 (2): 81-87, 1996

Mischke, Ch., Rützel, S., Hofmann, J., Wölfel, H.P., Belastung der Wirbelsäule durch Ganzkörperschwingungen mit variabler Frequenz, Intensität und Einleitungsrichtung, Abschlussbericht zu Projekt F 2028 der Bundesanstalt für Arbeitsschutz- und Arbeitsmedizin, Berlin, 2007, unveröffentlicht

Netter, F., Atlas der Anatomie des Menschen, Novartis AG, Basel, 1995

OECD, OECD Gesundheitsdaten, Durchschnittliche Lebenserwartung [OECD Health Data], Primärquelle: Statistisches Bundesamt, Gesundheitsberichterstattung des Bundes, in www.gbe-bund.de, Abrufdatum: 10.11.2009

Okunribido, O.O., Magnusson, M., Pope, M.H., Low back pain in drivers: The relative role of whole-body vibration, posture and manual material handling, Journal of Sound and Vibration, 298: 540-555, 2006

Pfeiffer, F.M., Ward, C.V., Abernathie, D.L., Smith, D.E., Alander, D.H., Finite Element Modelling of Lumbar Vertebrae, Conference of the American Society of Biomechanics, Stanford University, August 22-25, 2007

Pankoke, S., Hofmann, J., Wölfel, H.P., Weiterentwicklung eines Modells zur Berechnung von Kräften, die in der Lendenwirbelsäule wirksam werden. Bremerhaven; Wirtschaftsverlag NW, Schriftenreihe der Bundesanstalt für Arbeitsschutz und Arbeitsmedizin Dortmund/Berlin, Forschung FB 885, 2000

Pankoke, S., Hofmann, J., Wölfel, H.P., Determination of vibration-related spinal loads by numerical simulation. Clinical Biomechanics 16 (S1); S45-S56, 2001

Pollintine, P., Przybyla, A.S., Dolan, P., Adams, M.A., Neural arch load-bearing in old and degenerated spines, Journal of Biomechanics, 37 (2): 197-204, 2004

Race, A., Broom, N.D., Robertson, P., Effect of loading rate and hydration on the mechanical properties of the disc. Spine, 25(6): 662-9, 2000

RenShape Solutions, Casting Resin, RenCast® FC 53 Isocyanate / FC 53 Polyol, Quick setting polyurethane system, Huntsman Advanced Materials (Switzerland) GmbH, Publication no. T263e GB, 2004

Rochefort, E. de, Verver, M. M., Grunendahl, A., Mooi, H. G., Butenweg, Ch., Detailed Modelling of the Lumbar Spine for Investigation of Low Back Pain, SAE Technical Papers, Document Number 2005-01-2716, 2005

Rohlmann, A., Claes, L.E., Bergmann, G., Graichen, F., Neef, P., Wilke, H.J., Comparison of intradiscal pressures and spinal fixator loads for different body positions and exercises, Ergonomics, 44 (8): 781-794, 2001

Rohlmann, A., Zander, T., Schmidt, H., Wilke, H.-J., Bergmann, G., Analysis of the influence of disc degeneration on the mechanical behaviour of a lumbar motion segment using the finite element method, Journal of Biomechanics, 39: 2484-2490, 2006

Sandover J., The fatigue approach to vibration and health: is it a practical and viable way of predicting the effects on people? Journal of Sound and Vibration, 215: 699-721, 1998

Schmidt, H., Kettler, A., Heuer, F., Simon, U., Claes, L., Wilke, H.-J., Intradiscal Pressure, Shear Strain and Fiber Strain in the Intervertebral Disc under Combined Loading, Spine, 32(7):748-755, 2007

Seidel, H.; Blüthner, R.; Hinz, B., Effects of sinusoidal whole-body vibration on the lumbar spine: the stress-strain relationship. International Archives of Occupational and Environmental Health, 57 (3), 207-223, 1986

Seidel, H., Blüthner, R., Hinz, B., Schust, M., On the Health Risk of the Lumbar Spine due to Whole-Body Vibrations – Theoretical Approach, Experimental Data and Evaluation of Whole-Body Vibration, Journal of Sound and Vibration, 215 (4): 723-741, 1998

Seidel H., On the relationship between whole-body vibration exposure and spinal health risk. Industrial Health 43 (3), 361-377, 2005

Seidel, H., Pöpplau, B.M., Morlock, M.M., Püschel, K., Huber, G., The size of lumbar vertebral endplate areas—Prediction by anthropometric characteristics and significance for fatigue failure due to whole-body vibration, International Journal of Industrial Ergonomics, 38 (9-10): 844-855, 2008a

Seidel, H., Hinz, B., Hofmann, J., Menzel G., Intraspinal forces and health risk caused by whole-body vibration—Predictions for European drivers and different field conditions, International Journal of Industrial Ergonomics, 38 (9-10): 856-867, 2008b

Seidel, H., Blüthner, R., Hinz, B., Schust, M., Stresses in the lumbar spine due to whole-body vibration containing shocks. Experimental interdisciplinary study - anthropometry, biodynamics, biomechanical model, psychophysics and electromyography . The project formed part of the collaborative project on whole body vibration III; (Final Report), Bremerhaven; Wirtschaftsverlag NW, Schriftenreihe der Bundesanstalt für Arbeitsschutz und Arbeitsmedizin Dortmund/Berlin, Forschung Fb 777: 197, 1997

Shirazi-Adl, A., Analysis of large compression loads on lumbar spine in flexion and in torsion using a novel wrapping element, Journal of Biomechanics, 39: 267-275, 2006

Szabó, I., Höhere Technische Mechanik, 4. Auflage, Springer-Verlag, Berlin / Göttingen / Heidelberg, 1964

Thompson, J. P., Pearce, R. H., Schechter, M. T., Adams, M. E., Tsang, I. K. Y., Bishop, P. B., Preliminary evaluation of a scheme for grading the gross morphology of the human intervertebral disc, Spine, 15(5), 411-415,1990

VDI 2057 Part 1. Human exposure to mechanical vibrations, Whole-body vibration. VDI-Richtlinie, Verein Deutscher Ingenieure, Düsseldorf, 2002

VIBRISKS, Final Technical Report. Risks of occupational vibration exposures. FP5 Project No. QLK3-2002-02650, January 2003 to December 2006, http://www.humanvibration.com/vibrisks/index.html

Waters, T., Raches, C., Genaidy, A., Rashed, T., A new framework for evaluating potential risk of back disorders due to whole body vibration and repeated mechanical shock, Ergonomics, 50(3), 379-395, 2007

Wilke, H.J., Neef, P., Caimi, M., Hoogland, T., Claes, L.E., New in vivo measurements of pressures in the intervertebral disc in daily life, Spine, 24 (8): 755-762, 1999

Wilke, H., Neef, P., Hinz, B., Seidel, H., Claes, L., Intradiscal pressure together with anthropometric data - a data set for the validation of models, Clinical Biomechanics, 16 (S1): S111-126, 2001

Wilke, H.J., Rohlmann, A., Neller, S., Schultheiss, M., Bergmann, G., Graichen, F., Claes, L.E., Is it possible to simulate physiologic loading conditions by applying pure moments? A comparison of in vivo and in vitro load components in an internal fixator, Spine, 26 (6): 636-42, 2001b

Witt, F., Ein modulares System zur Datenaufnahme und differenzierten Regelung niederfrequenter Prozesse mittels serieller Schnittstelle; Diplomarbeit, supervisor Huber, 2007

Wölfel, H.P., Numerical models and hardware dummies for simulating whole-body vibration of human – an overview. In: Proceedings of the First American Conference on Human Vibration. DHHS (NIOSH) Publication No. 2006-140, June. Cincinnati: NIOSH – Publications Dissemination, 46-47, 2006

Yingling, V.R., McGill, S.M., Anterior Shear of Spinal Motion Segments Kinematics, Kinetics, and Resultant Injuries Observed in a Porcine Model, Spine, 24 (18): 1882-1889, 1999

Zander, T., Rohlmann, A., Calisse, J., Bergmann, G., Estimation of muscle forces in the lumbar spine during upper-body inclination, Clinical Biomechanics, 16: 73-80, 2001